



UNIVERSITAT<sub>DE</sub>  
BARCELONA

# Statistical thermodynamics of long-range interacting systems and near-field thermal radiation

Ivan Latella

**ADVERTIMENT.** La consulta d'aquesta tesi queda condicionada a l'acceptació de les següents condicions d'ús: La difusió d'aquesta tesi per mitjà del servei TDX ([www.tdx.cat](http://www.tdx.cat)) i a través del Dipòsit Digital de la UB ([diposit.ub.edu](http://diposit.ub.edu)) ha estat autoritzada pels titulars dels drets de propietat intel·lectual únicament per a usos privats emmarcats en activitats d'investigació i docència. No s'autoritza la seva reproducció amb finalitats de lucre ni la seva difusió i posada a disposició des d'un lloc aliè al servei TDX ni al Dipòsit Digital de la UB. No s'autoritza la presentació del seu contingut en una finestra o marc aliè a TDX o al Dipòsit Digital de la UB (framing). Aquesta reserva de drets afecta tant al resum de presentació de la tesi com als seus continguts. En la utilització o cita de parts de la tesi és obligat indicar el nom de la persona autora.

**ADVERTENCIA.** La consulta de esta tesis queda condicionada a la aceptación de las siguientes condiciones de uso: La difusión de esta tesis por medio del servicio TDR ([www.tdx.cat](http://www.tdx.cat)) y a través del Repositorio Digital de la UB ([diposit.ub.edu](http://diposit.ub.edu)) ha sido autorizada por los titulares de los derechos de propiedad intelectual únicamente para usos privados enmarcados en actividades de investigación y docencia. No se autoriza su reproducción con finalidades de lucro ni su difusión y puesta a disposición desde un sitio ajeno al servicio TDR o al Repositorio Digital de la UB. No se autoriza la presentación de su contenido en una ventana o marco ajeno a TDR o al Repositorio Digital de la UB (framing). Esta reserva de derechos afecta tanto al resumen de presentación de la tesis como a sus contenidos. En la utilización o cita de partes de la tesis es obligado indicar el nombre de la persona autora.

**WARNING.** On having consulted this thesis you're accepting the following use conditions: Spreading this thesis by the TDX ([www.tdx.cat](http://www.tdx.cat)) service and by the UB Digital Repository ([diposit.ub.edu](http://diposit.ub.edu)) has been authorized by the titular of the intellectual property rights only for private uses placed in investigation and teaching activities. Reproduction with lucrative aims is not authorized nor its spreading and availability from a site foreign to the TDX service or to the UB Digital Repository. Introducing its content in a window or frame foreign to the TDX service or to the UB Digital Repository is not authorized (framing). Those rights affect to the presentation summary of the thesis as well as to its contents. In the using or citation of parts of the thesis it's obliged to indicate the name of the author.

Ph.D. Thesis

**Statistical thermodynamics of long-range  
interacting systems and near-field thermal  
radiation**

IVAN LATELLA

Departament de Física de la Matèria Condensada,  
Facultat de Física



UNIVERSITAT DE  
BARCELONA



**Statistical thermodynamics of long-range interacting systems and  
near-field thermal radiation**

A dissertation presented by

Ivan Latella

to the Faculty of Physics of the University of Barcelona in partial fulfillment  
of the requirements for the degree of Doctor of Philosophy in Physics. This  
thesis was prepared under the supervision of

Dr. Agustín Pérez Madrid

from the Department of Condensed Matter Physics of the University of  
Barcelona.

Director: Dr. Agustín Pérez Madrid

Tutor: Dr. Giancarlo Franzese (University of Barcelona)



## Preface

This thesis reports on two main topics that have been studied from the perspective of statistical thermodynamics. The results presented in this dissertation concern, on the one hand, classical systems with long-range interactions and, on the other, thermal radiation in the near-field regime. Although both topics are examined within the realm of statistical thermodynamics, they are discussed separately in a self-contained manner and can be followed independently. After the introduction presented in Chapter 1, which covers both subjects, long-range interacting systems are considered in Chapters 2 and 3, whereas near-field thermal radiation is contemplated in Chapters 4 and 5. In Chapter 6, we summarize our findings and present the corresponding conclusions for the two topics.

Part of the original work presented in this thesis is currently in preparation for submission or has been submitted [1, 2], while another important part has already been published [3–9]. The publications included in this thesis are:

- [1] I. Latella, A. Pérez-Madrid, A. Campa, L. Casetti, and S. Ruffo. Long-range interacting systems in the unconstrained ensemble (*in preparation*).
- [2] A. Campa, L. Casetti, I. Latella, A. Pérez-Madrid, and S. Ruffo. Phase transitions in Thirring’s model, arXiv:1603.02602 (*submitted*).
- [3] I. Latella, A. Pérez-Madrid, L. C. Lapas, and J. M. Rubi. Near-field thermodynamics and nanoscale energy harvesting. *Phys. Scr.* **T165**, 014026 (2015).
- [4] I. Latella, A. Pérez-Madrid, J. M. Rubi, S.-A. Biehs, and P. Ben-Abdallah. Heat engine driven by photon tunneling in many-body systems. *Phys. Rev. Applied* **4**, 011001 (2015).
- [5] I. Latella, A. Pérez-Madrid, A. Campa, L. Casetti, and S. Ruffo. Thermodynamics of nonadditive systems. *Phys. Rev. Lett.* **114**, 230601 (2015).
- [6] I. Latella, A. Pérez-Madrid, and J. M. Rubi. Thermodynamics and energy conversion of near-field thermal radiation: maximum work and efficiency bounds. *Eur. Phys. J. Conferences* **79**, 01001 (2014).
- [7] I. Latella, A. Pérez-Madrid, L. C. Lapas, and J. M. Rubi. Near-field thermodynamics: Useful work, efficiency, and energy harvesting. *J. Appl. Phys.* **115**, 124307 (2014).
- [8] I. Latella and A. Pérez-Madrid. Local thermodynamics and the generalized Gibbs-Duhem equation in systems with long-range interactions. *Phys. Rev. E* **88**, 042135 (2013).

[9] I. Latella and A. Pérez-Madrid. Long-range interacting systems and the Gibbs-Duhem equation. In M. Pilotelli and G. P. Beretta, editors, *Proceedings of the 12th JETC*, page 437 (2013).

References [1, 2, 5, 8, 9] of the previous list belong to the framework of long-range interacting systems and are exposed in Chapters 2 and 3. The results published in [3, 4, 6, 7] correspond to the subject of near-field thermal radiation and are discussed in Chapters 4 and 5.

Ivan Latella  
Barcelona, April 2016

## Abstract

Two main topics are examined in this thesis: classical systems with long-range interactions and thermal radiation in the near-field regime. In the first part, we present a thermodynamic approach describing systems with long-range interactions which takes into account the intrinsic nonadditivity in these systems. The basic concept behind this approach is to consider a large ensemble of replicas of the system where the standard formulation of thermodynamics can be naturally applied and the properties of a single system can be consequently inferred. The formulation of the thermodynamic for these systems is in close connection with Hill's thermodynamics of systems with small number of particles. It is shown that systems with long-range interactions can attain equilibrium configurations in the unconstrained ensemble. In this statistical ensemble, the control parameters are the temperature, pressure, and chemical potential, while the energy, volume, and number of particles fluctuate. We consider a solvable model as a concrete example of a system that achieves stable equilibria in this ensemble. We also give a complete description of the phase-diagram of the Thirring model in both the microcanonical and the canonical ensemble, highlighting the main features of ensemble inequivalence. In the second part, we study energy and entropy fluxes of near-field thermal radiation in many-body systems, with application to energy-conversion processes. It is shown that the maximum work that can be obtained from the thermal radiation emitted by two planar sources in the near-field regime is much larger than that corresponding to the blackbody limit. This quantity as well as an upper bound for the efficiency of the process are computed from the formulation of thermodynamics in the near-field regime. The case when the difference of temperatures of the hot source and the environment is small, relevant for energy harvesting, is studied in detail. We also show that thermal radiation energy conversion can be more efficient in the near-field regime. Moreover, by analyzing the thermodynamic performance of three-body near-field heat engines, we demonstrate that the power they supply can be substantially larger than that of two-body systems, showing their strong potential for energy harvesting. Theoretical limits for energy and entropy fluxes in three-body systems are discussed and compared with their corresponding two-body counterparts. Such considerations confirm that the thermodynamic availability in energy-conversion processes driven by three-body photon tunneling can exceed the thermodynamic availability in two-body systems.



## Acknowledgements

In first place, I would like to express my sincere gratitude to my advisor Agustín Pérez Madrid for continuous support and encouragement, for his patience and motivation, and for giving me enough freedom to carry out this work following my intuition. I also want to thank him for his passion in countless discussions about the fascinating world of physics, and many other topics out of the academic life, those of the personal life, that vastly have contributed to what I take away from this experience.

I am deeply indebted to Philippe Ben-Abdallah, Svend-Age Biehs, Alessandro Campa, Lapo Casetti, Luciano C. Lapas, J. Miguel Rubi, and Stefano Ruffo, coauthors of the publications included in this thesis, who kindly clarified every single issue I addressed to them. This thesis would not been possible without their help.

During these years, I have had useful and interesting discussions with Dick Be-deaux, Ralph Chamberlin, Yan Levin, Takashi Mori, David Reguera, Tarcisio N. Teles, and Øivind Wilhelmsen. I extend my gratitude to all of them too.

I take this opportunity to thank all the friends and colleagues that I met in the faculty, who made this endeavor a memorable stage. In particular, I would like to mention Adriana, Albert, Blai G., Blai P., Carmen, Carlos, Dani, David, Genís, Guille, Luis, Marina, Markus, Martin, Miquel, Núria, Paco, Paolo, and Savitri. I also would like to thank Bea, Cristina, Elena, and Olga for priceless help with the bureaucratic tasks of the department.

Por supuesto, también quiero agradecer a la familia, por darme ánimos continuamente y haber ayudado en todo lo posible. A mi mamá Alicia, mis hermanas Romina y Silvana, mi hermano Adrian y mis tíos Alida y Remo, simplemente gracias. A mi familia y amigos de Barcelona, Daniel, Yanet, Kati, Simó, Rodrigo, Natalia, Victor y Juani, les agradezco por el apoyo y el afecto recibido durante estos años. Artífice de todo esto, además de agradecerle de corazón, a Tamara esta tesis va dedicada.

Financial support through an FPI scholarship (Grant No. BES-2012-054782) from the MINECO of the Spanish Government is gratefully acknowledged.



*to Tamara*



# CONTENTS

---

Preface . . . . .	v
Abstract . . . . .	vii
Acknowledgements . . . . .	ix
<b>1 Introduction</b>	<b>1</b>
1.1 Long-range interacting systems . . . . .	2
1.2 Near-field thermal radiation . . . . .	5
<b>2 Thermodynamics of long-range interacting systems</b>	<b>9</b>
2.1 Long-range interactions and nonadditivity . . . . .	9
2.1.1 Constrained ensembles . . . . .	12
2.1.2 The unconstrained ensemble . . . . .	17
2.2 Mean-field description . . . . .	20
2.2.1 Microcanonical ensemble . . . . .	21
2.2.2 Canonical ensemble . . . . .	25
2.2.3 Grand canonical ensemble . . . . .	27
2.2.4 Isobaric-isothermal ensemble . . . . .	30
2.2.5 Unconstrained ensemble . . . . .	32
2.3 Global and local relations . . . . .	35
2.3.1 Excess quantities . . . . .	35
2.3.2 Local equation of state . . . . .	37
2.3.3 Power-law interactions . . . . .	39
2.4 Response functions . . . . .	42
2.4.1 Concavity and convexity . . . . .	42
2.4.2 Response functions and ensemble inequivalence . . . . .	43
2.4.3 From microcanonical entropy to rescaled replica energy . . . . .	47
<b>3 Long-range interactions: models and applications</b>	<b>51</b>
3.1 Phase transitions in the Thirring model . . . . .	51
3.1.1 The Thirring model . . . . .	52
3.1.2 Landau theory: Microcanonical ensemble . . . . .	54

xiii

Contents

3.1.3	Landau theory: Canonical ensemble . . . . .	57
3.1.4	Microcanonical and canonical phase diagrams . . . . .	61
3.1.5	Replica energy and scaling . . . . .	65
3.2	Equilibria in the unconstrained ensemble . . . . .	68
3.2.1	Modified Thirring model . . . . .	69
3.2.2	Modified Thirring model under completely open conditions . . . . .	70
3.2.3	Comparison with the grand canonical ensemble . . . . .	76
3.2.4	Comparison with the canonical ensemble . . . . .	81
3.3	Thermodynamic relations and replica energy . . . . .	85
3.3.1	Self-gravitating isothermal spheres . . . . .	86
3.3.2	Modified Thirring model . . . . .	88
<b>4</b>	<b>Near-field thermodynamics out of thermal equilibrium</b>	<b>93</b>
4.1	Energy fluxes in three-body systems . . . . .	93
4.1.1	The Poynting vector . . . . .	95
4.1.2	Correlation functions and electric field . . . . .	97
4.1.3	Scattering coefficients . . . . .	101
4.1.4	Transmission coefficients . . . . .	103
4.2	Entropy fluxes in three-body systems . . . . .	105
4.3	Energy and entropy fluxes in two-body systems . . . . .	108
4.3.1	Finite bodies . . . . .	109
4.3.2	Semi-infinite bodies . . . . .	110
4.3.3	Blackbody limit . . . . .	112
4.4	Fluxes in the near-field regime . . . . .	112
4.4.1	Three-body systems . . . . .	113
4.4.2	Two-body systems . . . . .	114
4.4.3	Near-monochromatic approximation: the extreme near field . . . . .	115
<b>5</b>	<b>Near-field thermal radiation energy conversion</b>	<b>119</b>
5.1	Two-body near-field heat engines . . . . .	119
5.1.1	Thermodynamic availability and efficiency . . . . .	120
5.1.2	Energy harvesting from polar dielectric sources . . . . .	123
5.2	Many-body near-field heat engines . . . . .	126
5.2.1	Three-body vs. two-body near-field heat engines . . . . .	127
5.2.2	Theoretical limits in many-body systems . . . . .	134
<b>6</b>	<b>Summary and conclusions</b>	<b>137</b>
6.1	Replica energy as a degree of freedom . . . . .	137
6.2	Heat engines driven by photon tunneling . . . . .	139
6.3	Future directions . . . . .	140

<b>Appendix A Modified Thirring model: canonical critical point</b>	<b>143</b>
A.1 Free energy expansion . . . . .	143
A.2 Critical point . . . . .	144
<b>Appendix B Transmission coefficients for radiative heat transfer</b>	<b>145</b>
B.1 Coefficients for the electric field . . . . .	145
B.2 Transmission coefficients . . . . .	146
B.2.1 Transmission coefficients in the two-body system . . . . .	149
<b>Resumen</b>	<b>151</b>
<b>References</b>	<b>155</b>



# INTRODUCTION

---

Thermodynamics and statistical mechanics are complementary fields that describe the properties of a system subjected to given external conditions. While thermodynamics deals with the mathematical relations connecting such properties, statistical mechanics explains why a certain property takes the particular value observed in a concrete realization. The latter acts as a bridge from the microscopic behavior of the constituents of the systems to the global relationship among thermodynamic quantities. In this regard, from the point of view of both statistical mechanics and thermodynamics, finite systems may exhibit noteworthy properties differing from those of systems in the usual thermodynamic limit. For a physical system, the quality of being finite may arise in numerous situations and can be produced by different phenomena. This finiteness emerges, for instance, when the number of particles in the system is small or if the size of the system is comparable with a relevant length scale associated to the physics under consideration. In this work, we focus on statistical thermodynamics of two particular examples of finite systems: classical systems with long-range interactions and thermal radiation in the near-field regime.

In the first of these examples, we say that the interactions are long ranged when their range of interaction is comparable with the characteristic length defining the size of the system. Thus, a system with these interactions is finite with respect to the range of the interactions among its constituents. As a consequence of this property, systems with long-range interactions are nonadditive. This gives rise to a phenomenology which is in sharp contrast to that occurring in macroscopic system with short-range interactions. Remarkably, the equilibrium configurations in long-range interacting systems crucially depend on the particular control parameters specifying its thermodynamic states, namely, for these systems the different statistical ensembles may not be equivalent [10, 11]. In the second case, that is, near-field thermal radiation, the spectrum of the electromagnetic field in thermal equilibrium with a body at a given temperature possesses a characteristic wavelength defined by this

temperature, the so-called thermal wavelength. If two bodies interact exchanging heat by means of thermal radiation, the heat flux not only depends on the optical properties of the bodies and the temperatures at which they are thermalized, but also on the separation distance between such bodies. When this separation distance is smaller than the dominant thermal wavelength, we say that the radiative process occurs in the near-field regime. Considering that the system is the thermal radiation confined between the bodies, its size is given by the corresponding separation distance. The system is thus finite in the near-field regime, since its size is comparable with the thermal wavelength of the radiation. Such finite-size effects are not present in far-field thermal radiation, when the bodies are far from each other. The relevant point to highlight in this case is that the radiative heat transfer is significantly increased when reducing the separation distances to near-field scales [12]. Therefore, the finiteness just described can be seen as the common feature underlying characteristic properties of the systems with long-range interactions and of the near-field thermal radiation we examine in the following chapters.

In order to properly introduce both topics and make clear the objectives of the research presented in this thesis, the rest of this introductory chapter is divided in two sections setting out separate considerations on long-range interacting systems and near-field thermal radiation.

## 1.1 Long-range interacting systems

In recent years, the systematic study of systems with long-range interactions has attracted considerable attention, due to remarkable properties that significantly differ from those of short-range interacting systems [10, 11, 13, 14]. A great variety of systems in nature are governed by long-range interactions. Examples are self-gravitating systems [15–23], two-dimensional or geophysical fluids [21, 24–27], vortices [21], nuclear physics [28], spin systems [29–33], and plasmas [34–36]. In this context, also toy models such as, e.g., the Hamiltonian mean-field model [37, 38] and the self-gravitating ring model [39, 40] have been considered to demonstrate some features of these systems. Interactions in this kind of systems are characterized by a slowly decaying pair interaction potential that couples the constituent parts of the system at large distances. A potential is long ranged if it decays as or slower than  $1/r^a$ , with  $0 \leq a \leq d$ , at least in a region comparable with the total extension of the system, where  $r$  is the interparticle distance and  $d$  is the dimension of the embedding space [10]. As a result of these interactions, even in the proper thermodynamic limit each particle interacts with a number of particles that is a finite fraction of the whole, so that long-range interactions dominate over binary short-range ones.

Additivity plays a central role in the formulation of thermodynamics. If a sys-

tem is divided into different parts, each part possessing a certain energy, the system is said to be additive if the energy due to the interactions between these parts is negligible in comparison with the total energy [10, 11]. Because of additivity, the extensive quantities are linear functions of the system size and the thermodynamic potentials present always the same concavity. Macroscopic systems with short-range interactions are additive. In contrast, the energy due to interactions between different parts of the system cannot be neglected if these interactions are long-ranged, causing the system to be intrinsically nonadditive. Nonadditivity is thus clearly originated from the finiteness previously mentioned. This lack of additivity has been identified as the source of the unusual thermodynamic properties of systems with long-range interactions, typically associated with a curvature anomaly of the relevant thermodynamic potential. The same happens in small systems with short-range interactions, where the range of the interactions is of the order of the size of the system [28, 41]. The nonadditivity then leads to a thermostistical behavior not shown in macroscopic short-range interacting systems; as noted before, long-range interacting systems may present ensemble inequivalence [10, 18, 42–48]. For instance, the occurrence of negative heat capacities in the microcanonical ensemble leads to the inequivalence between the microcanonical and canonical ensembles, as we discuss in a moment with a well-known example. A peculiar thermodynamic property such as negative heat capacity is seen as unusual if one takes the thermodynamics of additive systems as a paradigm. In practice, properties of this kind are found in a large variety of systems in nature, ranging from atomic [49] to stellar clusters [16, 18–20].

Furthermore, the relaxation towards thermodynamic equilibrium in long-range systems proceeds in a different manner than that of systems with short-range interactions [50]. In short-range systems, internal collisions drive the system to a state characterized by a Maxwell-Boltzmann distribution function. To the contrary, in systems with long-range interactions with a large number of particles, the evolution is mainly collisionless and the system may remain trapped in a nonequilibrium quasistationary state that is not described by a Maxwell-Boltzmann distribution [50–54]. The time that the system spends in this quasistationary state depends on the number of particles and diverges if the number of particles is infinite. However, for a large but finite number of particles in a very long time limit, the system will evolve to a state of thermodynamic equilibrium characterized by a Maxwell-Boltzmann distribution if such a state exists [55]. These states of thermodynamic equilibrium given by the theory of ensembles in statistical mechanics are those we will focus on throughout this work.

Probably the most paradigmatic example of system with long-range interactions is the case of Newtonian gravity, that has served as a basis for developing methods for studying an important part of the phenomenology concerning the thermodynamics

of these systems. In this regard, the isothermal spheres model has been widely used to study self-gravitating systems in the mean-field approximation [15, 16, 19, 20, 56]. Although correlations are ignored in the mean-field approach, this description offers a mathematical tool for a suitable treatment of self-interactions in the system and turns out to be very accurate for a large number of particles [57, 58]. Some corrections are reasonably expected for not very large number of particles [59]. It is a well-known fact that self-gravitating systems possess equilibrium states with negative heat capacity, provided the system is isolated (microcanonical ensemble). Equilibrium in that case is ensured in a certain range in the space of parameters because isothermal spheres correspond to local maxima of the entropy with an extremely large lifetime that scales like the exponential of the number of particles [22]. In the microcanonical ensemble, self-gravitating isothermal spheres become unstable when the heat capacity passes from negative to positive, leading to what is known as gravothermal catastrophe [15–17]. When one of these systems is put in contact with a heat bath (canonical ensemble), the configurations with negative heat capacity cannot be realized and are replaced by a phase transition or isothermal collapse [18, 20, 60]. In the canonical ensemble, isothermal spheres correspond to states of local minimum of the Helmholtz free energy and the isothermal collapse sets in when the heat capacity passes from positive to negative [20]. The self-gravitating gas has also been studied in the grand canonical ensemble with the mean-field approach and Monte Carlo simulations [57, 58]. There, the instability sets in at a critical value of the parameter controlling the state of the system that is different from the critical values in the microcanonical and canonical ensembles [61, 62]. This example illustrates the fact that different ensemble representations are, in general, nonequivalent and that the behavior of the system strongly depends on the control parameter used to specify its thermodynamic state. In a wider scope, systems with an attractive interaction potential  $1/r^a$  with  $0 < a < 3$  in three dimensions were considered in the microcanonical ensemble [63, 64] and also there a critical energy was found below which these systems undergo a gravitational-like phase transition. Phase transitions in simplified models such as the self-gravitating ring model have also been studied [39, 40].

Although intense research on systems with long-range interactions has been carried out during the last few years from the statistical mechanics point of view, the thermodynamic framework concerning these systems in connection with nonadditivity has received much less attention. This is mainly due to the fact that statistical mechanics has to be necessarily contemplated in order to account for the microscopic interactions. Can nonadditivity be explicitly identified within the thermodynamic formalism, or does one merely have to settle for considering it through its implicit contribution to the usual thermodynamic potentials? Within this topic, the main objective of this thesis is to build a thermodynamic formalism suitable for long-range

interacting systems in which the role played by nonadditivity can be unambiguously determined and quantified.

As we shall see, the thermodynamic formalism described in Section 2.1 of the next chapter achieves the previous objective. There, we point out a close relationship existing between the thermodynamics of long-range interacting systems and Hill's thermodynamics of small systems [65]. Nonadditivity introduces a thermodynamic degree of freedom which, in particular, may lead to equilibrium configurations in completely open systems, namely, when the energy, volume, and number of particles fluctuate. This is discussed in Section 2.1.2 and complemented within the mean-field description in Section 2.2. Furthermore, we have mentioned that nonadditivity can give rise to curvature anomalies in the thermodynamic potentials, or thermodynamic characteristic functions, which is in turn associated with ensemble inequivalence. This matter is discussed in connection with the characteristic function corresponding to completely open systems in Section 2.4: it can be shown that this characteristic function is always concave in all its natural variables. In Chapter 3, we concentrate in specific models showing some of the particular aspects associated to systems with long-range interactions. In Section 3.1, we study in detail the phase diagrams of the Thirring model [18], a solvable model that describes a simplified version of a self-gravitating gas. The model undergoes first-order phase transitions which ends in a critical point in both the microcanonical and canonical ensembles. We obtain and compare these two phase diagrams. As a consequence of the ensemble inequivalence, neither the line nor the point have the same location in the phase diagram of the two ensembles. In Section 3.2, we consider a modification of the Thirring model that is stable under completely open conditions, and some thermodynamic relations in connection with the degree of freedom introduced by nonadditivity are studied in Section 3.3. Finally, a summary and general conclusions are presented in Section 6.1.

## 1.2 Near-field thermal radiation

The radiative heat transfer between bodies separated by a large distance is bounded by the blackbody limit [66]. In this limit, corresponding to the far-field regime, the power radiated by the bodies is given by the Stefan-Boltzmann law. When such a separation distance is reduced below the characteristic thermal wavelength of the radiation, that is, in the near-field regime, the radiative heat transfer is considerably enhanced as compared to the blackbody limit [12, 67–73]. The thermal wavelength of the radiation defining near-field scales is given by<sup>1</sup>  $\lambda_T = \hbar c/k_B T$ , where  $\hbar$  is

---

<sup>1</sup>Here and in Chapters 4 and 5 the thermal wavelength is taken as  $\lambda_T = \hbar c/k_B T$ . In Chapters 2 and 3 we consider systems with classical particles and with the same symbol denote the thermal

the reduced Planck constant,  $k_B$  is the Boltzmann constant,  $c$  is the speed of light in vacuum, and  $T$  is the temperature;  $\lambda_T$  is about  $7.6 \mu\text{m}$  at room temperature. Near-field radiative effects are relevant in many systems, such as scanning thermal microscopy [74], thermal radiation scanning tunnelling microscopy [75], the near-field thermal transistor [76], the generation of usable energy from thermal sources via thermophotovoltaic devices [77–82], and the recently reported photon thermal Hall effect between anisotropic particles [83] (recent reviews can be found, for instance, in [84, 85]). In addition, an useful control of the heat transfer has been predicted in many-body systems when intermediate bodies are used to connect two bodies in interaction [86–91]. This result offers the possibility of novel applications exploiting the physics of many-body systems, such as thermal memories [92] or heat engines driven by near-field thermal radiation [4].

For an electromagnetic plane wave characterized by the angular frequency  $\omega$ , the relation  $(\omega/c)^2 = k_x^2 + k_y^2 + k_z^2$  is satisfied in free space with all the wave vector components  $k_x$ ,  $k_y$ , and  $k_z$  being real quantities. However, in the presence of an interface lying, for instance, in the  $x$ - $y$  plane, Maxwell's equations permit solutions satisfying the corresponding boundary conditions for which  $\kappa^2 = k_x^2 + k_y^2 > \omega^2/c^2$ , leading to a pure imaginary component  $k_z = \sqrt{(\omega/c)^2 - \kappa^2}$ . Thus, these modes of the field decay as  $\exp(ik_z z) = \exp(-|k_z|z)$  in the direction perpendicular to the interface [93], as happens at the interface between a body emitting thermal radiation and vacuum. Such exponentially decaying waves are called evanescent waves and are modes of the electromagnetic field that do not propagate as the more usual traveling ones but stand localized in the vicinity of the body. These waves can transport energy if a second body is placed close enough to the first one, in such a way that the evanescent fields of both objects overlap between them. In this situation, the evanescent waves can be seen as perturbations tunneling through the gap between the bodies, carrying energy from one place to another. Because of the quantum nature of the electromagnetic radiation, the latter mechanism is also called photon tunneling [94]. This mechanism occupies a central place in near-field radiative heat transfer.

The description of the radiative heat transfer between closely spaced bodies is mainly due to the work of Polder and Van Hove [12], who introduced a theory based on the fluctuational electrodynamics approach of Rytov [95, 96]. The approach of Rytov and the work of Polder and Van Hove, later considered by Loomis and Maris [67], combine Maxwell's equations with the fluctuation-dissipation theorem [97, 98], leading to a macroscopic theory accounting for microscopic fluctuations inside the radiating body. The subjacent physics behind this theory is that the

---

wavelength  $\lambda_T = h/\sqrt{2\pi mT}$ , where  $h$  is a constant,  $m$  is the mass of a particle, and units such that  $k_B = 1$  are used.

charges in random thermal motion within a thermalized material generate fluctuating currents that radiate electromagnetic fields. These electromagnetic fields possess a thermal spectrum characterized by the temperature of the radiating body. Moreover, the energy carried by the electromagnetic fields emitted by this body can be absorbed and dissipated by another body receiving these fields, which constitutes the basic mechanism of radiative heat transfer [99]. Rytov's approach, in fact, not only takes into account thermal fluctuations of the electromagnetic field, but also purely quantum fluctuations that persist at zero temperature, namely, those associated to the zero-point energy. The latter, however, do not contribute to the net radiative heat transfer between the bodies. Using the fluctuational electrodynamics approach of Rytov, Lifshitz [100] described the van Der Waals forces between macroscopic bodies separated by a narrow vacuum gap, a theory generalized in [101] and that leads to the Casimir force [102] when the bodies are assumed to be perfect conductors. Purely quantum fluctuations of the electromagnetic field are more significant than thermal fluctuations in this case. These Casimir-Lifshitz forces, which will not be considered here, are intimately connected to the near-field radiative heat transfer we are interested in [103, 104]. Furthermore, on the basis of the fluctuational electrodynamics approach, one is able to describe the radiative heat transfer in both the far and near fields. The most important aspect of this approach is that it fully incorporates all participating modes, including the modes corresponding to evanescent states of the field. The heat transfer in the near-field regime is enhanced due to the tunneling of evanescent waves [94, 99, 105, 106].

In addition, while the net heat transfer vanishes when the interacting bodies are thermalized at the same temperature, there are certain effects in the near field that can be observed even at thermal equilibrium. Due to the contribution of evanescent modes, homogeneity is lost and the electromagnetic density of states becomes position-dependent close to an interface separating two media [107–109]. This implies that the thermodynamic functions also depend on this contribution [110, 111] and exhibit a very different behavior from the one shown in the far-field case. The local spectrum of near-field thermal emission has been reported in [112], showing that the characteristic spectrum of blackbody radiation is modified in the proximity of the source. Such aspects of the near-field thermal radiation will not be discussed in this thesis.

A relevant aspect of the thermal radiation to highlight at this point is that the electromagnetic fields not only carry energy, but also entropy. The balances of energy and entropy fluxes play a key role in any thermodynamic scheme describing energy-conversion processes. On the one hand, such schemes have been successfully implemented for blackbody radiation, leading to upper bounds for the efficiency of the process and the usable work flux that can be obtained from the system (see, for instance, references [113, 114]). On the other hand, since an advantageous control

of near-field heat transfer can be obtained in many-body systems, which includes energy flux amplification [88], a thermodynamic formulation dealing with many bodies in radiative interaction will be advantageous as well. The latter is our main interest within this topic.

In this context, the goal of this thesis is to provide a thermodynamic scheme describing near-field thermal radiation energy conversion in many-body systems. We analyze three-body systems explicitly, and discuss the general case of  $N$ -body systems in a particular situation. More specifically, in Chapter 4, we first consider energy fluxes in three-body systems. Following [103, 104], we compute the electromagnetic field in the vacuum regions between bodies of infinite transversal extension and finite width. This allows us to write the energy fluxes in a Landauer-like formalism [94, 115, 116], and obtain explicitly all the transmission coefficients in three- and two-body systems. From the energy fluxes and using these transmission coefficients, in Section 4.2 we obtain the corresponding entropy fluxes in three-body systems, and consider the two-body case in Section 4.3. With the knowledge of energy and entropy fluxes in the system and using thermodynamic arguments, we study energy-conversion processes involving near-field thermal radiation by computing upper bounds for the efficiency and the usable work flux that can be extracted from the radiation. This is done in Chapter 5. In Section 5.1, it is shown that the maximum work flux that can be obtained from the thermal radiation emitted by two polar sources in the near-field regime is much larger than that corresponding to the blackbody limit. The case when the difference of temperatures of the hot source and the environment is small, relevant for energy harvesting, is studied in some detail. It is also shown that thermal radiation energy conversion can be more efficient in the near-field regime, as compared to the case of blackbody radiation. In Section 5.2.1, by analyzing the thermodynamic performance of three-body near-field heat engines, we demonstrate that the power they supply can be substantially larger than that of two-body systems, showing their strong potential for energy harvesting. Theoretical limits for energy and entropy fluxes in three-body systems are discussed and compared with their corresponding two-body counterparts. Such considerations confirm that the thermodynamic availability in energy-conversion processes driven by photon tunneling in three-body systems can exceed the thermodynamic availability in two-body systems. In Section 5.2.2, theoretical limits in  $N$ -body systems are discussed. Finally, a summary and general conclusions are presented in Section 6.2.

# THERMODYNAMICS OF LONG-RANGE INTERACTING SYSTEMS

---

In this chapter we introduce a thermodynamic description in the equilibrium framework suitable for systems with long-range interactions. Emphasis is made on non-additivity, a remarkable property in these systems responsible for the occurrence of the rich phenomenology that is not present in the thermodynamics of short-range interacting systems. As we will discuss in detail, the approach we follow is in close connection with the thermodynamics of small systems. Here we concentrate on the thermodynamic formalism, while the discussion of concrete examples of systems with long-range interactions is postponed until the next chapter.

## 2.1 Long-range interactions and nonadditivity

The usual formulation of thermodynamics is based on the additivity of macroscopic systems [117]. Nevertheless, there are numerous examples of macroscopic systems that are not additive, due to the long-range character of the interaction among their constituents. Since statistical mechanics can be formulated for these systems [10,11], it suggests that the associated thermodynamics can be formulated as well. The thermodynamic approach discussed here, indeed, has to be understood as being that related to the usual statistical mechanics of long-range interacting systems [10,11].

The key idea is to convert the problem of the thermodynamics of a nonadditive system into one of the thermodynamics of an additive system, and use there the standard thermodynamic approach. This can be done by considering an ensemble of  $\mathcal{N}$  independent, equivalent, distinguishable replicas of the system. This ensemble of replicas not necessarily has to be interpreted as a real physical system; it can be seen as a contrived system that helps to infer thermodynamic properties of its single constituents. Since the ensemble can be as large as needed by taking  $\mathcal{N} \rightarrow \infty$ ,

it is in fact an additive system and, therefore, the standard equilibrium thermodynamic approach can be applied. An analogous theoretical framework implementing this idea was introduced by Hill [65, 118] for small systems. A small system, i.e., a system with a small number of particles, is not additive; but additivity is recovered, together with the usual thermodynamics of macroscopic systems, when the number of particles in the system goes to infinity, provided the range of the short-range interactions becomes negligible with respect to the system size. However, the situation we consider here is clearly different: we take from the beginning into account long-range interacting systems with a large number of particles. In such systems, no matter how large, the size of the system and the interaction range are comparable, and therefore these systems are always intrinsically nonadditive. The important point to highlight here is that no assumption is made in Hill's arguments regarding the size of the system when the thermodynamic formalism is established. He showed, in fact, that a nontrivial realization of this general thermodynamic approach is obtained if the system is small. More importantly, actually no assumption is made in his arguments about the elementary nature of the system itself; the only requirement is that the balance of energy in the equilibrium configurations of the system is dictated by the usual laws of thermodynamics. In addition, since for small systems, which are far from thermodynamic limit, ensemble equivalence does not hold in general, the thermodynamic equations in [65] are derived for several sets of different control parameters. Our task is then to show that such a framework applies for nonadditive systems with a large number of particles.

Let us thus consider a system with energy  $E$ , entropy  $S$ , volume  $V$ , and  $N$  particles. We now introduce an ensemble of independent, equivalent, and distinguishable replicas of the systems as a construction from which, as we will see, properties of the system itself can be inferred. We stress that, as usual in statistical ensembles, the replicas do not interact with each other. The total energy, entropy, volume, and number of particles of an ensemble of  $\mathcal{N}$  such systems are given by  $E_t = \mathcal{N}E$ ,  $S_t = \mathcal{N}S$ ,  $V_t = \mathcal{N}V$ , and  $N_t = \mathcal{N}N$ , respectively. The fundamental thermodynamic relation for the ensemble takes the form

$$dE_t = TdS_t - PdV_t + \mu dN_t + \mathcal{E}d\mathcal{N}, \quad (2.1)$$

where  $T$  is the temperature,  $P$  is the pressure exerted on the boundary of the systems, and  $\mu$  is the chemical potential of a single system. The last term on the right-hand side of equation (2.1) is the central ingredient that this approach incorporates, which accounts for the energy variation when the number of members of the ensemble  $\mathcal{N}$  varies, holding  $S_t$ ,  $V_t$  and  $N_t$  constant. Formally,

$$\mathcal{E} = \left( \frac{\partial E_t}{\partial \mathcal{N}} \right)_{S_t, V_t, N_t}. \quad (2.2)$$

The function  $\mathcal{E}$  is called replica energy<sup>1</sup> and quantifies the nonadditivity of the single systems; it vanishes for additive systems [5]. To see this, consider the following situation. Let us make a transformation in which an ensemble of  $\mathcal{N}_1$  replicas, each one with  $N_1$  particles, entropy  $S_1$  and volume  $V_1$ , becomes an ensemble of  $\mathcal{N}_2$  replicas, each one with  $N_2$  particles, entropy  $S_2$  and volume  $V_2$ , under the assumption that, for a given positive  $\xi$ , we have  $N_2 = N_1/\xi$ ,  $S_2 = S_1/\xi$ ,  $V_2 = V_1/\xi$ , but  $\mathcal{N}_2 = \xi\mathcal{N}_1$ . Clearly, in this case  $dS_t = dV_t = dN_t = 0$ , so that, from equation (2.1),  $dE_t = \mathcal{E}d\mathcal{N}$ . But in an additive system the energy is a linear homogeneous function of the entropy, volume and number of particles, i.e.,

$$E_2 \equiv E(S_2, V_2, N_2) = E(S_1/\xi, V_1/\xi, N_1/\xi) = E(S_1, V_1, N_1)/\xi \equiv E_1/\xi, \quad (2.3)$$

and therefore  $dE_t = 0$ , requiring  $\mathcal{E} = 0$ . Thus, we see that additivity implies  $\mathcal{E} = 0$ . Hence,  $\mathcal{E} \neq 0$  implies nonadditivity. On the other hand, for a nonadditive system the energy is not a linear homogeneous function of the entropy, volume and number of particles, and in general we will have  $\mathcal{E} \neq 0$ . Thinking for example of the case  $\xi = 2$ , this is a direct consequence of the fact that in a nonadditive system the interaction energy between the two halves of a macroscopic system is not negligible. Below we will show that  $\mathcal{E}$  is indeed a property of the system under consideration.

Notice that, according to (2.1), when adding replicas to the ensemble at constant  $S_t$ ,  $V_t$  and  $N_t$ , a subdivision of the system takes place. The result of this subdivision is not a collection of separate pieces of the system (subsystems) but whole systems with new values of entropy, volume, and number of particles. This gives us a criterion for regarding the system as additive ( $\mathcal{E} = 0$ ) or nonadditive ( $\mathcal{E} \neq 0$ ) without the need for defining subsystems.

Before proceeding, it is important to stress the following point. We are building a purely thermodynamic characterization of nonadditive systems, and we have singled out one thermodynamic quantity that is peculiar for this class of systems. However, we must be aware that one of the most striking facts in the statistical mechanics study of long-range systems, i.e., ensemble inequivalence, should produce a correspondence in a thermodynamic treatment, since ensemble inequivalence is connected to differences in the macroscopic states accessible to the systems when they are isolated or in contact with a thermostat [10,11]. The difference in the accessible macrostates translates into a difference in the equation of state between an isolated system and a thermostatted one, since, e.g., the temperature-energy relation of an isolated system in the range of convex entropy cannot hold for a thermalized system. These caveats do not spoil the central role of equation (2.1) in the present treatment; one should only consider that all the thermodynamic quantities in the equations,

---

<sup>1</sup>In Hill's book [65],  $\mathcal{E}$  is called subdivision potential. The name replica energy was suggested by Prof. D. Bedeaux [119].

like e.g.  $T$ ,  $S$ , and  $\mathcal{E}$  itself, are those corresponding to the actual physical conditions, and can be different according to whether the system is isolated or thermostatted.

Holding in equation (2.1) all single system properties constant yields

$$E d\mathcal{N} = T S d\mathcal{N} - P V d\mathcal{N} + \mu N d\mathcal{N} + \mathcal{E} d\mathcal{N}, \quad (2.4)$$

which can be integrated from 0 to  $\mathcal{N}$  giving

$$E_t = T S_t - P V_t + \mu N_t + \mathcal{E} \mathcal{N}. \quad (2.5)$$

Thus, for a single system one has

$$E = T S - P V + \mu N + \mathcal{E}, \quad (2.6)$$

together with the differential relations

$$dE = T dS - P dV + \mu dN, \quad (2.7)$$

$$d\mathcal{E} = -S dT + V dP - N d\mu. \quad (2.8)$$

Equation (2.7) is the usual first law of thermodynamics; equation (2.8) follows by requiring that the differentiation of  $E = T S - P V + \mu N + \mathcal{E}$  produces (2.7). Moreover, equation (2.8) shows that the well-known Gibbs-Duhem equation for additive systems does not hold here, and  $T$ ,  $P$ , and  $\mu$  may become independent due to the extra degree of freedom represented by  $\mathcal{E}$ . In the context of small systems, this independence between  $T$ ,  $P$ , and  $\mu$  has been exploited to consider completely open liquid-like clusters in a metastable supersaturated gas phase [120]. In addition, the deviations of small systems thermodynamics with respect to that of macroscopic systems have been shown in [121,122] using the grand canonical ensemble. Furthermore, this approach has also been used to study the critical behavior of ferromagnets [123] by considering an ensemble of physical subdivisions of a macroscopic sample; here we always consider replicas of the whole system under consideration.

### 2.1.1 Constrained ensembles

We have emphasized that all quantities appearing in the thermodynamic relations leading to (2.6), (2.7), and (2.8) are those corresponding to the actual physical conditions imposed on the system. Moreover, depending on the control parameters defining the state of the system, certain quantities fluctuate and other quantities are fixed. Distinguishing between these two kinds of quantities is relevant here, and it is convenient to set now the notation that will be used to indicate such a distinction when necessary: if the energy, volume, or number of particles are not control parameters, they are fluctuating quantities and will be denoted with a bar by  $\bar{E}$ ,  $\bar{V}$ ,

and  $\bar{N}$ , respectively. Thus, equations (2.6), (2.7), and (2.8) have to be understood for quantities with or without bars. In addition, we will refer to the variables  $E$ ,  $V$ , and  $N$  as constraint variables, and ensembles in which at least one of the constraint variables is a control parameter will be termed as constrained ensembles. In this way, the thermodynamic properties of an isolated system are obtained from a completely constrained ensemble in which all the constraint variables are control parameters, namely, the microcanonical ensemble. If none of the constraint variables is a control parameter, the system is said to be completely open and the associated ensemble is an unconstrained ensemble.

Ensemble inequivalence relies on the fact that the system can be sensitive to how the equilibrium configurations are established, that is, to the specific control parameters defining its state. Therefore, the thermodynamics of the system must be necessarily derived from the characteristic function (the entropy or the free energies) in the ensemble associated to the particular set of control parameters under consideration. In doing so, it is in general possible to obtain the replica energy from the corresponding characteristic function, except in the case where the replica energy itself is the characteristic function corresponding to a particular set of control parameters. In Section 2.1.2 we will show that the replica energy is the free energy associated to the unconstrained ensemble where the corresponding control parameters are  $T$ ,  $P$ , and  $\mu$ . Postponing until that section the discussion regarding this particular set of control parameters, now we focus on the relation between the replica energy and the characteristic functions in constrained ensembles (at least one of variables  $E$ ,  $V$ , and  $N$  is a control parameter). We restrict ourselves to some of the possible choices of control parameters, while other instances can be found in [65].

**Microcanonical ensemble:** Let us first consider the thermodynamics of an isolated system, so that the entropy is given as  $S = S(E, V, N)$  in the microcanonical ensemble. From (2.6), (2.7), and (2.8), the thermodynamic relations in this case are given by

$$-\frac{\mathcal{E}}{T} = S - \frac{1}{T}E - \frac{P}{T}V + \frac{\mu}{T}N, \quad (2.9)$$

$$dS = \frac{1}{T}dE + \frac{P}{T}dV - \frac{\mu}{T}dN, \quad (2.10)$$

$$d\mathcal{E} = -SdT + VdP - Nd\mu. \quad (2.11)$$

The replica energy can be written as  $\mathcal{E} = \mathcal{E}(E, V, N)$  by identifying  $T$ ,  $P$ , and  $\mu$  in (2.9) from the partial derivatives of the entropy with respect to their natural variables in (2.10). Alternatively, we can rewrite (2.9) and, using (2.10), express the

quantity  $\mathcal{S} \equiv -\mathcal{E}/T$  in the form

$$\mathcal{S} = S - E \left( \frac{\partial S}{\partial E} \right)_{V,N} - V \left( \frac{\partial S}{\partial V} \right)_{E,N} - N \left( \frac{\partial S}{\partial N} \right)_{E,V}. \quad (2.12)$$

Furthermore, the microcanonical entropy of a single system can be obtained from phase space considerations for the whole ensemble. Henceforth, the dimension of the embedding space is assumed to be  $d$ , and the momentum and position of the particle  $j$  in the system  $k$  are denoted by  $\mathbf{p}_{jk} \in \mathbb{R}^d$  and  $\mathbf{q}_{jk} \in \mathbb{R}^d$ , respectively. Taking into account that the  $\mathcal{N}$  systems are independent and equivalent, the Hamiltonian  $\mathcal{H}_t$  of the ensemble is given by

$$\mathcal{H}_t = \sum_{k=1}^{\mathcal{N}} \mathcal{H}_k, \quad (2.13)$$

where each individual Hamiltonian reads

$$\mathcal{H}_k = \sum_{j=1}^N \frac{|\mathbf{p}_{jk}|^2}{2m} + W(\mathbf{q}_{1k}, \dots, \mathbf{q}_{Nk}), \quad (2.14)$$

with  $m$  the mass of the particles. Here  $W$  is the potential energy of a single system that contains the long-range interactions. In addition, using units where  $k_B = 1$ , the total entropy is given by  $S_t = \ln \omega_t$ , where  $\omega_t = \omega_t(E_t, V_t, N_t, \mathcal{N})$  is the density of states obtained from the phase space of the ensemble. This density of states must be computed demanding not only that the total energy is fixed to  $E_t = \mathcal{N}E$ , but also that the energy of each single system is fixed to  $E$ . According to this, the energy constraint in phase space can be written as  $\rho(E_t) = \prod_{k=1}^{\mathcal{N}} \delta(E_t/\mathcal{N} - \mathcal{H}_k)$ . Since the systems are also considered to be distinguishable, the microcanonical density of states of the ensemble is therefore given by

$$\omega_t = \int \frac{\rho(E_t)}{(h^{dN} N!)^{\mathcal{N}}} \prod_{k=1}^{\mathcal{N}} d^{2dN} \Gamma_k = \omega^{\mathcal{N}}, \quad (2.15)$$

where  $h$  is a constant,  $d^{2dN} \Gamma_k = \prod_{j=1}^N d^d \mathbf{q}_{jk} d^d \mathbf{p}_{jk}$ , and  $\omega = \omega(E, V, N)$  is the density of states of a single system. Since the particles are confined to move within the walls of their own system, spatial integrations in (2.15) extend over the domains  $D_k$ , of volume  $V$ , satisfying  $\int_{D_k} d^d \mathbf{q}_{jk} = V$  for all  $j$  and  $k$ . Thus, in view of (2.15), as required we obtain

$$S_t = \mathcal{N} \ln \omega = \mathcal{N} S, \quad (2.16)$$

which highlights the fact that the information concerning nonadditivity is contained, in this case, in the microcanonical entropy  $S$  of a single system.

**Canonical ensemble:** Assume now that the system is put in contact with a heat bath and  $T$ ,  $V$ , and  $N$  are fixed. In this case, the energy of the system fluctuates. The appropriate characteristic function for the given control parameters is the Helmholtz free energy  $F = F(T, V, N)$ , satisfying

$$F = \bar{E} - TS. \quad (2.17)$$

This free energy is to be obtained as  $F = -T \ln Z$ , where  $Z = Z(T, V, N)$  is the canonical partition function of the system. From (2.6), (2.7), and (2.8), the thermodynamic relations in this case take the form

$$\mathcal{E} = F + PV - \mu N, \quad (2.18)$$

$$dF = -SdT - PdV + \mu dN, \quad (2.19)$$

$$d\mathcal{E} = -SdT + VdP - Nd\mu. \quad (2.20)$$

Moreover, in terms of the control parameters for this case, we can write  $\mathcal{E} = \mathcal{E}(T, V, N)$ . After identifying from (2.19) the pressure and the chemical potential, the replica energy can be computed as

$$\mathcal{E} = F - V \left( \frac{\partial F}{\partial V} \right)_{T, N} - N \left( \frac{\partial F}{\partial N} \right)_{T, V}. \quad (2.21)$$

The above discussion contains all the equations we need in the canonical ensemble. However, it is interesting to note that, alternatively, the same equations can be obtained if we write

$$dF_t = -S_t dT - PdV_t + \mu dN_t + \mathcal{E} d\mathcal{N} \quad (2.22)$$

as the equation giving the thermodynamics of the ensemble in the place of (2.1). Here  $F_t = -T \ln Z_t$  is the total Helmholtz free energy of the ensemble, where  $Z_t = Z_t(T, V_t, N_t, \mathcal{N})$  is the canonical partition function. Since the replicas are assumed to be independent, equivalent, and distinguishable, we can write

$$Z_t = \int \frac{e^{-\mathcal{H}_t/T}}{(h^{dN} N!)^{\mathcal{N}}} \prod_{k=1}^{\mathcal{N}} d^{2dN} \mathbf{\Gamma}_k = Z^{\mathcal{N}}, \quad (2.23)$$

and hence  $F_t = \mathcal{N}F = \mathcal{N}(\bar{E} - TS)$ . From (2.22), following a procedure analogous to that used to obtain (2.4) and the subsequent equations, one arrives at equations (2.18), (2.19), and (2.20). Although we will not do it here, a similar argument can be given also for the grand canonical and isobaric-isothermal ensembles discussed below.

**Grand canonical ensemble:** Let us consider now that the constraint in the number of particles is removed such that  $T$ ,  $V$ , and  $\mu$  are controlled. The energy and the number of particles of the system fluctuate, so that we take  $\bar{E}$  and  $\bar{N}$ , respectively, as their average values. In this case, the thermodynamics is given by the grand potential  $\Omega(T, V, \mu) = -T \ln \Xi(T, V, \mu)$  which satisfies

$$\Omega = \bar{E} - TS - \mu\bar{N}, \quad (2.24)$$

where  $\Xi$  is the grand canonical partition function. From (2.6), (2.7), and (2.8), we have

$$\mathcal{E} = \Omega + PV, \quad (2.25)$$

$$d\Omega = -SdT - PdV - \bar{N}d\mu, \quad (2.26)$$

$$d\mathcal{E} = -SdT + VdP - \bar{N}d\mu. \quad (2.27)$$

In addition, using (2.26) to evaluate the pressure in (2.25) yields

$$\mathcal{E} = \Omega - V \left( \frac{\partial \Omega}{\partial V} \right)_{T, \mu}. \quad (2.28)$$

**Isobaric-isothermal ensemble:** From a  $T, V, N$  system, one may allow fluctuations in the volume instead of the number of particles. In this case,  $T$ ,  $P$ , and  $N$  are to be taken as the appropriate control parameters, while in equilibrium configurations the energy and the volume will take average values  $\bar{E}$  and  $\bar{V}$ , respectively. The thermodynamics must be derived in the isobaric-isothermal ensemble from the Gibbs free energy  $G(T, P, N) = -T \ln \Delta(T, P, N)$ , where  $\Delta(T, P, N)$  is the isobaric-isothermal partition function. The Gibbs free energy satisfies

$$G = \bar{E} - TS + P\bar{V}. \quad (2.29)$$

From (2.6), (2.7), and (2.8), the corresponding thermodynamic equations are

$$\mathcal{E} = G - \mu N, \quad (2.30)$$

$$dG = -SdT + \bar{V}dP + \mu dN, \quad (2.31)$$

$$d\mathcal{E} = -SdT + \bar{V}dP - Nd\mu. \quad (2.32)$$

Moreover, using (2.31) to evaluate the chemical potential, in this ensemble we see that the replica energy is given by

$$\mathcal{E} = G - N \left( \frac{\partial G}{\partial N} \right)_{T, P}. \quad (2.33)$$

**Remark:** Comparing the thermodynamics for the different sets of control parameters that have been analyzed, we observe a common functional relation between the replica energy and the characteristic function under consideration. Equations (2.12), (2.21), (2.28), and (2.33) show that if the entropy, the Helmholtz energy, the grand potential or the Gibbs free energy, respectively, are linear homogeneous functions of their natural constraint variables, the replica energy necessarily vanishes. Conversely, if the replica energy is zero, the entropy, the Helmholtz free energy, the grand potential, and the Gibbs free energy are linear homogeneous functions of their natural constraint variables.

### 2.1.2 The unconstrained ensemble

A completely open system exchanges heat, work, and matter with its surroundings. That is, the energy, volume, and number of particles of the system fluctuate under completely open conditions. Thus, the control parameters that specify the thermodynamic state of the system are the temperature, pressure, and chemical potential. These control parameters are properties of a suitable reservoir that weakly interacts with the system, in the sense that, by means of some mechanism, it supplies heat, work, and matter, but it is not coupled by the interactions of the system. Furthermore, the unconstrained ensemble is the statistical ensemble that describes a completely open system (in the literature, this ensemble is also called “generalized” [124]). It was introduced by Guggenheim [125] (see also [126]), but did not receive much attention due to its lack of application in standard macroscopic systems. If the interactions in the system are short-ranged, the free energy associated to this ensemble is vanishingly small when the number of particles is large [125]. Physically, this is a consequence of the fact that temperature, pressure, and chemical potential cannot be treated as independent variables in this case, and thus they are not, taken together, suitable control parameters for macroscopic systems with short-range interactions. In case that the limit of a large number of particles is not assumed, however, the situation changes, as pointed out by Hill [65]. Small systems may have an extra degree of freedom which permits that equilibrium configurations in completely open conditions can be realized [65, 120, 127–129]. Nevertheless, when the size of the system is increased, the usual behavior of macroscopic systems is obtained [65, 121, 122], as long as the interactions remain short-ranged. Our aim here is to show that stable equilibrium configurations with a large number of particles may be realized in the unconstrained ensemble if the system possesses long-range interactions. Moreover, below we argue that the replica energy is the appropriate free energy defining stable configurations in this ensemble, and in Section 3.2 we consider a solvable model attaining equilibrium states under completely open conditions. To make our point clear, it is worth reviewing briefly the thermostatics

of completely open systems by establishing its connection to the unconstrained ensemble. The description of the unconstrained ensemble presented in this section is based on references [65] and [124], where the reader is referred to for an extended discussion (see also [125, 127, 130, 131]). In this section we restore conventional units for the Boltzmann constant  $k_B$ .

As we said before, the energy, volume, and number of particles of a completely open system are quantities that fluctuate due the interaction of the system with its surroundings. Let us consider the probability  $p_i(V, N)$  of the configuration of a system that is found in the state  $i$  with energy  $E_i$ , and possesses  $N$  particles in a volume  $V$ . Assume that this probability has the form

$$p_i(V, N) = \frac{\exp[-\alpha N - \beta E_i(V, N) - \gamma V]}{\Upsilon}, \quad (2.34)$$

where  $\alpha$ ,  $\beta$ , and  $\gamma$  are parameters that will be identified below and  $\Upsilon$  is the associated partition function given by

$$\Upsilon = \sum_{i, V, N} \exp[-\alpha N - \beta E_i(V, N) - \gamma V]. \quad (2.35)$$

Here discrete variables are used for simplicity. The ensemble average  $\bar{E}$  of the internal energy  $E$  is thus obtained as

$$\bar{E} = \sum_{i, V, N} E_i(V, N) p_i(V, N), \quad (2.36)$$

while the average number of particles  $\bar{N}$  and the average volume  $\bar{V}$  read

$$\bar{N} = \sum_{i, V, N} N p_i(V, N), \quad (2.37)$$

$$\bar{V} = \sum_{i, V, N} V p_i(V, N). \quad (2.38)$$

Now let us consider an infinitesimal change of the average internal energy in terms of changes in the probability,

$$d\bar{E} = \sum_{i, V, N} E_i(V, N) dp_i(V, N), \quad (2.39)$$

where the coefficients  $E_i(V, N)$  are assumed constant. Hence, using equation (2.34) to express  $E_i(V, N)$  and the condition  $\sum_{i, V, N} dp_i(V, N) = 0$ , equation (2.39) can be rewritten as

$$d\bar{E} = -\frac{1}{\beta} d \left[ \sum_{i, V, N} p_i(V, N) \ln p_i(V, N) \right] - \frac{\alpha}{\beta} d\bar{N} - \frac{\gamma}{\beta} d\bar{V}. \quad (2.40)$$

If the above equation is compared with the thermodynamic equation

$$d\bar{E} = TdS - Pd\bar{V} + \mu d\bar{N}, \quad (2.41)$$

one then recognizes  $k_{\text{B}}T = 1/\beta$ ,  $\mu = -\alpha/\beta$ ,  $P = \gamma/\beta$ , and the entropy

$$S = -k_{\text{B}} \sum_{i,V,N} p_i(V, N) \ln p_i(V, N). \quad (2.42)$$

Therefore, the probability (2.34) leads to the correct thermostatic description of completely open systems. Furthermore, substituting (2.34) in equation (2.42) with the previous identifications, one gets

$$\mathcal{E} = \bar{E} - TS + P\bar{V} - \mu\bar{N}, \quad (2.43)$$

where  $\mathcal{E}$  is introduced as

$$\mathcal{E}(T, P, \mu) \equiv -k_{\text{B}}T \ln \Upsilon(T, P, \mu). \quad (2.44)$$

Hence, the replica energy is the appropriate free energy from which the thermodynamics has to be derived in the unconstrained ensemble. By differentiation of equation (2.43) and using equation (2.41), one obtains

$$d\mathcal{E} = -SdT + \bar{V}dP - \bar{N}d\mu. \quad (2.45)$$

As a consequence of equation (2.45), the entropy, the average volume, and average number of particles are given as functions of  $T$ ,  $P$ , and  $\mu$  according to

$$-S = \left( \frac{\partial \mathcal{E}}{\partial T} \right)_{P, \mu}, \quad (2.46)$$

$$\bar{V} = \left( \frac{\partial \mathcal{E}}{\partial P} \right)_{T, \mu}, \quad (2.47)$$

$$-\bar{N} = \left( \frac{\partial \mathcal{E}}{\partial \mu} \right)_{T, P}. \quad (2.48)$$

Furthermore, the unconstrained partition function (2.35) can be written as

$$\Upsilon(T, P, \mu) = \sum_{V, N} Z(T, V, N) e^{\mu N / (k_{\text{B}}T)} e^{-PV / (k_{\text{B}}T)}, \quad (2.49)$$

where

$$Z(T, V, N) = \sum_i e^{-E_i(V, N) / (k_{\text{B}}T)} \quad (2.50)$$

is the canonical partition function. From equation (2.49), it is straightforward to connect  $\Upsilon$  with the partition function of another ensemble. For instance, one has

$$\Upsilon(T, P, \mu) = \sum_V \Xi(T, V, \mu) e^{-PV/(k_B T)}, \quad (2.51)$$

$\Xi(T, V, \mu)$  being the grand canonical partition function, or, analogously,

$$\Upsilon(T, P, \mu) = \sum_N \Delta(T, P, N) e^{\mu N/(k_B T)}, \quad (2.52)$$

where  $\Delta(T, P, N)$  is the isobaric-isothermal partition function.

For macroscopic systems with short-range interactions in the thermodynamic limit, the internal energy and the other thermodynamic potentials are linear homogeneous functions of the constraint variables and thus, from equation (2.43), one obtains  $\mathcal{E} = 0$ . We note that this case does not imply  $\Upsilon = 1$ , but that  $\mathcal{E}$  is negligible in the thermodynamic limit [124]. Thus, for this kind of systems, equation (2.45) reduces to the well-known Gibbs-Duhem equation.

## 2.2 Mean-field description

In this section we obtain a mean-field description for long-range interacting systems in various ensembles. We want to describe a system of  $N$  classical pointlike particles of equal mass  $m$  moving in a  $d$ -dimensional domain  $D$  of volume  $V \sim L^d$ ,  $L$  being a characteristic length defining the size of the system. The Hamiltonian of the system is

$$\mathcal{H}(\mathbf{p}, \mathbf{q}) = \sum_{i=1}^N \frac{|\mathbf{p}_i|^2}{2m} + \sum_{i>j}^N \phi(\mathbf{q}_i, \mathbf{q}_j), \quad (2.53)$$

where  $\mathbf{p}_i \in \mathbb{R}^d$  and  $\mathbf{q}_i \in \mathbb{R}^d$  are the momentum and position of particle  $i$ , respectively, with  $\mathbf{p} = (\mathbf{p}_1, \dots, \mathbf{p}_N)$  and  $\mathbf{q} = (\mathbf{q}_1, \dots, \mathbf{q}_N)$ . The interactions are introduced through the long-range pair interaction potential  $\phi(\mathbf{q}_i, \mathbf{q}_j)$  which depends on the positions of particles  $i$  and  $j$ . As an example, for interactions following a power law the potential takes the form

$$\phi(\mathbf{q}_i, \mathbf{q}_j) = \kappa |\mathbf{q}_i - \mathbf{q}_j|^{-a} \quad (2.54)$$

at large enough distances, where  $\kappa$  is a coupling constant and  $0 \leq a \leq d$ . In addition, we introduce the kinetic and potential energies  $E_0$  and  $W$ , respectively, which are given by

$$E_0 = \sum_{i=1}^N \frac{|\mathbf{p}_i|^2}{2m} \quad \text{and} \quad W = \sum_{i>j}^N \phi(\mathbf{q}_i, \mathbf{q}_j). \quad (2.55)$$

It is important to stress here that the interaction potential must be regular at short distances in order to avoid divergences and consistently define the statistical mechanics of the system [23]. Thus, if required, we consider implicitly a small distance cutoff regularizing the potential that is taken to be zero once the mean-field equilibrium configurations are obtained in the large  $N$  limit [23, 56, 57, 61]. In this way, short-range interactions are completely negligible in the mean-field description and quantities such as the total potential energy are assumed to exist and to be finite.

### 2.2.1 Microcanonical ensemble

In the microcanonical ensemble the state of the system is characterized by fixed values of the energy  $E$ , volume  $V$ , and number of particles  $N$ . The density of states accessible to the system is given by

$$\omega(E, V, N) = \frac{1}{h^{dN} N!} \int \delta(E - \mathcal{H}(\mathbf{p}, \mathbf{q})) d^{2dN} \mathbf{\Gamma}, \quad (2.56)$$

where  $d^{2dN} \mathbf{\Gamma} = \prod_{i=1}^N d^d \mathbf{p}_i d^d \mathbf{q}_i$ . Here spatial integrations extend over the  $d$ -dimensional domain  $D$ ,  $\int_D d^d \mathbf{q}_i = V$  for all  $i$ , and there are no restrictions on the domain of momenta; this will always be the case throughout the text unless another domain is specified. The microcanonical entropy is thus given by ( $k_B = 1$ )

$$S(E, V, N) = \ln \omega(E, V, N), \quad (2.57)$$

which as usual is defined up to an additive constant [132].

Using a Laplace representation for the Dirac  $\delta$  [11, 56], the density of states can be rewritten as

$$\omega(E, V, N) = \int_{\beta-i\infty}^{\beta+i\infty} \frac{d\beta_c}{2\pi i} e^{\beta_c E - \mathcal{F}(\beta_c, V, N)}, \quad (2.58)$$

where  $\beta = \text{Re}(\beta_c) > 0$  is the inverse temperature and

$$e^{-\mathcal{F}(\beta_c, V, N)} \equiv \int \frac{d^{2dN} \mathbf{\Gamma}}{N!} \frac{e^{-\beta_c \mathcal{H}(\mathbf{p}, \mathbf{q})}}{h^{dN}} = \int \frac{d^{dN} \mathbf{q}}{N!} \frac{e^{-\beta_c W(\mathbf{q})}}{\lambda_T^{dN}} \quad (2.59)$$

with  $d^{dN} \mathbf{q} = \prod_{i=1}^N d^d \mathbf{q}_i$  and

$$\lambda_T(\beta_c) = \sqrt{\frac{h^2 \beta_c}{2\pi m}}. \quad (2.60)$$

If the complex parameter  $\beta_c$  is evaluated at  $\beta_c = \beta = 1/T$ ,  $e^{-\mathcal{F}(\beta, V, N)} = Z(T, V, N)$  is the canonical partition function and  $\lambda_T$  is the thermal wavelength. Hence, (2.59) is the analytical continuation of the partition function to the complex plane [11].

Below we will see that, in fact,  $\beta_c$  must be taken to be real in order to satisfy the mean-field equations describing equilibrium configurations, and that then it is indeed the microcanonical inverse temperature given as a function of  $E$ ,  $V$ , and  $N$ .

In order to deal with (2.59), we generalize a method leading to the mean-field description of the system that was used by Thirring [18] to treat Newtonian gravity in  $d = 3$  (see also [57]). According to Thirring's method, the  $d$ -dimensional domain  $D$  of volume  $V$  is divided in  $M$  cells,  $1 \ll M \ll N$ , of volume  $v_a = V/M$ , so that  $\sum_{a=1}^M v_a = V$ . Each cell is located at  $\mathbf{x}_a = (x_a^1, x_a^2, \dots, x_a^d)$  and contains  $n_a \gg 1$  particles such that  $\sum_{a=1}^M n_a = N$ . This construction is self-consistent if the number of particles is large enough, so that the large  $N$  limit is implicitly assumed. It is also assumed that the size of each cell is small enough so that the potential can be considered constant through the cell, but, of course, it varies from cell to cell. Thus, it follows that the total potential energy can be approximated as

$$W \simeq \sum_{a>b}^M n_a n_b \phi(\mathbf{x}_a, \mathbf{x}_b). \quad (2.61)$$

Furthermore, we replace the integration on positions by a sum over occupation numbers according to [18]

$$\int \frac{d^{dN} \mathbf{q}}{N! \lambda_T^{dN}} \rightarrow \sum_{\{n_1, \dots, n_M\}} \delta_{N, \sum_{a=1}^M n_a} \prod_{a=1}^M \frac{1}{n_a!} \left( \frac{v_a}{\lambda_T^d} \right)^{n_a}, \quad (2.62)$$

where  $\{n_1, \dots, n_M\}$  means all possible values  $n_1, n_2, \dots, n_M$  of the occupation numbers and the Kronecker  $\delta$  restricts the total number of particles to  $N$ . Using this procedure, the right-hand side of (2.59) can be computed as

$$\int \frac{d^{dN} \mathbf{q}}{N!} \frac{e^{-\beta_c W(\mathbf{q})}}{\lambda_T^{dN}} \simeq \sum_{\{n_1, \dots, n_M\}} \delta_{N, \sum_{a=1}^M n_a} \prod_{a=1}^M \frac{1}{n_a!} \left( \frac{v_a}{\lambda_T^d} \right)^{n_a} e^{-\beta_c \sum_{a>b}^M n_a n_b \phi(\mathbf{x}_a, \mathbf{x}_b)}. \quad (2.63)$$

A continuum description can be obtained in the limit  $M \rightarrow \infty$  by introducing a number density whose value in each cell is given by  $n(\mathbf{x}_a) = n_a/v_a$ . Consequently, summations over the cells become spatial integrations over the domain  $D$ ,

$$\sum_{a=1}^M \rightarrow \int \frac{d^d \mathbf{x}}{v_a}, \quad (2.64)$$

and the summation over occupation number distributions becomes a functional integration in the number density, which will be symbolically denoted by

$$\sum_{\{n_1, \dots, n_M\}} \rightarrow \int \mathcal{D}n \quad (2.65)$$

and that can be understood as

$$\begin{aligned} \lim_{M \rightarrow \infty} \sum_{\{n_1, \dots, n_M\}} &= \lim_{M \rightarrow \infty} \left( \frac{V}{M} \right)^M \sum_{n_1=0}^{\infty} \frac{1}{v_1} \cdots \sum_{n_M=0}^{\infty} \frac{1}{v_M} \\ &= \lim_{M \rightarrow \infty} \left( \frac{V}{M} \right)^M \int_0^{\infty} \prod_{a=1}^M d \left( \frac{n_a}{v_a} \right) \equiv \int \mathcal{D}n(\mathbf{x}), \end{aligned} \quad (2.66)$$

where we have used that  $v_a = V/M$  for  $a = 1, \dots, M$ . Moreover, with Stirling's approximation, in the continuum limit we have

$$\prod_{a=1}^M \frac{1}{n_a!} \left( \frac{v_a}{\lambda_T^d} \right)^{n_a} \rightarrow \exp \left\{ - \int n(\mathbf{x}) \left[ \ln \left( n(\mathbf{x}) \lambda_T^d \right) - 1 \right] d^d \mathbf{x} \right\}, \quad (2.67)$$

whereas the Kronecker  $\delta$  restricting the number of particles can be represented in the form

$$\delta_{N, \sum_{a=1}^M n_a} = \int_{\alpha - i\pi}^{\alpha + i\pi} \frac{d\alpha_c}{2\pi i} e^{\alpha_c (N - \int n(\mathbf{x}) d^d \mathbf{x})} \quad (2.68)$$

with  $\alpha = \text{Re}(\alpha_c)$ .

Taking all the previous prescriptions into account, from equation (2.63), equation (2.59) can be written as

$$e^{-\mathcal{F}(\beta_c, V, N)} = \int_{\alpha - i\pi}^{\alpha + i\pi} \frac{d\alpha_c}{2\pi i} \int \mathcal{D}n e^{-\hat{\mathcal{F}}[n; \alpha_c, \beta_c, V, N]}, \quad (2.69)$$

where we have introduced the functional

$$\begin{aligned} \hat{\mathcal{F}}[n; \alpha_c, \beta_c, V, N] &= -\alpha_c \left( N - \int n(\mathbf{x}) d^d \mathbf{x} \right) + \int n(\mathbf{x}) \left[ \ln \left( n(\mathbf{x}) \lambda_T^d(\beta_c) \right) - 1 \right] d^d \mathbf{x} \\ &\quad + \frac{\beta_c}{2} \int n(\mathbf{x}) n(\mathbf{x}') \phi(\mathbf{x}, \mathbf{x}') d^d \mathbf{x} d^d \mathbf{x}', \end{aligned} \quad (2.70)$$

whose dependence on the volume is implicit in the integration domain. Accordingly, replacing (2.69) in (2.58) and using (2.57), the microcanonical entropy is given by

$$e^{S(E, V, N)} = \int_{\alpha - i\pi}^{\alpha + i\pi} \frac{d\alpha_c}{2\pi i} \int_{\beta - i\infty}^{\beta + i\infty} \frac{d\beta_c}{2\pi i} \int \mathcal{D}n e^{\hat{S}[n; \alpha_c, \beta_c, E, V, N]}, \quad (2.71)$$

where

$$\hat{S}[n; \alpha_c, \beta_c, E, V, N] = \beta_c E - \hat{\mathcal{F}}[n; \alpha_c, \beta_c, V, N]. \quad (2.72)$$

To proceed further, (2.71) will be evaluated using the saddle-point approximation in the large  $N$  limit. Since  $e^S$  is real and positive and we have started from the

analytical continuation of the canonical partition function, it can be argued that this integral will be dominated by a value of the integrand evaluated at the real parts of  $\alpha_c$  and  $\beta_c$  [11]. That is, the mean-field entropy is given by

$$S(E, V, N) = \sup_{n; \alpha, \beta} \hat{S}[n; \alpha, \beta, E, V, N] \quad (2.73)$$

with  $\alpha = \text{Re}(\alpha_c)$  and  $\beta = \text{Re}(\beta_c)$ . The solution to the variational problem (2.73) defines the thermodynamics of the system in the microcanonical ensemble. In order to find this solution, a full description of the system must be given; we have to specify the shape of the spatial domain and the function  $\phi(\mathbf{x}, \mathbf{x}')$  characterizing the interactions. However, if equilibrium configurations exist, the entropy of the system in these configurations corresponds to an extremum of  $\hat{S}$ . Thus, we can continue without further specifications and look for such an extremum. To decide whether this extremal solution actually maximizes  $\hat{S}$  according to (2.73), an additional second-order variational analysis has to be performed for each particular problem (a method for this analysis is discussed in [56]). This argument will also be followed for the other ensembles considered later on, adapted to the corresponding variational problem.

We now find the preceding extremum in the microcanonical ensemble. Setting to zero the derivative of  $\hat{S}$  with respect to  $\alpha$  and  $\beta$  yields

$$N = \int n(\mathbf{x}) d^d \mathbf{x}, \quad (2.74)$$

$$E = \frac{d}{2\beta} \int n(\mathbf{x}) d^d \mathbf{x} + W, \quad (2.75)$$

with

$$W = \frac{1}{2} \int n(\mathbf{x}) n(\mathbf{x}') \phi(\mathbf{x}, \mathbf{x}') d^d \mathbf{x} d^d \mathbf{x}' \equiv \frac{1}{2} \int n(\mathbf{x}) \Phi(\mathbf{x}) d^d \mathbf{x}, \quad (2.76)$$

where we have introduced the potential

$$\Phi(\mathbf{x}) \equiv \int n(\mathbf{x}') \phi(\mathbf{x}, \mathbf{x}') d^d \mathbf{x}'. \quad (2.77)$$

Moreover,

$$\delta \hat{S} = \int \left[ -\alpha - \ln \left( n(\mathbf{x}) \lambda_T^d \right) - \beta \Phi(\mathbf{x}) \right] \delta n(\mathbf{x}) d^d \mathbf{x}, \quad (2.78)$$

so that from the condition  $\delta \hat{S} / \delta n = 0$  it follows that

$$n(\mathbf{x}) = \lambda_T^{-d} \exp \left[ -\beta (\Phi(\mathbf{x}) - \mu) \right], \quad (2.79)$$

where  $\mu = -\alpha/\beta$  is the chemical potential, as will be shown below. We emphasize that in accordance with (2.73), here  $\beta = \beta(E, V, N)$  and  $\mu = \mu(E, V, N)$  such that  $\lambda_T(\beta)$  and the number density are functions of  $E$ ,  $V$ , and  $N$  as well. According to

the maximization problem, substituting (2.74) and (2.75) in (2.73) using (2.72) and (2.70), the mean-field entropy takes the form

$$S = \int n(\mathbf{x}) s(\mathbf{x}) d^d \mathbf{x}, \quad (2.80)$$

where we have introduced the local entropy per particle given by

$$s(\mathbf{x}) = -\ln \left( n(\mathbf{x}) \lambda_T^d \right) + \frac{2+d}{2}. \quad (2.81)$$

Furthermore, in the microcanonical ensemble we have

$$\frac{1}{T} = \left( \frac{\partial S}{\partial E} \right)_{V,N} = \frac{\partial \hat{S}}{\partial E}, \quad (2.82)$$

$$\frac{P}{T} = \left( \frac{\partial S}{\partial V} \right)_{E,N} = \frac{\partial \hat{S}}{\partial V}, \quad (2.83)$$

$$-\frac{\mu}{T} = \left( \frac{\partial S}{\partial N} \right)_{E,V} = \frac{\partial \hat{S}}{\partial N}, \quad (2.84)$$

where the expressions on the right-hand side must be evaluated at the solution of the variational problem (2.73) *after* computing the corresponding derivative of  $\hat{S}$ . That  $\beta$  and  $\mu$  are in fact the microcanonical inverse temperature and chemical potential can be verified from equations (2.82) and (2.84), since they straightforwardly lead to  $1/T = \beta(E, V, T)$  and  $-\mu/T = \alpha(E, V, T)$ . In order to obtain an useful expression for the pressure, the dependence of  $\hat{S}$  on the volume of the spatial domain  $D$  and the function  $\phi(\mathbf{x}, \mathbf{x}')$  characterizing the interactions have to be made explicit; we will come back to this point later on by considering interaction potentials decaying as a power law. We emphasize that the expression (2.80) for the entropy is an extremum of  $\hat{S}$ , and that a second-order variational analysis has to be performed to establish for which range of control parameters  $\hat{S}$  is really maximized. This procedure then depends on the specific interactions in the system.

### 2.2.2 Canonical ensemble

Here we consider that the control parameters specifying equilibrium configurations are the temperature  $T$ , the volume  $V$  and the number of particles  $N$ . The canonical partition function reads

$$Z(T, V, N) = \int \frac{d^{2dN} \mathbf{\Gamma}}{N!} \frac{e^{-\mathcal{H}(\mathbf{p}, \mathbf{q})/T}}{h^{dN}}. \quad (2.85)$$

According to the discussion in the preceding section, this partition function can also be written as

$$Z(T, V, N) = \int_{\alpha-i\pi}^{\alpha+i\pi} \frac{d\alpha_c}{2\pi i} \int \mathcal{D}n e^{-\hat{\mathcal{F}}[n; \alpha_c, \beta, V, N]}, \quad (2.86)$$

where  $\beta = 1/T$  and  $\hat{\mathcal{F}}[n; \alpha_c, \beta, V, N]$  is given by (2.70) with  $\beta_c = \beta$ . Instead of considering directly the Helmholtz free energy  $F(T, V, N) = -T \ln Z(T, V, N)$ , for convenience we introduce the rescaled free energy

$$\mathcal{F}(\beta, V, N) \equiv \beta F(1/\beta, V, N), \quad (2.87)$$

which can be identified from (2.86) and is given by the relation

$$e^{-\mathcal{F}(\beta, V, N)} = \int_{\alpha-i\pi}^{\alpha+i\pi} \frac{d\alpha_c}{2\pi i} \int \mathcal{D}n e^{-\hat{\mathcal{F}}[n; \alpha_c, \beta, V, N]}. \quad (2.88)$$

Using the saddle-point approximation in the large  $N$  limit, the rescaled free energy can be computed by solving the variational problem

$$\mathcal{F}(\beta, V, N) = \inf_{n; \alpha} \hat{\mathcal{F}}[n; \alpha, \beta, V, N], \quad (2.89)$$

where, as before, we only consider solutions for which  $\hat{\mathcal{F}}$  is evaluated at real  $\alpha = \text{Re}(\alpha_c)$ . If there are states of thermodynamic equilibrium in the canonical ensemble, the Helmholtz free energy of these states corresponds to an extremum of  $\hat{\mathcal{F}}$ . This extremum is what we will find below. As in the microcanonical case, a second-order variational analysis has to be performed to decide whether this extremal solution minimizes  $\hat{\mathcal{F}}$  according to (2.89).

From the condition  $\partial \hat{\mathcal{F}} / \partial \alpha = 0$ , we get

$$N = \int n(\mathbf{x}) d^d \mathbf{x}, \quad (2.90)$$

and since

$$\delta \hat{\mathcal{F}} = \int \left[ \ln \left( n(\mathbf{x}) \lambda_T^d \right) + \alpha + \beta \Phi(\mathbf{x}) \right] \delta n(\mathbf{x}) d^d \mathbf{x}, \quad (2.91)$$

the number density that extremizes  $\hat{\mathcal{F}}$  takes the form

$$n(\mathbf{x}) = \lambda_T^{-d} \exp[-\beta(\Phi(\mathbf{x}) - \mu)], \quad (2.92)$$

where  $\mu = -\alpha/\beta$  is the chemical potential (see below). Since  $\alpha$  is assumed to satisfy the variational problem (2.89), we remark that  $\mu = \mu(T, V, N)$  and hence the number density is a function of  $T$ ,  $V$ , and  $N$  as well.

The potential energy  $W$  and the potential  $\Phi(\mathbf{x})$  here have the same functional dependence on the number density as in the microcanonical ensemble, equations

(2.76) and (2.77). In spite of this fact, in the canonical ensemble they are, in general, different from the corresponding quantities in the microcanonical ensemble because of the different dependence of the number density on the control parameters, i.e.,  $W$  and  $\Phi(\mathbf{x})$  are here functions of  $T$ ,  $V$ , and  $N$ . An analogous consideration applies for the other ensembles studied below.

In the canonical ensemble we have

$$\bar{E} = \left( \frac{\partial \mathcal{F}}{\partial \beta} \right)_{V,N} = \frac{\partial \hat{\mathcal{F}}}{\partial \beta}, \quad (2.93)$$

$$-\frac{P}{T} = \left( \frac{\partial \mathcal{F}}{\partial V} \right)_{\beta,N} = \frac{\partial \hat{\mathcal{F}}}{\partial V}, \quad (2.94)$$

$$\frac{\mu}{T} = \left( \frac{\partial \mathcal{F}}{\partial N} \right)_{\beta,V} = \frac{\partial \hat{\mathcal{F}}}{\partial N}, \quad (2.95)$$

where the right-hand side must be evaluated, *after* computing the corresponding derivative of  $\hat{\mathcal{F}}$ , at the solution of the variational problem (2.89). Hence,

$$\bar{E}(T, V, N) = \frac{d}{2} T \int n(\mathbf{x}) d^d \mathbf{x} + W, \quad (2.96)$$

and from (2.95), we identify  $\mu$  as introduced in (2.92). Finally, using (2.90) in (2.89) with  $n(\mathbf{x})$  given by (2.92), the mean-field Helmholtz free energy in the canonical ensemble takes the form

$$F = \int n(\mathbf{x}) f(\mathbf{x}) d^d \mathbf{x}, \quad (2.97)$$

where

$$f(\mathbf{x}) = T \left[ \ln \left( n(\mathbf{x}) \lambda_T^d \right) - 1 \right] + \frac{1}{2} \Phi(\mathbf{x}) \quad (2.98)$$

is the local Helmholtz free energy per particle.

### 2.2.3 Grand canonical ensemble

In this case the control parameters are  $T$ ,  $V$ , and  $\mu$ , and the thermodynamics of the system is obtained from the grand potential

$$\Omega(T, V, \mu) = -T \ln \Xi(T, V, \mu). \quad (2.99)$$

The grand canonical partition function reads

$$\Xi(T, V, \mu) = \sum_{N=0}^{\infty} e^{\mu N/T} Z(T, V, N) = \sum_{N=0}^{\infty} \int_{\alpha-i\pi}^{\alpha+i\pi} \frac{d\alpha_c}{2\pi i} \int \mathcal{D}n e^{-\alpha N - \hat{\mathcal{F}}[n; \alpha_c, \beta, V, N]}, \quad (2.100)$$

where  $\alpha = -\mu/T$  and, as in the canonical case,  $\hat{\mathcal{F}}[n; \alpha_c, \beta, V, N]$  is given by (2.70) with  $\beta_c = \beta = 1/T$ . Since

$$\int_{\alpha-i\pi}^{\alpha+i\pi} \frac{d\alpha_c}{2\pi i} e^{\alpha_c(N - \int n(\mathbf{x})d^d\mathbf{x})} = \delta_{N, \int n(\mathbf{x})d^d\mathbf{x}}, \quad (2.101)$$

only the term with  $N = \int n(\mathbf{x})d^d\mathbf{x}$  survives in the summation over  $N$  in equation (2.100). Introducing the rescaled grand potential

$$\mathcal{L}(\alpha, \beta, V) \equiv \beta\Omega(1/\beta, V, -\alpha/\beta), \quad (2.102)$$

we get

$$e^{-\mathcal{L}(\alpha, \beta, V)} = \int \mathcal{D}n e^{-\hat{\mathcal{L}}[n; \alpha, \beta, V]}, \quad (2.103)$$

where

$$\begin{aligned} \hat{\mathcal{L}}[n; \alpha, \beta, V] &= \int n(\mathbf{x}) \left[ \ln \left( n(\mathbf{x}) \lambda_T^d(\beta) \right) - 1 + \alpha \right] d^d\mathbf{x} \\ &\quad + \frac{\beta}{2} \int n(\mathbf{x}) n(\mathbf{x}') \phi(\mathbf{x}, \mathbf{x}') d^d\mathbf{x} d^d\mathbf{x}'. \end{aligned} \quad (2.104)$$

We recall that the dependence of  $\hat{\mathcal{L}}$  on  $V$  is implicit through the domain of spatial integrations.

As has been done in the previous cases, we shall evaluate the integral (2.103) using the saddle-point approximation. At variance with the microcanonical and canonical ensembles, in this case we cannot invoke the large  $N$  limit to justify the saddle-point method, since here  $N$  is not a control parameter that can be chosen at convenience. Moreover, although the volume is a control parameter in this ensemble, we avoid the use of the large  $V$  limit directly because the grand potential is not, in general, a linear homogeneous function of the volume, namely,  $\Omega$  is not  $-PV$  if the replica energy is different from zero. Thus, we shall assume that the scaling laws of the system are such that the control parameters can be taken as large, in a proper thermodynamic limit, assuring that the variational problem associated with the saddle-point approximation holds. In this case

$$\mathcal{L}(\alpha, \beta, V) = \inf_n \hat{\mathcal{L}}[n; \alpha, \beta, V]. \quad (2.105)$$

These scaling laws are to be determined according to the system at hand; however, they must be consistent with a large average number of particles in order for the mean-field description to be suitable. We will refer to this assumption as the “large  $\bar{N}$  limit”.

Assuming (2.105), we look for an extremum of  $\hat{\mathcal{L}}$  performing variations with respect to  $n$ . We have

$$\delta\hat{\mathcal{L}} = \int \left[ \ln \left( n(\mathbf{x})\lambda_T^d \right) + \alpha + \beta\Phi(\mathbf{x}) \right] \delta n(\mathbf{x}) d^d\mathbf{x}, \quad (2.106)$$

so that the condition  $\delta\hat{\mathcal{L}}/\delta n = 0$  gives the number density as

$$n(\mathbf{x}) = \lambda_T^{-d} \exp[-\beta(\Phi(\mathbf{x}) - \mu)], \quad (2.107)$$

which now is a function of  $\alpha$ ,  $\beta$ , and  $V$ , or, equivalently, of  $T$ ,  $V$ , and  $\mu$ . Consequently, the potential  $\Phi(\mathbf{x})$  and the potential energy  $W$  are functions of  $T$ ,  $V$ , and  $\mu$  as well. Thus, from (2.105) we obtain the mean-field grand potential as

$$\Omega = \int n(\mathbf{x})\varpi(\mathbf{x}) d^d\mathbf{x}, \quad (2.108)$$

where the local grand potential per particle reads

$$\varpi(\mathbf{x}) = T \left[ \ln \left( n(\mathbf{x})\lambda_T^d \right) - 1 \right] - \mu + \frac{1}{2}\Phi(\mathbf{x}). \quad (2.109)$$

In addition, the following relations are obtained from the rescaled grand potential:

$$\bar{N} = \left( \frac{\partial \mathcal{L}}{\partial \alpha} \right)_{\beta, V} = \frac{\partial \hat{\mathcal{L}}}{\partial \alpha}, \quad (2.110)$$

$$\bar{E} = \left( \frac{\partial \mathcal{L}}{\partial \beta} \right)_{\alpha, V} = \frac{\partial \hat{\mathcal{L}}}{\partial \beta}, \quad (2.111)$$

$$-\frac{P}{T} = \left( \frac{\partial \mathcal{L}}{\partial V} \right)_{\alpha, \beta} = \frac{\partial \hat{\mathcal{L}}}{\partial V}, \quad (2.112)$$

where the right-hand side of the above equations must be evaluated using the solution of the variational problem (2.105) *after* performing the derivatives. Accordingly, if equilibrium configuration exist, the mean number of particles in the grand canonical ensemble is given by

$$\bar{N}(T, V, \mu) = \int n(\mathbf{x}) d^d\mathbf{x}, \quad (2.113)$$

while the internal energy reads

$$\bar{E}(T, V, \mu) = \frac{d}{2}T \int n(\mathbf{x}) d^d\mathbf{x} + W. \quad (2.114)$$

### 2.2.4 Isobaric-isothermal ensemble

In this ensemble the corresponding control parameters are  $T$ ,  $P$ , and  $N$ . The thermodynamics of the system is obtained from the Gibbs free energy

$$G(T, P, N) = -T \ln \Delta(T, P, N), \quad (2.115)$$

where the isobaric-isothermal partition function reads

$$\Delta(T, P, N) = \int dV e^{-PV/T} Z(T, V, N) = \int dV \int_{\alpha-i\pi}^{\alpha+i\pi} \frac{d\alpha_c}{2\pi i} \int \mathcal{D}n e^{-\gamma V - \hat{\mathcal{F}}[n; \alpha_c, \beta, V, N]}, \quad (2.116)$$

with  $\gamma = P/T$ . We now define the rescaled Gibbs free energy as

$$\mathcal{G}(N, \beta, \gamma) \equiv \beta G(1/\beta, \gamma/\beta, N), \quad (2.117)$$

which in turn is given by the relation

$$e^{-\mathcal{G}(N, \beta, \gamma)} = \int dV \int_{\alpha-i\pi}^{\alpha+i\pi} \frac{d\alpha_c}{2\pi i} \int \mathcal{D}n e^{-\hat{\mathcal{G}}[n; \alpha_c, V, N, \beta, \gamma]}, \quad (2.118)$$

where

$$\begin{aligned} \hat{\mathcal{G}}[n; \alpha_c, V, N, \beta, \gamma] &= -\alpha_c \left( N - \int n(\mathbf{x}) d^d \mathbf{x} \right) + \int n(\mathbf{x}) \left[ \ln \left( n(\mathbf{x}) \lambda_T^d(\beta) \right) - 1 \right] d^d \mathbf{x} \\ &\quad + \frac{\beta}{2} \int n(\mathbf{x}) n(\mathbf{x}') \phi(\mathbf{x}, \mathbf{x}') d^d \mathbf{x} d^d \mathbf{x}' + \gamma V. \end{aligned} \quad (2.119)$$

As before, we note that the dependence of  $\hat{\mathcal{G}}$  on  $V$  is also implicit through the domain of spatial integrations. Thus, in the large  $N$  limit we have

$$\mathcal{G}(N, \beta, \gamma) = \inf_{n; \alpha, V} \hat{\mathcal{G}}[n; \alpha, V, N, \beta, \gamma] \quad (2.120)$$

with  $\alpha = \text{Re}(\alpha_c)$ . From the condition  $\partial \hat{\mathcal{G}} / \partial \alpha = 0$ , we get

$$N = \int n(\mathbf{x}) d^d \mathbf{x}, \quad (2.121)$$

and since

$$\delta \hat{\mathcal{G}} = \int \left[ \ln \left( n(\mathbf{x}) \lambda_T^d \right) + \alpha + \beta \Phi(\mathbf{x}) \right] \delta n(\mathbf{x}) d^d \mathbf{x}, \quad (2.122)$$

the number density that extremizes the rescaled Gibbs free energy takes the form

$$n(\mathbf{x}) = \lambda_T^{-d} \exp \left[ -\beta (\Phi(\mathbf{x}) - \mu) \right], \quad (2.123)$$

where  $\mu = -\alpha/\beta$  is the chemical potential. Since  $\alpha$  is now assumed to satisfy the variational problem (2.120), we remark that  $\mu = \mu(T, P, N)$  and hence the number density is also a function of  $T$ ,  $P$ , and  $N$ . In addition, the average volume  $\bar{V}$  is given implicitly by (2.120), satisfying

$$\left. \frac{\partial}{\partial \bar{V}} \hat{\mathcal{G}} [n; \alpha, V, N, \beta, \gamma] \right|_{V=\bar{V}} = 0 \quad (2.124)$$

if the derivative exists. Notice that since the volume fluctuates, spatial integrations in the solution to the mean-field equations extend over a domain  $D$  of volume  $\bar{V}$  determined by the control parameters,  $\bar{V} = \bar{V}(T, P, N)$ . Accordingly, the potential  $\Phi(\mathbf{x})$  and the potential energy  $W$  are both functions of  $T$ ,  $P$ , and  $N$ .

From the rescaled Gibbs free energy obtained as an extremal solution of (2.120), the mean-field Gibbs free energy is given by

$$G = \int n(\mathbf{x})g(\mathbf{x}) \, d^d \mathbf{x}, \quad (2.125)$$

where

$$g(\mathbf{x}) = T \left[ \ln \left( n(\mathbf{x}) \lambda_T^d \right) - 1 \right] + P v(\mathbf{x}) + \frac{1}{2} \Phi(\mathbf{x}) \quad (2.126)$$

is the local Gibbs free energy per particle. Here  $v(\mathbf{x}) = 1/n(\mathbf{x})$  is the local volume per particle, or specific volume, such that

$$\bar{V}(T, P, N) = \int n(\mathbf{x})v(\mathbf{x}) \, d^d \mathbf{x}. \quad (2.127)$$

In addition, in view of the relation  $\mathcal{G} = -\ln \Delta$ , in the isobaric-isothermal ensemble we have

$$\frac{\mu}{T} = \left( \frac{\partial \mathcal{G}}{\partial N} \right)_{\beta, \gamma} = \frac{\partial \hat{\mathcal{G}}}{\partial N}, \quad (2.128)$$

$$\bar{E} = \left( \frac{\partial \mathcal{G}}{\partial \beta} \right)_{N, \gamma} = \frac{\partial \hat{\mathcal{G}}}{\partial \beta}, \quad (2.129)$$

$$\bar{V} = \left( \frac{\partial \mathcal{G}}{\partial \gamma} \right)_{N, \beta} = \frac{\partial \hat{\mathcal{G}}}{\partial \gamma}, \quad (2.130)$$

where, as usual, the right-hand side of these equations must be evaluated at the solution of the variational problem (2.120). The average energy in equilibrium configurations is thus given by

$$\bar{E}(T, P, N) = \frac{d}{2} T \int n(\mathbf{x}) \, d^d \mathbf{x} + W. \quad (2.131)$$

### 2.2.5 Unconstrained ensemble

In the previous ensembles at least one of the constraint variables is a control parameter. Here we consider that the energy, volume, and number of particles fluctuate, and their average values in equilibrium configurations are  $\bar{E}$ ,  $\bar{V}$ , and  $\bar{N}$ , respectively, if such configurations exist. The control parameters in this ensemble are thus  $T$ ,  $P$ , and  $\mu$ . In a completely equivalent manner, we will also consider  $\alpha = -\mu/T$ ,  $\beta = 1/T$ , and  $\gamma = P/T$  as the set of control parameters in this ensemble.

According to the discussion in Section 2.1.2, the unconstrained partition function is given by equation (2.51) in terms of the grand canonical partition function. Hence, taking the volume as a continuum variable we can write

$$\Upsilon(T, P, \mu) = \int dV \Xi(T, V, \mu) e^{-PV/T} = \int dV \int \mathcal{D}n e^{-\hat{\mathcal{L}}[n; \alpha, \beta, V] - \gamma V}. \quad (2.132)$$

Furthermore, we define the rescaled replica energy as

$$\mathcal{R}(\alpha, \beta, \gamma) \equiv \beta \mathcal{E}(1/\beta, \gamma/\beta, -\alpha/\beta). \quad (2.133)$$

Since the replica energy in the unconstrained ensemble is given by

$$\mathcal{E}(T, P, \mu) = -T \ln \Upsilon(T, P, \mu), \quad (2.134)$$

it follows that

$$e^{-\mathcal{R}(\alpha, \beta, \gamma)} = \int dV \int \mathcal{D}n e^{-\hat{\mathcal{R}}[n; V, \alpha, \beta, \gamma]}, \quad (2.135)$$

where we have introduced

$$\begin{aligned} \hat{\mathcal{R}}[n; V, \alpha, \beta, \gamma] = & \int n(\mathbf{x}) \left[ \ln \left( n(\mathbf{x}) \lambda_T^d(\beta) \right) - 1 + \alpha \right] d^d \mathbf{x} \\ & + \frac{\beta}{2} \int n(\mathbf{x}) n(\mathbf{x}') \phi(\mathbf{x}, \mathbf{x}') d^d \mathbf{x} d^d \mathbf{x}' + \gamma V \end{aligned} \quad (2.136)$$

by making use of equations (2.132) and (2.104). We recall that the dependence on  $V$  in the above expression is also implicit in the domain of spatial integrations.

Assuming the large  $\bar{N}$  limit and using the saddle-point approximation, the rescaled replica energy in this ensemble can be computed by solving the variational problem

$$\mathcal{R}(\alpha, \beta, \gamma) = \inf_{n; V} \hat{\mathcal{R}}[n; V, \alpha, \beta, \gamma]. \quad (2.137)$$

We note that the same variational problem would be obtained if instead of permitting fluctuations of the volume in the grand canonical ensemble, one allows fluctuations of the number of particles in the isobaric-isothermal ensemble. This can be seen

by writing  $\Upsilon$  in terms of  $\Delta$  with equation (2.52), and then expressing the isobaric-isothermal partition function with equation (2.118).

Following the same line of reasoning as in the previous ensembles, we look for an extremum of  $\hat{\mathcal{R}}$ . Variations with respect to the number density yield

$$\delta\hat{\mathcal{R}} = \int \left[ \ln \left( n(\mathbf{x}) \lambda_T^d \right) + \alpha + \beta\Phi(\mathbf{x}) \right] \delta n(\mathbf{x}) \, d^d \mathbf{x}, \quad (2.138)$$

and we get

$$n(\mathbf{x}) = \lambda_T^{-d} \exp[-\beta\Phi(\mathbf{x}) - \alpha], \quad (2.139)$$

also in the unconstrained ensemble, as expected. Moreover, the volume  $\bar{V}$  fulfills the extremal condition (2.137), satisfying

$$\left. \frac{\partial}{\partial V} \hat{\mathcal{R}}[n; V, \alpha, \beta, \gamma] \right|_{V=\bar{V}} = 0 \quad (2.140)$$

if the derivative exists, evaluated with the number density given by (2.139). Clearly, the number density and  $\bar{V}$  are functions of  $\alpha$ ,  $\beta$ , and  $\gamma$  (or  $T$ ,  $P$ , and  $\mu$ ). Since the volume fluctuates, as in the isobaric-isothermal ensemble, spatial integrations in the solution to the mean-field equations extend over a domain  $D$  of volume  $\bar{V}$  determined by the control parameters. In addition, using (2.137) and (2.136), from the expression for the function  $\mathcal{R}$  we can write the mean-field replica energy as

$$\mathcal{E} = \int n(\mathbf{x}) \varrho(\mathbf{x}) \, d^d \mathbf{x} \quad (2.141)$$

with the local replica energy per particle given by

$$\varrho(\mathbf{x}) = T \left[ \ln \left( n(\mathbf{x}) \lambda_T^d \right) - 1 \right] + Pv(\mathbf{x}) - \mu + \frac{1}{2}\Phi(\mathbf{x}). \quad (2.142)$$

As before,  $v(\mathbf{x}) = 1/n(\mathbf{x})$  is the local volume per particle such that

$$\bar{V}(T, P, \mu) = \int n(\mathbf{x}) v(\mathbf{x}) \, d^d \mathbf{x}. \quad (2.143)$$

In addition, using (2.139), the local replica energy per particle can be rewritten as

$$\varrho(\mathbf{x}) = Pv(\mathbf{x}) - T - \frac{1}{2}\Phi(\mathbf{x}). \quad (2.144)$$

Hence, multiplying both sides of (2.144) by the number density and integrating over the spatial domain leads to

$$\mathcal{E} = P\bar{V} - \bar{N}T - W \quad (2.145)$$

with the potential energy

$$W(T, P, \mu) = \frac{1}{2} \int n(\mathbf{x}) \Phi(\mathbf{x}) d^d \mathbf{x}. \quad (2.146)$$

After solving the mean-field equations in this ensemble, that is, the variational problem (2.137), we are able to compute the average value of the energy, volume, and number of particles in equilibrium configurations. Considering that the rescaled replica energy can be written as  $\mathcal{R} = -\ln \Upsilon$  and taking into account the form of the probability (2.34) for equilibrium states in the unconstrained ensemble, these average quantities are given by

$$\bar{N} = \left( \frac{\partial \mathcal{R}}{\partial \alpha} \right)_{\beta, \gamma} = \frac{\partial \hat{\mathcal{R}}}{\partial \alpha}, \quad (2.147)$$

$$\bar{E} = \left( \frac{\partial \mathcal{R}}{\partial \beta} \right)_{\alpha, \gamma} = \frac{\partial \hat{\mathcal{R}}}{\partial \beta}, \quad (2.148)$$

$$\bar{V} = \left( \frac{\partial \mathcal{R}}{\partial \gamma} \right)_{\alpha, \beta} = \frac{\partial \hat{\mathcal{R}}}{\partial \gamma}, \quad (2.149)$$

where, as before, the expressions on the right-hand side must be evaluated at the solution of the variational problem (2.137) *after* computing the corresponding derivative of  $\hat{\mathcal{R}}$ . The first two of these relations give

$$\bar{N}(T, P, \mu) = \int n(\mathbf{x}) d^d \mathbf{x}, \quad (2.150)$$

$$\bar{E}(T, P, \mu) = \frac{d}{2} \bar{N} T + W, \quad (2.151)$$

while the expression for  $\bar{V}$  cannot be given explicitly unless the dependence on the volume of the spatial domain is made explicit; the average volume is given implicitly through equation (2.140).

Since the equation giving the infinitesimal changes of the replica energy is

$$d\mathcal{E} = -SdT + \bar{V}dP - \bar{N}d\mu, \quad (2.152)$$

the entropy, volume, and number of particles can be obtained as a partial derivatives of  $\mathcal{E}$  with respect to the corresponding control parameter, see equations (2.46), (2.47), and (2.48). In order to compute these derivatives in the mean-field description, it is convenient to define  $\hat{\mathcal{E}} \equiv T\hat{\mathcal{R}}$ , which can be written as

$$\begin{aligned} \hat{\mathcal{E}}[n; V, T, P, \mu] &= T \int n(\mathbf{x}) \left[ \ln \left( n(\mathbf{x}) \lambda_T^d(T) \right) - 1 - \frac{\mu}{T} \right] d^d \mathbf{x} \\ &+ \frac{1}{2} \int n(\mathbf{x}) n(\mathbf{x}') \phi(\mathbf{x}, \mathbf{x}') d^d \mathbf{x} d^d \mathbf{x}' + PV. \end{aligned} \quad (2.153)$$

According to this, the entropy is given by

$$S = - \left( \frac{\partial \mathcal{E}}{\partial T} \right)_{P, \mu} = - \frac{\partial \hat{\mathcal{E}}}{\partial T} = - \int n(\mathbf{x}) \left[ \ln \left( n(\mathbf{x}) \lambda_T^d \right) - \frac{2+d}{2} \right] d^d \mathbf{x}, \quad (2.154)$$

where the right-hand side must be evaluated at  $n(\mathbf{x})$  and  $\bar{V}$  satisfying (2.137). The average number of particles given by (2.48) obviously coincides with (2.150), whereas the average volume, as before, cannot be given explicitly through equation (2.47) in the mean-field description unless the dependence on the volume of the spatial domain is made explicit. Finally, we note that in the unconstrained ensemble, the energy can also be obtained from the relation

$$\mathcal{E} = \bar{E} - TS + P\bar{V} - \mu\bar{N}, \quad (2.155)$$

which can be combined with (2.145) giving  $\bar{E} = TS + \mu\bar{N} - \bar{N}T - W$ . From the latter equation and after manipulating the expression for the entropy (2.154), one readily gets (2.151).

We emphasize that the replica energy has been found here as an extremum of  $\hat{\mathcal{R}}$  according to the variational problem (2.137), since equilibrium configurations correspond to an extremal solution of this problem if they exist. As noted previously, in order to decide whether this extremal solution actually minimizes  $\hat{R}$  according to (2.137), a second-order variational analysis has to be performed for the particular system under consideration. This will establish the range of control parameters defining the states of equilibrium in the unconstrained ensemble.

## 2.3 Global and local relations

Here we consider some useful relations between thermodynamic quantities both at local and global levels. In particular, we consider the long-range interactions as producing an “excess” of the thermodynamic quantities, and how this is related to the replica energy. As an example, interacting potentials decaying like a power law are considered at the end of this section.

### 2.3.1 Excess quantities

In the case of long-range interacting systems, the contribution of the long-range interactions to the replica energy can be further concretized if the thermodynamic quantities are separated into a part evaluated without long-range interactions and the corresponding excess produced by these interactions. Assuming that there are no short-range interactions, so that the potential energy is only due to long-range

interactions, we write the entropy and energy as  $S = S^{(i)} + S^{(e)}$  and  $E = E^{(i)} + E^{(e)}$ , respectively, with  $E^{(e)} = W$ . Here, quantities labeled with (i) correspond to the ideal gas contribution, while (e) indicates the excess produced by the long-range interactions. Analogously, we write  $\mu = \mu^{(i)} + \mu^{(e)}$  and  $P = P^{(i)} + P^{(e)}$ . Using these expressions, from (2.6) one obtains (for quantities with or without bars)

$$\mathcal{E} = W - TS^{(e)} + P^{(e)}V - \mu^{(e)}N \quad (2.156)$$

since in the absence of long-range interactions  $TS^{(i)} = E^{(i)} + P^{(i)}V - \mu^{(i)}N$  [5]. If we include also short-range interactions, and not only ideal contributions, the last statement is still true if the splitting to account for the excess produced by long-range interactions is performed in such a way that equation (2.156) is satisfied. Expression (2.156) for the replica energy can be significantly simplified using the mean-field approximation in the large  $N$  limit.

The mean-field entropy written in terms of the number density formally takes the form

$$S = - \int n(\mathbf{x}) \left[ \ln \left( n(\mathbf{x}) \lambda_T^d \right) - \frac{2+d}{2} \right] d^d \mathbf{x}, \quad (2.157)$$

regardless of the set of control parameters used to define the state of the system. This fact has been explicitly shown in the microcanonical and unconstrained cases, equations (2.80) and (2.154), respectively, while in other ensembles (2.157) can be obtained from the corresponding characteristic function. Nonetheless, we emphasize that the number density, the thermal wavelength, and the integration domain in (2.157) are those corresponding to the actual physical conditions imposed on the system, and differ between the various ensembles. Moreover, from the expression for the number density, we can write the chemical potential as

$$\mu = T \ln \left( n(\mathbf{x}) \lambda_T^d \right) + \Phi(\mathbf{x}). \quad (2.158)$$

Multiplying both sides of (2.158) by the number density and integrating over the spatial domain one obtains

$$\mu N = T \int d^d \mathbf{x} n(\mathbf{x}) \ln \left[ \lambda_T^d n(\mathbf{x}) \right] + 2W. \quad (2.159)$$

From these expressions for the entropy and chemical potential, the relation between their excess parts can be explicitly written down. Since  $S^{(i)}$  and  $\mu^{(i)}$  can be obtained from (2.157) and (2.159), respectively, by setting  $\Phi(\mathbf{x}) = 0$ , the excess quantities  $S^{(e)} = S - S^{(i)}$  and  $\mu^{(e)} = \mu - \mu^{(i)}$  follow straightforwardly. As a consequence, one has  $\mu^{(e)}N = -TS^{(e)} + 2W$ , and therefore [5]

$$\mathcal{E} = P^{(e)}V - W. \quad (2.160)$$

Here  $P^{(e)} = P - P^{(i)} = P - NT/V$ . Equation (2.160) for the replica energy is particularly useful since it does not involve entropy and chemical potential. Notice that this expression for the replica energy has already been obtained in the unconstrained ensemble, equation (2.145), where the energy, volume, and number of particles fluctuate.

### 2.3.2 Local equation of state

The formulation of thermodynamics in terms of local variables is well known (see, for instance, references [133,134]) and here we implement this formalism for systems with long-range interactions. In the previous sections we wrote the thermodynamic potentials as integrals over the spatial domain of the system, which leads to a natural definition of local quantities per particle. Analogously, the local energy per particle can be written as

$$e(\mathbf{x}) = e_0 + \frac{1}{2}\Phi(\mathbf{x}), \quad (2.161)$$

where  $e_0 = \frac{d}{2}T$  is the local kinetic energy per particle, such that the total energy  $E$  and kinetic energy  $E_0$  are given by

$$E = \int n(\mathbf{x})e(\mathbf{x}) d^d\mathbf{x} \quad (2.162)$$

$$E_0 = \int n(\mathbf{x})e_0 d^d\mathbf{x}. \quad (2.163)$$

In the preceding sections we have also introduced the local volume per particle  $v(\mathbf{x}) = 1/n(\mathbf{x})$ , which obviously leads to  $V = \int n(\mathbf{x})v(\mathbf{x}) d^d\mathbf{x}$ .

Once local variables are defined, the local equation of state can be obtained. In order to do that, it is useful to write the local entropy per particle in a convenient way. From (2.81) one obtains [8]

$$s(\mathbf{x}) = \ln \left[ v(\mathbf{x}) \left( \frac{4\pi m}{dh^2} e_0 \right)^{d/2} \right] + \frac{2+d}{2}, \quad (2.164)$$

such that  $S = \int n(\mathbf{x})s(\mathbf{x}) d^d\mathbf{x}$ . The local entropy per particle (2.164) is a Sackur-Tetrode-like equation in  $d$  dimensions formulated in terms of local variables. Long-range interactions are included in the local volume through its dependence on the interaction potential, thus leading also to an implicit dependence of the local entropy on the interaction potential. The local entropy per particle is therefore explicitly obtained as a function of the local variables  $e_0$  and  $v$ ,  $s = s(e_0, v)$ . Thus, in the equilibrium framework, one infers that the local internal energy only has contributions coming from kinetic degrees of freedom while long-range interactions in the

system play the role of an external field that locally perturbs the gas. In addition, local thermodynamic equilibrium implies the relations [133, 134]

$$\frac{1}{T} = \left( \frac{\partial s}{\partial e_0} \right)_v \quad \text{and} \quad \frac{p}{T} = \left( \frac{\partial s}{\partial v} \right)_{e_0}, \quad (2.165)$$

where the second of these relations is the local equation of state of the system,  $p$  being the local pressure. In our case, this local equation of state is indeed the one corresponding to an isothermal ideal gas,

$$p(\mathbf{x}) = n(\mathbf{x})T, \quad (2.166)$$

which is valid for any long-range pair interaction potential that can be suitably represented with the mean-field description. The pressure  $P$  we have been considering throughout the text is the local pressure  $p(\mathbf{x})$  evaluated at the boundary of the spatial domain of the system,  $P = p(\mathbf{x})|_{\mathbf{x} \in \partial D}$ . Since the mean-field local entropy per particle takes the same functional form in the different ensembles, the above equation of state is valid in all these ensembles, too. Note that the condition of local thermodynamic equilibrium, together with the relations (2.165) determining temperature and pressure are assumed as a hypothesis in the framework of non-equilibrium thermodynamics, but in contrast in our approach they are derived from the condition that the whole system is in equilibrium. Moreover, while the local equation of state (2.166) is usually derived by considering the condition of hydrostatic equilibrium [58, 135], here it was derived directly from the local entropy [8].

To get more insight in the relation between local thermodynamic variables, we use (2.158) and write the chemical potential as

$$\mu = \mu_0(\mathbf{x}) + \Phi(\mathbf{x}), \quad (2.167)$$

where

$$\mu_0(\mathbf{x}) = T \ln \left( n(\mathbf{x}) \lambda_T^d \right) \quad (2.168)$$

possesses the same functional dependence on the number density as the chemical potential of the ideal gas, but with the density depending on the position as a consequence of the interactions. From (2.164), (2.168), and the local equation of state (2.166), one obtains [8]

$$Ts(\mathbf{x}) = e_0 + p(\mathbf{x})v(\mathbf{x}) - \mu_0(\mathbf{x}), \quad (2.169)$$

which can be further rearranged in the form

$$Ts(\mathbf{x}) = [e_0 + \Phi(\mathbf{x})] + p(\mathbf{x})v(\mathbf{x}) - \mu. \quad (2.170)$$

The term in square brackets in (2.170) is the total energy of a particle at the point  $\mathbf{x}$ ; locally the potential  $\Phi(\mathbf{x})$  acts like an external field. However, the difference between  $\Phi(\mathbf{x})$  and an authentic external field becomes manifest when one sums the contribution of the whole system: multiplying  $[e_0 + \Phi(\mathbf{x})]$  by the number density and integrating over the spatial domain does not give the total energy (2.162). In order to obtain the total energy one must take into account that the total potential energy is due to self-interactions of the system and this is the reason why we have defined the local energy per particle according to (2.161) (the total potential energy is a functional quadratic in the number density). In this respect, using (2.161), equation (2.170) can be alternatively written in the form

$$Ts(\mathbf{x}) = e(\mathbf{x}) + p(\mathbf{x})v(\mathbf{x}) - \mu + \frac{1}{2}\Phi(\mathbf{x}), \quad (2.171)$$

where the last term on the right-hand side highlights the fact that self-interactions of the system are important in the case under consideration.

### 2.3.3 Power-law interactions

Useful relations between global quantities can be obtained by integration of the local equations. Multiplying both sides of (2.171) by  $n(\mathbf{x})$  and integrating over the spatial domain yields

$$TS = E + \frac{2}{d}E_0 - \mu N + W. \quad (2.172)$$

We now want to convert the above expression into an equation in which the quantity  $PV$  appears explicitly related to the other thermodynamic quantities, where  $P$  is the local pressure  $p(\mathbf{x})$  evaluated at the boundary of the system. In order to do that, the form of the pair interaction potential has to be taken into account and the global equation of state has to be considered. This will also lead to an explicit identification of the replica energy.

To proceed, let us consider a long-range interaction potential of the form

$$\phi(\mathbf{q}_i, \mathbf{q}_j) = \kappa |\mathbf{q}_i - \mathbf{q}_j|^{-a} \quad (2.173)$$

with  $0 \leq a \leq d$ ,  $\kappa$  being a coupling constant. The total energy and the interaction potential can be rescaled by introducing [57, 64]

$$\Lambda \equiv \frac{V^{a/d} E}{|\kappa| N^2}, \quad (2.174)$$

$$\varphi_{ij} \equiv \frac{V^{a/d}}{|\kappa| N^2} \phi(\mathbf{q}_i, \mathbf{q}_j) = \frac{\kappa}{|\kappa| N^2} |\mathbf{r}_i - \mathbf{r}_j|^{-a}, \quad (2.175)$$

where we have used  $\mathbf{q}_i = V^{1/d}\mathbf{r}_i$ . Notice that the energy scales like  $N^2$ , as is well known for this kind of systems [136]. Below we first discuss the thermodynamics in the microcanonical ensemble, and afterwards consider the other ensembles.

In the microcanonical description the density of states can be computed as

$$\omega(E, V, N) = \frac{1}{h^{dN}N!} \int \delta(E - \mathcal{H}(\mathbf{p}, \mathbf{q})) d^{2dN}\mathbf{\Gamma} = BV^{N(1-a/2)}\Sigma(\Lambda), \quad (2.176)$$

where the prefactor  $B = B(N, a, d)$  does not depend on either  $E$  or  $V$ , and we have introduced

$$\Sigma(\Lambda) \equiv \int d^{dN}\mathbf{r} \left( \Lambda - \sum_{i>j} \varphi_{ij} \right)^{dN/2} \quad (2.177)$$

using that  $dN/2 - 1 \approx dN/2$  in the large  $N$  limit. In (2.177) the integration is carried over the dimensionless variables  $\mathbf{r}_i$  with  $d^{dN}\mathbf{r} = \prod_i^N d^d\mathbf{r}_i$ . Thus, the microcanonical entropy takes the form

$$S = N \left( 1 - \frac{a}{2} \right) \ln V + \ln \Sigma(\Lambda) + \ln B. \quad (2.178)$$

In addition, using that

$$\frac{\partial \Lambda}{\partial E} = \frac{\Lambda}{E} \quad \text{and} \quad \frac{\partial \Lambda}{\partial V} = \frac{a}{d} \frac{\Lambda}{V}, \quad (2.179)$$

one obtains the following thermodynamic relations [57]:

$$\frac{1}{\bar{T}} = \left( \frac{\partial S}{\partial E} \right)_{V,N} = \frac{\Lambda}{E} \frac{\partial \ln \Sigma(\Lambda)}{\partial \Lambda}, \quad (2.180)$$

$$\frac{P}{\bar{T}} = \left( \frac{\partial S}{\partial V} \right)_{E,N} = \frac{N}{V} \left( 1 - \frac{a}{2} \right) + \frac{a\Lambda}{dV} \frac{\partial \ln \Sigma(\Lambda)}{\partial \Lambda}, \quad (2.181)$$

Combining the above equations and using that  $E = E_0 + W$  with  $E_0 = d/2NT$ , one gets

$$\frac{PV}{NT} = 1 + \frac{a}{d} \frac{W}{NT}, \quad (2.182)$$

which is the microcanonical equation of state of the system. Moreover, the virial theorem can be obtained from this equation,

$$2E_0 + aW = dPV, \quad (2.183)$$

which is particularly useful to express relations between global quantities. Although equation (2.182) has been derived in the microcanonical ensemble, it is a relation at a thermodynamical level and holds also for a different set of control parameters if

the associated equilibrium configurations exist; one has to consider each quantity in this equation as defined by the actual physical conditions imposed on the system. Below we describe, however, a procedure to obtain equation (2.182) in the mean-field canonical description, which can be easily extended to other cases.

Consider the functional (2.70) in the canonical ensemble, and the change of variables  $\mathbf{x} = V^{1/d}\mathbf{r}$  for which  $d^d\mathbf{x} = Vd^d\mathbf{r}$ . Since the integration of the number density over the spatial domain is equal to the number of particles regardless of the volume of the system, we introduce a rescaled number density  $\tilde{n}(\mathbf{r}) = n(\mathbf{x})V$ , so that  $n(\mathbf{x})d^d\mathbf{x} = \tilde{n}(\mathbf{r})d^d\mathbf{r}$ . We then have

$$\begin{aligned} \hat{\mathcal{F}}[\tilde{n}; \alpha, \beta, V, N] = & -\alpha \left( N - \int \tilde{n}(\mathbf{r}) d^d\mathbf{r} \right) + \int \tilde{n}(\mathbf{r}) \left[ \ln \left( \frac{\tilde{n}(\mathbf{r})}{V} \lambda_T^d(\beta) \right) - 1 \right] d^d\mathbf{r} \\ & + \frac{\beta}{V^{a/d}} \frac{\kappa}{2} \int \frac{\tilde{n}(\mathbf{r})\tilde{n}(\mathbf{r}')}{|\mathbf{r} - \mathbf{r}'|^a} d^d\mathbf{r} d^d\mathbf{r}'. \end{aligned} \quad (2.184)$$

Since

$$\delta\hat{\mathcal{F}} = \int \left[ \ln \left( \frac{\tilde{n}(\mathbf{r})}{V} \lambda_T^d \right) + \alpha + \frac{\beta}{V^{a/d}} \tilde{\Phi}(\mathbf{r}) \right] \delta\tilde{n}(\mathbf{r}) d^d\mathbf{r}, \quad (2.185)$$

the rescaled number density that extremizes  $\hat{\mathcal{F}}$  is given by

$$\tilde{n}(\mathbf{r}) = \frac{V}{\lambda_T^d} \exp \left[ -\beta \left( V^{-a/d} \tilde{\Phi}(\mathbf{r}) - \mu \right) \right], \quad (2.186)$$

where  $\mu = -\alpha/\beta$  and

$$\tilde{\Phi}(\mathbf{r}) = \kappa \int \frac{\tilde{n}(\mathbf{r}')}{|\mathbf{r} - \mathbf{r}'|^a} d^d\mathbf{r}' = V^{a/d} \kappa \int \frac{n(\mathbf{x}')}{|\mathbf{x} - \mathbf{x}'|^a} d^d\mathbf{x}' = V^{a/d} \Phi(\mathbf{x}). \quad (2.187)$$

Notice that, by construction, replacing the potential (2.187) in the number density (2.186) one automatically obtains  $\tilde{n}(\mathbf{r}) = n(\mathbf{x})V$ . Here the number of particles is fixed by the condition  $\partial\hat{\mathcal{F}}/\partial\alpha = 0$ , leading to

$$N = \int \tilde{n}(\mathbf{r}) d^d\mathbf{r} = \int n(\mathbf{x}) d^d\mathbf{x}. \quad (2.188)$$

Furthermore, the pressure is obtained from the relation

$$-\frac{P}{T} = \left( \frac{\partial\mathcal{F}}{\partial V} \right)_{\beta, N} = \frac{\partial\hat{\mathcal{F}}}{\partial V} = -\frac{N}{V} - \frac{a}{d} \frac{\beta W}{V}, \quad (2.189)$$

where

$$W = \frac{1}{V^{a/d}} \frac{\kappa}{2} \int \frac{\tilde{n}(\mathbf{r})\tilde{n}(\mathbf{r}')}{|\mathbf{r} - \mathbf{r}'|^a} d^d\mathbf{r} d^d\mathbf{r}' = \frac{\kappa}{2} \int \frac{n(\mathbf{x})n(\mathbf{x}')}{|\mathbf{x} - \mathbf{x}'|^a} d^d\mathbf{x} d^d\mathbf{x}'. \quad (2.190)$$

Thus, equation (2.182) is readily obtained from the relation (2.189).

For interaction potentials decaying as a power law, it is useful to introduce the parameter  $\sigma$  defined as

$$\sigma \equiv \frac{d-a}{d}, \quad 0 \leq \sigma \leq 1, \quad (2.191)$$

which together with (2.183) enables us to rewrite (2.172) in the form

$$TS = E + PV - \mu N + \sigma W. \quad (2.192)$$

The marginal case  $a = d$  corresponds to systems with  $\sigma = 0$ , so that the above equation and the related thermodynamic potentials reduce to the usual ones in short-range interactions thermodynamics. By comparison of (2.192) with equation (2.6), we identify the replica energy for power-law interacting potentials as [8]

$$\mathcal{E} = -\sigma W. \quad (2.193)$$

According to this, we note that the usual Gibbs-Duhem equation is recovered for the marginal case  $a = d$ . Also, note that for  $a > d$  the mean-field approximation fails, and therefore one cannot use the last expression to infer that  $\mathcal{E} \neq 0$ . Recently, it has been argued in [137] that with a suitable modification of the interaction potential corresponding to the marginal case in  $d = 3$ , the usual Gibbs-Duhem equation can also be violated. Such interactions describe a dipolar gas, and the associated replica energy accounts for the dependence of the thermodynamic functions on the shape of the container enclosing the gas. Besides, it has been shown in [138] that the modification of Gibbs-Duhem and the associated equation (2.192) for the self-gravitating gas ( $d = 3$ ,  $a = 1$ ) can be used to obtain the scaling properties and the thermodynamic limit satisfied by the system.

## 2.4 Response functions

As is well known, the inequivalence of ensembles can be related to the occurrence of negative response functions [11]. Here we are particularly interested in the inequivalence between the unconstrained ensemble and other ensembles. This inequivalence can be examined with the help of the properties of the Legendre-Fenchel transformation, as usually done in more common cases [47, 139, 140]. It is therefore instructive to consider first the inequivalence between constrained ensembles.

### 2.4.1 Concavity and convexity

Before discussing the connection between response functions and ensemble inequivalence, let us recall some standard definitions and properties that are needed for our

purpose. We say that the function  $y(x)$  is concave ( $\cap$ -shaped) if for any  $x_1$  and  $x_2$  in the interval of definition and for any  $\lambda \in [0, 1]$ , it satisfies

$$y(\lambda x_1 + (1 - \lambda)x_2) \geq \lambda y(x_1) + (1 - \lambda)y(x_2). \quad (2.194)$$

When the inequality is satisfied strictly for all  $x_1 \neq x_2$ , the function is strictly concave. If  $y(x)$  is concave and twice-differentiable, we necessarily must have  $y''(x) \leq 0$ . Moreover, the concave envelope of a function  $y(x)$  which is not necessarily concave is defined as the smallest concave function  $h(x)$  such that  $h(x) \geq y(x)$  for all  $x$  in the domain of definition. We also say that the function  $y(x)$  is nonconcave if it does not coincide with its concave envelope. Besides, the function  $y(x)$  is said to be convex ( $\cup$ -shaped) if

$$y(\lambda x_1 + (1 - \lambda)x_2) \leq \lambda y(x_1) + (1 - \lambda)y(x_2), \quad (2.195)$$

and strictly convex if the inequality is satisfied strictly for all  $x_1 \neq x_2$ . If  $y(x)$  is convex and twice-differentiable, it necessarily follows that  $y''(x) \geq 0$ . In addition, the convex envelope of a function  $y(x)$  which is not necessarily convex is defined as the largest convex function  $h(x)$  such that  $h(x) \leq y(x)$ . We also say that the function  $y(x)$  is nonconvex if it does not coincide with its convex envelope.

### 2.4.2 Response functions and ensemble inequivalence

Consider now the microcanonical and canonical ensembles. Taking advantage of the Dirac  $\delta$  in the microcanonical density of states (2.56), we rewrite the canonical partition function (2.85) as  $Z = e^{-\mathcal{F}}$ , in such a way that

$$e^{-\mathcal{F}(\beta, V, N)} = \int dE \omega(E, V, N) e^{-\beta E} = \int dE e^{S(E, V, N) - \beta E} \quad (2.196)$$

with  $\beta$  being the inverse canonical temperature,  $\mathcal{F} = \beta F$  the rescaled Helmholtz free energy, and  $S = S(E, V, N)$  the microcanonical entropy. Assuming the large  $N$  limit, we can compute the integral on the right-hand side of (2.196) using the saddle-point approximation and write

$$\mathcal{F}(\beta, V, N) = \inf_E [\beta E - S(E, V, N)]. \quad (2.197)$$

We thus obtain the rescaled Helmholtz free energy as the Legendre-Fenchel transform of the microcanonical entropy with respect to the energy [11, 47, 139, 140], which reduces to the usual Legendre transformation if the entropy is differentiable and concave in  $E$  at constant  $V$  and  $N$ .

On the one hand, the Legendre-Fenchel transform of any function, as defined in (2.197), is always a concave function [140]. This very remarkable property guarantees that the rescaled free energy  $\mathcal{F}$  is always concave with respect to  $\beta$ . Therefore,

if  $\mathcal{F}$  is twice-differentiable, using (2.93) we have

$$\left(\frac{\partial \bar{E}}{\partial \beta}\right)_{V,N} = \left(\frac{\partial^2 \mathcal{F}}{\partial \beta^2}\right)_{V,N} \leq 0, \quad (2.198)$$

which ensures that the response function

$$C_{V,N} = \left(\frac{\partial \bar{E}}{\partial T}\right)_{V,N} \geq 0, \quad (2.199)$$

that is, the heat capacity, is a nonnegative quantity in the canonical ensemble. On the other hand, it is well-known that the lack of additivity can induce a convex region in the microcanonical entropy as a function of the energy. Hence, the quantity

$$\frac{1}{C_{V,N}} = \left(\frac{\partial T}{\partial E}\right)_{V,N} = -T^2 \left(\frac{\partial^2 S}{\partial E^2}\right)_{V,N} \quad (2.200)$$

can be negative in the microcanonical ensemble (hereafter we use, for simplicity, the same symbol to represent the response functions in the different ensembles). If  $C_{V,N}$  is negative in the microcanonical ensemble, the entropy does not coincide with its concave envelope. Negative heat capacities in the microcanonical ensemble are not forbidden by any fundamental requirement, and in fact we will consider some models of isolated systems showing this property in the next chapter. Besides, according to equation (2.199), equilibrium states with negative heat capacity cannot be realized if the system is put in contact with an infinite thermal bath (canonical ensemble). It is therefore clear that states associated with the convex region of the entropy (with respect to  $E$ ) in the microcanonical ensemble have no correspondence in the canonical ensemble. Thus, stated succinctly, if the microcanonical entropy does not coincide with its concave envelope<sup>2</sup> with respect to  $E$ , the microcanonical and canonical ensembles are not equivalent [11, 43, 47, 139, 140].

It should be stressed that negative heat capacity may arise in the microcanonical ensemble due to the fact that the energy is a constraint variable, i.e., it is fixed in any equilibrium configuration. Hence, there are no fluctuations of this quantity bringing the system to an unstable state, as could happen if the system is put in contact with a thermostat at a fixed temperature. In the same way, in principle, in the microcanonical ensemble the system could exhibit a convex region in the entropy as

---

<sup>2</sup>The concave envelope can be obtained by applying twice the Legendre-Fenchel transformation. Put  $S^*(\beta) = \inf_E [\beta E - S(E)]$  and  $S^{**}(E) = \inf_\beta [\beta E - S^*(\beta)]$  at constant  $V$  and  $N$ . Thus,  $S^{**}(E)$  is the concave envelope of  $S(E)$  with respect to  $E$ . A suitable definition of the Legendre-Fenchel transformation with a supremum instead of an infimum yields always convex functions; applying twice this transformation one obtains the convex envelope of the function [140].

a function of the other constraint variables,  $V$  or  $N$ . The microcanonical entropy can be nonconcave in any of its natural variables, all of them being constraint variables. For those variables, such a nonconcave behavior can be reflected in the canonical ensemble, since in this case both  $V$  and  $N$  are constraint variables as well.

In the grand canonical ensemble, the number of particles is not constrained. Let us write the grand canonical partition function  $\Xi = e^{-\mathcal{L}}$  as

$$e^{-\mathcal{L}(\alpha, \beta, V)} = \sum_{N=0}^{\infty} e^{\mu N/T} Z(T, V, N) = \sum_{N=0}^{\infty} e^{-\alpha N - \mathcal{F}(\beta, V, N)}, \quad (2.201)$$

where  $\alpha = -\mu/T$ . The rescaled grand potential  $\mathcal{L} = \beta\Omega$  is thus given by the term that dominates the sum according to

$$\mathcal{L}(\alpha, \beta, V) = \inf_N [\alpha N + \mathcal{F}(\beta, V, N)], \quad (2.202)$$

which is the Legendre-Fenchel transform of  $-\mathcal{F} = -\beta F$  with respect to  $N$ . The above expression ensures that  $\mathcal{L}$  is always concave in  $\alpha$ . Its concavity with respect to  $\beta$  is inherited from  $\mathcal{F}$ , which can be seen explicitly using that

$$\mathcal{L}(\alpha, \beta, V) = \inf_{E, N} [\alpha N + \beta E - S(E, V, N)]. \quad (2.203)$$

Hence, if  $\mathcal{L}$  is twice-differentiable with respect to  $\alpha$ , from (2.113) we have

$$\left( \frac{\partial \bar{N}}{\partial \alpha} \right)_{\beta, V} = \left( \frac{\partial^2 \mathcal{L}}{\partial \alpha^2} \right)_{\beta, V} \leq 0, \quad (2.204)$$

so that in the grand canonical ensemble

$$M_{T, V} \equiv \left( \frac{\partial \bar{N}}{\partial \mu} \right)_{T, V} \geq 0. \quad (2.205)$$

Here  $M_{T, V}$  is a response function (just as the heat capacity) telling us that in the grand canonical ensemble the number of particles increases whenever the chemical potential increases, holding  $T$  and  $V$  constant. Notice that this response function can be written as  $M_{T, V} = \beta N / \Gamma$ , where  $\Gamma$  is the thermodynamic factor given by [122]

$$\frac{1}{\Gamma} = \frac{1}{\beta} \left( \frac{\partial \ln \bar{N}}{\partial \mu} \right)_{T, V}. \quad (2.206)$$

Moreover, for macroscopic short-range interacting systems, the usual Gibbs-Duhem equation holds, so that the function  $M_{T, V}$  can be directly related to the isothermal

compressibility<sup>3</sup>  $\kappa_T$ . In the latter case, the sign of  $M_{T,V}$  can be inferred from the sign of  $\kappa_T$ , namely, they are both positive quantities. However, if the replica energy is different from zero, the signs of these response functions are independent from each other, in general. Furthermore, in the canonical ensemble there is no mechanism ensuring that

$$\frac{1}{M_{T,V}} = \left( \frac{\partial \mu}{\partial N} \right)_{T,V} = \left( \frac{\partial^2 F}{\partial N^2} \right)_{T,V} \quad (2.207)$$

is a positive quantity, since the Helmholtz free energy is not necessarily convex with respect to  $N$ . If the Helmholtz free energy does not coincide with its convex envelope with respect to  $N$ , the canonical and grand canonical ensembles are not equivalent.

In the isothermal-isobaric ensemble, where the volume is not a constraint variable, for the partition function  $\Delta = e^{-\mathcal{G}}$  we get

$$e^{-\mathcal{G}(N,\beta,\gamma)} = \int dV e^{-PV/T} Z(T, V, N) = \int dV e^{-\gamma V - \mathcal{F}(\beta, V, N)}, \quad (2.208)$$

where  $\gamma = P/T$ . Hence, the saddle-point approximation gives the rescaled Gibbs free energy  $\mathcal{G} = \beta G$  as

$$\mathcal{G}(N, \beta, \gamma) = \inf_V [\gamma V + \mathcal{F}(\beta, V, N)], \quad (2.209)$$

which is the Legendre-Fenchel transform of  $-\mathcal{F}$  with respect to  $V$ . Moreover, using (2.197) we can also write

$$\mathcal{G}(N, \beta, \gamma) = \inf_{E,V} [\beta E + \gamma V - S(E, V, N)], \quad (2.210)$$

from which we infer that  $\mathcal{G}$  is concave in both  $\beta$  and  $\gamma$ . In particular, if  $\mathcal{G}$  is twice-differentiable with respect to  $\gamma$ , we can assert that

$$\left( \frac{\partial \bar{V}}{\partial \gamma} \right)_{N,\beta} = \left( \frac{\partial^2 \mathcal{G}}{\partial \gamma^2} \right)_{N,\beta} \leq 0, \quad (2.211)$$

<sup>3</sup>For macroscopic short-range interacting systems, we can take  $n = \bar{N}/V$  and write

$$M_{T,V} = \left( \frac{\partial \bar{N}}{\partial \mu} \right)_{T,V} = V \left( \frac{\partial n}{\partial \mu} \right)_T = V \left( \frac{\partial P}{\partial \mu} \right)_T \left( \frac{\partial n}{\partial P} \right)_T.$$

Since Gibbs-Duhem holds in this case ( $\mathcal{E} = 0$ ), under isothermal conditions we have  $dP = nd\mu$ . Hence, using that  $\partial n / \partial P = -n^2 \partial(1/n) / \partial P$ ,  $\kappa_T$  is related to  $M_{T,V}$  according to

$$M_{T,V} = Vn \left( \frac{\partial n}{\partial P} \right)_T = -\frac{\bar{N}n}{V} \left( \frac{\partial V}{\partial P} \right)_{T,\bar{N}} = \bar{N}n\kappa_T.$$

and therefore that the isothermal compressibility in the isobaric-isothermal ensemble is nonnegative,

$$\kappa_T = -\frac{1}{\bar{V}} \left( \frac{\partial \bar{V}}{\partial P} \right)_{T,N} \geq 0. \quad (2.212)$$

This is what we expect on physical grounds, since states with negative  $\kappa_T$  cannot be stable under volume fluctuations. Furthermore, for convenience, instead of the isothermal compressibility  $\kappa_T$  we will consider the quantity  $K_{T,N} = \bar{V} \kappa_T$  as a response function, where the subscript  $N$  is written to emphasize that it is also computed at constant number of particles. Then, in the isobaric-isothermal ensemble

$$K_{T,N} = - \left( \frac{\partial \bar{V}}{\partial P} \right)_{T,N} \geq 0. \quad (2.213)$$

If the volume is a constraint variable which is always fixed in any equilibrium configuration, however, states with negative isothermal compressibility or, equivalently, negative  $K_{T,N}$  can be realized. In the canonical ensemble we have

$$\frac{1}{K_{T,N}} = - \left( \frac{\partial P}{\partial V} \right)_{T,N} = \left( \frac{\partial^2 F}{\partial V^2} \right)_{T,N}, \quad (2.214)$$

which is not restricted to be a positive quantity since the Helmholtz free energy is not necessarily convex with respect to  $V$ . According to this, the isobaric-isothermal and canonical ensembles are not equivalent if the Helmholtz free energy does not coincide with its convex envelope with respect to  $V$ .

### 2.4.3 From microcanonical entropy to rescaled replica energy

Continuing the discussion of the preceding section, here we focus on the unconstrained ensemble and its connection with the other ensembles. Since the unconstrained ensemble describes the thermodynamics of completely open systems, it can be seen as the opposite situation of the one described by the microcanonical ensemble where the systems are isolated. Such an opposition, in a certain sense, is reflected in the curvature of the thermodynamic characteristic functions. We shall see that the characteristic function of completely open systems, the rescaled replica energy, possesses always a very well defined concavity with respect to all its natural variables (none of them being a constraint variable), while, as noted previously, the microcanonical entropy can be nonconcave in any of its natural variables (all of them being constraint variables).

In the case where the energy, volume, and number of particles fluctuate, we can combine (2.132) with (2.196) and (2.201) to write the unconstrained partition

function  $\Upsilon = e^{-\mathcal{R}}$  as a function of the microcanonical entropy, that is

$$e^{-\mathcal{R}(\alpha,\beta,\gamma)} = \int dE \int dV \sum_{N=0}^{\infty} e^{S(E,V,N) - \alpha N - \beta E - \gamma V}. \quad (2.215)$$

We recall that the rescaled replica energy is given by  $\mathcal{R} = \beta \mathcal{E}$  and that considering the set of control parameters  $\alpha = -\mu/T$ ,  $\beta = 1/T$ , and  $\gamma = P/T$  is completely equivalent to considering  $T$ ,  $P$ , and  $\mu$ . Moreover, evaluating (2.215) in a saddle-point approximation we have

$$\mathcal{R}(\alpha, \beta, \gamma) = \inf_{E,V,N} [\alpha N + \beta E + \gamma V - S(E, V, N)], \quad (2.216)$$

which ensures that  $\mathcal{R}$  is completely concave, implying that it is also separately concave in  $\alpha$ ,  $\beta$ , and  $\gamma$ . Therefore, if the rescaled replica energy is twice-differentiable, in the unconstrained ensemble we get

$$\left( \frac{\partial \bar{N}}{\partial \alpha} \right)_{\beta, \gamma} = \left( \frac{\partial^2 \mathcal{R}}{\partial \alpha^2} \right)_{\beta, \gamma} \leq 0, \quad (2.217)$$

$$\left( \frac{\partial \bar{E}}{\partial \beta} \right)_{\alpha, \gamma} = \left( \frac{\partial^2 \mathcal{R}}{\partial \beta^2} \right)_{\alpha, \gamma} \leq 0, \quad (2.218)$$

$$\left( \frac{\partial \bar{V}}{\partial \gamma} \right)_{\alpha, \beta} = \left( \frac{\partial^2 \mathcal{R}}{\partial \gamma^2} \right)_{\alpha, \beta} \leq 0. \quad (2.219)$$

Using that  $\alpha = -\mu/T$ ,  $\beta = 1/T$ , and  $\gamma = P/T$ , equations (2.217), (2.218), and (2.219) imply that the response functions

$$M_{T,P} \equiv \left( \frac{\partial \bar{N}}{\partial \mu} \right)_{T,P} \geq 0, \quad (2.220)$$

$$C_{\alpha,\gamma} \equiv \left( \frac{\partial \bar{E}}{\partial T} \right)_{\mu/T, P/T} \geq 0, \quad (2.221)$$

$$K_{T,\mu} \equiv - \left( \frac{\partial \bar{V}}{\partial P} \right)_{T,\mu} \geq 0, \quad (2.222)$$

respectively, are nonnegative in the unconstrained ensemble. On the one hand, the rescaled replica energy can be related to the rescaled grand potential via

$$e^{-\mathcal{R}(\alpha,\beta,\gamma)} = \int dV \Xi(T, V, \mu) e^{-PV/T} = \int dV e^{-\mathcal{L}(\alpha,\beta,V) - \gamma V}. \quad (2.223)$$

Using the saddle-point approximation, we then have

$$\mathcal{R}(\alpha, \beta, \gamma) = \inf_V [\gamma V + \mathcal{L}(\alpha, \beta, V)], \quad (2.224)$$

so that  $\mathcal{R}$  is expressed as the Legendre-Fenchel transform of  $-\mathcal{L} = -\beta\Omega$  with respect to  $V$ . Thus, considering the response function  $K_{T,\mu}$ , we can obtain a sufficient criterion for the occurrence of inequivalence between the unconstrained and the grand canonical ensembles. In the grand canonical ensemble we have

$$\frac{1}{K_{T,\mu}} = - \left( \frac{\partial P}{\partial V} \right)_{T,\mu} = \left( \frac{\partial^2 \Omega}{\partial V^2} \right)_{T,\mu}, \quad (2.225)$$

which can be a negative quantity since the grand potential is not necessarily a convex function in  $V$ . Hence, taking into account equation (2.222), if the grand potential does not coincide with its convex envelope with respect to  $V$ , the grand canonical and unconstrained ensembles are not equivalent. On the other hand, we can write

$$e^{-\mathcal{R}(\alpha,\beta,\gamma)} = \sum_{N=0}^{\infty} \Delta(T, P, N) e^{\mu N/T} = \sum_{N=0}^{\infty} e^{-\mathcal{G}(N,\beta,\gamma) - \alpha N}, \quad (2.226)$$

which relates the rescaled replica energy to the rescaled Gibbs free energy, and therefore we obtain  $\mathcal{R}$  as the Legendre-Fenchel transform of  $-\mathcal{G} = -\beta G$  with respect to  $N$ ,

$$\mathcal{R}(\alpha, \beta, \gamma) = \inf_N [\alpha N + \mathcal{G}(N, \beta, \gamma)]. \quad (2.227)$$

Now let us consider the response function  $M_{T,P}$  in the isobaric-isothermal ensemble. In this case,

$$\frac{1}{M_{T,P}} = \left( \frac{\partial \mu}{\partial N} \right)_{T,P} = \left( \frac{\partial^2 G}{\partial N^2} \right)_{T,P} \quad (2.228)$$

is not restricted to be a positive quantity since the Gibbs free energy is not necessarily convex in  $N$ . Therefore, in view of (2.220), the unconstrained and isobaric-isothermal ensembles are not equivalent if the Gibbs free energy does not coincide with its convex envelope with respect to  $N$ .

To finish the discussion of this section, we observe briefly that in the same manner nonconcavity of the entropy  $S$  or nonconvexity of the thermodynamic potentials  $F$ ,  $\Omega$ , and  $G$  with respect to their natural constraint variables ( $E$ ,  $V$ , or  $N$ ) leads to ensemble inequivalence.



## LONG-RANGE INTERACTIONS: MODELS AND APPLICATIONS

---

After having analyzed various theoretical aspects of the thermostatics of long-range interacting systems, in this chapter we consider some models that exhibit the associated phenomenology. In Section 3.1, we study in detail the microcanonical and canonical phase diagrams of the Thirring model [18]. Because of ensemble inequivalence, these phase diagrams are different. In Section 3.2, a modification of this model is introduced, which presents equilibrium configurations in the unconstrained ensemble. Finally, in Section 3.3 some thermodynamic relations for self-gravitating systems [15–23] and for the modified Thirring model are examined in connection with the replica energy.

### 3.1 Phase transitions in the Thirring model

A seminal work on negative specific heat was written by Walter Thirring [18]. In that paper he introduced a simple model that reproduces some of the properties of self-gravitating systems. He showed that the model exhibits negative specific heat and temperature jumps in the microcanonical ensemble and that they are both absent, and replaced by a first-order phase transition, in the canonical ensemble. In the last decade, ensemble inequivalence in nonadditive systems has become an established fact [11], and several different models have been shown to display such a feature. However, quite surprisingly, a detailed study of the full phase diagram in both the microcanonical and the canonical ensemble of the Thirring model has not yet been performed. Moreover, the analysis of ensemble inequivalence has been restricted in general to models which are endowed with specific symmetries of the order parameter. We are here thinking, for instance, to models of magnetic systems which, in absence of an external field, are invariant under a sign change  $m \rightarrow -m$  of

magnetization  $m$ . These models have typically a phase diagram with a line of second order phase transitions which ends at a tricritical point. This latter has a different location in different ensembles [48]. Thirring's model does not possess this symmetry and, as we will show, the line of first-order phase transitions terminates at a critical point, as it happens for the gas-liquid phase transitions in fluids. At variance with what is found for models with symmetries, ensemble inequivalence manifests itself in Thirring's model by a different location of the critical point. This feature was already found for a model studied mainly for its non equilibrium properties [141]. Finally, the mean-field character of Thirring's model allows us to employ a Landau expansion [98] of thermodynamic potentials and to determine analytically the location of the critical point in both the microcanonical and canonical ensembles.

### 3.1.1 The Thirring model

The Thirring model is a minimal model that describes a confined system with regularized attractive interactions that mimic those of a self-gravitating gas [142]. In this model,  $N$  particles are enclosed in a volume  $V$  with a Hamiltonian of the form (2.53) in three dimensions. The interactions of the model are defined by the nonlocal potential [18]

$$\phi(\mathbf{q}_i, \mathbf{q}_j) = -2\nu\theta_{V_0}(\mathbf{q}_i)\theta_{V_0}(\mathbf{q}_j), \quad (3.1)$$

where  $\nu > 0$  is a constant, and  $\theta_{V_0}(\mathbf{q}_i) = 1$  if  $\mathbf{q}_i \in V_0$  and vanishes otherwise, where  $V_0 < V$  is the core volume. Particles outside  $V_0$  are free, so that the total potential energy in the large  $N$  limit is given by

$$\sum_{i>j}^N \phi(\mathbf{q}_i, \mathbf{q}_j) = -\nu N_0^2, \quad (3.2)$$

where  $N_0$  is the number of particles in  $V_0$  for a given configuration. Notice that, as a consequence of the interaction potential (3.1), the system is nonadditive [5] and exhibits the rich phenomenology common in long-range interacting systems. In particular, the microcanonical and canonical ensembles are not equivalent, as will be shown below.

Let us consider the thermodynamics of the system when it is isolated. The density of states in phase space can be written as a sum over all possible values of the number of particles in the core [18]

$$\omega(E, V, N) = \sum_{N_0} e^{\hat{S}(E, V, N, N_0)}, \quad (3.3)$$

in such a way that the maximization of  $\hat{S}(E, V, N, N_0)$  leads to the microcanonical entropy in the large  $N$  limit,

$$S(E, V, N) = \sup_{N_0} \hat{S}(E, V, N, N_0) \quad (3.4)$$

Here and below we use units in which  $k_B = 1$ . Furthermore, introducing the fraction of free particles  $n_g$  (fraction of particles outside  $V_0$ ), the reduced energy  $\varepsilon$ , and the reduced volume  $\eta$ , given by

$$n_g = 1 - \frac{N_0}{N}, \quad \varepsilon = \frac{E}{\nu N^2} + 1, \quad \eta = \ln \left( \frac{V - V_0}{V_0} \right), \quad (3.5)$$

the function  $\hat{S}$  in (3.3) can be written as  $\hat{S} \equiv N\hat{s}$  with [18]

$$\hat{s}(n_g, \varepsilon, \eta) = \frac{3}{2} \ln [\varepsilon - 2n_g + n_g^2] - (1 - n_g) \ln(1 - n_g) - n_g \ln n_g + n_g \eta, \quad (3.6)$$

where in (3.6) we have neglected constant terms. The microcanonical entropy per particle  $s = S/N$  is thus given by

$$s(\varepsilon, \eta) = \hat{s}(\bar{n}_g, \varepsilon, \eta) = \sup_{n_g} \hat{s}(n_g, \varepsilon, \eta), \quad (3.7)$$

where  $\bar{n}_g = \bar{n}_g(\varepsilon, \eta)$  is the value of  $n_g$  that maximizes (3.6). The energy  $E$ , being the sum of the potential energy (3.2) and of the kinetic energy, is bounded from below by  $-\nu N^2$ , such that for the reduced energy we have  $\varepsilon \geq 0$ . Furthermore, for a given reduced energy in the range  $0 \leq \varepsilon < 1$ , the fraction of free particles  $n_g$  is bounded from above by  $1 - \sqrt{1 - \varepsilon}$ , from the fact that the kinetic energy is nonnegative. On the other hand, for  $\varepsilon \geq 1$  the fraction  $n_g$  can take any value in the range  $0 \leq n_g \leq 1$ . In turn, this guarantees that the argument of the logarithm in equation (3.6) is never negative. The reduced temperature  $\tau = T/(\nu N)$ , where  $T$  is the temperature, takes the form

$$\frac{1}{\tau(\varepsilon, \eta)} = \left. \frac{\partial}{\partial \varepsilon} \hat{s}(n_g, \varepsilon, \eta) \right|_{n_g = \bar{n}_g} = \frac{3}{2} (\varepsilon - 2\bar{n}_g + \bar{n}_g^2)^{-1}, \quad (3.8)$$

which is guaranteed to be positive from the same observation made above.

In the canonical ensemble, the system is assumed to be in contact with a thermostat, in such a way that the reduced temperature  $\tau$  is fixed and the energy fluctuates. The reduced canonical free energy per particle is defined by  $\varphi \equiv F/(NT)$ ,  $F$  being the canonical free energy. It can be obtained from the microcanonical entropy by computing its Legendre-Fenchel transform, namely,

$$\varphi(\tau, \eta) = \inf_{\varepsilon} \left[ \frac{\varepsilon}{\tau} - s(\varepsilon, \eta) \right]. \quad (3.9)$$

The reduced free energy can also be written as

$$\varphi(\tau, \eta) = \hat{\varphi}(\bar{n}_g, \tau, \eta) = \inf_{n_g} \hat{\varphi}(n_g, \tau, \eta), \quad (3.10)$$

where

$$\hat{\varphi}(n_g, \tau, \eta) = \inf_{\varepsilon} \left[ \frac{\varepsilon}{\tau} - \hat{s}(n_g, \varepsilon, \eta) \right], \quad (3.11)$$

and now the fraction of free particles that minimizes the free energy is a function of the temperature,  $\bar{n}_g = \bar{n}_g(\tau, \eta)$ . In this case, using (3.6), the expression (3.11) can be computed to give

$$\hat{\varphi}(n_g, \tau, \eta) = -\frac{3}{2} \ln \left( \frac{3\tau}{2} \right) + \frac{2n_g - n_g^2}{\tau} + (1 - n_g) \ln(1 - n_g) + n_g \ln n_g - n_g \eta + \frac{3}{2}. \quad (3.12)$$

Obviously, the constant terms neglected in the entropy (3.6) are not included. The mean value  $\bar{\varepsilon}$  of the reduced energy in the canonical ensemble is given by

$$\bar{\varepsilon}(\tau, \eta) = -\tau^2 \frac{\partial}{\partial \tau} \hat{\varphi}(n_g, \tau, \eta) \Big|_{n_g = \bar{n}_g} = \frac{3\tau}{2} + 2\bar{n}_g - \bar{n}_g^2. \quad (3.13)$$

An interesting feature of the system is that it undergoes first-order phase transitions in both the microcanonical and canonical ensembles. Using the Landau theory of phase transitions, below we study the critical points in the two ensembles and show explicitly that they differ from each other.

### 3.1.2 Landau theory: Microcanonical ensemble

Let us introduce the deviation  $m = n_g - \bar{n}_g$  of the fraction of free particles  $n_g$  with respect to a certain reference value  $\bar{n}_g$ . This reference value will be the one maximizing equation (3.6), i.e., the equilibrium value. Thus, we perform a Landau expansion of the entropy (3.6) in powers of  $m$  around  $\bar{n}_g$ ,

$$\begin{aligned} \hat{s}(m, \varepsilon, \eta) &= a_s(\bar{n}_g, \varepsilon, \eta) + b_s(\bar{n}_g, \varepsilon, \eta)m + c_s(\bar{n}_g, \varepsilon, \eta)m^2 + d_s(\bar{n}_g, \varepsilon, \eta)m^3 \\ &\quad + e_s(\bar{n}_g, \varepsilon, \eta)m^4 + \mathcal{O}(m^5), \end{aligned} \quad (3.14)$$

where the coefficients are given by

$$a_s(\bar{n}_g, \varepsilon, \eta) = \frac{3}{2} \ln \left( \varepsilon - 2\bar{n}_g + \bar{n}_g^2 \right) - (1 - \bar{n}_g) \ln(1 - \bar{n}_g) - \bar{n}_g \ln \bar{n}_g + \bar{n}_g \eta, \quad (3.15)$$

$$b_s(\bar{n}_g, \varepsilon, \eta) = \ln \left( \frac{1 - \bar{n}_g}{\bar{n}_g} \right) - \frac{3(1 - \bar{n}_g)}{\varepsilon - 2\bar{n}_g + \bar{n}_g^2} + \eta, \quad (3.16)$$

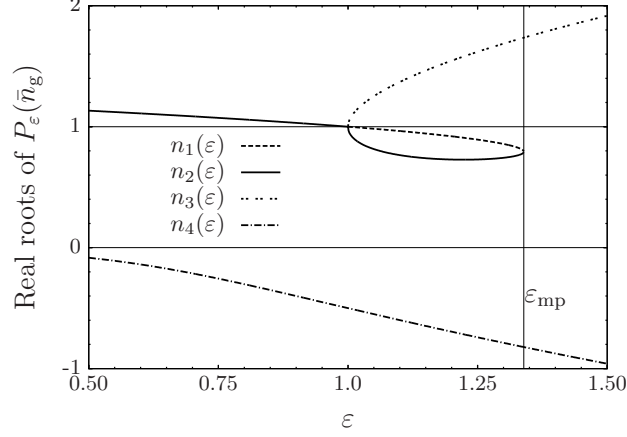


**Figure 3.1:** Real roots of  $P_\varepsilon(\bar{n}_g)$  as a function of the reduced energy  $\varepsilon$ . Since, by definition,  $0 \leq \bar{n}_g \leq 1$ , the roots  $n_3(\varepsilon)$  and  $n_4(\varepsilon)$  are not to be considered. The roots  $n_1(\varepsilon)$  and  $n_2(\varepsilon)$  become equal at  $\varepsilon_{\text{mp}}$ , the energy at the microcanonical critical point. Taken from [2].

$$c_s(\bar{n}_g, \varepsilon, \eta) = \frac{P_\varepsilon(\bar{n}_g)}{2(1 - \bar{n}_g)\bar{n}_g(\varepsilon - 2\bar{n}_g + \bar{n}_g^2)^2}, \quad (3.17)$$

$$d_s(\bar{n}_g, \varepsilon, \eta) = \frac{1 - 2\bar{n}_g}{6(1 - \bar{n}_g)^2\bar{n}_g^2} + \frac{3(1 - \bar{n}_g)}{(\varepsilon - 2\bar{n}_g + \bar{n}_g^2)^2} - \frac{4(1 - \bar{n}_g)^3}{(\varepsilon - 2\bar{n}_g + \bar{n}_g^2)^3}, \quad (3.18)$$

$$e_s(\bar{n}_g, \varepsilon, \eta) = -\frac{\bar{n}_g^3 + (1 - \bar{n}_g)^3}{12(1 - \bar{n}_g)^3\bar{n}_g^3} - \frac{3}{4(\varepsilon - 2\bar{n}_g + \bar{n}_g^2)^2} - \frac{6(1 - \varepsilon)(1 - \bar{n}_g)^2}{(\varepsilon - 2\bar{n}_g + \bar{n}_g^2)^4}, \quad (3.19)$$

with

$$P_\varepsilon(\bar{n}_g) \equiv 2\bar{n}_g^4 - 5\bar{n}_g^3 + (8 - 5\varepsilon)\bar{n}_g^2 + (7\varepsilon - 6)\bar{n}_g - \varepsilon^2. \quad (3.20)$$

We note that the equilibrium states require the conditions  $b_s(\bar{n}_g, \varepsilon, \eta) = 0$ , defining  $\bar{n}_g = \bar{n}_g(\varepsilon, \eta)$ , and  $c_s(\bar{n}_g, \varepsilon, \eta) \leq 0$ . It is not difficult to see that for  $0 \leq \varepsilon \leq 1$  these conditions are satisfied by only one value of  $\bar{n}_g$ ; therefore a phase transition can occur only for  $\varepsilon > 1$ .

### Microcanonical critical point

The microcanonical phase diagram in the  $(\varepsilon, \eta)$  plane exhibits a line of first-order phase transitions that ends at a critical point specified by the reduced energy and volume  $\varepsilon_{\text{mp}}$  and  $\eta_{\text{mp}}$ , respectively, corresponding to a fraction of free particles  $\bar{n}_g =$

$n_{\text{mp}}$ . Such critical values can be obtained by solving the system of equations

$$\begin{aligned} b_s(n_{\text{mp}}, \varepsilon_{\text{mp}}, \eta_{\text{mp}}) &= 0, \\ c_s(n_{\text{mp}}, \varepsilon_{\text{mp}}, \eta_{\text{mp}}) &= 0, \\ d_s(n_{\text{mp}}, \varepsilon_{\text{mp}}, \eta_{\text{mp}}) &= 0. \end{aligned} \quad (3.21)$$

In order to find the critical point, consider the quartic polynomial  $P_\varepsilon(\bar{n}_g)$  given by (3.20); when  $P_\varepsilon(\bar{n}_g)$  vanishes, also the coefficient  $c_s$  vanishes. Let us denote the roots of  $P_\varepsilon(\bar{n}_g)$  by  $n_i(\varepsilon)$ ,  $i = 1, \dots, 4$ . Two of these roots, say,  $n_3(\varepsilon)$  and  $n_4(\varepsilon)$ , lie outside the interval  $[0, 1)$  when they are real: since the fraction  $\bar{n}_g$  is bounded,  $0 \leq \bar{n}_g \leq 1$ , these roots are not to be considered. The other two roots,  $n_1(\varepsilon)$  and  $n_2(\varepsilon)$ , can be real or complex, depending on the value of  $\varepsilon$ , and are given by

$$n_1(\varepsilon) = \frac{\sqrt{3}}{24} \left\{ \frac{15}{\sqrt{3}} + z_2(\varepsilon) - \left[ 2z_1(\varepsilon) - 18\sqrt{3} \frac{(8\varepsilon + 1)}{z_2(\varepsilon)} \right]^{1/2} \right\}, \quad (3.22)$$

$$n_2(\varepsilon) = \frac{\sqrt{3}}{24} \left\{ \frac{15}{\sqrt{3}} - z_2(\varepsilon) + \left[ 2z_1(\varepsilon) + 18\sqrt{3} \frac{(8\varepsilon + 1)}{z_2(\varepsilon)} \right]^{1/2} \right\}, \quad (3.23)$$

where

$$z_1(\varepsilon) = 16(5\varepsilon - 8) - \frac{4(\varepsilon - 1)(\varepsilon + 26)}{z_3(\varepsilon)} - 4z_3(\varepsilon) + 75, \quad (3.24)$$

$$z_2(\varepsilon) = \left[ 80\varepsilon + 8z_3(\varepsilon) + \frac{8(\varepsilon - 1)(\varepsilon + 26)}{z_3(\varepsilon)} - 53 \right]^{1/2}, \quad (3.25)$$

$$z_3(\varepsilon) = \left[ \frac{3\sqrt{3}}{2} \sqrt{-\Delta_P(\varepsilon)} + (1374 - 485\varepsilon)\varepsilon^2 - 1293\varepsilon + 404 \right]^{1/3}, \quad (3.26)$$

and

$$\Delta_P(\varepsilon) = -36(\varepsilon - 1)^3 (968\varepsilon^3 - 2581\varepsilon^2 + 2276\varepsilon - 744) \quad (3.27)$$

is the discriminant of  $P_\varepsilon(\bar{n}_g)$ . When  $n_1(\varepsilon)$  and  $n_2(\varepsilon)$  are real, they lie in the interval  $(0, 1]$  for a certain range of energies  $\varepsilon$ . To visualize this situation, in figure 3.1 we plot the real roots of  $P_\varepsilon(\bar{n}_g)$  as function of  $\varepsilon$ . In addition, these roots are real and different when the discriminant is positive, are real and coincide when  $\Delta_P(\varepsilon)$  vanishes, and become complex when  $\Delta_P(\varepsilon)$  is negative. Thus, the solution of the system (3.21) is characterized by the condition  $\Delta_P(\varepsilon_{\text{mp}}) = 0$ , in such a way that  $n_{\text{mp}} = n_1(\varepsilon_{\text{mp}}) = n_2(\varepsilon_{\text{mp}})$ . This can be seen by noting that  $c_s$  is continuous for  $\bar{n}_g$  between  $n_1$  and  $n_2$ , and that

$$d_s(\bar{n}_g, \varepsilon, \eta) = \frac{1}{3} \frac{\partial}{\partial \bar{n}_g} c_s(\bar{n}_g, \varepsilon, \eta), \quad (3.28)$$

so that the value of  $\bar{n}_g$  that cancels out  $d_s$  must lie between  $n_1$  and  $n_2$ . Therefore, if the fraction  $\bar{n}_g = n_{\text{mp}}$  cancels out both  $c_s$  and  $d_s$ , we have  $n_{\text{mp}} = n_1 = n_2$ , which is precisely what happens when the discriminant vanishes,  $\Delta_P(\varepsilon_{\text{mp}}) = 0$ . Furthermore, in such a case, from  $b_s(n_{\text{mp}}, \varepsilon_{\text{mp}}, \eta_{\text{mp}}) = 0$ , the critical reduced volume can be unequivocally determined as

$$\eta_{\text{mp}} = \frac{3(1 - n_{\text{mp}})}{\varepsilon_{\text{mp}} - 2n_{\text{mp}} + n_{\text{mp}}^2} - \ln \left( \frac{1 - n_{\text{mp}}}{n_{\text{mp}}} \right). \quad (3.29)$$

The discriminant  $\Delta_P(\varepsilon)$ , equation (3.27), is a polynomial of degree six in  $\varepsilon$ . It has four real roots and two complex roots: three of these real roots are found at  $\varepsilon_0 = 1$ , and the remaining real root is given by

$$\varepsilon_{\text{mp}} = \frac{(k_1 + k_2)^{1/3} + (k_1 - k_2)^{1/3} + 2581}{2904} \simeq 1.339, \quad (3.30)$$

with the numerical coefficients  $k_1 = 1016263261$  and  $k_2 = 37792656\sqrt{723}$ . We note that  $\varepsilon_0$  is not the critical energy at the critical point, since one has  $n_1(\varepsilon_0) = n_2(\varepsilon_0) = 1$  and, hence, this corresponds, from equation (3.29), to a state with  $\eta \rightarrow \infty$ . The critical fraction can be obtained by evaluating equations (3.22) or (3.23) at the critical energy  $\varepsilon_{\text{mp}}$ , yielding  $n_{\text{mp}} \simeq 0.7929$ . Finally, from (3.29), the critical reduced volume is given by  $\eta_{\text{mp}} \simeq 2.969$ .

In addition, we note that phase transitions can occur only for  $\varepsilon$  such that  $\varepsilon_0 < \varepsilon < \varepsilon_{\text{mp}}$ , since for  $\varepsilon < 1$ , as noted before, the condition  $b_s(\bar{n}_g, \varepsilon, \eta) = 0$  defines only one state of equilibrium. In figure 3.2 we show the microcanonical phase diagram in the  $(\varepsilon, \eta)$  plane, with the line of first order transition points terminating at the critical point. The features of the microcanonical and canonical phase diagrams are commented later.

### 3.1.3 Landau theory: Canonical ensemble

We are interested in showing how the phase diagram in the canonical ensemble differs from the diagram obtained in the microcanonical ensemble. Following [141], we introduce the deviation  $q = \varepsilon - \bar{\varepsilon}$  of the energy with respect to the mean value  $\bar{\varepsilon}$  and perform an expansion in powers of  $q$  of the entropy in such a way that

$$\begin{aligned} \frac{\varepsilon}{\tau} - \hat{s}(m, \varepsilon, \eta) = & \frac{\bar{\varepsilon} + q}{\tau} - a_0 - a_1 q - a_2 q^2 - a_3 q^3 - (b_0 + b_1 q + b_2 q^2) m \\ & - (c_0 + c_1 q) m^2 - d_0 m^3 + \mathcal{O}(m^4), \end{aligned} \quad (3.31)$$

where we have used (3.14) and the coefficients of the expansion are given by

$$\alpha_k \equiv \frac{1}{k!} \left. \frac{\partial^k}{\partial \varepsilon^k} \alpha_s(\bar{n}_g, \varepsilon, \eta) \right|_{\varepsilon = \bar{\varepsilon}}, \quad \alpha = a, b, c. \quad (3.32)$$

Fixing the temperature to that of the state at which  $\varepsilon = \bar{\varepsilon}$  and  $m = 0$ , such that

$$\frac{1}{\tau} = \left. \frac{\partial}{\partial \varepsilon} \hat{s}(m, \varepsilon, \eta) \right|_{m=0, \varepsilon=\bar{\varepsilon}} = a_1, \quad (3.33)$$

and minimizing (3.31) with respect to  $q$  yields

$$q = -\frac{b_1}{2a_2}m - \frac{4a_2^2c_1 - 4a_2b_1b_2 + 3a_3b_1^2}{8a_2^3}m^2 + \mathcal{O}(m^3), \quad (3.34)$$

as well as a second solution given by

$$q_2 = -\frac{2a_2}{3a_3} - \frac{2b_2}{3a_3}m - q. \quad (3.35)$$

We do not consider the solution  $q_2$  because it does not vanish at  $m = 0$ . Therefore, using equations (3.33) and (3.34) in (3.31) and replacing the latter in (3.11) gives

$$\begin{aligned} \hat{\varphi}(m, \tau, \eta) &= \frac{\bar{\varepsilon}}{\tau} - a_0 - b_0m + \left( \frac{b_1^2}{4a_2} - c_0 \right) m^2 \\ &+ \left( \frac{4a_2^2b_1c_1 - 2a_2b_1^2b_2 + a_3b_1^3}{8a_2^3} - d_0 \right) m^3 + \mathcal{O}(m^4). \end{aligned} \quad (3.36)$$

By writing the free energy as

$$\begin{aligned} \hat{\varphi}(m, \tau, \eta) &= a_\varphi(\bar{n}_g, \tau, \eta) + b_\varphi(\bar{n}_g, \tau, \eta)m + c_\varphi(\bar{n}_g, \tau, \eta)m^2 + d_\varphi(\bar{n}_g, \tau, \eta)m^3 \\ &+ e_\varphi(\bar{n}_g, \tau, \eta)m^4 + \mathcal{O}(m^5), \end{aligned} \quad (3.37)$$

one identifies the coefficients

$$a_\varphi(\bar{n}_g, \tau, \eta) = \frac{\bar{\varepsilon}}{\tau} - a_0, \quad (3.38)$$

$$b_\varphi(\bar{n}_g, \tau, \eta) = -b_0, \quad (3.39)$$

$$c_\varphi(\bar{n}_g, \tau, \eta) = \frac{b_1^2}{4a_2} - c_0, \quad (3.40)$$

$$d_\varphi(\bar{n}_g, \tau, \eta) = \frac{4a_2^2b_1c_1 - 2a_2b_1^2b_2 + a_3b_1^3}{8a_2^3} - d_0, \quad (3.41)$$

where the mean energy  $\bar{\varepsilon}$  must be taken as a function of  $\tau$  whose dependence is obtained through (3.33). Since  $\hat{s}(m, \bar{\varepsilon}, \eta) = a_0 + b_0m + c_0m^2 + d_0m^3 + \mathcal{O}(m^4)$ , the previous procedure provides the firsts terms of the Landau expansion of the canonical free energy as functions of the coefficients of the expansion of the microcanonical entropy at a certain energy  $\varepsilon = \bar{\varepsilon}$ . We observe that the coefficients  $c_\varphi$  and  $d_\varphi$  do

not vanish at the same critical conditions that  $c_0$  and  $d_0$  do. Hence, the critical point in the canonical ensemble will be different from the corresponding one in the microcanonical ensemble.

We highlight that we have started from a generic Landau expansion of the entropy. For the Thirring model  $\bar{\varepsilon}$  is given by (3.13) and the coefficients in the microcanonical ensemble by equations (3.15)-(3.19), so that using equations (3.39), (3.40), and (3.41) one obtains

$$b_\varphi(\bar{n}_g, \tau, \eta) = \frac{2(1 - \bar{n}_g)}{\tau} - \ln \left( \frac{1 - \bar{n}_g}{\bar{n}_g} \right) - \eta, \quad (3.42)$$

$$c_\varphi(\bar{n}_g, \tau, \eta) = \frac{Q_\tau(\bar{n}_g)}{\tau(1 - \bar{n}_g)\bar{n}_g}, \quad (3.43)$$

$$d_\varphi(\bar{n}_g, \tau, \eta) = \frac{1}{6} \left[ -\frac{1}{\bar{n}_g^2} + \frac{1}{(1 - \bar{n}_g)^2} \right], \quad (3.44)$$

with

$$Q_\tau(\bar{n}_g) \equiv \bar{n}_g^2 - \bar{n}_g + \frac{\tau}{2}. \quad (3.45)$$

The equilibrium states in the canonical ensemble require the conditions  $b_\varphi(\bar{n}_g, \tau, \eta) = 0$ , defining  $\bar{n}_g = \bar{n}_g(\tau, \eta)$ , and  $c_\varphi(\bar{n}_g, \tau, \eta) \geq 0$ .

### Canonical critical point

As it happens in the microcanonical ensemble in the  $(\varepsilon, \eta)$  plane, the canonical phase diagram exhibits in the  $(\tau, \eta)$  plane a line of first-order phase transition that ends at a critical point, here specified by the reduced temperature and volume  $\tau_{\text{cp}}$  and  $\eta_{\text{cp}}$ , respectively, for which the fraction of free particles is denoted by  $n_{\text{cp}}$ . The critical parameters can now be obtained by solving the system of equations

$$\begin{aligned} b_\varphi(n_{\text{cp}}, \tau_{\text{cp}}, \eta_{\text{cp}}) &= 0, \\ c_\varphi(n_{\text{cp}}, \tau_{\text{cp}}, \eta_{\text{cp}}) &= 0, \\ d_\varphi(n_{\text{cp}}, \tau_{\text{cp}}, \eta_{\text{cp}}) &= 0. \end{aligned} \quad (3.46)$$

Since  $d_\varphi$  depends only on  $\bar{n}_g$ , one immediately obtains that the critical point can occur only for  $n_{\text{cp}} = \bar{n}_g = 1/2$ . Substituting it in equation (3.43) or equation (3.45) one then finds that the critical temperature is  $\tau_{\text{cp}} = 1/2$ . Finally, replacing these values in equation (3.42) we get that  $\eta_{\text{cp}} = 2$ . However, it is useful to consider the discriminant of the quadratic polynomial  $Q_\tau(\bar{n}_g)$ , given in equation (3.45), following a procedure analogous to that used in the microcanonical case, where the discriminant of the quartic polynomial  $P_\varepsilon(\bar{n}_g)$  was studied. The discriminant of  $Q_\tau(\bar{n}_g)$

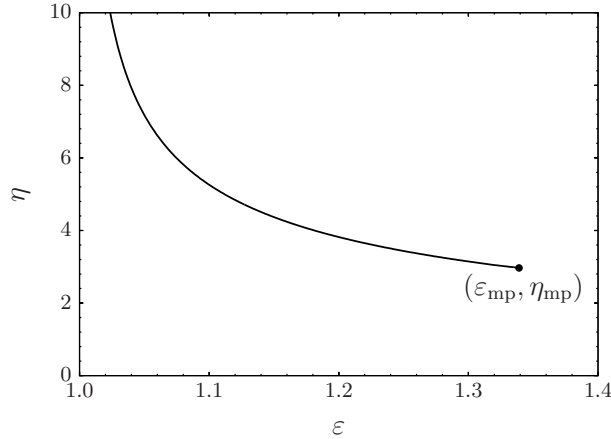


**Figure 3.2:** Phase diagram in the  $(\varepsilon, \eta)$  plane, showing the transition line in the microcanonical ensemble. The plot shows the curve  $\eta(\varepsilon)$  which represents the points defined by the reduced energy  $\varepsilon$  and reduced volume  $\eta$  at which first-order phase transitions take place in the microcanonical ensemble. The transition line terminates at a critical point represented by the point  $(\varepsilon_{\text{mp}}, \eta_{\text{mp}})$ . The values of the critical parameters are  $\varepsilon_{\text{mp}} \simeq 1.339$  and  $\eta_{\text{mp}} \simeq 2.969$ . Taken from [2].

takes the form  $\Delta_Q(\tau) = 1 - 2\tau$ , and we know that the critical temperature satisfies  $\Delta_Q(\tau_{\text{cp}}) = 0$ , giving  $\tau_{\text{cp}} = 1/2$ . In this case, the roots of  $Q_\tau(\bar{n}_g)$ , given by

$$n_1(\tau) = \frac{1}{2} - \frac{\sqrt{\Delta_Q(\tau)}}{2}, \quad (3.47)$$

$$n_2(\tau) = \frac{1}{2} + \frac{\sqrt{\Delta_Q(\tau)}}{2}, \quad (3.48)$$

coincide and are equal to  $n_{\text{cp}} = 1/2$ . The last expressions also show that for  $\tau > \tau_{\text{cp}}$ ,  $Q_\tau(\bar{n}_g)$  has no real roots and, hence, the second order coefficient  $c_\varphi$  does not vanish. This means that in such a case the condition  $b_\varphi(\bar{n}_g, \tau, \eta) = 0$  defines only one state of equilibrium, and, therefore, phase transitions can only occur if  $\tau < 1/2$ .

We emphasize that, for the Thirring model, the coefficients (3.42), (3.43), and (3.44) of the Landau expansion can be alternatively obtained from the free energy (3.12), instead of the method we employed here. In fact, from (3.12), the remaining coefficient of (3.37) takes the form

$$e_\varphi(\bar{n}_g, \tau, \eta) = \frac{1}{12} \left[ \frac{1}{\bar{n}_g^3} + \frac{1}{(1 - \bar{n}_g)^3} \right]. \quad (3.49)$$

However, taking into account that the expansions (3.14) and (3.31) do not depend on the model, some general conclusions can be obtained from this method. From

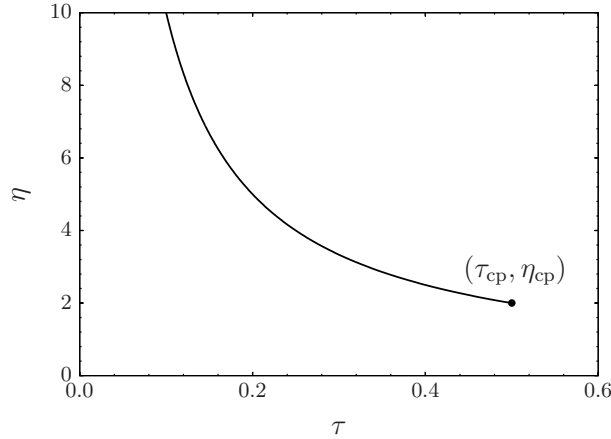


**Figure 3.3:** Phase diagram in the  $(\tau, \eta)$  plane, showing the transition line in the canonical ensemble. The plot shows the curve  $\eta(\tau)$  which represents the points defined by the reduced temperature  $\tau$  and reduced volume  $\eta$  at which first-order phase transitions take place in the canonical ensemble. The transition line terminates at a critical point represented by the point  $(\tau_{\text{cp}}, \eta_{\text{cp}})$ . The values of the critical parameters are  $\tau_{\text{cp}} = 1/2$  and  $\eta_{\text{cp}} = 2$ . Taken from [2].

equation (40) one sees that at the canonical critical point, where  $c_\varphi = 0$ ,  $c_0$  is different from zero if  $b_1 \neq 0$ , implying that the two critical points do not coincide in general, regardless of the model. Of course, for a particular model, the Landau expansion may present a symmetry with respect to the order parameter that enforces the condition  $b_1 = 0$  [141]; here we consider that there is no such a symmetry. Furthermore, it is important to stress that, according to the Landau theory, we are assuming analyticity of the free energy at the canonical critical point. Analyticity here can be assumed because the system is nonadditive and for these systems actually there is no phase separation at the transition line. Therefore, this discussion does not apply to short-range interacting systems, since these systems do undergo phase separation at a first-order transition, which, in addition, occurs under the same conditions in the different ensembles.

### 3.1.4 Microcanonical and canonical phase diagrams

In this section we will draw a comparison between the microcanonical and canonical phase diagrams. Since the transition is first-order in both ensembles, the two equilibrium configurations associated to the transition are characterized by a jump in  $\bar{n}_g$  and, hence, in the associated thermodynamic properties (those which are not control parameters).

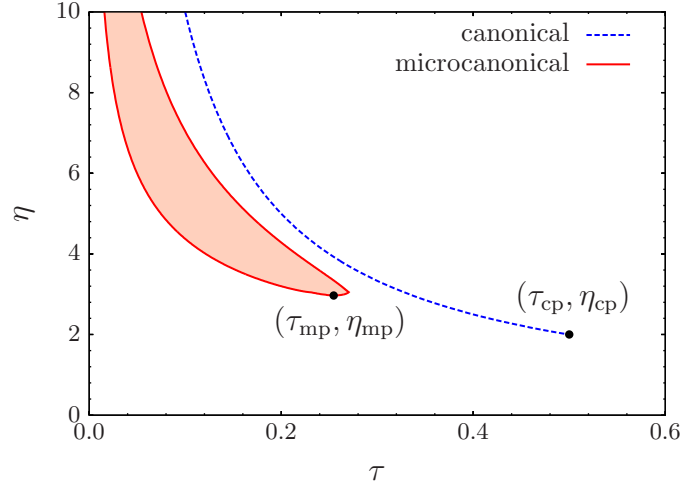


**Figure 3.4:** Comparison of the microcanonical and canonical phase diagrams. The reduced volume  $\eta$  is shown as a function of the temperature  $\tau$  at the transition line of the two ensembles. In the microcanonical ensemble, there are two temperature branches that join at the critical point. The temperatures within the region between this two branches are forbidden in the microcanonical ensemble. In the canonical ensemble,  $\tau$  is a control parameter and, thus, has no discontinuity at the transition line. The critical parameters are  $\tau_{\text{mp}} \simeq 0.2547$ ,  $\eta_{\text{mp}} \simeq 2.969$ ,  $\tau_{\text{cp}} = 1/2$  and  $\eta_{\text{cp}} = 2$ . Taken from [2].

In figure 3.2, we plotted the microcanonical transition line  $\eta(\varepsilon)$ . This line indicates the points  $(\varepsilon, \eta)$  at which phase transition takes place, i.e., when the entropy reaches the same value at the two maxima. We emphasize that both  $\varepsilon$  and  $\eta$  are control parameters in the microcanonical ensemble. In the figure 3.3, we showed the canonical transition line  $\eta(\tau)$  containing the points  $(\tau, \eta)$  at which a phase transition occurs in the canonical ensemble, corresponding to the coincidence of the two free energy minima. We recall that  $\tau$  and  $\eta$  are the control parameters in this ensemble.

On the one hand, in the microcanonical case, the jump in  $\bar{n}_g$  produces a jump in the temperature. This can be seen in figure 3.4 in the microcanonical phase diagram in the  $(\tau, \eta)$  plane: we plot  $\eta$  at the transition line as a function of the microcanonical temperature  $\tau$ . The phase diagram has two branches starting at small temperatures and high  $\eta$  that join smoothly at the critical point. According to (3.8), the microcanonical temperature at the critical point is  $\tau_{\text{mp}} \simeq 0.2547$ . We highlight that the temperatures between the two branches of the phase diagram are forbidden for the system in the microcanonical ensemble. In addition, for comparison purposes, in figure 3.4 the canonical phase diagram is also shown, where  $\tau$  is a control parameter and thus has no discontinuity. We observe that the microcanonical and canonical critical points are far from each other and that the temperatures corresponding to the canonical phase transition are allowed in the microcanonical

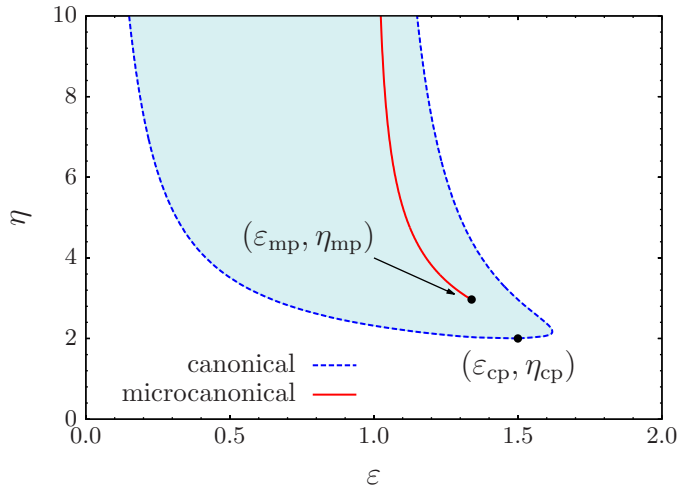


**Figure 3.5:** Comparison of the microcanonical and canonical phase diagrams. The reduced volume  $\eta$  is shown as a function of the reduced energy  $\varepsilon$  at the transition line of the two ensembles. In the canonical ensemble, there are two energy branches that join at the critical point. The energies within the region between this two branches are forbidden in the canonical ensemble. In the microcanonical ensemble,  $\varepsilon$  is a control parameter and, thus, has no discontinuity at the transition line. The critical parameters are  $\varepsilon_{\text{mp}} \simeq 1.339$ ,  $\eta_{\text{mp}} \simeq 2.969$ ,  $\varepsilon_{\text{cp}} = 3/2$  and  $\eta_{\text{cp}} = 2$ . Taken from [2].

ensemble. On the other hand, in the canonical ensemble the jump in  $\bar{n}_g$  at the transition produces a jump in the energy, as shown in figure 3.5 in the phase diagram in the  $(\varepsilon, \eta)$  plane. In this diagram, there are two energy branches that join smoothly at the canonical critical point, the energy at this point being  $\varepsilon_{\text{cp}} = 3/2$ . Moreover, due to the jump, the values of the energy between the two branches are forbidden in the canonical ensemble. We finally observe that the energies at the transition line in the microcanonical ensemble, also shown in figure 3.5, lie within the region of forbidden canonical energies.

To get a clearer picture of the behavior of the system when the energy is a control parameter, in comparison with the situation in which the system is in contact with a thermostat at fixed temperature, in the figure 3.6 we show several caloric curves in both the microcanonical and canonical ensembles. These curves are shown for different values of the reduced volume  $\eta$ . When  $\eta \leq \eta_{\text{cp}}$ , the temperature-energy relation  $\tau(\varepsilon, \eta)$  is invertible, in the sense that  $\varepsilon(\tau, \eta)$  can be unequivocally obtained from it, and the microcanonical and canonical ensembles are equivalent. Notice that in this case the Legendre-Fenchel transform (3.9) reduces to the usual Legendre transform. For values of  $\eta$  such that the temperature-energy relation is not invertible in the microcanonical ensemble, the system undergoes a first order phase transition in the canonical ensemble. Moreover, for  $\eta > \eta_{\text{mp}}$ , the microcanonical

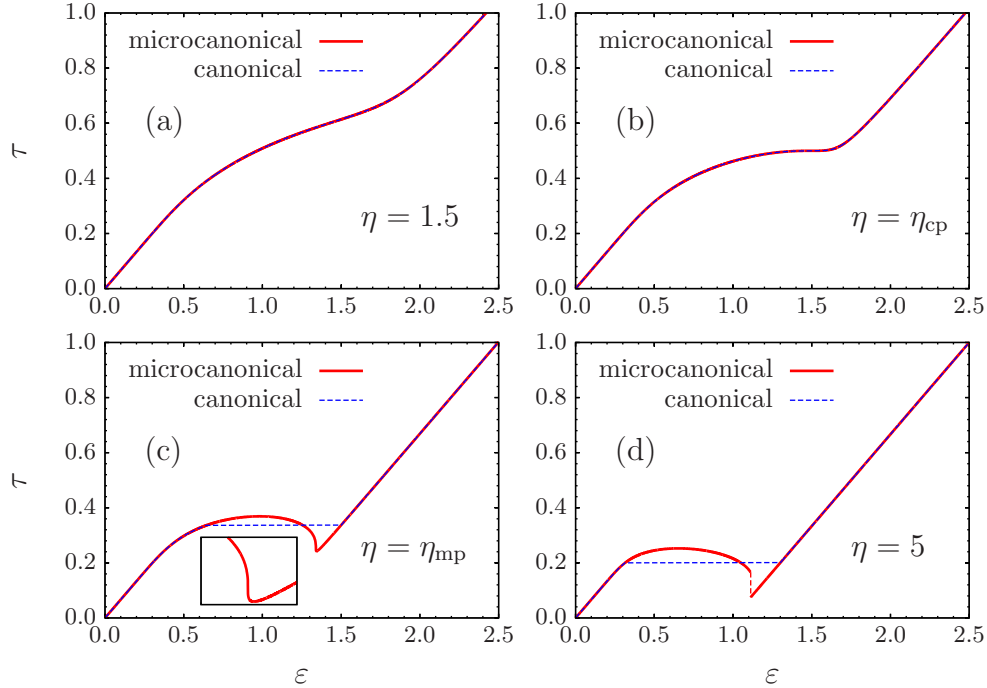


**Figure 3.6:** Caloric curves in the microcanonical and canonical ensembles for several values of the reduced volume  $\eta$ . For  $\eta \geq \eta_{\text{cp}}$  the two ensembles are equivalent, as shown in (a) and (b). In (c) and (d), a region of negative specific heat in the microcanonical ensemble appears for  $\eta > \eta_{\text{cp}}$ , which is jumped over by a first order transition in the canonical ensemble. In (c), the curve has a vertical tangent when approaching from both the left and the right to the critical energy  $\varepsilon_{\text{mp}}$ , occurring just before the local minimum (see the enlargement in the inset). For  $\eta > \eta_{\text{mp}}$ , in (d), the system develops a temperature jump in the microcanonical ensemble. This jump is denoted with a red dashed line. Taken from [2].

phase transition is always jumped over by the transition in the canonical ensemble. This is, of course, in agreement with the fact that the microcanonical critical point ( $\eta = \eta_{\text{mp}}$ ) lies in the region of forbidden energies in the canonical ensemble.

It is interesting to note that the regions of ensemble inequivalence and the occurrence of phase transitions in both ensembles can be deduced from singular points in the  $s(\varepsilon, \eta)$  curve or, equivalently, from the microcanonical temperature-energy relation  $\tau(\varepsilon, \eta)$ . We identify two different codimension 1 singularities, as classified in [43]. Notice that here  $\eta$  is the (only one) parameter, in addition to the energy, that can produce a change in the structure of  $s(\varepsilon, \eta)$  or the caloric curve. These singular points can be observed in the figure 3.6, as we discuss in what follows. At  $\eta = \eta_{\text{cp}}$ , a singularity arises due to convexification, in which a point with horizontal tangent appears in the curve  $\tau(\varepsilon, \eta_{\text{cp}})$  (the entropy is concave at this point). This corre-

sponds to the canonical critical point. The second singularity occurs at  $\eta = \eta_{\text{mp}}$ , which is a maximization singularity, in that a point with vertical tangent appears in the curve  $\tau(\varepsilon, \eta_{\text{mp}})$ . Such a point correspond to the microcanonical critical point.

### 3.1.5 Replica energy and scaling

While phase diagrams have been studied in detail, there are still other aspects of interest in the thermodynamics of this model. In particular, we want to study how the entropy scales when the constraint variables are scaled. As the replica energy does not vanish for this system, which will be shown below, one expects that the entropy scales nonlinearly if the constraint variables are linearly scaled. This fact, indeed, will be confirmed by the following analysis.

The Thirring model is of mean-field type, so that the treatment given in Section 2.2.1 for the microcanonical ensemble applies in this case. According to this, the microcanonical entropy of the system in an equilibrium configuration can be written as

$$S = - \int n(\mathbf{x}) \left[ \ln \left( n(\mathbf{x}) \lambda_T^3 \right) - \frac{5}{2} \right] d^3 \mathbf{x}, \quad (3.50)$$

where  $n(\mathbf{x})$  and  $\lambda_T$  are to be determined according to the variational problem (2.73). Since the interactions are described by the pair potential (3.1), the number density is given by

$$n(\mathbf{x}) = \begin{cases} N(1 - n_g)/V_0 & \text{if } \mathbf{x} \in V_0 \\ N n_g / (V - V_0) & \text{if } \mathbf{x} \notin V_0 \end{cases} \quad (3.51)$$

evaluated at the fraction of free-gas particles  $n_g = \bar{n}_g$  that maximizes the entropy. In addition, the potential energy of the system is

$$W = -\nu N^2 (1 - n_g)^2 \Big|_{n_g = \bar{n}_g}, \quad (3.52)$$

so that using (2.75) the microcanonical temperature can be written as

$$T = \frac{2\nu N}{3} \left[ \Lambda + (1 - n_g)^2 \right]_{n_g = \bar{n}_g}, \quad (3.53)$$

where we have introduced the reduced energy  $\Lambda \equiv E/(\nu N^2)$  which is related to  $\varepsilon$  according to  $\Lambda = \varepsilon - 1$ ; we use  $\Lambda$  instead of  $\varepsilon$  because the former variable is more appropriate to studying the scaling laws of the system. In terms of the temperature (3.53), the thermal wavelength is given by

$$\lambda_T = \frac{\lambda_0}{\sqrt{N}} \left[ \Lambda + (1 - n_g)^2 \right]^{-1/2} \quad (3.54)$$

evaluated at  $n_g = \bar{n}_g$ , where  $\lambda_0 = \sqrt{3\hbar^2/(4\pi\nu m)}$ . Therefore, taking into account equations (3.52) and (3.53) together with the number density (3.51) and the thermal wavelength (3.54), the functional (2.72) takes the form

$$\begin{aligned} \hat{S} = & \frac{3}{2}N \ln \left[ \Lambda + (1 - n_g)^2 \right] - N(1 - n_g) \ln (1 - n_g) - Nn_g \ln n_g \\ & + Nn_g\eta - N \ln (e^\eta + 1) + N \ln (cVN^{1/2}), \end{aligned} \quad (3.55)$$

where  $c = e^{5/2}\lambda_0^{-3}$  and we recall that  $\eta = \ln(V/V_0 - 1)$ . Because of we have imposed the conservation of the number of particles in using (3.51) and the dependence of the temperature on the control parameters via (3.54), the variational problem (2.73) now reads

$$S(E, V, N) = \sup_{n_g} \hat{S}[n_g, E, V, N] \quad (3.56)$$

with  $n_g$  as the only variational parameter, and where the dependence on  $E$  and  $V$  is implicit through  $\Lambda$  and  $\eta$ , respectively. For fixed  $E$ ,  $V$ , and  $N$ , and according to the above variational problem, the fraction  $\bar{n}_g = \bar{n}_g(\Lambda, \eta)$  that defines the equilibrium states of the system is then obtained by solving

$$\frac{3(1 - \bar{n}_g)}{\Lambda + (1 - \bar{n}_g)^2} - \ln \left( \frac{1 - \bar{n}_g}{\bar{n}_g} \right) - \eta = 0. \quad (3.57)$$

The microcanonical entropy per particle  $s(\Lambda, \eta) \equiv S(E, V, N)/N$  takes the form

$$\begin{aligned} s(\Lambda, \eta) = & \frac{3}{2} \ln \left[ \Lambda + (1 - \bar{n}_g)^2 \right] - (1 - \bar{n}_g) \ln(1 - \bar{n}_g) \\ & - \bar{n}_g \ln \bar{n}_g + \bar{n}_g\eta - \ln (e^\eta + 1) + s_0 \\ \equiv & s_1(\Lambda, \eta) + s_0, \end{aligned} \quad (3.58)$$

with  $s_0 = \ln(cVN^{1/2})$ . The entropy per particle (3.58) contains the constant terms we neglected in the previous section when constructing the microcanonical phase diagram, as can be seen by comparison of equations (3.55) and (3.6). Such terms are relevant for the scaling laws. We remark, however, that the equilibrium states obtained from the solution of (3.57) are the same as those we considered in the previous section (that is why these terms could be omitted).

Since the particles outside the core are free, the pressure  $P$  at the boundary of the system is clearly given by  $P(V - V_0) = N\bar{n}_gT$ , which can also be obtained from

$$\frac{P}{T} = \left( \frac{\partial S}{\partial V} \right)_{E, N} = \left. \frac{\partial \hat{S}}{\partial V} \right|_{n_g = \bar{n}_g}. \quad (3.59)$$

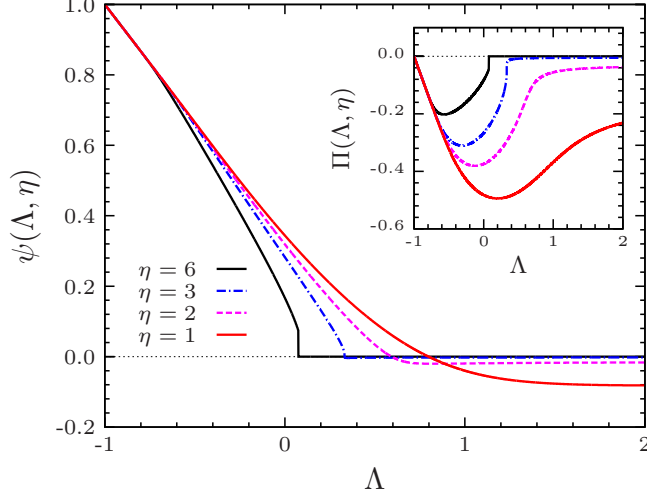


**Figure 3.7:** Microcanonical reduced replica energy for the Thirring model as a function of the reduced energy for different values of  $\eta$ . In the inset we show  $\Pi(\Lambda, \eta) = P^{(e)}V/(\nu N^2)$ , which is one of the contributions to the reduced replica energy; the other contribution,  $-W/(\nu N^2)$ , decreases for increasing  $\Lambda$  and  $\eta$ . Taken from [5].

Taking into account that the excess pressure is given by  $P^{(e)} = P - NT/V$ , we introduce

$$\Pi(\Lambda, \eta) \equiv \frac{P^{(e)}V}{\nu N^2} = \tau [\bar{n}_g (1 + e^{-\eta}) - 1], \quad (3.60)$$

where  $\tau = T/(\nu N)$  with  $T$  obtained from (3.53). In addition, the replica energy can be computed from the relation  $\mathcal{E} = -W + P^{(e)}V$ , so that we define the reduced microcanonical replica energy as

$$\psi \equiv \frac{\mathcal{E}}{\nu N^2} = (1 - \bar{n}_g)^2 + \tau [\bar{n}_g (1 + e^{-\eta}) - 1]. \quad (3.61)$$

Using (3.57) to express  $e^{-\eta}$  in (3.61), it is not difficult to see that for  $\bar{n}_g > 0$  and  $\Lambda \gg 3(1 - \bar{n}_g)$ ,  $\psi$  approaches  $W/(\nu N^2) = -(1 - \bar{n}_g)^2$ , which, in turn, decreases in modulus for increasing  $\eta$ . This behavior can be seen in figure 3.7 for different values of the reduced volume  $\eta$ . Notice that in the plot  $\psi$  presents a jump at a value of  $\Lambda$  slightly greater than zero for  $\eta = 6$ ; this is because the system undergoes a phase transition and the replica energy contains this information.

Furthermore, in order to evince the intrinsic nonadditivity of the system, we now study how the entropy behaves when the constraint variables are scaled. With this purpose, we introduce a scale factor  $\xi \geq 1$  and a scale transformation that acts on a quantity  $Q$  such that  $Q' = \xi Q$ . Since  $E'/(\nu N'^2) = \Lambda/\xi$  and  $V' = \xi V$ , the dimensionless parameters  $\Lambda$  and  $\eta$  transform according to  $\Lambda \rightarrow \tilde{\Lambda} = \Lambda/\xi$  and  $\eta \rightarrow \tilde{\eta} =$

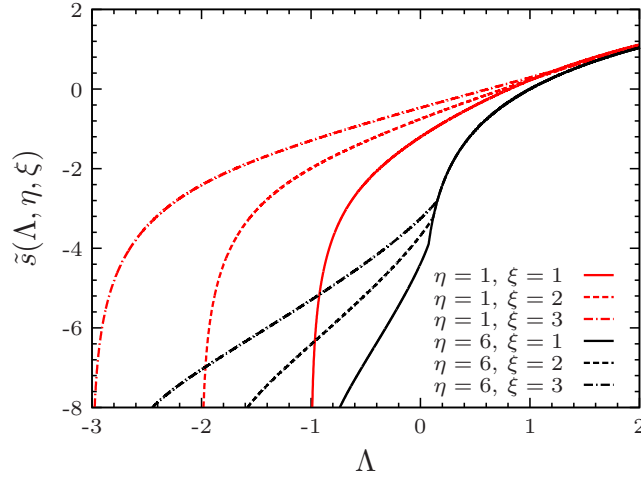


**Figure 3.8:** Scaled microcanonical entropy per particle for the Thirring model as a function of  $\Lambda$  for different values of the scale factor and the reduced volume  $\eta$ . The curves get close to each other for values of  $\Lambda$  for which the replica energy becomes relatively small. Even for high energies, nonadditivity makes impossible a strict scaling regime. Taken from [5].

$\ln[\xi(e^\eta + 1) - 1]$ . We can write  $S'(E', V', N')/N' = s_1(\tilde{\Lambda}, \tilde{\eta}) + \ln(cVN^{1/2}) + \frac{3}{2} \ln \xi$ , where the last term comes from the scaling of the volume and the number of particles in  $s_0$ . The fraction  $\tilde{n}_g$  now is obtained from (3.57) with  $\tilde{\Lambda}$  and  $\tilde{\eta}$  in the place of  $\Lambda$  and  $\eta$ , respectively. Moreover, the entropy per particle of the fully scaled system can be expressed as a function of the parameters of the system without scaling by defining  $\tilde{s}(\Lambda, \eta, \xi) \equiv s_1(\tilde{\Lambda}, \tilde{\eta}) + \frac{3}{2} \ln \xi$ , where we have subtracted  $s_0$  for convenience since it does not depend on  $\xi$ . The scaled entropy per particle  $\tilde{s}$  is shown in figure 3.8. Due to the nonadditivity, it is clearly seen that the entropy strongly depends on the scale transformation, as expected. As the energy increases, however, in this case the system becomes, so to speak, more additive since the curves tend to run together, although they never touch each other. If the entropy were a linear homogeneous function of  $E$ ,  $V$ , and  $N$ , all curves would collapse into a single one. The interesting fact is that the nonadditivity becomes less noticeable when the replica energy is relatively small, as should be expected since  $\mathcal{E} = 0$  for additive systems.

## 3.2 Equilibria in the unconstrained ensemble

As anticipated in Section 2.1.2, here we consider a model showing states of thermodynamic equilibrium in the unconstrained ensemble. The model introduced below is a modification of the Thirring model, which contains an additional term in the

Hamiltonian accounting for the interaction of particles outside the core region. Furthermore, the equilibrium configurations of the model in the unconstrained ensemble are compared with those of the grand canonical and canonical ensembles. This comparison is in agreement with known results: the more the ensemble is constrained by fixing the energy, volume, or number of particles, the larger the space of parameters defining the equilibrium configurations.

### 3.2.1 Modified Thirring model

We now introduce a model that, as discussed in the following sections, attains equilibrium configurations under completely open conditions. As in the preceding section, consider a system of  $N$  particles in a volume  $V$  with a Hamiltonian of the form (2.53) in three dimensions. The interactions in this model are defined by

$$\phi(\mathbf{q}_i, \mathbf{q}_j) = -2\nu [\theta_{V_0}(\mathbf{q}_i)\theta_{V_0}(\mathbf{q}_j) + b\theta_{V_1}(\mathbf{q}_i)\theta_{V_1}(\mathbf{q}_j)], \quad (3.62)$$

where the above functions are given

$$\begin{aligned} \theta_{V_0}(\mathbf{q}_i) &= \begin{cases} 1 & \text{if } \mathbf{q}_i \in V_0 \\ 0 & \text{if } \mathbf{q}_i \notin V_0 \end{cases}, \\ \theta_{V_1}(\mathbf{q}_i) &= \begin{cases} 1 & \text{if } \mathbf{q}_i \notin V_0 \\ 0 & \text{if } \mathbf{q}_i \in V_0 \end{cases}, \end{aligned} \quad (3.63)$$

and  $\nu > 0$  and  $b$  are constants. As before,  $V_0$  is the volume of an internal region of the system such that  $V_0 < V$ , and  $V_1$  is the volume of the region outside  $V_0$  so that  $V_1 = V - V_0$ . In this way,  $V_0$  is a parameter of the interaction potential that do not depend on the state of the system. Hence, the total potential energy in the large  $N$  limit is given by

$$\hat{W}(N_0, N_1) \equiv \sum_{i>j}^N \phi(\mathbf{q}_i, \mathbf{q}_j) = -\nu (N_0^2 + bN_1^2), \quad (3.64)$$

where  $N_0$  is the number of particles in  $V_0$  and  $N_1 = N - N_0$  is the number of particles in  $V_1$  for a given configuration. Notice that  $N_0 = N_0(\mathbf{q})$  and  $N_1 = N_1(\mathbf{q})$ , so that  $\hat{W}$  depends implicitly on the position of all particles. The Thirring model is obtained in the particular case  $b = 0$ . Furthermore, the model is solvable in the different statistical ensembles, and below we focus on the unconstrained ensemble and compare it with the canonical and grand canonical cases. In the following sections it will become clear why we consider this modification of the model.

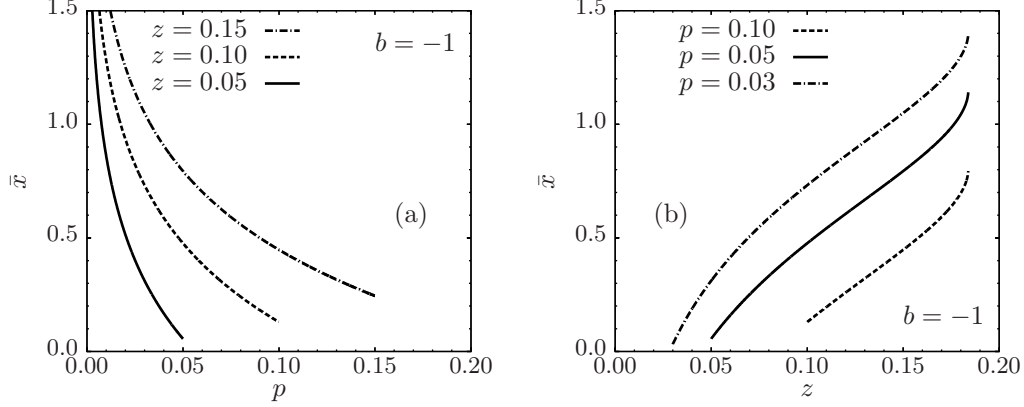


**Figure 3.9:** Reduced number of particles  $\bar{x}$  for the modified Thirring model with  $b = -1$  in the unconstrained ensemble: in (a), as a function of the reduced pressure  $p$  with constant fugacity  $z$ , and, in (b), as a function of the fugacity with constant reduced pressure. We remind that in this and in the following four figures we have, as requested by stability in the unconstrained ensemble,  $p < z$  and  $z < 1/(2e)$ . Taken from [1].

### 3.2.2 Modified Thirring model under completely open conditions

Here we study the stability of the modified Thirring model in the unconstrained ensemble. Thus, we will assume that the system is in contact with a reservoir characterized by fixed temperature  $T$ , pressure  $P$ , and chemical potential  $\mu$ .

Consider the canonical partition function for this model, which is given by

$$Z(T, V, N) = \int \frac{d^{3N} \mathbf{q} d^{3N} \mathbf{p}}{h^{3N} N!} e^{-\beta \mathcal{H}(\mathbf{p}, \mathbf{q})} = \int \frac{d^{3N} \mathbf{q}}{N!} \frac{e^{-\beta \hat{W}(N_0, N_1)}}{\lambda_T^{3N}}, \quad (3.65)$$

Thus, using equation (2.49), the unconstrained partition function becomes (we take  $V$  as a continuous variable)

$$\Upsilon(T, P, \mu) = \int dV \sum_N \int \frac{d^{3N} \mathbf{q}}{N!} \lambda_T^{-3N} e^{-\beta \hat{W}(N_0, N_1) + \beta \mu N - \beta P V}. \quad (3.66)$$

Following Thirring's method [18], as done in Section 2.2, the partition function can be computed by replacing the integral over coordinates with a sum over the occupation numbers in each region of the system,

$$\int \frac{d^{3N} \mathbf{q}}{N!} \rightarrow \sum_{N_0, N_1} \delta_{N, N_0 + N_1} \frac{V_0^{N_0} V_1^{N_1}}{N_0! N_1!}, \quad (3.67)$$

where the sum runs over all possible values of  $N_0$  and  $N_1$  and the Kronecker  $\delta$  enforces the condition  $N = N_0 + N_1$ . This leads to

$$\Upsilon(T, P, \mu) = \int dV \sum_{N_0, N_1} e^{-\beta \hat{\mathcal{E}}(T, P, \mu, V, N_0, N_1)}, \quad (3.68)$$

where we have introduced (from now on we omit writing down explicitly the dependence on the control parameters)

$$\hat{\mathcal{E}}(V, N_0, N_1) = \hat{W}(N_0, N_1) + PV - T \sum_k N_k + T \sum_k N_k \left[ \ln \left( N_k \frac{\lambda_T^3}{V_k} \right) - \frac{\mu}{T} \right], \quad (3.69)$$

with  $k = 0, 1$ , and we have used Stirling's approximation. Since the replica energy is given by  $\mathcal{E} = -T \ln \Upsilon$ , using the saddle-point approximation one obtains

$$\mathcal{E} = \inf_{V, N_0, N_1} \hat{\mathcal{E}}(V, N_0, N_1). \quad (3.70)$$

Thus, minimization with respect to  $V$ ,  $N_0$ , and  $N_1$  requires that

$$P = \frac{T \bar{N}_1}{\bar{V} - V_0}, \quad (3.71)$$

$$\mu = -2\nu \bar{N}_0 + T \ln \left( \frac{\bar{N}_0}{V_0} \lambda_T^3 \right), \quad (3.72)$$

$$\mu = -2b\nu \bar{N}_1 + T \ln \left( \frac{\bar{N}_1}{\bar{V} - V_0} \lambda_T^3 \right), \quad (3.73)$$

where  $\bar{V}$ ,  $\bar{N}_0$ , and  $\bar{N}_1$  are the values of the volume and the number of particles in each region that minimizes the replica energy. It is clear that  $\bar{V}$ ,  $\bar{N}_0$ , and  $\bar{N}_1$  are functions of  $T$ ,  $P$ , and  $\mu$ , whose dependence is implicit through equations (3.71), (3.72), and (3.73). The mean value of the total number of particles is then given by  $\bar{N} = \sum_k \bar{N}_k$ . Moreover, the total potential energy for stable configurations in the unconstrained ensemble becomes

$$W \equiv \hat{W}(\bar{N}_0, \bar{N}_1) = -\nu (\bar{N}_0^2 + b\bar{N}_1^2). \quad (3.74)$$

Hence, notice that from equations (3.72) and (3.73) one obtains

$$\mu \bar{N} = T \sum_k \bar{N}_k \ln \left( \frac{\bar{N}_k}{V_k} \lambda_T^3 \right) + 2W, \quad (3.75)$$

with  $V_1 = \bar{V} - V_0$ . Therefore, using equations (3.69) and (3.70), we see, again, that the replica energy takes the form

$$\mathcal{E} = -W + P^{(e)} \bar{V}, \quad (3.76)$$

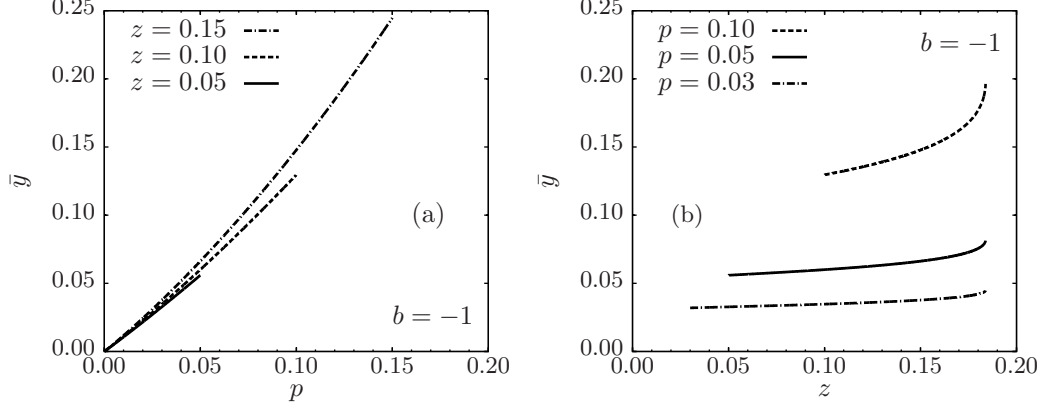


**Figure 3.10:** Reduced density  $\bar{y}$  for the modified Thirring model with  $b = -1$  in the unconstrained ensemble: in (a), as a function of the reduced pressure  $p$  with constant fugacity  $z$ , and, in (b), as a function of the fugacity with constant reduced pressure. Taken from [1].

where  $P^{(e)} = P - \bar{N}T/\bar{V}$  is the excess pressure.

In order to study the stability of the system in the unconstrained ensemble, we introduce the dimensionless variables

$$v = \frac{V - V_0}{V_0}, \quad x_0 = \frac{\nu N_0}{T}, \quad x_1 = \frac{\nu N_1}{T}, \quad (3.77)$$

which will be denoted as  $\bar{v}$ ,  $\bar{x}_0$ , and  $\bar{x}_1$  when evaluated at  $\bar{V}$ ,  $\bar{N}_0$ , and  $\bar{N}_1$ , respectively. In addition, we define the reduced pressure  $p$  and the relative fugacity  $z$  by

$$p \equiv \frac{\nu V_0}{T^2} P, \quad z \equiv e^{(\mu - \mu_0)/T}, \quad (3.78)$$

where

$$\mu_0 = T \ln \left( \frac{T \lambda_T^3}{\nu V_0} \right). \quad (3.79)$$

Since controlling  $T$ ,  $P$ , and  $\mu$  is equivalent to controlling  $T$ ,  $p$ , and  $z$ , the latter set of variables can be taken as the set of control parameters in this ensemble. Using these variables, from equations (3.71), (3.72), and (3.73) one obtains

$$\bar{x}_0 = z e^{2\bar{x}_0}, \quad (3.80)$$

$$\bar{x}_1(p, z) = \frac{1}{2b} \ln \left( \frac{p}{z} \right), \quad (3.81)$$

$$\bar{v}(p, z) = \frac{1}{2bp} \ln \left( \frac{p}{z} \right), \quad (3.82)$$

where equation (3.80) defines implicitly  $\bar{x}_0 = \bar{x}_0(z)$ . Furthermore, let us consider the reduced replica energy  $\varphi_U = \nu \hat{\mathcal{E}}/T^2$  and the function  $\hat{\varphi}_U = \nu \hat{\mathcal{E}}/T^2$ , where, using equations (3.77) and (3.78), the latter can be written as

$$\hat{\varphi}_U(v, x_0, x_1) = x_0 \left[ \ln \left( \frac{x_0}{z} \right) - 1 \right] - x_0^2 + p(v+1) + x_1 \left[ \ln \left( \frac{x_1}{vz} \right) - 1 \right] - bx_1^2. \quad (3.83)$$

We note that with the dimensionless quantities, i.e., in the reduced replica energy and in equations (3.80)-(3.82), the temperature does not appear; therefore  $T$  acts as a simple scaling factor. The condition (3.70) becomes

$$\varphi_U(\bar{v}, \bar{x}_0, \bar{x}_1) = \inf_{v, x_0, x_1} \hat{\varphi}_U(v, x_0, x_1). \quad (3.84)$$

Since the Hessian matrix  $H_U$  associated to  $\hat{\varphi}_U$  at the stationary point  $(\bar{v}, \bar{x}_0, \bar{x}_1)$  takes the form

$$H_U = \begin{pmatrix} 2bp^2 \ln^{-1}(p/z) & 0 & -2bp \ln^{-1}(p/z) \\ 0 & 1/\bar{x}_0 - 2 & 0 \\ -2bp \ln^{-1}(p/z) & 0 & 2b [\ln^{-1}(p/z) - 1] \end{pmatrix}, \quad (3.85)$$

one infers that  $\bar{v}$ ,  $\bar{x}_0$ , and  $\bar{x}_1$  lead to a minimum of replica energy when

$$\bar{x}_0 < 1/2, \quad b < 0, \quad p < z. \quad (3.86)$$

The last two inequalities guarantee, from equations (3.81) and (3.82), that  $\bar{x}_1 > 0$  and  $\bar{v} > 0$ . Moreover, equation (3.80) has two positive solutions if  $0 < z < z_0$  with  $z_0 = 1/(2e) \approx 0.1839$ , while no real solution exists for  $z > z_0$ . Notice that the smallest of the roots of equation (3.80) is that corresponding to  $0 < \bar{x}_0 < 1/2$ . Thus, this implies that the fugacity can not be arbitrarily large in order for the system to be stable, and that

$$0 < p < z < z_0. \quad (3.87)$$

Therefore, we conclude that stable configurations in the unconstrained ensemble can indeed be realized. In addition, we stress that there are no different states minimizing the replica energy for the same control parameters in the stability region, hence the model has no phase transitions in the unconstrained ensemble. Furthermore, it is clear that equations (3.81) and (3.82) are not well defined when  $b = 0$ . As a consequence, the Thirring model ( $b = 0$ ) does not attain stable equilibrium states in this ensemble; in this case,  $T$ ,  $P$ , and  $\mu$  can not be taken as independent control parameters, just as happens for macroscopic systems with short-range interactions. We will come back to this point in Section 3.3. As a concluding remark regarding the stability of this particular model in the unconstrained ensemble, we note that the condition  $b < 0$  means that the interactions within the outer parts of the system

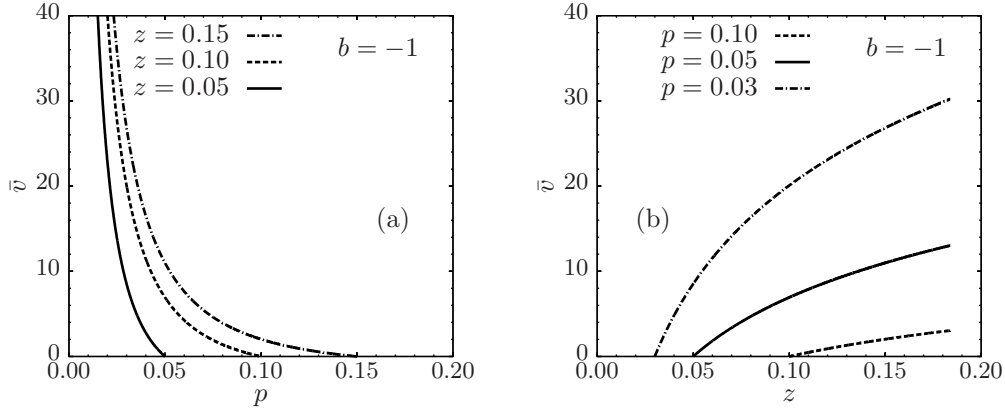


**Figure 3.11:** Reduced volume  $\bar{v}$  for the modified Thirring model with  $b = -1$  in the unconstrained ensemble: in (a), as a function of the reduced pressure  $p$  with constant fugacity  $z$ , and, in (b), as a function of the fugacity with constant reduced pressure. Taken from [1].

must be repulsive to guaranty equilibrium configurations. This prevents the system to collapse under completely open conditions in the appropriate range of control parameters.

In order to get further insight in the nature of the system, let us introduce the reduced number of particles  $\bar{x}$  and reduced density  $\bar{y}$  defined as

$$\bar{x}(p, z) = \frac{\nu \bar{N}}{T} = \bar{x}_0 + \bar{x}_1, \quad (3.88)$$

$$\bar{y}(p, z) = \frac{\nu V_0 \bar{N}}{T \bar{V}} = \frac{\bar{x}_0 + \bar{x}_1}{\bar{v} + 1}. \quad (3.89)$$

The behavior of these thermodynamic functions in the unconstrained ensemble can be quantitatively described for the model we are studying. Thus, the reduced number of particles  $\bar{x}(p, z)$  is shown in figure 3.9(a) as a function of the reduced pressure  $p$  with constant fugacity  $z$ , while in figure 3.9(b) is plotted as a function of the fugacity with constant reduced pressure. In figure 3.10(a), the reduced density  $\bar{y}(p, z)$  is represented as a function of the reduced pressure  $p$  with constant fugacity  $z$ , and, in figure 3.10(b), as a function of the fugacity with constant reduced pressure. Furthermore, in figure 3.11(a), we plot the reduced volume  $\bar{v}(p, z)$ , as given by the equation (3.82), as a function of the reduced pressure  $p$  for fixed values of the fugacity  $z$ . In the figure 3.11(b), we show  $\bar{v}$  as a function of  $z$  holding the pressure constant. In all these graphics we have set the parameter  $b$  of the model to  $b = -1$ .

Let us also consider the response functions  $K_{T,N}$  and  $M_{T,V}$  (see Section 2.4)

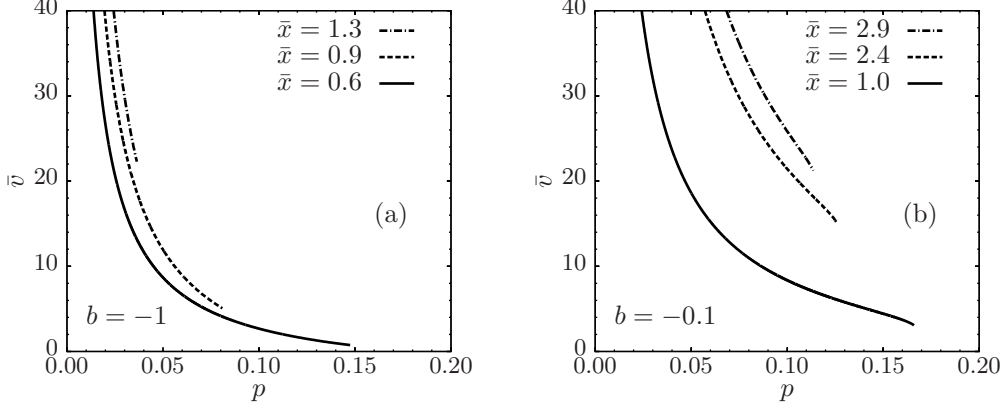


**Figure 3.12:** (a) Reduced volume  $\bar{v}$  as a function of the reduced pressure  $p$  in the unconstrained ensemble, where  $\bar{x}$  is held constant and  $b = -1$ . (b) Reduced density as a function of the reduced pressure at constant  $\bar{x}$ , but with  $b = -0.1$ . Taken from [1].

defined according to

$$K_{T,N} = - \left( \frac{\partial \bar{V}}{\partial \bar{P}} \right)_{T, \bar{N}} = - \frac{\nu V_0^2}{T^2} \left( \frac{\partial \bar{v}}{\partial p} \right)_{\bar{x}}, \quad (3.90)$$

$$M_{T,V} = \left( \frac{\partial \bar{N}}{\partial \mu} \right)_{T, \bar{V}} = \frac{z(\bar{v} + 1)}{\nu} \left( \frac{\partial \bar{y}}{\partial z} \right)_{\bar{v}}. \quad (3.91)$$

These response functions will be useful to compare the unconstrained ensemble with the canonical ensemble, and we recall that  $K_{T,N}$  is related to the isothermal compressibility  $\kappa_T$ , according to

$$K_{T,N} = \bar{V} \kappa_T. \quad (3.92)$$

In fact, here we are only interested in the signs of  $K_{T,N}$  and  $M_{T,V}$ , which can be seen by plotting the curves  $\bar{v}$  vs.  $p$  with constant  $\bar{x}$ , and  $\bar{y}$  vs.  $z$  with constant  $\bar{v}$ , respectively. Since  $\bar{x}$  is not a control parameter, the curve  $\bar{v}$  vs.  $p$  with constant  $\bar{x}$  represents the evolution of  $\bar{v}$  as a function of  $p$  through a series of equilibrium states where the actual control parameters,  $p$  and  $z$  in this case, are chosen in such a way that  $\bar{x}$  takes the same value in all these states. This can be achieved if the reduced pressure is parametrized as

$$p_{\bar{x}}(z) = z \exp \{ 2b[\bar{x} - \bar{x}_0(z)] \} \quad (3.93)$$

for the given  $\bar{x}$ , where we have used equations (3.81) and (3.88). Moreover, since the reduced pressure is always lower than  $z$  in equilibrium configurations, equation (3.93) must be restricted only to values of  $z$  satisfying the condition  $b[\bar{x} - \bar{x}_0(z)] < 0$ . Hence,

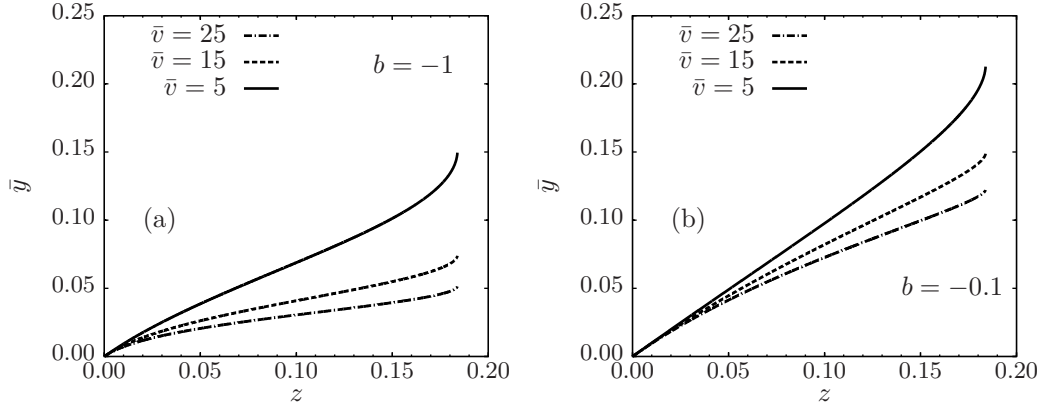


**Figure 3.13:** (a) Reduced density  $\bar{y}$  as a function of the fugacity  $z$  in the unconstrained ensemble, where the reduced volume  $\bar{v}$  is held constant and  $b = -1$ . (b) Reduced density as a function of the fugacity at constant  $\bar{v}$ , but with  $b = -0.1$ . Taken from [1].

the curve  $\bar{v}$  vs.  $p$  with constant  $\bar{x}$  is obtained by parametrically plotting  $p_{\bar{x}}(z)$  and  $\bar{v}(p_{\bar{x}}(z), z)$  using  $z$  as a parameter. The curve  $\bar{y}$  vs.  $z$  with constant  $\bar{v}$  can be obtained in analogous manner by choosing  $p$  and  $z$  in such a way that  $\bar{v}$  takes always the same value. In this case the reduced pressure is given by  $p = p_{\bar{v}}(z)$ , where, from equation (3.82),  $p_{\bar{v}}(z)$  is the (numerical) solution of the equation

$$\bar{v} = \frac{1}{2bp_{\bar{v}}} \ln \left( \frac{p_{\bar{v}}}{z} \right) \quad (3.94)$$

with fixed values of the reduced volume  $\bar{v}$ . As the reduced density  $\bar{y}$  is given by equation (3.89) as a function of  $p$  and  $z$ , the curve  $\bar{y}$  vs.  $z$  with constant  $\bar{v}$  is obtained from equation (3.89) using  $p = p_{\bar{v}}(z)$ .

According to the precedent discussion, in figures 3.12(a)-(b) we observe that  $\bar{v}$  is a decreasing function of  $p$  when  $\bar{x}$  is fixed. This means that  $K_{T,N}$  is positive for these configurations. Furthermore, as can be seen in figures 3.13(a)-(b),  $\bar{y}$  increases for increasing  $z$  with fixed  $\bar{v}$ , which indicates that the response function  $M_{T,V}$  is also positive. Below we will show that the response functions in this model can be negative in the canonical ensemble, where  $V$  and  $N$  are fixed control parameters.

### 3.2.3 Comparison with the grand canonical ensemble

We now constrain the system by fixing the volume, so that the control parameters in this case are  $T$ ,  $V$ , and  $\mu$ , which corresponds to the grand canonical ensemble. Using equation (3.65), the grand canonical partition function  $\Xi = \sum_N e^{\beta\mu N} Z$  can

be written as

$$\Xi = \sum_N \int \frac{d^{3N} \mathbf{q}}{N!} \lambda_T^{-3N} e^{-\beta \hat{W}(N_0, N_1) + \beta \mu N}. \quad (3.95)$$

Thus, as before, replacing the integrals over positions by a sum over all possible values of the number of particles in the two regions, according to (3.67), one gets

$$\Xi = \sum_{N_0, N_1} e^{-\beta \hat{\Omega}(N_0, N_1)}, \quad (3.96)$$

where, using Stirling's approximation in the large  $N$  limit,

$$\hat{\Omega}(N_0, N_1) = \hat{W}(N_0, N_1) - T \sum_k N_k + T \sum_k N_k \left[ \ln \left( N_k \frac{\lambda_T^3}{V_k} \right) - \frac{\mu}{T} \right]. \quad (3.97)$$

With the saddle-point approximation, the grand potential is given by

$$\Omega = \inf_{N_0, N_1} \hat{\Omega}(N_0, N_1). \quad (3.98)$$

The minimization with respect to  $N_0$  and  $N_1$  leads to

$$\mu = -2\nu \bar{N}_0 + T \ln \left( \frac{\bar{N}_0}{V_0} \lambda_T^3 \right), \quad (3.99)$$

$$\mu = -2b\nu \bar{N}_1 + T \ln \left( \frac{\bar{N}_1}{V - V_0} \lambda_T^3 \right), \quad (3.100)$$

where now  $\bar{N}_0$  and  $\bar{N}_1$ , being functions of  $T$ ,  $V$ , and  $\mu$ , are the number of particles in each region that minimize the grand potential. The total mean number of particles is then given by  $\bar{N} = \bar{N}_0 + \bar{N}_1$ . In addition, in the grand canonical ensemble, the pressure is given by

$$P = - \left( \frac{\partial \Omega}{\partial V} \right)_{T, \mu} = - \left( \frac{\partial \hat{\Omega}}{\partial V} \right)_{T, \mu}, \quad (3.101)$$

where the expression containing  $\hat{\Omega}$  must be evaluated at  $N_0 = \bar{N}_0$  and  $N_1 = \bar{N}_1$ . Thus, for the modified Thirring model, one obtains

$$P = \frac{T \bar{N}_1}{V - V_0}. \quad (3.102)$$

According to the discussion in Section 2.1.1, the replica energy in the grand canonical ensemble is given by

$$\mathcal{E} = \Omega + PV = \Omega - V \left( \frac{\partial \Omega}{\partial V} \right)_{T, \mu}. \quad (3.103)$$

From equation (3.103), using (3.97) evaluated at  $N_0 = \bar{N}_0$  and  $N_1 = \bar{N}_1$ , one obtains the usual expression

$$\mathcal{E} = -W + P^{(e)}V, \quad (3.104)$$

with the excess pressure  $P^{(e)} = P - \bar{N}T/V$ . We stress that, in this case, the replica energy is a function of  $T$ ,  $V$ , and  $\mu$ .

In order to study the stability of the system, we introduce the reduced grand potential  $\varphi_G = \nu\Omega/T^2$  and the associated function  $\hat{\varphi}_G = \nu\hat{\Omega}/T^2$ , which are both related through

$$\varphi_G(\bar{x}_0, \bar{x}_1) = \inf_{x_0, x_1} \hat{\varphi}_G(x_0, x_1). \quad (3.105)$$

Here  $x_0 = \nu N_0/T$  and  $x_1 = \nu N_1/T$ , so that  $\bar{x}_0 = \nu\bar{N}_0/T$  and  $\bar{x}_1 = \nu\bar{N}_1/T$  are the corresponding quantities that minimize  $\hat{\varphi}_G$ , defining thus the equilibrium configurations in the grand canonical ensemble. From (3.97), we obtain

$$\hat{\varphi}_G(x_0, x_1) = x_0 \left[ \ln \left( \frac{x_0}{z} \right) - 1 \right] - x_0^2 + x_1 \left[ \ln \left( \frac{x_1}{zv} \right) - 1 \right] - bx_1^2, \quad (3.106)$$

with the relative fugacity  $z = e^{(\mu - \mu_0)/T}$  and the reduced volume  $v = (V - V_0)/V_0$ . Here the variables  $z$  and  $v$  can be taken as control parameters together with  $T$ . We note that, analogously to what occurred for the reduced replica energy in the previous section, the temperature  $T$  does not appear explicitly in the reduced grand potential. In dimensionless variables, equations (3.99) and (3.100) can be rewritten as

$$\bar{x}_0 = ze^{2\bar{x}_0}, \quad (3.107)$$

$$\bar{x}_1 = zve^{2b\bar{x}_1}. \quad (3.108)$$

Furthermore, the Hessian matrix  $H_G$  associated to  $\hat{\varphi}_G$  at the stationary point  $(\bar{x}_0, \bar{x}_1)$  takes the form

$$H_G = \begin{pmatrix} 1/\bar{x}_0 - 2 & 0 \\ 0 & 1/\bar{x}_1 - 2b \end{pmatrix}, \quad (3.109)$$

and, therefore, one finds that  $\hat{\varphi}_G$  can be minimized if

$$\bar{x}_0 < 1/2, \quad 1/\bar{x}_1 > 2b. \quad (3.110)$$

We thus observe that, as before, equation (3.107) has two solutions if  $0 < z < z_0$  with  $z_0 = 1/(2e)$ , and that the smallest of the roots of (3.107) is that corresponding to  $0 < \bar{x}_0 < 1/2$ . Besides, on the one hand, equation (3.108) has always one solution if  $b \leq 0$ . On the other hand, when  $b > 0$ , (3.108) has two solutions if  $0 < z < z_1(v)$ , where

$$z_1(v) = \frac{1}{2ebv}, \quad (3.111)$$

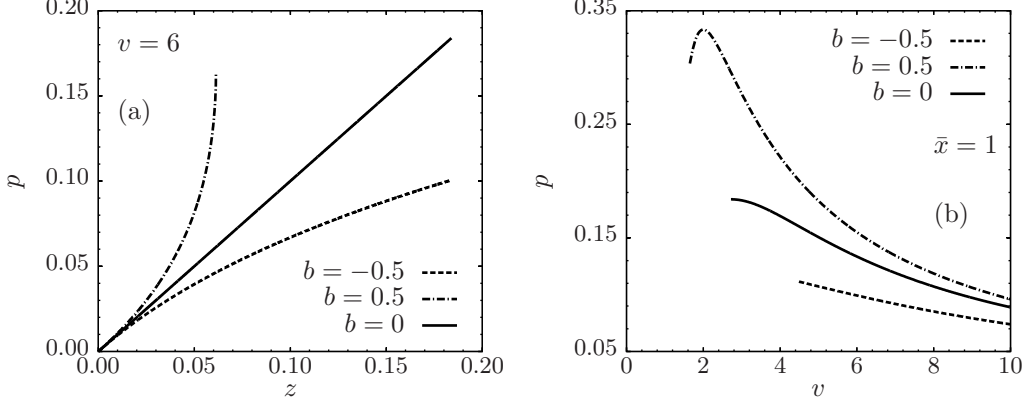


**Figure 3.14:** Modified Thirring model in the grand canonical ensemble. (a) Reduced pressure as a function of the fugacity for constant reduced volume  $v$ . For  $b < 0$ , the reduced pressure is always smaller than the fugacity, while, for  $b > 0$ , it is shown that  $p > z$ . In the case  $b = 0$ , the condition  $p = z$  is always satisfied. (b) Pressure as a function of the volume with constant reduced number of particles  $\bar{x}$ . In the case  $b = 0.5$ , the portion of the curve with positive slope correspond to states of negative isothermal compressibility. Taken from [1].

in such a way that the smallest of these solutions satisfies the condition (3.110). At  $z = z_1(v)$ , the only solution is given by  $\bar{x}_1 = 1/(2b)$ , and, hence, it corresponds to an unstable state. Therefore, equations (3.107) and (3.108) can be solved simultaneously to give stable equilibria if

$$0 < z < z_G(v), \quad (3.112)$$

where

$$z_G(v) = \begin{cases} z_0 & \text{if } b \leq 0 \\ \min[z_0, z_1(v)] & \text{if } b > 0 \end{cases}. \quad (3.113)$$

We note that for given values of the control parameters, the saddle-point equations define only one state, and, hence, there are no phase transitions in the grand canonical ensemble. We also remark that the Thirring model ( $b = 0$ ) is stable in the grand canonical ensemble if  $0 < z < z_0$ .

In the grand canonical ensemble, we now introduce the reduced number of particles, density, and pressure given by

$$\bar{x}(v, z) = \frac{\nu \bar{N}}{T} = \bar{x}_0 + \bar{x}_1, \quad (3.114)$$

$$\bar{y}(v, z) = \frac{\nu V_0 \bar{N}}{T V} = \frac{\bar{x}_0 + \bar{x}_1}{v + 1}, \quad (3.115)$$

$$p(v, z) = \frac{\nu V_0 P}{T^2} = \frac{\bar{x}_1}{v}, \quad (3.116)$$

respectively. In addition, the response functions are given by

$$\frac{1}{K_{T,N}} = - \left( \frac{\partial P}{\partial V} \right)_{T, \bar{N}} = - \frac{T^2}{\nu V_0^2} \left( \frac{\partial p}{\partial v} \right)_{\bar{x}}, \quad (3.117)$$

$$M_{T,V} = \left( \frac{\partial \bar{N}}{\partial \mu} \right)_{T,V} = \frac{z(v+1)}{\nu} \left( \frac{\partial \bar{y}}{\partial z} \right)_v. \quad (3.118)$$

Hence, in view of equation (3.117), to put in evidence the sign of  $K_{T,N}$ , one has to plot  $p$  as function of  $v$  by holding  $\bar{x}$  constant. Since  $\bar{x}$  is not a control parameter in the grand canonical ensemble, the curve  $p$  vs.  $v$  with constant  $\bar{x}$  represents the evolution of  $p$  as a function of  $v$  through a series of equilibrium states characterized by the same  $\bar{x}$ . By combining equations (3.107) and (3.108),  $z$  can in fact be chosen in such a way that  $\bar{x}$  remains constant when  $v$  is varied. Using this values of  $z$  in equations (3.116), we obtain the curve  $p$  vs.  $v$  with constant  $\bar{x}$ . Besides, the sign of  $M_{T,V}$  can be directly seen by plotting  $z$  vs.  $\bar{y}$  at constant  $v$ , since  $\bar{y} = \bar{y}(v, z)$  as given by equation (3.115).

For  $b < 0$ , the pressure-volume relation is invertible in the grand canonical ensemble. That is, from equations (3.108) and (3.116) we can write

$$v = \frac{1}{2bp(v, z)} \ln \left[ \frac{p(v, z)}{z} \right], \quad (3.119)$$

which for constant  $z$  defines the same relation as in the unconstrained ensemble. Moreover, the stability conditions are the same in the two ensembles for  $b < 0$ . Therefore, in the modified Thirring model, the grand canonical and unconstrained ensembles are equivalent when  $b < 0$ .

Since also the class of models with  $b \geq 0$  are stable in the grand canonical ensemble, the phenomenology in this case is richer than in the unconstrained case. For instance, equilibrium configurations with  $p \geq z$  or with negative isothermal compressibility are not stable under completely open conditions, while these configurations can be realized with fixed volume. In figure 3.14(a), we show  $p$  as a function of  $z$  with fixed  $v$  for different values of the parameter  $b$ . It can be seen that  $p > z$  when  $b > 0$ , while  $p < z$  when  $b < 0$  as it happens in the unconstrained ensemble. In addition, in this graphic we observe that  $p = z$  for  $b = 0$ , a general feature the Thirring model. All the curves in figure 3.14(a) finish at  $z = z_G(v)$ , since beyond this critical fugacity the stability is lost in the grand canonical ensemble. In figure 3.14(b),  $p$  is plotted as a function of  $v$  by holding  $\bar{x}$  constant, where also different values of  $b$  are chosen. Since holding  $\bar{x}$  constant determines the value of

the fugacity when  $v$  is varied, the curves start at the minimum value of  $v$  for which the condition  $0 < z < z_G(v)$  is satisfied, ensuring thus the stability of the configurations. As a remarkable fact, a region where  $K_{T,N} < 0$  is observed for  $b = 0.5$ , which corresponds to the points of the curve with positive slope. Configurations in such a region have negative isothermal compressibility.

### 3.2.4 Comparison with the canonical ensemble

In order to understand better the behavior of the system in the unconstrained ensemble, it is instructive to compare its states of equilibrium with the corresponding ones in the canonical ensemble. Hence, we consider now that the control parameters are  $T$ ,  $V$ , and  $N$ . Using (3.67) and the integral representation

$$\delta_{N,N_0+N_1} = \int_{\alpha-i\pi}^{\alpha+i\pi} \frac{d\alpha_c}{2\pi i} e^{\alpha_c(N-N_0-N_1)} \quad (3.120)$$

with  $\text{Re}(\alpha_c) = \alpha = -\mu/T$ , the canonical partition function (3.65) can be written as

$$Z = \int_{\alpha-i\pi}^{\alpha+i\pi} \frac{d\alpha_c}{2\pi i} \sum_{N_0, N_1} e^{-\hat{F}(\alpha_c, N_0, N_1)/T}, \quad (3.121)$$

where, for large  $N$ ,

$$\hat{F}(\alpha_c, N_0, N_1) = -\alpha_c T \left( N - \sum_k N_k \right) + \hat{W}(N_0, N_1) + T \sum_k N_k \left[ \ln \left( \frac{N_k}{V_k} \lambda_T^3 \right) - 1 \right]. \quad (3.122)$$

The canonical Helmholtz free energy is thus given by

$$F = \inf_{\alpha, N_0, N_1} \hat{F}(\alpha, N_0, N_1), \quad (3.123)$$

where we only look for solutions evaluated at real  $\alpha = \text{Re}(\alpha_c)$ . Moreover, minimization with respect to  $\alpha$  enforces that  $\bar{N}_1 = N - \bar{N}_0$ , while minimization with respect to  $N_0$  and  $N_1$  leads to

$$\mu = -2\nu \bar{N}_0 + T \ln \left( \frac{\bar{N}_0}{V_0} \lambda_T^3 \right), \quad (3.124)$$

$$\mu = -2\nu b(N - \bar{N}_0) + T \ln \left( \frac{N - \bar{N}_0}{V - V_0} \lambda_T^3 \right), \quad (3.125)$$

where we have used that  $\alpha = -\mu/T$ , and where the bars denote that the corresponding quantity minimizes the canonical free energy. In view of

$$\mu = \left( \frac{\partial F}{\partial N} \right)_{T,V} = \left( \frac{\partial \hat{F}}{\partial N} \right)_{T,V}, \quad (3.126)$$

where the expression containing  $\hat{F}$  is evaluated at  $\alpha = -\mu/T$ ,  $N_0 = \bar{N}_0$ , and  $N_1 = \bar{N}_1$ , we note that  $\mu$  is indeed the chemical potential of the system, that in the canonical ensemble is no more a control parameter. Equating the right hand sides of (3.124) and (3.125) we get an equation for  $\bar{N}_0$  as a function of  $T$ ,  $V$  and  $N$ . Furthermore, the pressure is given by

$$P = - \left( \frac{\partial F}{\partial V} \right)_{T,N} = - \left( \frac{\partial \hat{F}}{\partial V} \right)_{T,N}, \quad (3.127)$$

so that

$$P = \frac{T\bar{N}_1}{V - V_0}. \quad (3.128)$$

We now turn our attention to the replica energy in the canonical ensemble. It is given by (see Section 2.1.1)

$$\mathcal{E} = F + PV - \mu N = F - V \left( \frac{\partial F}{\partial V} \right)_{T,N} - N \left( \frac{\partial F}{\partial N} \right)_{T,V}, \quad (3.129)$$

From equation (3.129) and (3.122), we again obtain

$$\mathcal{E} = -W + P^{(e)}V, \quad (3.130)$$

where  $P^{(e)} = P - NT/V$ .

Furthermore, taking  $x = \nu N/T$  and  $v = (V - V_0)/V_0$  as control parameters, and, as before, introducing  $\bar{x}_0 = \nu \bar{N}_0/T$  in the canonical ensemble, equations (3.124) and (3.125) can be combined into

$$2bx - 2(1+b)\bar{x}_0 + \ln \left( \frac{\bar{x}_0}{x - \bar{x}_0} \right) + \ln v = 0, \quad (3.131)$$

Notice that  $\bar{x}_0/x = \bar{N}_0/N$  represents the fraction of particles inside the volume  $V_0$ , so that  $0 \leq \bar{x}_0/x \leq 1$ . Equation (3.131) defines  $\bar{x}_0 = \bar{x}_0(x, v)$  in this ensemble, and, depending on the parameters, it can have two solutions. Again, in reduced variables the temperature does not appear. The solution determining the equilibrium states corresponds to  $x_0 = \bar{x}_0$  that minimizes the canonical free energy, or, equivalently, the reduced free energy  $\varphi_C = \nu F/T^2$ . From equation (3.122) and according to the variational problem for this ensemble, one obtains

$$\varphi_C(\bar{x}_0) = \inf_{x_0} \hat{\varphi}_C(x_0) \quad (3.132)$$

with

$$\hat{\varphi}_C(x_0) = 2bx_0 - (1+b)x_0^2 + x_0 \ln \left( \frac{x_0}{x - x_0} \right) + x \ln \left( 1 - \frac{x_0}{x} \right) + x_0 \ln v, \quad (3.133)$$

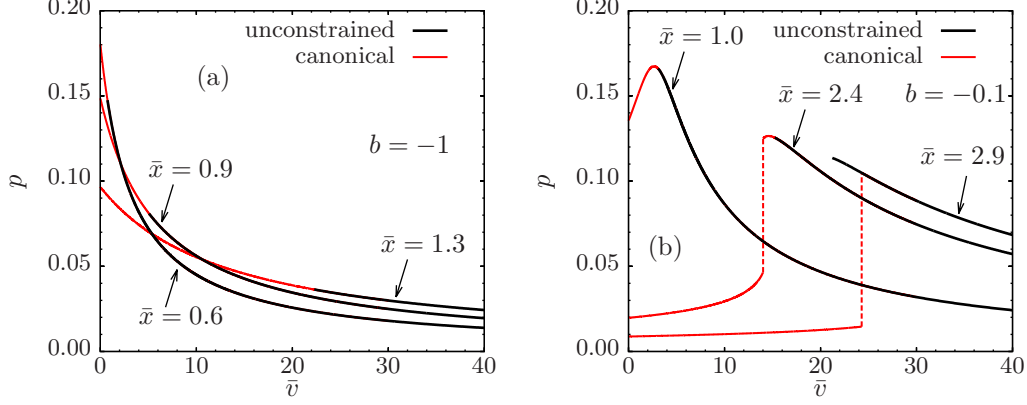


**Figure 3.15:** Comparison between the unconstrained and the canonical ensembles in the modified Thirring model. (a) The black lines indicate the reduced pressure  $p$  as a function of the reduced volume  $\bar{v}$  in the unconstrained ensemble, where the reduced number of particles  $\bar{x}$  is held constant for  $b = -1$ . The red lines show the analogous curves in the canonical ensemble, where  $v$  and  $x$  are fixed to the same values of  $\bar{v}$  and  $\bar{x}$ , respectively. (b) The graphics shows the same as in (a), but with  $b = -0.1$  and different values of  $\bar{x}$ . For  $b = -0.1$  the model shows first-order phase transitions in the canonical ensemble, indicated with red-dashed lines. In both (a) and (b), the curves in the canonical ensemble continue to the right superposed upon the curves in the unconstrained ensemble. Taken from [1].

where we have used that  $\bar{N}_1 = N - \bar{N}_0$ , and omitted terms that do not depend on  $x_0$ . It is interesting to note that equation (3.131) can have more than one solution, so that the model may exhibit phase transitions. In the Appendix A we discuss how to obtain the critical point for the modified Thirring model in the canonical ensemble.

Once (3.131) is solved satisfying (3.132), the relative fugacity  $z = e^{(\mu - \mu_0)/T}$  can be computed from equation (3.124), since this equation can be rewritten as

$$z(x, v) = \bar{x}_0 e^{-2\bar{x}_0}. \quad (3.134)$$

Furthermore, the reduced pressure  $p = \nu V_0 P / T^2$  takes the form

$$p(x, v) = \frac{x - \bar{x}_0}{v}. \quad (3.135)$$

The response functions in the canonical ensemble are given by

$$\frac{1}{K_{T,N}} = \left( \frac{\partial^2 F}{\partial V^2} \right)_{T,N} = -\frac{T^2}{\nu V_0^2} \left( \frac{\partial p}{\partial v} \right)_x, \quad (3.136)$$

$$\frac{1}{M_{T,V}} = \left( \frac{\partial^2 F}{\partial N^2} \right)_{T,V} = \frac{\nu}{z(v+1)} \left( \frac{\partial z}{\partial y} \right)_v, \quad (3.137)$$

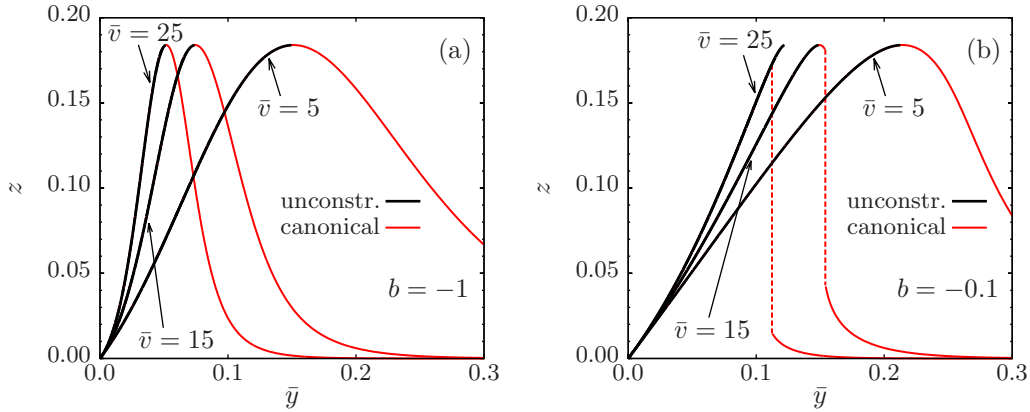


**Figure 3.16:** Comparison between the unconstrained and the canonical ensembles in the modified Thirring model. (a) The black lines represent the fugacity  $z$  as a function of the reduced density  $\bar{y}$  in the unconstrained ensemble. Here the reduced volume  $\bar{v}$  is held constant and we set  $b = -1$ . The red lines show the analogous curves in the canonical ensemble, where  $y$  and  $v$  are fixed to the same values of  $\bar{y}$  and  $\bar{v}$ , respectively. In (b), the graphic shows the same as in (a), but with  $b = -0.1$ . The jumps correspond to first-order phase transitions in the canonical ensemble (red-dashed lines). In both (a) and (b), the curves in the canonical ensemble continue to the left superposed upon the curves in the unconstrained ensemble. Taken from [1].

where we have introduced the reduced density

$$y = \frac{\nu V_0 N}{T V} = \frac{x}{v + 1}. \quad (3.138)$$

As discussed in Section 3.2.2, the sign of the response functions  $K_{T,N}$  and  $M_{T,V}$  can be inferred from the slopes of the curves  $p(v)$  at constant  $x$  and  $z(y)$  at constant  $v$ , respectively. Here we want to compare these curves with the corresponding ones in the unconstrained ensemble. We do this for negative values of  $b$ , for which the unconstrained and the grand canonical ensembles are equivalent. Then, the curves represent also the comparison between the canonical and grand canonical ensembles when  $b < 0$ . Thus, in figure 3.15(a) we show  $p$  as a function of  $\bar{v}$  in the unconstrained ensemble with  $b = -1$ , where  $\bar{x}$  is held constant. The corresponding curves in the canonical ensemble are also shown in this graphic, where  $v$  and  $x$  are fixed to the same values of  $\bar{v}$  and  $\bar{x}$ , respectively. In figure 3.15(b), these curves are represented for  $b = -0.1$  and different values of  $\bar{x}$ , where it can be appreciated that the model presents first-order phase transitions in the canonical ensemble, as indicated by the jumps in the pressure. We remark that in the figure 3.15(b), the three curves in the canonical ensemble present a portion with positive slope, indicating negative isothermal compressibility ( $K_{T,N} < 0$ ). In particular, the slopes of

the curves with  $\bar{x} = 2.4$  and  $\bar{x} = 2.9$  are positive before the jump. In addition, in figure 3.16(a) we represent  $z$  as a function of  $\bar{y}$  in the unconstrained ensemble, where  $\bar{v}$  is held constant and we set  $b = -1$ . We also show the analogous curves in the canonical ensemble, where  $y$  and  $v$  are fixed to the same values of  $\bar{y}$  and  $\bar{v}$ , respectively. In figure 3.16(b), these curves are shown for  $b = -0.1$ . The jumps in the fugacity correspond to first-order phase transitions in the canonical ensemble. Notice that in figures 3.16(a)-(b) the curves  $z(y)$  have a portion with negative slope, indicating  $M_{T,V} < 0$ . We note that the two ensembles are not equivalent, and, in particular, that the considered response functions can be negative in the canonical ensemble.

### 3.3 Thermodynamic relations and replica energy

As shown in Section 2.1, when the replica energy is written as a function of  $T$ ,  $P$ , and  $\mu$  satisfies the relation

$$d\mathcal{E} = -SdT + VdP - Nd\mu. \quad (3.139)$$

This relation holds even if  $T$ ,  $P$ , and  $\mu$  are not the actual control parameters specifying the state of the system; in such a case  $T$ ,  $P$ , and  $\mu$  themselves must be understood as functions of the control parameters. From the above equation one obtains

$$-S = \left( \frac{\partial \mathcal{E}}{\partial T} \right)_{P,\mu}, \quad (3.140)$$

$$V = \left( \frac{\partial \mathcal{E}}{\partial P} \right)_{T,\mu}, \quad (3.141)$$

$$-N = \left( \frac{\partial \mathcal{E}}{\partial \mu} \right)_{T,P}. \quad (3.142)$$

These equations, in fact, are thermodynamic relations valid in any ensemble; with this in mind, we do not use here a bar over the variables to indicate whether a certain quantity fluctuates or not. In order for equations (3.140), (3.141), and (3.142) to be satisfied, however, the system must have enough thermodynamic degrees of freedom permitting that  $T$ ,  $P$ , and  $\mu$  can be taken as a set of independent variables. Below we show that this is indeed possible for self-gravitating isothermal spheres. We emphasize that the fact that  $T$ ,  $P$ , and  $\mu$  can be taken as a set of independent variables does not guarantee that the system attains equilibrium configurations in the unconstrained ensemble; to establish the latter, the corresponding second-order variational analysis ensuring that the replica energy can be minimized in the unconstrained ensemble must be performed. After the discussion regarding self-gravitating

systems, we comment on the aforementioned thermodynamic degrees of freedom in the modified Thirring model.

### 3.3.1 Self-gravitating isothermal spheres

The characterization of global thermodynamic quantities of self-gravitating isothermal spheres is well understood and here we will just consider it as an example to illustrate the relations (3.140), (3.141), and (3.142). In particular, the first of these relations will be used to obtain the entropy of the self-gravitating gas. We will write down only the necessary expressions to carry out our task and refer the reader to [19, 20, 22] for details.

The interactions of a self-gravitating gas are a particular case of power-law decaying interactions, as considered in Section 2.3.3. For this case we have  $a = 1$ , thus  $\sigma = 2/3$ , with the coupling  $\kappa = -G_N m^2$ , where  $G_N$  is Newton's constant. Also, Newtonian systems satisfy the Poisson-Boltzmann equation which, after introducing the dimensionless variables  $\xi = [4\pi|\kappa|\beta n(0)]^{1/2}x$  and  $\psi = \beta(\Phi(x) - \Phi(0))$ , becomes the Emden equation

$$\frac{1}{\xi^2} \frac{d}{d\xi} \left( \xi^2 \frac{d}{d\xi} \psi \right) = e^{-\psi}. \quad (3.143)$$

Here  $x = |\mathbf{x}|$ ,  $\mathbf{x}$  being the position of a point within the system, and  $\beta = 1/T$  is the inverse temperature, while  $n(0)$  and  $\Phi(0)$  are the number density and the potential at the origin, respectively. Global thermodynamic quantities are expressed in terms of these variables evaluated at the boundary of the system, thus, for convenience, one introduces

$$\xi_0 = (4\pi|\kappa|\beta n(0))^{1/2}R, \quad \psi_0 = \psi(\xi_0), \quad \text{and} \quad \psi'_0 = \psi'(\xi_0), \quad (3.144)$$

where primes denote the derivative with respect to  $\xi$  and  $R$  is the radius of spherical container. Moreover, with a suitable change of variables, the Emden equation can be transformed into a first-order differential equation [143]. When such variables, usually denoted by  $(v, u)$ , are evaluated at  $\xi = \xi_0$  and  $\psi = \psi_0$ , with  $\psi' = \psi'_0$ , they read

$$v_0 = \xi_0 \psi'_0 \quad \text{and} \quad u_0 = \frac{\xi_0 e^{-\psi_0}}{\psi'_0}, \quad (3.145)$$

and therefore satisfy

$$\frac{du_0}{dv_0} = -\frac{u_0(u_0 + v_0 - 3)}{v_0(u_0 - 1)}. \quad (3.146)$$

Furthermore, it can be shown [19, 20] that the inverse temperature and the potential energy can be written as

$$\frac{1}{T} = \frac{Rv_0}{|\kappa|N}, \quad (3.147)$$

$$W = NT(u_0 - 3). \quad (3.148)$$

Because of the replica energy is ( $\sigma = 2/3$ )

$$\mathcal{E} = -\frac{2}{3}W \quad (3.149)$$

in this case, what we need is to express the potential energy as a function of  $T$ ,  $P$ , and  $\mu$  only. Since the potential at the boundary of the system is  $\Phi(R) = \kappa N/R$ , using (2.167) yields

$$N = \frac{R}{|\kappa|} \left[ T \ln \left( \frac{P\lambda_T^3}{T} \right) - \mu \right], \quad (3.150)$$

where we have taken into account the local equation of state so that  $P = n(R)T$ . From (3.150) and (3.147) one sees that

$$v_0(T, P, \mu) = \ln \left( \frac{P\lambda_T^3}{T} \right) - \frac{\mu}{T} \quad (3.151)$$

and therefore

$$\left( \frac{\partial v_0}{\partial T} \right)_{P, \mu} = \frac{1}{T} \left( \frac{\mu}{T} - \frac{5}{2} \right). \quad (3.152)$$

Combining (3.148) and the global equation of state (2.182) one obtains  $3PV = NTu_0$  and hence, using (3.147) to express  $N$  the radius can be written as

$$R = T \left( \frac{v_0 u_0}{4\pi|\kappa|P} \right)^{1/2}. \quad (3.153)$$

Using (3.147) and (3.153), the potential energy (3.148) takes the form

$$W(T, P, \mu) = \frac{T^3 v_0^{3/2}}{(4\pi|\kappa|^3 P)^{1/2}} \left( u_0^{3/2} - 3u_0^{1/2} \right), \quad (3.154)$$

which depends only on the desired variables since  $u_0 = u_0(v_0(T, P, \mu))$ . We then have

$$\left( \frac{\partial \mathcal{E}}{\partial T} \right)_{P, \mu} = -\frac{W}{2T} - \frac{W}{v_0} \left( \frac{\partial v_0}{\partial T} \right)_{P, \mu} \left[ 1 + \frac{v_0(u_0 - 1)}{u_0(u_0 - 3)} \frac{du_0}{dv_0} \right]. \quad (3.155)$$

Therefore, according to the expression

$$S = - \left( \frac{\partial \mathcal{E}}{\partial T} \right)_{P, \mu} \quad (3.156)$$

and using (3.146), (3.148), and (3.152), from equation (3.155) the entropy is obtained as

$$S = N \left[ 2u_0 - \frac{\mu}{T} - \frac{7}{2} \right]. \quad (3.157)$$

Using that with equation (3.147) the thermal wavelength can be expressed as

$$\lambda_T = \left[ h^2 / (2\pi m T) \right]^{1/2} = \left[ h^2 R v_0 / (2\pi m |\kappa| N) \right]^{1/2} \quad (3.158)$$

and that  $P/T = N u_0 / (3V)$ , from (3.151) one gets

$$\frac{\mu}{T} = \frac{1}{2} \ln(v_0) + \ln(v_0 u_0) - v_0 - \frac{1}{2} \ln \left( 2^7 \pi^5 m^3 |\kappa|^3 R^3 N / h^6 \right). \quad (3.159)$$

Thus the entropy (3.157) becomes

$$S = N \left[ v_0 + 2u_0 - \frac{1}{2} \ln(v_0) - \ln(v_0 u_0) - 3 \right] + S_0, \quad (3.160)$$

as given in [22], with  $S_0 = N/2 \ln [2^7 \pi^5 m^3 |\kappa|^3 R^3 N / (eh^6)]$ . This verifies equation (3.140) for the self-gravitating gas. The verification of the remaining equations (3.141) and (3.142) follows from an analogous procedure.

### 3.3.2 Modified Thirring model

The present discussion is to emphasize that a situation may exist in which the replica energy is different from zero, but  $T$ ,  $P$ , and  $\mu$  cannot be taken as a set of independent variables. This can happen in an ensemble different from the unconstrained one. When  $T$ ,  $P$ , and  $\mu$  cannot be taken as independent in the unconstrained ensemble, the mean-field equations will not lead to a minimum of replica energy and therefore, equations (3.139)-(3.142) are meaningless.

Let us assume that the system is itself constrained such that, for instance,  $\mu = \mu(T, P)$ . In this case, equation (3.139) becomes

$$d\mathcal{E} = - \left[ S + N \left( \frac{\partial \mu}{\partial T} \right)_P \right] dT + \left[ V - N \left( \frac{\partial \mu}{\partial P} \right)_T \right] dP, \quad (3.161)$$

which establishes a functional relation  $\mathcal{E} = \mathcal{E}(T, P)$ . Thus, one actually has

$$\left( \frac{\partial \mathcal{E}}{\partial T} \right)_P = -S - N \left( \frac{\partial \mu}{\partial T} \right)_P, \quad (3.162)$$

$$\left( \frac{\partial \mathcal{E}}{\partial P} \right)_T = V - N \left( \frac{\partial \mu}{\partial P} \right)_T, \quad (3.163)$$

which are the relations satisfied in this case instead of equations (3.140) and (3.141). This is equivalent to directly consider a constraint  $\mathcal{E} = \mathcal{E}(T, P)$  in equation (3.139), which yields

$$N d\mu = - \left[ S + \left( \frac{\partial \mathcal{E}}{\partial T} \right)_P \right] dT + \left[ V - \left( \frac{\partial \mathcal{E}}{\partial P} \right)_T \right] dP. \quad (3.164)$$

The above expression shows that the usual Gibbs-Duhem equation is not valid when the replica energy is different from zero even if  $T$ ,  $P$ , and  $\mu$  are not a set of independent variables. Moreover, analogous equations can be obtained if one considers any other functional relation constraining  $T$ ,  $P$ , and  $\mu$ .

To go further, consider an arbitrary  $d$ -dimensional system with long-range interactions whose number density at a point  $\mathbf{x} \in \mathbb{R}^d$  is given by

$$n(\mathbf{x}) = \frac{1}{\lambda_T^d} \exp \left[ \frac{\mu - \Phi(\mathbf{x})}{T} \right], \quad (3.165)$$

where  $\Phi(\mathbf{x})$  is the mean-field potential. On the one hand, according to our considerations in Section 2.3.2, the local pressure is given by  $p(\mathbf{x}) = n(\mathbf{x})T$  when short-range interactions are completely ignored, and the pressure  $P$  is  $p(\mathbf{x})$  evaluated at the boundary of the system. Consider also that the mean-field potential is not completely arbitrary but it always vanishes at the boundary of the system, regardless of the thermodynamic state of the system. This will enforce the condition

$$\mu = T \ln \left( \frac{P \lambda_T^d}{T} \right). \quad (3.166)$$

On the other hand, we have seen in Section 2.3.1 that the chemical potential and the entropy of the system satisfy

$$\mu N = T \int n(\mathbf{x}) \ln \left[ n(\mathbf{x}) \lambda_T^d \right] d^d \mathbf{x} + 2W, \quad (3.167)$$

$$S = - \int n(\mathbf{x}) \ln \left[ n(\mathbf{x}) \lambda_T^d \right] d^d \mathbf{x} + \frac{2+d}{2} N, \quad (3.168)$$

where  $W$  is the potential energy. Thus, using equation (3.166) in equations (3.162) and (3.163), and then using equations (3.167) and (3.168) leads to

$$\left( \frac{\partial \mathcal{E}}{\partial T} \right)_P = - \frac{2W}{T}, \quad (3.169)$$

$$\left( \frac{\partial \mathcal{E}}{\partial P} \right)_T = \frac{P^{(e)} V}{P}, \quad (3.170)$$

where  $P^{(e)} = P - NT/V$ . Hence, with the particular constraint (3.166), equations (3.169) and (3.170) hold in place of equations (3.140) and (3.141).

The interesting fact here is that the modified Thirring model can be used to test these general considerations. In Section 3.2.2 we found that in the case  $b = 0$  the model never attains equilibrium configurations in the unconstrained ensemble. As we shall see below, this is due to the fact that, for the case  $b = 0$ , the chemical

potential satisfies equation (3.166) (with  $d = 3$ ), and thus  $T$ ,  $P$ , and  $\mu$  cannot be taken as independent variables. But first we will check that for  $b \neq 0$  the entropy can be computed from equation (3.140), showing that  $T$ ,  $P$ , and  $\mu$  can actually be taken as independent variables in this case. This, of course, is in agreement with the statistical mechanics description of the system obtained in Section 3.2.2.

To check the validity of equation (3.140), we need to write the replica energy as a function of  $T$ ,  $P$ , and  $\mu$ . We note that  $\Phi(\mathbf{x}) = -2\nu [N_0\theta_{V_0}(\mathbf{x}) + bN_1\theta_{V_1}(\mathbf{x})]$  and  $N_1/V_1 = P/T$  for the modified Thirring model. Thus, evaluating the number density (3.165) at any point  $\mathbf{x}$  in  $V_1$  and rearranging terms gives us

$$\mu = T \ln \left( \frac{P\lambda_T^3}{T} \right) - 2\nu b N_1, \quad (3.171)$$

which defines  $N_1 = N_1(T, P, \mu)$  if  $b \neq 0$ . Analogously, evaluating (3.165) at any point  $\mathbf{x}$  in  $V_0$  yields

$$\mu = T \ln \left( \frac{N_0\lambda_T^3}{V_0} \right) - 2\nu N_0, \quad (3.172)$$

which defines implicitly  $N_0 = N_0(T, \mu)$ . Therefore, when  $b \neq 0$ , we have

$$\left( \frac{\partial N_0}{\partial T} \right)_{P, \mu} = \frac{2\nu N_0^2 + \mu N_0 - \frac{3}{2} N_0 T}{(2\nu N_0 - T) T}, \quad (3.173)$$

$$\left( \frac{\partial N_1}{\partial T} \right)_{P, \mu} = \frac{N_1}{T} + \frac{1}{2b\nu} \left( \frac{\mu}{T} - \frac{5}{2} \right). \quad (3.174)$$

Since

$$\mathcal{E} = -W + P^{(e)}V = \nu (N_0^2 + bN_1^2) + PV_0 - N_0T, \quad (3.175)$$

the replica energy is implicitly given as a function of  $T$ ,  $P$ , and  $\mu$  by means of equations (3.171) and (3.172). Hence,

$$\left( \frac{\partial \mathcal{E}}{\partial T} \right)_{P, \mu} = \sum_k N_k \left[ \ln \left( \frac{N_k \lambda_T^3}{V_k} \right) - \frac{5}{2} \right], \quad (3.176)$$

where we have rearranged terms using equations (3.171) and (3.172). By comparing with equation (3.168), we thus see that the right-hand side of equation (3.176) is indeed  $-S$ . This confirms that when  $b \neq 0$ , the system has enough thermodynamic degrees of freedom to take  $T$ ,  $P$ , and  $\mu$  as a set of independent variables. To see whether the configurations are stable or not, however, one must perform an analysis of the second-order variations of the appropriate free energy, as we have done in Section 3.2.2, for instance, depending on the actual physical conditions imposed by the corresponding control parameters.

In view of equation (3.171), it is now obvious that if  $b = 0$ , the chemical potential is given by equation (3.166) and that

$$2\nu N_0 = T \ln \left( \frac{N_0 T}{P V_0} \right) \quad (3.177)$$

defines implicitly  $N_0 = N_0(T, P)$ . Hence,

$$\left( \frac{\partial N_0}{\partial T} \right)_P = \frac{N_0}{T} \left( \frac{2\nu N_0 + T}{2\nu N_0 - T} \right). \quad (3.178)$$

Using equation (3.178) and since in this case  $\mathcal{E} = \nu N_0^2 + P V_0 - N_0 T$ , it is easy to see that

$$\left( \frac{\partial \mathcal{E}}{\partial T} \right)_P = \frac{2\nu N_0^2}{T} = -\frac{2W}{T}, \quad (3.179)$$

in agreement with equation (3.169). These arguments show that, although the replica energy is different from zero, in the Thirring model ( $b = 0$ ) one can not take  $T$ ,  $P$ , and  $\mu$  as a set of independent variables.



# NEAR-FIELD THERMODYNAMICS OUT OF THERMAL EQUILIBRIUM

---

For separation distances between two bodies below the characteristic thermal wavelength of the radiation, the radiative heat transfer is considerably enhanced as compared to the blackbody limit [12,67–70]. Moreover, at near-field scales, the tunneling of evanescent electromagnetic waves dominates the heat transfer. Such a mechanism of heat transfer, also called photon tunneling, can be further enhanced in many-body systems [76,86,88,104] when passive intermediate bodies (relays) are used to connect two bodies in interaction. This fact encourages a systematic study of radiative heat transfer in many-body systems. In this chapter we approach this matter from a thermostatistical point of view and focus on the description of energy and entropy fluxes in these systems. In contrast with the previous chapters, the thermostatistics of the thermal radiation presented below characterizes situations that are globally out of thermal equilibrium. This is the relevant case accounting for the energy conversion processes discussed in Chapter 5 and many other applications involving near-field radiative heat transfer. We begin by considering the problem of three bodies in mutual radiative interaction in both the far-field and near-field regimes. Hence, the description of two bodies in interaction is derived as a particular case, and in Section 4.4 we identify the dominant contributions in the near-field regime for three-body and two-body systems.

## 4.1 Energy fluxes in three-body systems

In this section we introduce the system of our interest and discuss how to obtain the transmission coefficients associated to this system. The transmission coefficients contain the information about the radiative transport properties of the system, in such a way that they play a crucial role in the thermodynamics of the problem. We

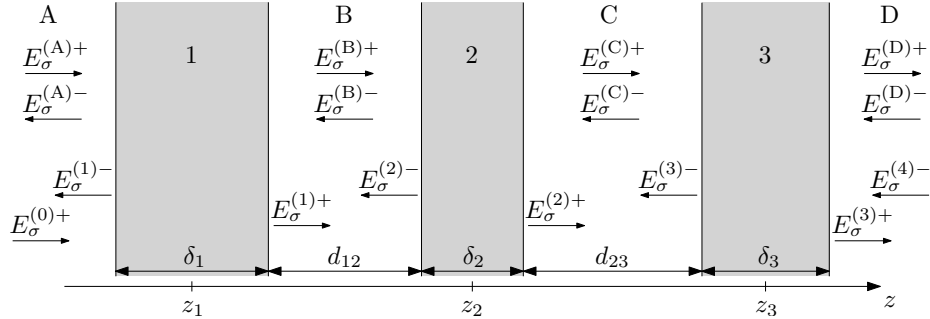


**Figure 4.1:** Representation of the three-body system. The bodies 1, 2, and 3 define four vacuum regions that are indicated with A, B, C, and D. The contributions to the total electric field in each region are also indicated.

will present an outline of the derivation of the energy flux in three-body systems following references [104] and [103]. The motivation for reproducing this derivation is to introduce the physics of the problem and the methods that can be employed to handle it. From here, in Section 4.1.4, we obtain all the transmission coefficients of the three-body system in both the far and near fields. This will allow us to write the energy flux in Landauer-like form [94, 115, 116, 144, 145].

Consider the distribution of bodies according to the geometry illustrated in the figure 4.1, where three bodies, denoted by 1, 2, and 3, with planar surfaces and infinite transversal extension are separated by vacuum. This distribution of bodies defines four vacuum regions labeled with A, B, C, and D, which are also indicated in the figure 4.1. In general, we consider that the bodies are made of different materials. Moreover, the body  $\alpha$ , with  $\alpha = 1, 2, 3$ , has thickness  $\delta_\alpha$  and is placed at  $z_\alpha$  on the  $z$  axis, as shown in the figure, while its transversal extension lies on the  $x$ - $y$  plane. Furthermore, we assume that the body  $\alpha$  is maintained at a fixed temperature  $T_\alpha$  by means of some external source. We also assume that the environment on the left of the whole three-body system is thermalized at a temperature  $T_0$ , while the environment on the right of the system is thermalized at a temperature  $T_4$ . This introduces a minor modification with respect to the case considered in [104], where  $T_0 = T_4$  is assumed.

Before going further, let us first recall the main mechanism behind thermal radiative transfer in systems as the one we want to study. Basically, materials in thermal equilibrium possess charges in random thermal motion that generate fluctuating currents, and these currents, in turn, radiate electromagnetic fields [105]. These charges can be electrons in metals or ions in polar materials. Although in neutral materials the random density charges, currents, and the generated electromagnetic fields vanish in average [146], the energy radiated by these thermal fields is not null. This

can be understood by realizing that the energy radiated is proportional to averaged contributions that are quadratic in the fields (see below). Since the fields are correlated, averaged quadratic contributions do not vanish [99]. Furthermore, as is well known, describing thermal radiation is an intrinsically quantum mechanical problem. With this in mind, we will treat the electromagnetic field classically and introduce its quantum nature using the fluctuation-dissipation theorem [97, 98].

### 4.1.1 The Poynting vector

We want to compute the net energy flux across a surface within any of the vacuum regions of the system and, from here, be able to identify the transmission coefficients. The electric field at a point  $\mathbf{R} = (x, y, z)$  and time  $t$  in such vacuum regions, which is created by the fluctuating currents inside the materials, can be expressed as a Fourier expansion given by

$$\mathbf{E}^{(\gamma)}(\mathbf{R}, t) = \int_{-\infty}^{\infty} \frac{d\omega}{2\pi} e^{-i\omega t} \mathbf{E}^{(\gamma)}(\mathbf{R}, \omega), \quad (4.1)$$

where  $\omega$  is the frequency and the label  $\gamma = A, B, C, D$  indicates the corresponding vacuum region. We require that  $\mathbf{E}^{(\gamma)}(\mathbf{R}, -\omega) = \mathbf{E}^{(\gamma)*}(\mathbf{R}, \omega)$  in order for the field  $\mathbf{E}^{(\gamma)}(\mathbf{R}, t)$  to be real, where the asterisk denotes complex conjugate. In addition, the components  $\mathbf{E}^{(\gamma)}(\mathbf{R}, \omega)$  can be decomposed using a plane-wave description [104], in such a way that a single mode the field is specified by the frequency  $\omega$ , the component  $\boldsymbol{\kappa} = (k_x, k_y)$  of the wave vector on the  $x$ - $y$  plane, the two polarizations  $\sigma = s, p$ , and the direction of propagation along the  $z$  axis which is denoted by  $\phi$ . The latter can take two values:  $\phi = +$  indicating propagation to the right and  $\phi = -$  that indicates propagation to the left. The total wave vector reads  $\mathbf{K}^\phi = (\boldsymbol{\kappa}, \phi k_z)$ , where the component  $k_z$  is given by

$$k_z = \sqrt{(\omega/c)^2 - \boldsymbol{\kappa}^2}. \quad (4.2)$$

We note that when  $\kappa = |\boldsymbol{\kappa}| \leq \omega/c$ , the component  $k_z$  is real and, therefore, the wave is propagative. When  $\kappa > \omega/c$ ,  $k_z$  is imaginary and the associated wave is evanescent. Evanescent waves are nonpropagative modes of the field, for which  $\phi$  indicates the direction along with the amplitude of the wave decays. Thus, taking this plane-wave decomposition into account, the single-frequency component of the electric field can be written as

$$\mathbf{E}^{(\gamma)}(\mathbf{R}, \omega) = \sum_{\phi, \sigma} \int \frac{d^2\boldsymbol{\kappa}}{(2\pi)^2} e^{i\mathbf{K}^\phi \cdot \mathbf{R}} \hat{\boldsymbol{\epsilon}}_\sigma^\phi(\boldsymbol{\kappa}, \omega) E_\sigma^{(\gamma)\phi}(\boldsymbol{\kappa}, \omega), \quad (4.3)$$

where  $E_\sigma^{(\gamma)\phi}(\boldsymbol{\kappa}, \omega)$  are the components of the electric field in this decomposition and  $\hat{\boldsymbol{\epsilon}}_\sigma^\phi(\boldsymbol{\kappa}, \omega)$  are the polarization vectors given by [104]

$$\hat{\boldsymbol{\epsilon}}_p^\phi(\boldsymbol{\kappa}, \omega) = \hat{\boldsymbol{\epsilon}}_s^\phi(\boldsymbol{\kappa}, \omega) \times \frac{c}{\omega} \mathbf{K}^\phi = \frac{c}{\omega} (-\kappa \hat{\mathbf{z}} + \phi k_z \hat{\boldsymbol{\kappa}}), \quad (4.4)$$

$$\hat{\boldsymbol{\epsilon}}_s^\phi(\boldsymbol{\kappa}, \omega) = \hat{\mathbf{z}} \times \hat{\boldsymbol{\kappa}} = \frac{1}{\kappa} (-k_y \hat{\mathbf{x}} + k_x \hat{\mathbf{y}}), \quad (4.5)$$

where  $\hat{\boldsymbol{\kappa}} = \boldsymbol{\kappa}/\kappa$  and  $\hat{\mathbf{x}}, \hat{\mathbf{y}},$  and  $\hat{\mathbf{z}}$  are unitary vectors along the  $x, y,$  and  $z$  axis, respectively. We thus have (for positive frequencies only)

$$\mathbf{E}^{(\gamma)}(\mathbf{R}, t) = \int_0^\infty \frac{d\omega}{2\pi} e^{-i\omega t} \sum_{\phi, \sigma} \int \frac{d^2\boldsymbol{\kappa}}{(2\pi)^2} e^{i\mathbf{K}^\phi \cdot \mathbf{R}} \hat{\boldsymbol{\epsilon}}_\sigma^\phi(\boldsymbol{\kappa}, \omega) E_\sigma^{(\gamma)\phi}(\boldsymbol{\kappa}, \omega) + \text{c.c.} \quad (4.6)$$

Besides, according to Maxwell's equations, the magnetic field  $\mathbf{B}^{(\gamma)}(\mathbf{R}, t)$  satisfies

$$\nabla \times \mathbf{E}^{(\gamma)}(\mathbf{R}, t) = -\frac{\partial}{\partial t} \mathbf{B}^{(\gamma)}(\mathbf{R}, t). \quad (4.7)$$

Hence, the Fourier components  $\mathbf{B}^{(\gamma)}(\mathbf{R}, \omega)$  can be obtained and expanded in terms of the plane-wave components of the electric field  $E_\sigma^{(\gamma)\phi}(\boldsymbol{\kappa}, \omega)$ . The magnetic field is then given by

$$\mathbf{B}^{(\gamma)}(\mathbf{R}, t) = \int_0^\infty \frac{d\omega}{2\pi c} e^{-i\omega t} \sum_{\phi, \sigma} \int \frac{d^2\boldsymbol{\kappa}}{(2\pi)^2} e^{i\mathbf{K}^\phi \cdot \mathbf{R}} \hat{\boldsymbol{\beta}}_\sigma^\phi(\boldsymbol{\kappa}, \omega) E_\sigma^{(\gamma)\phi}(\boldsymbol{\kappa}, \omega) + \text{c.c.}, \quad (4.8)$$

where  $\hat{\boldsymbol{\beta}}_p^\phi(\boldsymbol{\kappa}, \omega) = -\hat{\boldsymbol{\epsilon}}_s^\phi(\boldsymbol{\kappa}, \omega)$  and  $\hat{\boldsymbol{\beta}}_s^\phi(\boldsymbol{\kappa}, \omega) = \hat{\boldsymbol{\epsilon}}_p^\phi(\boldsymbol{\kappa}, \omega)$ .

Once suitable expressions for the electric and magnetic fields are known, the energy carried by these fields per unit area of the emitter and per unit of time, i.e., the energy flux, can be computed. This is obtained through the Poynting vector

$$\mathbf{S}^{(\gamma)}(\mathbf{R}, t) = \varepsilon_0 c^2 \mathbf{E}^{(\gamma)}(\mathbf{R}, t) \times \mathbf{B}^{(\gamma)}(\mathbf{R}, t), \quad (4.9)$$

where  $\varepsilon_0$  is the vacuum permittivity. In fact, we only need the averaged component of the Poynting vector along the  $z$  axis, which is the component in the direction perpendicular to the surfaces of the bodies. In Cartesian components, we have

$$\langle S_i^{(\gamma)}(\mathbf{R}, t) \rangle = \varepsilon_0 c^2 \sum_{j,k} \epsilon_{ijk} \langle E_j^{(\gamma)}(\mathbf{R}, t) B_k^{(\gamma)}(\mathbf{R}, t) \rangle, \quad (4.10)$$

where  $\langle \dots \rangle$  indicates symmetrized statistical average and  $\epsilon_{ijk}$  are the Levi-Civita symbols with  $i, j, k = x, y, z$ . In order to compute this quantity, we introduce the correlation functions  $C_\sigma^{(\gamma)\phi\phi'}(\boldsymbol{\kappa}, \omega)$  which are defined according to

$$\langle E_\sigma^{(\gamma)\phi}(\boldsymbol{\kappa}, \omega) E_{\sigma'}^{(\gamma)\phi'*}(\boldsymbol{\kappa}', \omega') \rangle = (2\pi)^3 \delta(\omega - \omega') \delta(\boldsymbol{\kappa} - \boldsymbol{\kappa}') \delta_{\sigma\sigma'} C_\sigma^{(\gamma)\phi\phi'}(\boldsymbol{\kappa}, \omega). \quad (4.11)$$

Thus, from (4.10) and (4.11), after manipulating the polarization vectors, the averaged  $z$  component of the Poynting vector takes the form

$$\begin{aligned}\Phi_\gamma &\equiv \langle S_z^{(\gamma)}(\mathbf{R}, t) \rangle \\ &= \int_0^\infty \frac{d\omega}{2\pi} \sum_\sigma \sum_{\phi, \phi'} \int \frac{d^2\boldsymbol{\kappa}}{(2\pi)^2} e^{i(\phi k_z - \phi' k_z^*)z} \frac{\varepsilon_0 c^2}{\omega} (\phi k_z + \phi' k_z^*) C_\sigma^{(\gamma)\phi\phi'}(\boldsymbol{\kappa}, \omega).\end{aligned}\quad (4.12)$$

We observe that, as a consequence of (4.11), the energy flux  $\Phi_\gamma$  is stationary and invariant under translations in the  $x$ - $y$  plane, and depends on the  $z$  coordinate belonging to region  $\gamma$ .

Introducing the projectors on the propagative and evanescent sectors  $\Pi^{(\text{pw})}$  and  $\Pi^{(\text{ew})}$ , respectively, defined by

$$\Pi^{(\text{pw})} \equiv \theta(\omega - c\kappa), \quad (4.13)$$

$$\Pi^{(\text{ew})} \equiv \theta(c\kappa - \omega), \quad (4.14)$$

where  $\theta(x)$  is the Heaviside step function, and since  $k_z$  is pure imaginary when  $c\kappa > \omega$ , the energy flux (4.12) can be rewritten as [104]

$$\begin{aligned}\Phi_\gamma &= \int_0^\infty \frac{d\omega}{2\pi} \sum_\sigma \sum_{\phi, \phi'} \int \frac{d^2\boldsymbol{\kappa}}{(2\pi)^2} \left[ \delta_{\phi\phi'} \Pi^{(\text{pw})} + (1 - \delta_{\phi\phi'}) \Pi^{(\text{ew})} \right] \\ &\quad \times \frac{2\varepsilon_0 c^2 \phi k_z}{\omega} C_\sigma^{(\gamma)\phi\phi'}(\boldsymbol{\kappa}, \omega).\end{aligned}\quad (4.15)$$

Therefore, to go further, the correlation functions are required. Notice that the dependence on  $z$  in equation (4.15) is still present and will become evident when choosing the correlation functions of the total field in a particular region  $\gamma$  of the system.

### 4.1.2 Correlation functions and electric field

The total electric field in each region of the system depends on the fields generated by all the bodies as well as on the background fields present in the left and right environments. Thus, the total contribution to the mode  $E_\sigma^{(\gamma)\phi}(\boldsymbol{\kappa}, \omega)$  in region  $\gamma$  depends on the modes  $E_\sigma^{(\alpha)\phi}(\boldsymbol{\kappa}, \omega)$  that are scattered through the system, where  $\alpha = 1, 2, 3$  indicates that the corresponding mode is radiated by the body  $\alpha$ , and  $\alpha = 0$  and  $\alpha = 4$  indicate that the mode comes from the background radiation of the left and right environments, respectively. Moreover, to take into account the scattering of modes through the system, we introduce the reflection and transmission coefficients  $\rho_\sigma^{(\alpha)\phi}(\boldsymbol{\kappa}, \omega)$  and  $\tau_\sigma^{(\alpha)}(\boldsymbol{\kappa}, \omega)$  associated to body  $\alpha$  (see below). For the

reflection coefficients,  $\phi = +, -$  specify the direction of propagation of the outgoing field (the incoming field propagates in the direction  $-\phi$ ), while, according to the geometry of the system, the transmission coefficients do not depend on  $\phi$  [103,104].

According to the previous argument and considering the scheme shown in figure 4.1, the field in each region satisfies the following system of equations [104]:

$$\begin{aligned}
E_\sigma^{(A)+} &= E_\sigma^{(0)+} \\
E_\sigma^{(A)-} &= E_\sigma^{(1)-} + \rho_\sigma^{(1)-} E_\sigma^{(0)+} + \tau_\sigma^{(1)} E_\sigma^{(B)-} \\
E_\sigma^{(B)+} &= E_\sigma^{(1)+} + \rho_\sigma^{(1)+} E_\sigma^{(B)-} + \tau_\sigma^{(1)} E_\sigma^{(0)+} \\
E_\sigma^{(B)-} &= E_\sigma^{(2)-} + \rho_\sigma^{(2)-} E_\sigma^{(B)+} + \tau_\sigma^{(2)} E_\sigma^{(C)-} \\
E_\sigma^{(C)+} &= E_\sigma^{(2)+} + \rho_\sigma^{(2)+} E_\sigma^{(C)-} + \tau_\sigma^{(2)} E_\sigma^{(B)+} \\
E_\sigma^{(C)-} &= E_\sigma^{(3)-} + \rho_\sigma^{(3)-} E_\sigma^{(C)+} + \tau_\sigma^{(3)} E_\sigma^{(4)-} \\
E_\sigma^{(D)+} &= E_\sigma^{(3)+} + \rho_\sigma^{(3)+} E_\sigma^{(4)-} + \tau_\sigma^{(3)} E_\sigma^{(C)+} \\
E_\sigma^{(D)-} &= E_\sigma^{(4)-},
\end{aligned} \tag{4.16}$$

where, for simplicity, we have omitted the dependence on  $\boldsymbol{\kappa}$  and  $\omega$ . The solution of the system (4.16) for the components  $E_\sigma^{(\gamma)\phi}$  can be written as a linear combination of the form

$$E_\sigma^{(\gamma)\phi}(\boldsymbol{\kappa}, \omega) = \sum_{\alpha, \eta} L_{(\alpha)\eta}^{(\gamma)\phi}(\sigma, \boldsymbol{\kappa}, \omega) E_\sigma^{(\alpha)\eta}(\boldsymbol{\kappa}, \omega), \tag{4.17}$$

$$\gamma = \text{A, B, C, D}, \quad \alpha = 0, 1, 2, 3, 4, \quad \phi, \eta = +, -$$

with the coefficients  $L_{(\alpha)\eta}^{(\gamma)\phi}(\sigma, \boldsymbol{\kappa}, \omega)$  being given in Appendix B.

For the particular geometry of the system under consideration (see figure 4.1), the above introduced reflection and transmission coefficients take the form [104]

$$\rho_\sigma^{(\alpha)\phi} = \rho_\sigma^{(\alpha)} e^{-2i\phi k_z(z_\alpha + \phi\delta_\alpha/2)}, \tag{4.18}$$

$$\rho_\sigma^{(\alpha)} = r_{\alpha\sigma} \frac{1 - e^{2ik_{\alpha z}\delta_\alpha}}{1 - r_{\alpha\sigma}^2 e^{2ik_{\alpha z}\delta_\alpha}}, \tag{4.19}$$

$$\tau_\sigma^{(\alpha)} = \frac{t_{\alpha\sigma} \bar{t}_{\alpha\sigma} e^{i(k_{\alpha z} - k_z)\delta_\alpha}}{1 - r_{\alpha\sigma}^2 e^{2ik_{\alpha z}\delta_\alpha}}, \tag{4.20}$$

for  $\alpha = 1, 2, 3$ . Here, the  $z$ -component of the wave vector inside the media reads

$$k_{\alpha z} = \sqrt{(\omega/c)^2 \varepsilon_\alpha - \boldsymbol{\kappa}^2}, \tag{4.21}$$

and the vacuum-medium Fresnel reflection coefficients for each polarization  $\sigma$  are given by

$$r_{\alpha p} = \frac{\varepsilon_\alpha k_z - k_{\alpha z}}{\varepsilon_\alpha k_z + k_{\alpha z}}, \quad r_{\alpha s} = \frac{k_z - k_{\alpha z}}{k_z + k_{\alpha z}}, \tag{4.22}$$

where  $\varepsilon_\alpha(\omega)$  is the dielectric permittivity of the body  $\alpha$ . The vacuum-medium and medium-vacuum transmission coefficients,  $t_{\alpha\sigma}$  and  $\bar{t}_{\alpha\sigma}$ , respectively, read as

$$t_{\alpha p} = \frac{2\sqrt{\varepsilon_\alpha}k_z}{\varepsilon_\alpha k_z + k_{\alpha z}}, \quad t_{\alpha s} = \frac{2k_z}{k_z + k_{\alpha z}}, \quad (4.23)$$

$$\bar{t}_{\alpha p} = \frac{2\sqrt{\varepsilon_\alpha}k_{\alpha z}}{\varepsilon_\alpha k_z + k_{\alpha z}}, \quad \bar{t}_{\alpha s} = \frac{2k_{\alpha z}}{k_z + k_{\alpha z}}. \quad (4.24)$$

Let us now return to the discussion concerning the correlation functions. We will assume that the correlation function of the total field in region  $\gamma$  can be expressed in a simple way in terms of the correlation functions of the source fields. This can be achieved under the assumption of local thermal equilibrium [96]. That is, we assume that each body radiates as it would do at equilibrium at its own temperature [104]. Thus, the single modes of the radiation emitted by the bodies ( $\alpha = 1, 2, 3$ ) and the modes of the environmental radiation ( $\alpha = 0, 4$ ) are not correlated to each other. Denoting by  $C_\sigma^{(\alpha)\phi\phi'}(\boldsymbol{\kappa}, \omega)$  the correlation functions of these source fields, the assumption of local thermal equilibrium leads to

$$\begin{aligned} \left\langle E_\sigma^{(\alpha)\phi}(\boldsymbol{\kappa}, \omega) E_{\sigma'}^{(\alpha')\phi'*}(\boldsymbol{\kappa}', \omega') \right\rangle &= (2\pi)^3 \delta(\omega - \omega') \delta(\boldsymbol{\kappa} - \boldsymbol{\kappa}') \delta_{\sigma\sigma'} \delta_{\alpha\alpha'} \\ &\times C_\sigma^{(\alpha)\phi\phi'}(\boldsymbol{\kappa}, \omega) \end{aligned} \quad (4.25)$$

for  $\alpha, \alpha' = 0, 1, 2, 3, 4$ . In addition, since

$$\begin{aligned} \left\langle E_\sigma^{(\gamma)\phi}(\boldsymbol{\kappa}, \omega) E_{\sigma'}^{(\gamma)\phi'*}(\boldsymbol{\kappa}', \omega') \right\rangle &= \sum_{\alpha, \alpha'} \sum_{\eta, \eta'} L_{(\alpha)\eta}^{(\gamma)\phi}(\sigma, \boldsymbol{\kappa}, \omega) L_{(\alpha')\eta'}^{(\gamma)\phi'*}(\sigma', \boldsymbol{\kappa}', \omega') \\ &\times \left\langle E_\sigma^{(\alpha)\eta}(\boldsymbol{\kappa}, \omega) E_{\sigma'}^{(\alpha')\eta'*}(\boldsymbol{\kappa}', \omega') \right\rangle, \end{aligned} \quad (4.26)$$

using (4.25) one obtains

$$\begin{aligned} \left\langle E_\sigma^{(\gamma)\phi}(\boldsymbol{\kappa}, \omega) E_{\sigma'}^{(\gamma)\phi'*}(\boldsymbol{\kappa}', \omega') \right\rangle &= (2\pi)^3 \delta(\omega - \omega') \delta(\boldsymbol{\kappa} - \boldsymbol{\kappa}') \delta_{\sigma\sigma'} \\ &\times \sum_{\alpha} \sum_{\eta, \eta'} L_{(\alpha)\eta}^{(\gamma)\phi}(\sigma, \boldsymbol{\kappa}, \omega) L_{(\alpha)\eta'}^{(\gamma)\phi'*}(\sigma', \boldsymbol{\kappa}, \omega) \\ &\times C_\sigma^{(\alpha)\eta\eta'}(\boldsymbol{\kappa}, \omega). \end{aligned} \quad (4.27)$$

Therefore, the correlation function of the total field in region  $\gamma$  can be read from (4.27) in terms of the correlation functions of the source fields, yielding

$$C_\sigma^{(\gamma)\phi\phi'}(\boldsymbol{\kappa}, \omega) = \sum_{\alpha} \sum_{\eta, \eta'} L_{(\alpha)\eta}^{(\gamma)\phi}(\sigma, \boldsymbol{\kappa}, \omega) L_{(\alpha)\eta'}^{(\gamma)\phi'*}(\sigma, \boldsymbol{\kappa}, \omega) C_\sigma^{(\alpha)\eta\eta'}(\boldsymbol{\kappa}, \omega). \quad (4.28)$$

To proceed, we need the expressions of the correlation functions of the source fields. These functions can be obtained by using the assumption of local thermal

equilibrium and the fluctuation-dissipation theorem. The fluctuation-dissipation theorem states that the fluctuations of the total field outside a body in thermal equilibrium with the environment at temperature  $T_\alpha$  satisfy [97, 98, 147]

$$\langle E_i(\mathbf{R}, \omega) E_j^*(\mathbf{R}', \omega') \rangle = \frac{4\pi\omega}{\varepsilon_0 c^2} \Theta(\omega, T_\alpha) \delta(\omega - \omega') \operatorname{Im} G_{ij}(\mathbf{R}, \mathbf{R}'; \omega), \quad (4.29)$$

where we have introduced

$$\Theta(\omega, T_\alpha) = \frac{\hbar\omega}{2} \coth\left(\frac{\hbar\omega}{2k_B T_\alpha}\right) = \hbar\omega \left[ n(\omega, T_\alpha) + \frac{1}{2} \right] \quad (4.30)$$

with

$$n(\omega, T_\alpha) = \left[ e^{\hbar\omega/k_B T_\alpha} - 1 \right]^{-1} \quad (4.31)$$

being the distribution of thermal photons at temperature  $T_\alpha$ . In (4.29), we have also introduced  $G_{ij}(\mathbf{R}, \mathbf{R}'; \omega)$ , the Cartesian components of the dyadic Green's function  $\mathbb{G}(\mathbf{R}, \mathbf{R}'; \omega)$  defined by the solution of the equation

$$\left[ \nabla_{\mathbf{R}} \times \nabla_{\mathbf{R}} - \frac{\omega^2}{c^2} \varepsilon(\omega, \mathbf{R}) \right] \mathbb{G}(\mathbf{R}, \mathbf{R}'; \omega) = \mathbb{I} \delta(\mathbf{R} - \mathbf{R}'), \quad (4.32)$$

where  $\varepsilon(\omega, \mathbf{R})$  is the permittivity of the medium and  $\mathbb{I}$  is the unit dyad. As discussed in detail in [103], the assumption of local thermal equilibrium allows us to use the fluctuation-dissipation theorem (4.29) with the Green's function of a system consisting only of the body under consideration in thermal equilibrium with the environment, i.e., without taking into account the other bodies. This permits the identification of the correlation functions of the source fields  $C_\sigma^{(\alpha)\phi\phi'}$ . Moreover, the Green's function is related to the reflection and transmission coefficients of the body, so that the correlation functions also depend on these coefficients. As a result, after employing the plane-wave decomposition in (4.29), the correlation functions of the fields emitted by the bodies  $\alpha = 1, 2, 3$  when  $\phi = \phi'$  are given by [103]

$$\begin{aligned} C_\sigma^{(\alpha)\phi\phi'} &= \frac{\omega}{2\varepsilon_0 c^2 k_z} \Theta(\omega, T_\alpha) \\ &\times \left[ \Pi^{(\text{pw})} \left( 1 - \rho_\sigma^{(\alpha)\phi} \rho_\sigma^{(\alpha)\phi*} - \tau_\sigma^{(\alpha)} \tau_\sigma^{(\alpha)*} \right) + \Pi^{(\text{ew})} \left( \rho_\sigma^{(\alpha)\phi} - \rho_\sigma^{(\alpha)\phi*} \right) \right]. \end{aligned} \quad (4.33)$$

Analogously, for the bodies  $\alpha = 1, 2, 3$  when  $\phi \neq \phi'$ , one has [103]

$$\begin{aligned} C_\sigma^{(\alpha)\phi\phi'} &= \frac{\omega}{2\varepsilon_0 c^2 k_z} \Theta(\omega, T_\alpha) \\ &\times \left[ -\Pi^{(\text{pw})} \left( \rho_\sigma^{(\alpha)\phi} \tau_\sigma^{(\alpha)*} + \rho_\sigma^{(\alpha)\phi'} \tau_\sigma^{(\alpha)} \right) + \Pi^{(\text{ew})} \left( \tau_\sigma^{(\alpha)} - \tau_\sigma^{(\alpha)*} \right) \right]. \end{aligned} \quad (4.34)$$

In addition, the correlation functions of the environmental radiation in equilibrium at temperature  $T_\alpha$ , for  $\alpha = 0, 4$ , are given by [103]

$$C_\sigma^{(\alpha)\phi\phi'} = \frac{\omega}{2\varepsilon_0 c^2 k_z} \Theta(\omega, T_\alpha) \Pi^{(\text{pw})} \delta_{\phi\phi'}, \quad (4.35)$$

which, in particular, do not depend on the polarization.

Summarizing, we have now the expressions of the correlation functions of the source fields  $C_\sigma^{(\alpha)\phi\phi'}$ . With these correlation functions, the correlation function of the total field in region  $\gamma$ ,  $C_\sigma^{(\gamma)\phi\phi'}$ , can be obtained using (4.28). Moreover, the dependence on  $\gamma$ , the region that is being considered, is introduced through the coefficients  $L_{(\alpha)\eta}^{(\gamma)\phi}$  in (4.28). Thus, the energy flux  $\Phi_\gamma$  in region  $\gamma$  can be computed using (4.15) with the correlations functions obtained from (4.28). The next step would be to write the energy flux in a suitable form by means of the transmission coefficients of the system, but, before doing that, in the next section we will define the scattering coefficients that allows us to express relevant quantities in a compact and intuitive form.

### 4.1.3 Scattering coefficients

The many-body scattering operators introduced in references [103, 104], which for our geometry reduce simply to coefficients, are a useful tool that permits writing physical quantities in a convenient way. These coefficients take into account the presence of two or three bodies at the same time. Moreover, all these coefficients depend on the the wave vector  $\boldsymbol{\kappa}$  and the frequency  $\omega$  of the scattered mode of the electromagnetic field; for simplicity, below we omit writing down explicitly this dependence.

Consider, for instance, the cavity formed by bodies 1 and 2 (that is, the vacuum gap between these bodies). Because of the optical properties of the materials, in the cavity there will be an infinite series of multiple reflections between the bodies. We denote by  $u_\sigma^{(1,2)}$  the coefficient accounting for these multiple reflections associated to the field emitted by body 1 towards body 2, which can be written as

$$u_\sigma^{(1,2)} = \sum_{n=0}^{\infty} \left( \rho_\sigma^{(1)+} \rho_\sigma^{(2)-} \right)^n = \left( 1 - \rho_\sigma^{(1)+} \rho_\sigma^{(2)-} \right)^{-1}. \quad (4.36)$$

In the same way, the coefficient accounting for the multiple reflections in the cavity associated to the field emitted by body 2 towards body 1 can be written as

$$u_\sigma^{(2,1)} = \sum_{n=0}^{\infty} \left( \rho_\sigma^{(2)-} \rho_\sigma^{(1)+} \right)^n = \left( 1 - \rho_\sigma^{(2)-} \rho_\sigma^{(1)+} \right)^{-1} = u_\sigma^{(1,2)}. \quad (4.37)$$

For the cavity formed by bodies 2 and 3, we have

$$u_{\sigma}^{(2,3)} = u_{\sigma}^{(3,2)} = \sum_{n=0}^{\infty} \left( \rho_{\sigma}^{(2)+} \rho_{\sigma}^{(3)-} \right)^n = \left( 1 - \rho_{\sigma}^{(2)+} \rho_{\sigma}^{(3)-} \right)^{-1}. \quad (4.38)$$

In addition, the two-body reflection and transmission coefficients related to bodies 1 and 2 are given by

$$\rho_{\sigma}^{(12)+} = \rho_{\sigma}^{(2)+} + \tau_{\sigma}^{(2)} u_{\sigma}^{(1,2)} \rho_{\sigma}^{(1)+} \tau_{\sigma}^{(2)}, \quad (4.39)$$

$$\rho_{\sigma}^{(12)-} = \rho_{\sigma}^{(1)-} + \tau_{\sigma}^{(1)} u_{\sigma}^{(1,2)} \rho_{\sigma}^{(2)-} \tau_{\sigma}^{(1)}, \quad (4.40)$$

$$\tau_{\sigma}^{(12)} = \tau_{\sigma}^{(1)} u_{\sigma}^{(1,2)} \tau_{\sigma}^{(2)}, \quad (4.41)$$

while for bodies 2 and 3 read as

$$\rho_{\sigma}^{(23)+} = \rho_{\sigma}^{(3)+} + \tau_{\sigma}^{(3)} u_{\sigma}^{(2,3)} \rho_{\sigma}^{(2)+} \tau_{\sigma}^{(3)}, \quad (4.42)$$

$$\rho_{\sigma}^{(23)-} = \rho_{\sigma}^{(2)-} + \tau_{\sigma}^{(2)} u_{\sigma}^{(2,3)} \rho_{\sigma}^{(3)-} \tau_{\sigma}^{(2)}, \quad (4.43)$$

$$\tau_{\sigma}^{(23)} = \tau_{\sigma}^{(2)} u_{\sigma}^{(2,3)} \tau_{\sigma}^{(3)}. \quad (4.44)$$

The coefficient  $\rho_{\sigma}^{(23)+}$ , for example, accounts for the reflection of a mode to the right due to bodies 2 and 3 together: it has a direct contribution from the reflection produced by body 3, and a contribution that takes into account that the mode is transmitted by body 3 into the cavity, undergoes multiple reflections, is reflected to the right by body 2, and finally leaves the cavity by transmission through body 3. The coefficient  $\tau_{\sigma}^{(23)}$  represents transmission through body 2, multiple reflections between bodies 2 and 3, and transmission through body 3. The rest of the many-body scattering coefficients can be interpreted in a similar way.

Finally, using the two-body reflection coefficients, the three-body intracavity coefficients are given by

$$u_{\sigma}^{(1,23)} = u_{\sigma}^{(23,1)} = \left( 1 - \rho_{\sigma}^{(1)+} \rho_{\sigma}^{(23)-} \right)^{-1}, \quad (4.45)$$

$$u_{\sigma}^{(12,3)} = u_{\sigma}^{(3,12)} = \left( 1 - \rho_{\sigma}^{(12)+} \rho_{\sigma}^{(3)-} \right)^{-1}, \quad (4.46)$$

and the three-body reflection and transmission coefficients take the form

$$\rho_{\sigma}^{(123)+} = \rho_{\sigma}^{(3)+} + \tau_{\sigma}^{(3)} u_{\sigma}^{(12,3)} \rho_{\sigma}^{(12)+} \tau_{\sigma}^{(3)}, \quad (4.47)$$

$$\rho_{\sigma}^{(123)-} = \rho_{\sigma}^{(12)-} + \tau_{\sigma}^{(12)} u_{\sigma}^{(12,3)} \rho_{\sigma}^{(3)-} \tau_{\sigma}^{(12)}, \quad (4.48)$$

$$\tau_{\sigma}^{(123)} = \tau_{\sigma}^{(12)} u_{\sigma}^{(12,3)} \tau_{\sigma}^{(3)}, \quad (4.49)$$

or, identically,

$$\rho_{\sigma}^{(123)+} = \rho_{\sigma}^{(23)+} + \tau_{\sigma}^{(23)} u_{\sigma}^{(1,23)} \rho_{\sigma}^{(1)+} \tau_{\sigma}^{(23)}, \quad (4.50)$$

$$\rho_{\sigma}^{(123)-} = \rho_{\sigma}^{(1)-} + \tau_{\sigma}^{(1)} u_{\sigma}^{(1,23)} \rho_{\sigma}^{(23)-} \tau_{\sigma}^{(1)}, \quad (4.51)$$

$$\tau_{\sigma}^{(123)} = \tau_{\sigma}^{(1)} u_{\sigma}^{(1,23)} \tau_{\sigma}^{(23)}. \quad (4.52)$$

The coefficients  $L_{(\alpha)\eta}^{(\gamma)\phi}$ , defined in equation (4.17) and given in Appendix B, can be suitably written in terms of these many-body scattering coefficients. Thus, quantities depending on  $L_{(\alpha)\eta}^{(\gamma)\phi}$ , e.g., the energy flux, are functions of the scattering coefficients as well.

#### 4.1.4 Transmission coefficients

Here we want to write the energy flux in terms of the transmission coefficients of the system (this coefficients will be introduced below). In this way, as noted previously, the energy flux exchanged between the different parts of the system can be expressed by using a Landauer-like formalism [94, 115, 116]. This formalism is advantageous because it permits a straightforward extension of the results obtained here to the general case of a  $N$ -body systems (see Section 5.2.2). Of course, this does not avoid the fact that the expressions for the transmission coefficients must be obtained for each particular case. Below, we consider a three-body system from which, in the proper limit, the two-body configuration can also be derived.

First, let us make some convenient definitions. We introduce the coefficients  $K_{\phi\phi'}^{(\alpha)\eta\eta'}(\sigma, \boldsymbol{\kappa}, \omega)$  for the source fields defined according to

$$\left[ \Pi^{(\text{pw})} \delta_{\phi\phi'} + \Pi^{(\text{ew})} (1 - \delta_{\phi\phi'}) \right] C_{\sigma}^{(\alpha)\eta\eta'}(\boldsymbol{\kappa}, \omega) \equiv \frac{\omega}{2\varepsilon_0 c^2 k_z} \Theta(\omega, T_{\alpha}) K_{\phi\phi'}^{(\alpha)\eta\eta'}(\sigma, \boldsymbol{\kappa}, \omega). \quad (4.53)$$

Hence, the energy flux (4.15) becomes

$$\Phi_{\gamma} = \int_0^{\infty} \frac{d\omega}{2\pi} \sum_{\sigma} \int \frac{d^2\boldsymbol{\kappa}}{(2\pi)^2} \sum_{\alpha} \Theta(\omega, T_{\alpha}) X_{\sigma(\alpha)}^{(\gamma)}(\boldsymbol{\kappa}, \omega), \quad (4.54)$$

where

$$X_{\sigma(\alpha)}^{(\gamma)}(\boldsymbol{\kappa}, \omega) = \sum_{\phi, \phi'} \sum_{\eta, \eta'} \phi L_{(\alpha)\eta}^{(\gamma)\phi}(\sigma, \boldsymbol{\kappa}, \omega) L_{(\alpha)\eta'}^{(\gamma)\phi'*}(\sigma, \boldsymbol{\kappa}, \omega) K_{\phi\phi'}^{(\alpha)\eta\eta'}(\sigma, \boldsymbol{\kappa}, \omega). \quad (4.55)$$

Furthermore, we note that the dependence on the temperature in (4.54) is explicit through the functions  $\Theta(\omega, T_{\alpha})$ . Besides, if all the bodies are thermalized at the

same equilibrium temperature, say at temperature  $T$ , the flux  $\Phi_\gamma$  must vanish in each region  $\gamma$ :

$$0 = \int_0^\infty \frac{d\omega}{2\pi} \sum_\sigma \int \frac{d^2\boldsymbol{\kappa}}{(2\pi)^2} \Theta(\omega, T) \sum_\alpha X_{\sigma(\alpha)}^{(\gamma)}(\boldsymbol{\kappa}, \omega). \quad (4.56)$$

As a consequence, the coefficients  $X_{\sigma(\alpha)}^{(\gamma)}$  necessarily satisfy the relation

$$\sum_\alpha X_{\sigma(\alpha)}^{(\gamma)}(\boldsymbol{\kappa}, \omega) = 0. \quad (4.57)$$

Finally, defining  $n_\alpha(\omega) \equiv n(\omega, T_\alpha)$  and

$$n_{\alpha,\beta}(\omega) \equiv n_\alpha(\omega) - n_\beta(\omega) = \frac{1}{\hbar\omega} [\Theta(\omega, T_\alpha) - \Theta(\omega, T_\beta)], \quad (4.58)$$

and using the relation (4.57), the energy flux (4.54) can be rewritten as

$$\Phi_\gamma = \int_0^\infty \frac{d\omega}{2\pi} \hbar\omega \sum_\sigma \int \frac{d^2\boldsymbol{\kappa}}{(2\pi)^2} \sum_{\alpha=0}^3 n_{\alpha,\alpha+1}(\omega) \mathcal{T}_{\sigma,\gamma}^{\alpha,\alpha+1}(\boldsymbol{\kappa}, \omega), \quad (4.59)$$

where we have introduced the desired transmission coefficients of the system associated to region  $\gamma$ ,

$$\mathcal{T}_{\sigma,\gamma}^{\alpha,\alpha+1}(\boldsymbol{\kappa}, \omega) = \sum_{\beta=0}^{\alpha} X_{\sigma(\beta)}^{(\gamma)}(\boldsymbol{\kappa}, \omega). \quad (4.60)$$

All the transmission coefficients of the three-body system are given explicitly in Appendix B. We observe that the transmission coefficients in regions A and D are affected by  $\Pi^{(\text{pw})}$  only, and therefore, the projection of the energy flux on the evanescent sector vanishes in these regions. Thus, only propagative modes contribute to the energy flux in the external parts of the system. This is expected because, in those regions, the three-body system can be seen as a single radiating object. However, in regions B and C the situation is different. For instance, the coefficient associated to bodies 1 and 2 in region B is given by (see Appendix B)

$$\mathcal{T}_{\sigma,\text{B}}^{1,2} = \Pi^{(\text{pw})} \frac{\left(1 - |\rho_\sigma^{(1)+}|^2\right) \left(1 - |\rho_\sigma^{(23)-}|^2\right)}{\left|1 - \rho_\sigma^{(1)+} \rho_\sigma^{(23)-}\right|^2} + \Pi^{(\text{ew})} \frac{4\text{Im}\left(\rho_\sigma^{(1)+}\right) \text{Im}\left(\rho_\sigma^{(23)-}\right)}{\left|1 - \rho_\sigma^{(1)+} \rho_\sigma^{(23)-}\right|^2}. \quad (4.61)$$

In the internal regions of the system, that is, in the cavity formed by bodies 1 and 2 and in the cavity formed by bodies 2 and 3, also evanescent waves contribute to the energy flux. However, the contribution of these modes will be significant only if the

vacuum gaps are narrow enough to prevent the rapid decay of the evanescent field. In particular, if the separation between the bodies is small as compared with the thermal wavelength of the radiation, i.e., in the near-field regime, the contribution of evanescent waves to the energy flux is dominant [12, 105, 106].

Lastly, we can also compute the net energy flux on each body of the system by taking into account the difference of energy fluxes in the regions surrounding each body. Denoting by  $\Phi^{(1)} = \Phi_A - \Phi_B$ ,  $\Phi^{(2)} = \Phi_B - \Phi_C$ , and  $\Phi^{(3)} = \Phi_C - \Phi_D$  the net energy flux on the bodies 1, 2, and 3, respectively, these energy fluxes can be written as

$$\Phi^{(1)} = \int_0^\infty \frac{d\omega}{2\pi} \hbar\omega \sum_\sigma \int \frac{d^2\boldsymbol{\kappa}}{(2\pi)^2} \sum_{\alpha=0}^3 n_{\alpha,\alpha+1} \left( \mathcal{T}_{\sigma,A}^{\alpha,\alpha+1} - \mathcal{T}_{\sigma,B}^{\alpha,\alpha+1} \right), \quad (4.62)$$

$$\Phi^{(2)} = \int_0^\infty \frac{d\omega}{2\pi} \hbar\omega \sum_\sigma \int \frac{d^2\boldsymbol{\kappa}}{(2\pi)^2} \sum_{\alpha=0}^3 n_{\alpha,\alpha+1} \left( \mathcal{T}_{\sigma,B}^{\alpha,\alpha+1} - \mathcal{T}_{\sigma,C}^{\alpha,\alpha+1} \right), \quad (4.63)$$

$$\Phi^{(3)} = \int_0^\infty \frac{d\omega}{2\pi} \hbar\omega \sum_\sigma \int \frac{d^2\boldsymbol{\kappa}}{(2\pi)^2} \sum_{\alpha=0}^3 n_{\alpha,\alpha+1} \left( \mathcal{T}_{\sigma,C}^{\alpha,\alpha+1} - \mathcal{T}_{\sigma,D}^{\alpha,\alpha+1} \right). \quad (4.64)$$

## 4.2 Entropy fluxes in three-body systems

In addition to energy fluxes, entropy fluxes play a crucial role in the thermodynamics of the system. These fluxes represent the entropy radiated by the sources, hence, carried by the radiation, per unit area of the emitter and per unit of time. As discussed in the next chapter, these quantities are essential to obtain the thermodynamic availability of the system, which provides an upper bound for the energy flux that can be converted into usable work flux. Thus, here we are interested, in particular, in computing these quantities to be able to exploit the thermodynamic formalism in energy-conversion processes.

As a starting point to compute the entropy fluxes, we have to consider the fact that the thermal radiation in the system is produced by several sources at, in general, different temperatures. Thus, first we need to identify the energy flux of thermal radiation coming from the different constituents of the system that are in local thermal equilibrium at a given individual temperature and, from here, compute the associated partial entropy flux. Then, the corresponding total entropy flux will be given by the sum of all the partial ones. This is implemented by noting that the partial energy fluxes  $\Phi_\alpha^{(\beta)}(T_\alpha)$  on body  $\beta$ , characterized only by the temperature  $T_\alpha$ , can be identified from equations (4.62), (4.63), and (4.64) which give the total

energy fluxes  $\Phi^{(\beta)}$  on body  $\beta$ . In other words, we need the fluxes  $\Phi_\alpha^{(\beta)}(T_\alpha)$  such that

$$\Phi^{(\beta)} = \sum_\alpha \Phi_\alpha^{(\beta)}(T_\alpha). \quad (4.65)$$

In the case of  $\Phi^{(1)}$ , given by (4.62), the partial fluxes  $\Phi_\alpha^{(1)}(T_\alpha)$  are readily obtained as

$$\Phi_\alpha^{(1)}(T_\alpha) = \int_0^\infty \frac{d\omega}{2\pi} \hbar\omega \sum_\sigma \int \frac{d^2\kappa}{(2\pi)^2} n_\alpha \left( \mathcal{T}_{\sigma,A}^{\alpha,\alpha+1} - \mathcal{T}_{\sigma,B}^{\alpha,\alpha+1} - \mathcal{T}_{\sigma,A}^{\alpha-1,\alpha} + \mathcal{T}_{\sigma,B}^{\alpha-1,\alpha} \right), \quad (4.66)$$

for  $\alpha = 1, 2, 3$ , and

$$\Phi_0^{(1)}(T_0) = \int_0^\infty \frac{d\omega}{2\pi} \hbar\omega \sum_\sigma \int \frac{d^2\kappa}{(2\pi)^2} n_0 \left( \mathcal{T}_{\sigma,A}^{0,1} - \mathcal{T}_{\sigma,B}^{0,1} \right) \quad (4.67)$$

$$\Phi_4^{(1)}(T_4) = \int_0^\infty \frac{d\omega}{2\pi} \hbar\omega \sum_\sigma \int \frac{d^2\kappa}{(2\pi)^2} n_4 \left( \mathcal{T}_{\sigma,B}^{3,4} - \mathcal{T}_{\sigma,A}^{3,4} \right) \quad (4.68)$$

in the other cases, where each  $\Phi_\alpha^{(1)}(T_\alpha)$  depends only on the temperature  $T_\alpha$  through the photon distributions  $n_\alpha$ . It is not difficult to see from (4.63) and (4.64) that the fluxes  $\Phi_\alpha^{(2)}$  and  $\Phi_\alpha^{(3)}$  can be obtained from the previous expression for  $\Phi_\alpha^{(1)}$  by changing  $A \rightarrow B$ ,  $B \rightarrow C$  and  $A \rightarrow C$ ,  $B \rightarrow D$ , respectively. In addition, since local thermal equilibrium is assumed, the partial entropy fluxes  $\Psi_\alpha^{(\beta)}(T_\alpha)$  on body  $\beta$  must satisfy the thermodynamic relation

$$\frac{1}{T_\alpha} = \frac{d\Psi_\alpha^{(\beta)}}{d\Phi_\alpha^{(\beta)}}. \quad (4.69)$$

The above differential equation can be integrated to give

$$\Psi_\alpha^{(\beta)}(T_\alpha) - \Psi_\alpha^{(\beta)}(T_r) = \int_{T_r}^{T_\alpha} dT' \frac{1}{T'} \frac{d}{dT'} \Phi_\alpha^{(\beta)}(T'), \quad (4.70)$$

where  $T_r$  and  $\Psi_\alpha^{(\beta)}(T_r)$  are the temperature and the entropy flux corresponding to an arbitrary reference state, respectively.

In order to obtain the entropy fluxes from (4.70), we introduce the functions

$$m_\alpha(\omega) \equiv m(\omega, T_\alpha) = [1 + n_\alpha(\omega)] \ln [1 + n_\alpha(\omega)] - n_\alpha(\omega) \ln n_\alpha(\omega) \quad (4.71)$$

and  $m_{\alpha,\beta}(\omega) \equiv m_\alpha(\omega) - m_\beta(\omega)$ , which satisfy

$$m_{\alpha,r}(\omega) = \frac{\hbar\omega}{k_B} \int_{T_r}^{T_\alpha} dT' \frac{1}{T'} \frac{d}{dT'} n(\omega, T'). \quad (4.72)$$

Moreover, we assume that the temperature dependence of the optical properties of the bodies, which could be included in the transmission coefficients of the system, can be neglected in a certain range of working temperatures. Thus, if all the temperatures  $T_\alpha$  and the arbitrary temperature  $T_r$  lie within this range of working temperatures, we can safely use (4.70) by taking the photon distributions  $n(\omega, T_\alpha)$  included in  $\Phi_\alpha^{(\beta)}(T_\alpha)$  as the only temperature-dependent properties. This assumption, in fact, was already considered implicitly when we identified the energy fluxes  $\Phi_\alpha^{(\beta)}(T_\alpha)$ .

Furthermore, the total entropy flux  $\Psi^{(\beta)}$  on body  $\beta$  is given by the sum of all the partial entropy fluxes,

$$\Psi^{(\beta)} = \sum_\alpha \left[ \Psi_\alpha^{(\beta)}(T_\alpha) - \Psi_\alpha^{(\beta)}(T_r) \right]. \quad (4.73)$$

Using (4.70) and (4.72) with the previous considerations, for the body 1 we get

$$\begin{aligned} \Psi_\alpha^{(1)}(T_\alpha) - \Psi_\alpha^{(1)}(T_r) &= \int_0^\infty \frac{d\omega}{2\pi} k_B \sum_\sigma \int \frac{d^2\boldsymbol{\kappa}}{(2\pi)^2} m_{\alpha,r} \\ &\times \left( \mathcal{T}_{\sigma,A}^{\alpha,\alpha+1} - \mathcal{T}_{\sigma,B}^{\alpha,\alpha+1} - \mathcal{T}_{\sigma,A}^{\alpha-1,\alpha} + \mathcal{T}_{\sigma,B}^{\alpha-1,\alpha} \right), \end{aligned} \quad (4.74)$$

for  $\alpha = 1, 2, 3$ , and

$$\Psi_0^{(1)}(T_0) - \Psi_0^{(1)}(T_r) = \int_0^\infty \frac{d\omega}{2\pi} k_B \sum_\sigma \int \frac{d^2\boldsymbol{\kappa}}{(2\pi)^2} m_{0,r} \left( \mathcal{T}_{\sigma,A}^{0,1} - \mathcal{T}_{\sigma,B}^{0,1} \right) \quad (4.75)$$

$$\Psi_4^{(1)}(T_4) - \Psi_4^{(1)}(T_r) = \int_0^\infty \frac{d\omega}{2\pi} k_B \sum_\sigma \int \frac{d^2\boldsymbol{\kappa}}{(2\pi)^2} m_{4,r} \left( \mathcal{T}_{\sigma,B}^{3,4} - \mathcal{T}_{\sigma,A}^{3,4} \right) \quad (4.76)$$

in the cases  $\alpha = 0, 4$ . The fluxes  $\Psi_\alpha^{(2)}(T_\alpha) - \Psi_\alpha^{(2)}(T_r)$  and  $\Psi_\alpha^{(2)}(T_\alpha) - \Psi_\alpha^{(2)}(T_r)$  on bodies 2 and 3 can be obtained from the previous expression for the body 1 by changing  $A \rightarrow B$ ,  $B \rightarrow C$  and  $A \rightarrow C$ ,  $B \rightarrow D$ , respectively. Hence, from (4.73), we now can write down the total entropy fluxes  $\Psi^{(\beta)}$  on each body  $\beta$ . This yields

$$\Psi^{(1)} = \int_0^\infty \frac{d\omega}{2\pi} k_B \sum_\sigma \int \frac{d^2\boldsymbol{\kappa}}{(2\pi)^2} \sum_{\alpha=0}^3 m_{\alpha,\alpha+1} \left( \mathcal{T}_{\sigma,A}^{\alpha,\alpha+1} - \mathcal{T}_{\sigma,B}^{\alpha,\alpha+1} \right), \quad (4.77)$$

$$\Psi^{(2)} = \int_0^\infty \frac{d\omega}{2\pi} k_B \sum_\sigma \int \frac{d^2\boldsymbol{\kappa}}{(2\pi)^2} \sum_{\alpha=0}^3 m_{\alpha,\alpha+1} \left( \mathcal{T}_{\sigma,B}^{\alpha,\alpha+1} - \mathcal{T}_{\sigma,C}^{\alpha,\alpha+1} \right), \quad (4.78)$$

$$\Psi^{(3)} = \int_0^\infty \frac{d\omega}{2\pi} k_B \sum_\sigma \int \frac{d^2\boldsymbol{\kappa}}{(2\pi)^2} \sum_{\alpha=0}^3 m_{\alpha,\alpha+1} \left( \mathcal{T}_{\sigma,C}^{\alpha,\alpha+1} - \mathcal{T}_{\sigma,D}^{\alpha,\alpha+1} \right). \quad (4.79)$$

Thus, we note that all contributions associated with the arbitrary reference state cancel out because only differences of entropy fluxes are involved. This can be explicitly seen by realizing that when collecting all terms containing the function  $m_r$  for, e.g, body 1, one ends with a contribution from the transmission coefficients that takes the form

$$\mathcal{T}_{\sigma,A}^{0,1} - \mathcal{T}_{\sigma,B}^{0,1} + \sum_{\alpha=1}^3 \left( \mathcal{T}_{\sigma,A}^{\alpha,\alpha+1} - \mathcal{T}_{\sigma,B}^{\alpha,\alpha+1} - \mathcal{T}_{\sigma,A}^{\alpha-1,\alpha} + \mathcal{T}_{\sigma,B}^{\alpha-1,\alpha} \right) - \mathcal{T}_{\sigma,A}^{3,4} + \mathcal{T}_{\sigma,B}^{3,4} = 0, \quad (4.80)$$

and analogous expressions for bodies 2 and 3 with the substitutions  $A \rightarrow B$ ,  $B \rightarrow C$  and  $A \rightarrow C$ ,  $B \rightarrow D$ , respectively.

As a final remark, we want to stress that these expressions for the entropy fluxes can be equivalently obtained if one considers [3, 4, 6, 7]

$$\Psi_{\alpha}^{(\beta)}(T_{\alpha}) = \int_0^{T_{\alpha}} dT' \frac{1}{T'} \frac{d}{dT'} \Phi_{\alpha}^{(\beta)}(T') \quad (4.81)$$

instead of equation (4.70) to compute the partial entropy fluxes. In this case the reference state corresponds to that for which  $T_r = 0$  and  $\Psi_{\alpha}^{(\beta)}(T_r) = 0$ . Our aim here was to show explicitly that it is not necessary to assume that the optical properties of the materials does not depend on the temperature in the whole interval  $(0, T_{\alpha})$  but only in a smaller interval containing the temperatures of the problem at hand. In addition, if we are allowed to neglect the temperature dependence of the transmission coefficients when computing the energy fluxes, we can proceed in the same manner for the entropy fluxes as well. This ensures that when using optical data describing the material properties measured at a given temperature, the error introduced in computing entropy fluxes will not be so big if the system is working at temperatures close to that at which the optical data were measured. This argument holds, of course, also for the two-body systems considered below, which are a particular case of the one presented here, and can be generalized to the many-body case.

### 4.3 Energy and entropy fluxes in two-body systems

So far we have considered a system consisting of three bodies of finite size in thermal radiative interaction. From here, as discussed below, the thermostatics of a two-body system can be obtained as a particular case. First we obtain the energy and entropy fluxes assuming that the bodies are finite, and afterwards we discuss the limit in which they are semi-infinite. This, in turn, allows us to easily obtain the particular case of blackbody radiation.

### 4.3.1 Finite bodies

A two-body system can be obtained as a limiting case by appropriately removing, for instance, the body 3. This can be done simply by assuming that the medium in body 3 is a vacuum, thus taking its dielectric permittivity as  $\varepsilon_3 = 1$ . Under this assumption, the Fresnel reflection coefficients vanish,  $r_{3\sigma} = 0$ , and the vacuum-medium and medium-vacuum transmission coefficients become unity,  $t_{3\sigma} = 1$  and  $\bar{t}_{3\sigma} = 1$ , respectively. Hence, the reflection and transmission coefficients of body 3 turn into  $\rho_\sigma^{(3)\phi} = 0$  and  $\tau_\sigma^{(3)} = 1$ , in accordance with equations (4.18) and (4.20). Since now medium 3 is a vacuum, for convenience, we take the temperature  $T_3$  to be that of right environment and forget about the temperature  $T_4$  by setting  $T_4 = T_3$ . For the same reason, here we formally ignore region D. Thus, we are left with bodies 1 and 2 that define three vacuum regions, A, B, and C.

Using that  $\rho_\sigma^{(3)\phi} = 0$  and  $\tau_\sigma^{(3)} = 1$ , it is easy to see that the following two-body scattering coefficients become  $\rho_\sigma^{(23)\phi} \rightarrow \rho_\sigma^{(2)\phi}$ ,  $\tau_\sigma^{(23)} \rightarrow \tau_\sigma^{(2)}$ , and  $u_\sigma^{(2,3)} \rightarrow 1$ , while the three-body coefficients take the form  $u_\sigma^{(1,23)} \rightarrow u_\sigma^{(1,2)}$ ,  $u_\sigma^{(12,3)} \rightarrow 1$ ,  $\rho_\sigma^{(123)\phi} \rightarrow \rho_\sigma^{(12)\phi}$ , and  $\tau_\sigma^{(123)} \rightarrow \tau_\sigma^{(12)}$ . By taking into account these prescriptions, the transmission coefficients of the two-body system can be obtained from those of the three-body system. These transmission coefficients are all given explicitly in Appendix B. It can be seen that in regions A and C only propagative modes contribute to the transfer. In the cavity, i.e., region B, however, there is also contribution of evanescent modes. This contribution of the evanescent field enters through the transmission coefficient associated to bodies 1 and 2 in this region, which takes the form

$$\mathcal{T}_{\sigma,B}^{1,2} = \Pi^{(\text{pw})} \frac{\left(1 - |\rho_\sigma^{(1)+}|^2\right) \left(1 - |\rho_\sigma^{(2)-}|^2\right)}{\left|1 - \rho_\sigma^{(1)+} \rho_\sigma^{(2)-}\right|^2} + \Pi^{(\text{ew})} \frac{4\text{Im}\left(\rho_\sigma^{(1)+}\right) \text{Im}\left(\rho_\sigma^{(2)-}\right)}{\left|1 - \rho_\sigma^{(1)+} \rho_\sigma^{(2)-}\right|^2}. \quad (4.82)$$

In the two-body system, the total energy flux on bodies 1 and 2,  $\Phi^{(1)}$  and  $\Phi^{(2)}$ , respectively, are given by

$$\Phi^{(1)} = \int_0^\infty \frac{d\omega}{2\pi} \hbar\omega \sum_\sigma \int \frac{d^2\boldsymbol{\kappa}}{(2\pi)^2} \sum_{\alpha=0}^2 n_{\alpha,\alpha+1} \left(\mathcal{T}_{\sigma,A}^{\alpha,\alpha+1} - \mathcal{T}_{\sigma,B}^{\alpha,\alpha+1}\right), \quad (4.83)$$

$$\Phi^{(2)} = \int_0^\infty \frac{d\omega}{2\pi} \hbar\omega \sum_\sigma \int \frac{d^2\boldsymbol{\kappa}}{(2\pi)^2} \sum_{\alpha=0}^2 n_{\alpha,\alpha+1} \left(\mathcal{T}_{\sigma,B}^{\alpha,\alpha+1} - \mathcal{T}_{\sigma,C}^{\alpha,\alpha+1}\right). \quad (4.84)$$

Likewise, the total entropy fluxes on body 1 and 2,  $\Psi^{(1)}$  and  $\Psi^{(2)}$ , respectively, can be written as

$$\Psi^{(1)} = \int_0^\infty \frac{d\omega}{2\pi} k_B \sum_\sigma \int \frac{d^2\boldsymbol{\kappa}}{(2\pi)^2} \sum_{\alpha=0}^2 m_{\alpha,\alpha+1} \left(\mathcal{T}_{\sigma,A}^{\alpha,\alpha+1} - \mathcal{T}_{\sigma,B}^{\alpha,\alpha+1}\right), \quad (4.85)$$

$$\Psi^{(2)} = \int_0^\infty \frac{d\omega}{2\pi} k_B \sum_\sigma \int \frac{d^2\boldsymbol{\kappa}}{(2\pi)^2} \sum_{\alpha=0}^2 m_{\alpha,\alpha+1} \left( \mathcal{T}_{\sigma,B}^{\alpha,\alpha+1} - \mathcal{T}_{\sigma,C}^{\alpha,\alpha+1} \right). \quad (4.86)$$

### 4.3.2 Semi-infinite bodies

Here we consider the situation in which bodies 1 and 2 are two semi-infinite media. First, we set the temperature of the left environment to  $T_0 = T_1$  and that of the right environment to  $T_3 = T_2$ . We also take  $\tau_\sigma^{(1)} \rightarrow 0$  and  $\tau_\sigma^{(2)} \rightarrow 0$ , since there is no transmission through the bodies when the thicknesses  $\delta_1$  and  $\delta_2$  tend to infinity [103]. Under these assumptions,  $\mathcal{T}_{\sigma,B}^{1,2}$  is the only transmission coefficient that survives in the expressions for the fluxes  $\Phi^{(1)}$  and  $\Phi^{(2)}$  given by (4.83) and (4.84). That is,

$$\Phi^{(1)} = - \int_0^\infty \frac{d\omega}{2\pi} \hbar\omega \sum_\sigma \int \frac{d^2\boldsymbol{\kappa}}{(2\pi)^2} n_{1,2}(\omega) \mathcal{T}_\sigma(\boldsymbol{\kappa}, \omega, d), \quad (4.87)$$

$$\Phi^{(2)} = \int_0^\infty \frac{d\omega}{2\pi} \hbar\omega \sum_\sigma \int \frac{d^2\boldsymbol{\kappa}}{(2\pi)^2} n_{1,2}(\omega) \mathcal{T}_\sigma(\boldsymbol{\kappa}, \omega, d), \quad (4.88)$$

where we denote by  $\mathcal{T}_\sigma(\boldsymbol{\kappa}, \omega, d)$  the transmission coefficient  $\mathcal{T}_{\sigma,B}^{1,2}$  of the two-body system in the limiting case where the two bodies are semi-infinite, while  $d$  is the separation distance between them,  $d \equiv d_{12}$ . Thus, the coefficient  $\mathcal{T}_\sigma(\boldsymbol{\kappa}, \omega, d)$  can be obtained from (4.82) in this limit, which will be done in what follows.

Since  $d = z_2 - z_1 - \delta_1/2 - \delta_2/2$  remains finite when the bodies are considered as semi-infinite (see the figure 4.1), we have  $\rho_\sigma^{(1)+} \rho_\sigma^{(2)-} = \rho_\sigma^{(1)} \rho_\sigma^{(2)} e^{2ik_z d}$  and

$$\Pi^{(\text{ew})} \text{Im} \left( \rho_\sigma^{(1)+} \right) \text{Im} \left( \rho_\sigma^{(2)-} \right) = \Pi^{(\text{ew})} \text{Im} \left( \rho_\sigma^{(1)} \right) \text{Im} \left( \rho_\sigma^{(2)} \right) e^{-2|k_z|d}. \quad (4.89)$$

The property  $\Pi^{(\text{pw})} \left| \rho_\sigma^{(\alpha)\phi} \right|^2 = \Pi^{(\text{pw})} \left| \rho_\sigma^{(\alpha)} \right|^2$  is also useful for this purpose. Furthermore, in the limit of infinite thickness, the reflection coefficients of the bodies become the usual Fresnel reflection coefficients [103],  $\rho_\sigma^{(\alpha)} \rightarrow r_{\alpha\sigma}$ , given in (4.22). According to this, the transmission coefficient (4.82) becomes [115, 116]

$$\mathcal{T}_\sigma = \Pi^{(\text{pw})} \frac{\left(1 - |r_{1\sigma}|^2\right) \left(1 - |r_{2\sigma}|^2\right)}{|1 - r_{1\sigma} r_{2\sigma} e^{2ik_z d}|^2} + \Pi^{(\text{ew})} \frac{4\text{Im}(r_{1\sigma}) \text{Im}(r_{2\sigma}) e^{-2|k_z|d}}{|1 - r_{1\sigma} r_{2\sigma} e^{-2|k_z|d}|^2}. \quad (4.90)$$

From the above result, we obtain the well-know expression for the net energy flux in the cavity as a function of the separation distance,  $\Phi(d)$ , which equals the total

flux on body 2 and can be written as [12, 99, 105, 106, 148]

$$\begin{aligned} \Phi(d) &= \sum_{\sigma} \int_0^{\infty} d\omega \hbar\omega n_{1,2}(\omega) \\ &\times \left[ \int_0^{\omega/c} \frac{d\kappa \kappa}{(2\pi)^2} \frac{(1 - |r_{1\sigma}|^2)(1 - |r_{2\sigma}|^2)}{|1 - r_{1\sigma}r_{2\sigma}e^{2ik_z d}|^2} \right. \\ &\quad \left. + \int_{\omega/c}^{\infty} \frac{d\kappa \kappa}{(2\pi)^2} \frac{4\text{Im}(r_{1\sigma})\text{Im}(r_{2\sigma})e^{-2|k_z|d}}{|1 - r_{1\sigma}r_{2\sigma}e^{-2|k_z|d}|^2} \right], \end{aligned} \quad (4.91)$$

where we have used that  $d^2\boldsymbol{\kappa} = 2\pi\kappa d\kappa$ . In equivalent way, we can write

$$\Phi(d) = \int_0^{\infty} d\omega \hbar\omega n_{1,2}(\omega) \varphi(\omega, d) \quad (4.92)$$

with the quantity  $\varphi(\omega, d)$  easily recognizable from (4.91). In references [3, 6, 7],  $\varphi(\omega, d)$  is called the spectral flux of modes and is given by

$$\begin{aligned} \varphi(\omega, d) &= \sum_{\sigma} \left[ \int_0^{\omega/c} \frac{d\kappa \kappa}{(2\pi)^2} \frac{(1 - |r_{1\sigma}|^2)(1 - |r_{2\sigma}|^2)}{|1 - r_{1\sigma}r_{2\sigma}e^{2ik_z d}|^2} \right. \\ &\quad \left. + \int_{\omega/c}^{\infty} \frac{d\kappa \kappa}{(2\pi)^2} \frac{4\text{Im}(r_{1\sigma})\text{Im}(r_{2\sigma})e^{-2|k_z|d}}{|1 - r_{1\sigma}r_{2\sigma}e^{-2|k_z|d}|^2} \right]. \end{aligned} \quad (4.93)$$

In terms of the transmission coefficients of the system, it reads as

$$\varphi(\omega, d) = \sum_{\sigma} \int \frac{d^2\boldsymbol{\kappa}}{(2\pi)^3} \mathcal{T}_{\sigma}(\boldsymbol{\kappa}, \omega, d). \quad (4.94)$$

To conclude, we write the total entropy fluxes on bodies 1 and 2 when the bodies are semi-infinite,

$$\Psi^{(1)} = - \int_0^{\infty} \frac{d\omega}{2\pi} k_B \sum_{\sigma} \int \frac{d^2\boldsymbol{\kappa}}{(2\pi)^2} m_{1,2}(\omega) \mathcal{T}_{\sigma}(\boldsymbol{\kappa}, \omega, d), \quad (4.95)$$

$$\Psi^{(2)} = \int_0^{\infty} \frac{d\omega}{2\pi} k_B \sum_{\sigma} \int \frac{d^2\boldsymbol{\kappa}}{(2\pi)^2} m_{1,2}(\omega) \mathcal{T}_{\sigma}(\boldsymbol{\kappa}, \omega, d), \quad (4.96)$$

and introduce the net entropy flux in the cavity  $\Psi(d) = \Psi^{(2)}$  which can be written as [7]

$$\Psi(d) = \int_0^{\infty} d\omega k_B m_{1,2}(\omega) \varphi(\omega, d). \quad (4.97)$$

### 4.3.3 Blackbody limit

The case of blackbody radiation [66] is obtained by assuming that the materials are perfect absorbers, so that  $r_{1\sigma} = r_{2\sigma} = 0$ . Using this in (4.93), the contribution of evanescent waves vanishes and the spectral flux of modes becomes

$$\varphi_{\text{bb}}(\omega) = \left( \frac{\omega}{2\pi c} \right)^2, \quad (4.98)$$

where the subscript bb refers to blackbody. Thus, when the energy flux (4.92) is evaluated with  $\varphi = \varphi_{\text{bb}}$ , it reduces to the Stefan-Boltzmann law

$$\Phi_{\text{bb}} = \sigma_{\text{SB}} (T_1^4 - T_2^4), \quad (4.99)$$

where  $\sigma_{\text{SB}} = \pi^2 k_{\text{B}}^4 / 60 \hbar^3 c^2$  is the Stefan-Boltzmann constant. Since evanescent waves are completely neglected here, the idealized case of blackbody radiation and the associated Stefan-Boltzmann law constitute a limit for the radiative heat transfer between largely separated bodies, in the far field. This is precisely the limit that can be overcome in the near-field regime [12, 68–70]. Moreover, the entropy flux for blackbody radiation, obtained from (4.97) with  $\varphi = \varphi_{\text{bb}}$ , takes the well-known form

$$\Psi_{\text{bb}} = \frac{4}{3} \sigma_{\text{SB}} (T_1^3 - T_2^3). \quad (4.100)$$

## 4.4 Fluxes in the near-field regime

In the previous sections, the energy and entropy fluxes were derived for arbitrary separation distances between the bodies, thus taking into account both far-field and near-field contributions. Here we consider the particular situation in which these separation distances are small as compared with the thermal wavelength  $\lambda_T = \hbar c / k_{\text{B}} T$  ( $\lambda_T \approx 7.6 \mu\text{m}$  when  $T = 300 \text{ K}$ ). This ensures that the radiative heat transfer takes place in the near-field regime. Furthermore, it is a well-known fact that the contribution of evanescent waves to the heat transfer is dominant in the near-field regime [12, 99, 105, 106]. Since evanescent waves are nonpropagative modes of the electromagnetic field, the associated heat transfer can be seen as mediated by the tunneling of photons between the sources [94]. Thus, photon tunneling mainly dominates the fluxes of energy and entropy in the near-field regime. Moreover, we will assume that the contribution of propagative waves can be completely neglected in this regime.

For further purpose, below we rewrite the energy and entropy fluxes for three- and two-body systems, and their corresponding transmission coefficients, maintaining

only the dominant contribution of evanescent modes. We will also show with some detail, in a particular situation, that when the materials support a resonant surface wave, the fluxes are near-monochromatic in the near field.

#### 4.4.1 Three-body systems

We are now interested in considering near-field effects associated to the projections of the fluxes on the evanescent sector. These effects can only be given in the vacuum gaps between the bodies, since the contribution of evanescent waves is only present in these region of the system. In the three-body system, we thus have to consider regions B and C. Moreover, in those regions, the contribution to the fluxes coming from the interaction of the bodies with the environmental fields at  $T_0$  and  $T_4$  is only due to propagative waves, and, hence, can be neglected. The relevant transmission coefficients are, therefore, given by

$$\mathcal{T}_{\sigma,B}^{1,2} = \frac{4\text{Im}(\rho_{\sigma}^{(1)+})\text{Im}(\rho_{\sigma}^{(23)-})}{|1 - \rho_{\sigma}^{(1)+}\rho_{\sigma}^{(23)-}|^2}, \quad (4.101)$$

$$\mathcal{T}_{\sigma,B}^{2,3} = \frac{4|\tau_{\sigma}^{(2)}|^2\text{Im}(\rho_{\sigma}^{(1)+})\text{Im}(\rho_{\sigma}^{(3)-})}{|1 - \rho_{\sigma}^{(1)+}\rho_{\sigma}^{(23)-}|^2|1 - \rho_{\sigma}^{(2)+}\rho_{\sigma}^{(3)-}|^2}, \quad (4.102)$$

$$\mathcal{T}_{\sigma,C}^{1,2} = \frac{4|\tau_{\sigma}^{(2)}|^2\text{Im}(\rho_{\sigma}^{(1)+})\text{Im}(\rho_{\sigma}^{(3)-})}{|1 - \rho_{\sigma}^{(12)+}\rho_{\sigma}^{(3)-}|^2|1 - \rho_{\sigma}^{(1)+}\rho_{\sigma}^{(2)-}|^2}, \quad (4.103)$$

$$\mathcal{T}_{\sigma,C}^{2,3} = \frac{4\text{Im}(\rho_{\sigma}^{(12)+})\text{Im}(\rho_{\sigma}^{(3)-})}{|1 - \rho_{\sigma}^{(12)+}\rho_{\sigma}^{(3)-}|^2}, \quad (4.104)$$

where we have taken into account that the fluxes containing these coefficients will be projected on the evanescent sector in which  $\Pi^{(\text{ew})} = 1$ . Hence, using the above expressions for the transmission coefficients and from (4.62), (4.63), and (4.64), in the near-field regime, the total energy fluxes on the bodies 1, 2, and 3 take the form

$$\Phi^{(1)} = - \int_0^{\infty} \frac{d\omega}{2\pi} \hbar\omega \sum_{\sigma} \int_{c\kappa > \omega} \frac{d^2\boldsymbol{\kappa}}{(2\pi)^2} \sum_{\alpha=1}^2 n_{\alpha,\alpha+1} \mathcal{T}_{\sigma,B}^{\alpha,\alpha+1}, \quad (4.105)$$

$$\Phi^{(2)} = \int_0^{\infty} \frac{d\omega}{2\pi} \hbar\omega \sum_{\sigma} \int_{c\kappa > \omega} \frac{d^2\boldsymbol{\kappa}}{(2\pi)^2} \sum_{\alpha=1}^2 n_{\alpha,\alpha+1} (\mathcal{T}_{\sigma,B}^{\alpha,\alpha+1} - \mathcal{T}_{\sigma,C}^{\alpha,\alpha+1}), \quad (4.106)$$

$$\Phi^{(3)} = \int_0^{\infty} \frac{d\omega}{2\pi} \hbar\omega \sum_{\sigma} \int_{c\kappa > \omega} \frac{d^2\boldsymbol{\kappa}}{(2\pi)^2} \sum_{\alpha=1}^2 n_{\alpha,\alpha+1} \mathcal{T}_{\sigma,C}^{\alpha,\alpha+1}. \quad (4.107)$$

In analogous manner, from (4.77), (4.78), and (4.79), in the near-field regime, the total entropy fluxes on the bodies 1, 2, and 3 become

$$\Psi^{(1)} = - \int_0^\infty \frac{d\omega}{2\pi} k_B \sum_\sigma \int_{c\kappa > \omega} \frac{d^2\kappa}{(2\pi)^2} \sum_{\alpha=1}^2 m_{\alpha,\alpha+1} \mathcal{T}_{\sigma,B}^{\alpha,\alpha+1}, \quad (4.108)$$

$$\Psi^{(2)} = \int_0^\infty \frac{d\omega}{2\pi} k_B \sum_\sigma \int_{c\kappa > \omega} \frac{d^2\kappa}{(2\pi)^2} \sum_{\alpha=1}^2 m_{\alpha,\alpha+1} \left( \mathcal{T}_{\sigma,B}^{\alpha,\alpha+1} - \mathcal{T}_{\sigma,C}^{\alpha,\alpha+1} \right), \quad (4.109)$$

$$\Psi^{(3)} = \int_0^\infty \frac{d\omega}{2\pi} k_B \sum_\sigma \int_{c\kappa > \omega} \frac{d^2\kappa}{(2\pi)^2} \sum_{\alpha=1}^2 m_{\alpha,\alpha+1} \mathcal{T}_{\sigma,C}^{\alpha,\alpha+1}. \quad (4.110)$$

#### 4.4.2 Two-body systems

In the two-body system considered previously in Section 4.3.1, the contribution of evanescent waves occurs only in region B, the cavity formed by bodies 1 and 2. In this region, in turn, the bodies are coupled with the environmental fields characterized by the temperatures  $T_0$  and  $T_3$  only through propagative waves, so that these contributions to the fluxes can be neglected. Thus, as before, taking into account that the fluxes will be projected on the evanescent sector, the relevant transmission coefficient in this case is given by

$$\mathcal{T}_{\sigma,B}^{1,2} = \frac{4\text{Im}(\rho_\sigma^{(1)+}) \text{Im}(\rho_\sigma^{(2)-})}{|1 - \rho_\sigma^{(1)+} \rho_\sigma^{(2)-}|^2}. \quad (4.111)$$

As a consequence, in the near field, the total energy flux on bodies 1 and 2 become

$$\Phi^{(1)} = - \int_0^\infty \frac{d\omega}{2\pi} \hbar\omega \sum_\sigma \int_{c\kappa > \omega} \frac{d^2\kappa}{(2\pi)^2} n_{1,2} \mathcal{T}_{\sigma,B}^{1,2}, \quad (4.112)$$

$$\Phi^{(2)} = \int_0^\infty \frac{d\omega}{2\pi} \hbar\omega \sum_\sigma \int_{c\kappa > \omega} \frac{d^2\kappa}{(2\pi)^2} n_{1,2} \mathcal{T}_{\sigma,B}^{1,2}, \quad (4.113)$$

while the total entropy fluxes take the form

$$\Psi^{(1)} = - \int_0^\infty \frac{d\omega}{2\pi} k_B \sum_\sigma \int_{c\kappa > \omega} \frac{d^2\kappa}{(2\pi)^2} m_{1,2} \mathcal{T}_{\sigma,B}^{1,2}, \quad (4.114)$$

$$\Psi^{(2)} = \int_0^\infty \frac{d\omega}{2\pi} k_B \sum_\sigma \int_{c\kappa > \omega} \frac{d^2\kappa}{(2\pi)^2} m_{1,2} \mathcal{T}_{\sigma,B}^{1,2}. \quad (4.115)$$

### 4.4.3 Near-monochromatic approximation: the extreme near field

In this section we study a two-body system in which the two bodies are semi-infinite and are separated by a distance  $d \ll \lambda_T$ . The regime for which the separation distance is very small as compared with the thermal wavelength is called extreme near-field regime. For simplicity, we assume now that the two bodies are made of the same material, in such a way that the Fresnel reflection coefficients are the same for the two bodies,  $r_\sigma \equiv r_{1\sigma} = r_{2\sigma}$ . In addition, it is important to emphasize here that we are assuming throughout the text that the permittivity of the material is local, which means that the permittivity at a given point is not correlated with its value at a different point [149]. This fact imposes a restriction in the minimum value that can be assumed for  $d$ , since below a certain separation distance, non-local effects have to be necessarily taken into account. For dielectrics, the minimum value for the separations can be assumed to be the interatomic distance, while for metals it is given by the Thomas-Fermi screening length [115, 149–152]. Moreover, below we will see that the fluxes behave as  $\sim 1/d^2$  in this regime; the divergence at  $d \rightarrow 0$ , which is unphysical, is due to the local approach in which this minimum distance is not incorporated.

Furthermore, we assume that the material is polar dielectric. At the surface of these materials, that is, at the material-vacuum interface, the coupling of optical phononic excitations with the electromagnetic fields results in the so-called surface phonon polaritons (SPPs). These surface waves can be thermally excited at the nanoscale, since their characteristic frequency is typically located in the infrared [99, 105, 153]. It can be seen analytically that the heat transfer is near-monochromatic in the near field and that the associated spectrum is strongly peaked at the frequency of the SPP. This theoretical result [154], derived below, will be used in the next chapter to compare the thermodynamics of energy-conversion processes involving near-field thermal radiation with other results in the literature concerning near-monochromatic radiation.

According to (4.92) and (4.97), the net energy and entropy fluxes on body 2,  $\Phi(d)$  and  $\Psi(d)$ , respectively, in the near-field regime can be written as

$$\Phi(d) = \int_0^\infty d\omega \hbar\omega n_{1,2}(\omega) \varphi_{\text{nf}}(\omega, d). \quad (4.116)$$

$$\Psi(d) = \int_0^\infty d\omega k_B m_{1,2}(\omega) \varphi_{\text{nf}}(\omega, d), \quad (4.117)$$

where we have introduced the near-field contribution to the spectral flux of modes

$$\varphi_{\text{nf}}(\omega, d) = \sum_\sigma \int_{\omega/c}^\infty \frac{d\kappa \kappa}{(2\pi)^2} \frac{4\text{Im}^2(r_\sigma) e^{-2|k_z|d}}{|1 - r_\sigma^2 e^{-2|k_z|d}|^2} \quad (4.118)$$

for two identical bodies. The expression (4.118) is obtained from (4.93) by keeping only the term corresponding to evanescent waves.

For polar materials and when  $d \ll \lambda_T$ , the spectral flux of modes is mainly dominated by<sup>1</sup>  $p$ -polarized evanescent modes [105, 106]. This allows us to consider only the term with  $\sigma = p$  in (4.118), and neglect that with  $\sigma = s$ . Furthermore, assuming the electrostatic limit in which  $\kappa \gg \omega/c$ , so that  $|k_z| \simeq \kappa$ , the Fresnel reflection coefficient for  $p$ -polarized waves does not depend on  $\kappa$  and can be written as

$$r_p(\omega) \simeq \frac{\varepsilon(\omega) - 1}{\varepsilon(\omega) + 1}. \quad (4.119)$$

Under these assumptions, the spectral flux of modes can be approximated by

$$\begin{aligned} \varphi_{\text{nf}}(\omega, d) &\simeq \frac{1}{\pi^2} \text{Im}^2[r_p(\omega)] \int_0^\infty \frac{d\kappa \kappa e^{-2\kappa d}}{|1 - r_p^2(\omega) e^{-2\kappa d}|^2} \\ &= \frac{1}{\pi^2} \frac{\text{Im}^2[r_p(\omega)]}{\text{Im}[r_p^2(\omega)]} \text{Im} \int_0^\infty \frac{d\kappa \kappa r_p^2(\omega) e^{-2\kappa d}}{1 - r_p^2(\omega) e^{-2\kappa d}}. \end{aligned} \quad (4.120)$$

The integral in (4.120) can be computed to give

$$\varphi_{\text{nf}}(\omega, d) = \text{Im} \left\{ \frac{\text{Li}_2[r_p^2(\omega)]}{4\pi^2 d^2 f(\omega)} \right\}, \quad (4.121)$$

where  $\text{Li}_2(z)$  is the dilogarithm function<sup>2</sup>, we have introduced [154]

$$f(\omega) = \frac{\text{Im}[r_p^2(\omega)]}{\text{Im}^2[r_p(\omega)]} \quad (4.122)$$

and used that  $f(\omega)$  is a real-valued function. As a result, using the approximation given by (4.121), the energy flux can be written as

$$\Phi(d) = \text{Im} \left\{ \mathcal{P} \int_0^\infty d\omega \hbar\omega n_{1,2}(\omega) \frac{\text{Li}_2[r_p^2(\omega)]}{4\pi^2 d^2 f(\omega)} \right\}, \quad (4.123)$$

where  $\mathcal{P}$  denotes the Cauchy principal value: this gives the correct prescription to compute the integral, since its integrand has simple poles arising from the zeros of

<sup>1</sup>In the cases where the materials are metals,  $s$ -polarized evanescent modes can be the dominant contribution [150], so that the treatment given here is not applicable in those cases.

<sup>2</sup>The dilogarithm is defined for complex  $z$  by

$$\text{Li}_2(z) = - \int_0^z dt \frac{\ln(1-t)}{t}.$$

the function  $f(\omega)$ . We will come back to this point later on. Besides, we note that an expression analogous to (4.123) can be obtained for the entropy flux  $\Psi(d)$ .

Let us assume that the permittivity of the material can be suitably described by the Lorentz model

$$\varepsilon(\omega) = \varepsilon_\infty \left( \frac{\omega_L^2 - \omega^2 - i\Gamma\omega}{\omega_T^2 - \omega^2 - i\Gamma\omega} \right), \quad (4.124)$$

where  $\varepsilon_\infty$ ,  $\omega_L$ ,  $\omega_T$ , and  $\Gamma$  are material-dependent parameters. In particular,  $\Gamma$  takes into account the losses in the material. This model is adequate for describing materials such as silicon carbide (SiC) or hexagonal boron nitride (hBN), among others. Thus, introducing

$$\omega_0 = \left( \frac{\varepsilon_\infty \omega_L^2 + \omega_T^2}{\varepsilon_\infty + 1} \right)^{1/2}, \quad (4.125)$$

$$\omega_1 = \left( \frac{\varepsilon_\infty \omega_L^2 + \omega_T^2}{\varepsilon_\infty + 1} \right)^{1/2}, \quad (4.126)$$

and assuming that  $\Gamma$  is small as compared with the other characteristic frequencies  $\omega_L$  and  $\omega_T$ , the function  $f(\omega)$  is given by

$$f(\omega) = -\frac{2(\omega^2 - \omega_0^2)(\omega^2 - \omega_1^2)}{\omega(\omega_0^2 - \omega_1^2)\Gamma}. \quad (4.127)$$

We thus see that  $1/f(\omega)$  has simple poles at  $\omega_0$  and  $\omega_1$  on the real positive axis. The resonance frequency  $\omega_0$  is the frequency of the single-surface SPP supported by the material, which, according (4.124), satisfies  $\text{Re}[\varepsilon(\omega_0)] = -1$  in the limit of small losses. In addition, the frequency  $\omega_1$  is the Christiansen frequency of the material that satisfies  $\text{Re}[\varepsilon(\omega_1)] = 1$  (in the limit of small losses).

To compute (4.123), we can perform an integration in the complex plane by choosing a contour consisting of the real positive axis excluding the poles at  $\omega_0$  and  $\omega_1$ , a quarter of circle joining the positive real infinity with the positive imaginary infinity, and a path returning to the origin along the positive imaginary axis excluding the poles due to the photon distributions. The poles of the Fresnel reflection coefficient are located at the lower half-plane, so that they do not contribute in this contour integration [154]. Since the integration along the semicircle vanishes and the imaginary part of the contribution from the integration along the imaginary axis can be neglected [154], one obtains

$$\text{Im} \left\{ \mathcal{P} \int_0^\infty d\omega \hbar\omega n_{1,2}(\omega) \frac{\text{Li}_2[r_p^2(\omega)]}{4\pi^2 d^2 f(\omega)} \right\} = \text{Im} \left\{ i\pi \sum_{j=0,1} \text{Res}(\omega_j) \right\}, \quad (4.128)$$

where

$$\text{Res}(\omega_j) = \hbar\omega_j n_{1,2}(\omega_j) \frac{\text{Li}_2[r_p^2(\omega_j)]}{4\pi^2 d^2 f'(\omega_j)} \quad (4.129)$$

is the residue of the integrand evaluated at the poles and

$$f'(\omega) = \frac{df(\omega)}{d\omega}. \quad (4.130)$$

However, the contribution coming from  $\omega_1$  is small as compared with that from  $\omega_0$  and can also be neglected. Taking this into account, equation (4.123) becomes

$$\Phi(d) = \hbar\omega_0 n_{1,2}(\omega_0) \frac{\text{Re} \left\{ \text{Li}_2[r_p^2(\omega_0)] \right\}}{4\pi d^2 f'(\omega_0)}, \quad (4.131)$$

where  $f'(\omega_0) \simeq -4/\Gamma$ . Equation (4.131) shows that the radiation is highly monochromatic with dominant frequency  $\omega_0$ , so that the tunneling of SPPs is the main mechanism of heat transfer in this regime. Moreover, by comparing (4.131) with (4.116), although not shown rigorously, we see that in this near-monochromatic approximation the spectral flux of modes behaves as

$$\varphi_{\text{nf}}(\omega, d) = g_d(\omega) \delta(\omega - \omega_0), \quad (4.132)$$

with

$$g_d(\omega) = \frac{\text{Re} \left\{ \text{Li}_2[r_p^2(\omega)] \right\}}{4\pi d^2 f'(\omega)}. \quad (4.133)$$

The above result is valid for the radiation emitted by the polar materials under consideration and in the presence of a nearby second surface made of the same material. The function  $g_d(\omega)$ , which is restricted to the frequency of the resonant mode due to the Dirac  $\delta$  in (4.132), contains the information about the emissivity of the material and the typical dependence  $1/d^2$  on the gap size in this regime [99]. In addition, this functional form of the spectral flux of modes allows us to easily compute the flux associated to other thermodynamic quantities. The entropy flux of the radiation in this regime is therefore given by

$$\Psi(d) = \int_0^\infty d\omega k_B m_{1,2}(\omega) \varphi_{\text{nf}}(\omega, d) = k_B m_{1,2}(\omega_0) g_d(\omega_0). \quad (4.134)$$

We have to emphasize that the several approximations employed to obtain the above results can be tested by integrating numerically equations (4.116) and (4.117). This imposes some restrictions in the range of applicability of the near-monochromatic approximation: indicatively, the separation distances have to be  $d < \lambda_T/100$  and the temperatures lower than 1000 K [154]. The accuracy of the results presented in the next chapter, which are within these ranges, is better than 2% for both SiC and hBN.

# NEAR-FIELD THERMAL RADIATION ENERGY CONVERSION

---

A heat engine may, in general, be conceived as a device that converts part of the heat coming from a hot source of energy into mechanical work throughout an appropriate conversion system [117]. In contactless devices this heat is transferred to the converter by radiation, only. At large separation distances the maximum power which can be transmitted is bounded by the blackbody limit [66]. On the contrary, at separation distances smaller than the thermal wavelength, heat can be transferred to the converter also by photon tunneling, so that the flux can become several orders of magnitude larger than in the far-field regime, as shown theoretically [12] and experimentally [68, 69, 74, 155–157]. Furthermore, it could be shown theoretically and experimentally that near-field thermophotovoltaic conversion devices can be used to harvest this energy by transferring it towards a  $p$ - $n$  junction [77, 158], that is an example of an energy-conversion mechanism. Thanks to the tunneling of surface phonon polaritons (SPPs) supported by the primary source, this energy transfer is near-monochromatic, which is very advantageous for the energy conversion with a photovoltaic cell [77–79, 82]. In this chapter, we study the thermodynamic performance of such near-field heat engines, emphasizing their potential for energy harvesting. First, we consider in Section 5.1 these heat engines as implemented in two-body systems. In Section 5.2, three-body heat engines are analyzed and compared with the two-body case. Finally, in the latter section, we also discuss some implications in the general case of many-body near-field heat engines.

## 5.1 Two-body near-field heat engines

Here we consider the thermodynamics of near-field thermal radiation and its application to energy harvesting. We focus on the radiation emitted by two identical

semi-infinite polar media at different temperatures and separated by a vacuum gap of width  $d$ , and compute the maximum work flux that can be extracted from this system, the so-called thermodynamic availability. How to compute upper bounds for the efficiency is also discussed. The analysis performed below is done by taking advantage of the analytical results obtained in Section 4.4.3 using the near-monochromatic approximation, which allows us to easily identify the physical properties behind the problem.

In particular, we concentrate on the case where the temperature difference between the hot source and the receiver is small. In these conditions, on the one hand, converters working in the far field not only have low efficiencies, but also the power they supply is poor. This is due to the fact that converters in the far field require high temperature sources to operate in optimal conditions [81]. On the other hand, although the efficiency remains low if the temperature difference between the source and the receiver is small, the delivered power is notably higher for converters working in the near field. Thus, near-field radiation brings out the possibility of energy harvesting from sources of moderate temperature at the nanoscale.

### 5.1.1 Thermodynamic availability and efficiency

In order to define the thermodynamic scheme of the energy-conversion process, let us consider the radiation emitted by the surface of one of these materials (body 1) at temperature  $T_h$  to the second radiating surface (body 2) at temperature  $T_c$ , assuming  $T_c < T_h$ . Henceforth, body 1 will be referred to as the hot body and body 2 as the cold body. Now consider a converter that transforms the energy flux of the radiation incoming on the surface of the cold body, delivering a certain amount of work flux  $\dot{W}$ . We do not need to specify how the converter operates because here we focus on upper bounds for the work flux and the efficiency, as will become clear below.

The converter can be thought of as coupled to the cold body. In turn, this body is assumed to be thermalized due to the interaction with a thermostat. Thus, the energy flux balance equation on the cold body can be written as

$$\Phi(d) = \dot{Q} + \dot{W}, \quad (5.1)$$

where  $\dot{Q}$  is the heat flux delivered to a cold sink (due to the interaction with the thermostat at temperature  $T_c$ ) and  $\Phi(d)$  is the energy flux on this body due to its interaction with the other body. Furthermore, according to the formulation of the second law of thermodynamics [133], one has

$$\Psi_c - \Psi(d) = \Psi_g \geq 0, \quad (5.2)$$

where  $\Psi_g$  is the entropy production due to irreversibilities in the processes,  $\Psi_c$  is the entropy flux delivered to the cold sink, and  $\Psi(d)$  is the entropy flux of the radiation due to the interaction between the bodies. This entropy production  $\Psi_g$  accounts for dissipative processes in the thermalization of excited electrons at the surface of the cold body [114]. In addition, we have also assumed that in the converter there are no sources either of energy or entropy. Moreover, equations (5.1) and (5.2) are closely linked because  $\Psi_c = \dot{Q}/T_c$  and hence,  $\dot{Q} = T_c\Psi(d) + T_c\Psi_g$ . Under these conditions, the work flux provided by the device reads

$$\dot{W} = \Phi(d) - T_c\Psi(d) - T_c\Psi_g, \quad (5.3)$$

and in the limiting case when there is no entropy production, one has an ideal work flux

$$\dot{W} \equiv \Phi(d) - T_c\Psi(d). \quad (5.4)$$

Therefore,  $\dot{W}$  is the maximum work flux that can be obtained in the process of conversion of the incoming energy flux, namely, it represents the thermodynamic availability of the system. It should be emphasized that the definition (5.4) gives us an upper bound for the actual work flux that can be obtained, regardless of the entropy that is being generated in the system due to irreversibilities.

According to the discussion of Section 4.4.3, for two identical semi-infinite bodies made of a polar dielectric in the extreme near-field regime ( $d \ll \lambda_T$ ), the energy and entropy fluxes on the cold body are given by

$$\Phi(d) = \hbar\omega_0 n_{h,c}(\omega_0) g_d(\omega_0), \quad (5.5)$$

$$\Psi(d) = k_B m_{h,c}(\omega_0) g_d(\omega_0), \quad (5.6)$$

where  $\omega_0$  is the frequency of the SPP supported by the material and  $g_d(\omega_0)$  is given by (4.133). Here,  $n_{h,c}(\omega_0) = n(\omega_0, T_r) - n(\omega_0, T_c)$  and, analogously,  $m_{h,c}(\omega_0) = m(\omega_0, T_r) - m(\omega_0, T_c)$ . Thus, the thermodynamic availability is given by

$$\dot{W} = g_d(\omega_0) [\hbar\omega_0 n_{h,c}(\omega_0) - k_B T_c m_{h,c}(\omega_0)]. \quad (5.7)$$

Furthermore, the thermodynamic efficiency of the energy-conversion process,  $\eta$ , is given by the ratio of the available work flux to the input energy flux [159]. We can take  $\Phi(d)$  as the input energy flux, since this quantity is the net energy flux in the cavity that is radiated on the cold body. From here, one has

$$\eta = \frac{\dot{W}}{\Phi(d)} = \frac{\dot{W} - T_c\Psi_g}{\Phi(d)}. \quad (5.8)$$

An upper bound  $\bar{\eta}$  for the efficiency is therefore obtained by considering that the work flux is ideal,

$$\bar{\eta} = \frac{\dot{W}}{\Phi(d)} \geq \eta. \quad (5.9)$$

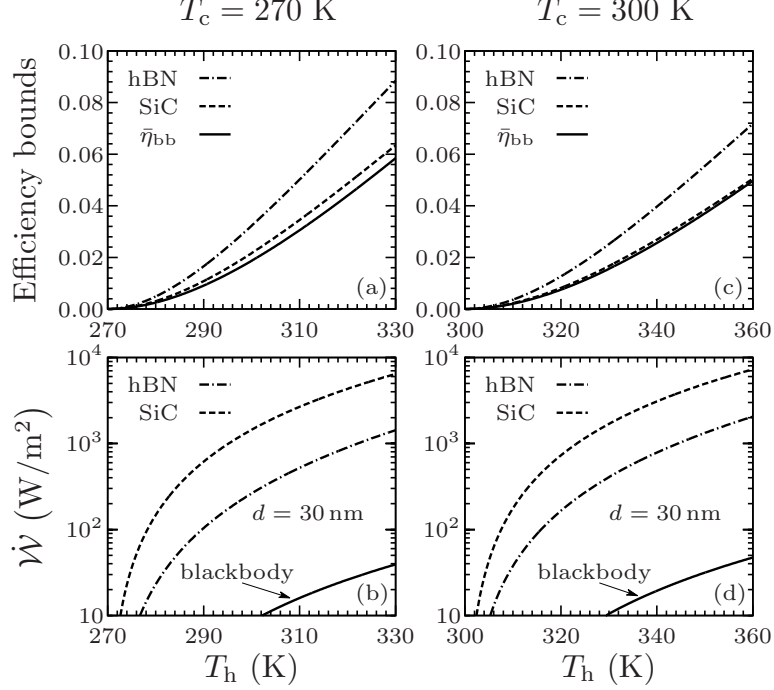


**Figure 5.1:** Efficiency bound  $\bar{\eta}_0$  and maximum work flux  $\dot{W}$  as a function of the temperature of the hot source  $T_h$  for two different environmental temperatures  $T_c$ . In (a) and (b) these quantities are plotted for  $T_c = 270$  K, while in (c) and (d) for  $T_c = 300$  K. The quantities  $\bar{\eta}_{bb}$  and  $\dot{W}_{bb}$  corresponding to blackbody radiation are also shown. Taken from [7].

The efficiency defined in this way is appropriated for analyzing the intrinsic performance of the device in operating conditions. However, in order to compare the performance of near-field heat engines with far-field radiative energy-conversion mechanisms, it is convenient to introduce the efficiency

$$\bar{\eta}_0 = \frac{\dot{W}}{\Phi_0(d)} \leq \bar{\eta}, \quad (5.10)$$

where

$$\Phi_0(d) = \int_0^\infty d\omega \hbar\omega n_h(\omega) \varphi_{nf}(\omega, d) = \hbar\omega_0 n_h(\omega_0) g_d(\omega_0) \quad (5.11)$$

is the energy flux radiated by the hot body towards the converter without taking into account the feedback energy flux emitted by the cold body on the hot body. We remark that  $\Phi_0(d)$  depends only on the temperature  $T_h$  through the photon distribution  $n_h(\omega_0) = n(\omega_0, T_h)$ . Thus, we can write

$$\bar{\eta}_0 = \frac{\hbar\omega_0 n_{h,c}(\omega_0) - k_B T_c m_{h,c}(\omega_0)}{\hbar\omega_0 n_h(\omega_0)}, \quad (5.12)$$

	$\varepsilon_\infty$	$\omega_L$ (rad s <sup>-1</sup> )	$\omega_T$ (rad s <sup>-1</sup> )	$\Gamma$ (rad s <sup>-1</sup> )	$\omega_0$ (rad s <sup>-1</sup> )
SiC	6.7	$1.83 \times 10^{14}$	$1.49 \times 10^{14}$	$8.97 \times 10^{11}$	$1.79 \times 10^{14}$
hBN	4.9	$3.03 \times 10^{14}$	$2.57 \times 10^{14}$	$1.00 \times 10^{12}$	$2.96 \times 10^{14}$

**Table 5.1:** Parameters for the Lorentz (4.124) describing the dielectric constant  $\varepsilon(\omega)$  of SiC and hBN, and the frequency  $\omega_0$  of the SPP supported by the material. The SiC optical data are taken from [160] and those for hBN are taken from [82].

which corresponds to the efficiency of near-monochromatic radiation, as obtained in [113] with general considerations, a result being valid in the far field as well. For fixed temperatures, the upper bound  $\bar{\eta}_0$  increases as the resonant frequency increases, but its growth is limited by the Carnot efficiency  $\eta_C$ , since  $\lim_{\omega_0 \rightarrow \infty} \bar{\eta}_0 = 1 - T_c/T_h = \eta_C$  (the delivered power vanishes in this limit). Thus, for convenience, in this section we will continue to use the efficiency  $\bar{\eta}_0$ , since the efficiency defined in this way<sup>1</sup> is suitable for comparing our results with those corresponding to blackbody radiation [7]. In Section 5.2, the intrinsic efficiency of the energy-conversion process will be quantified using  $\bar{\eta}$ .

### 5.1.2 Energy harvesting from polar dielectric sources

The maximum work flux that can be extracted from the radiation in the near-field regime is considerably higher than that obtained from blackbody radiation, as shown in figure 5.1 for SiC and hBN setting  $d = 30$  nm, where also the bounds  $\bar{\eta}_0$  for the efficiency are plotted. The properties of these materials are described according to the Lorentz model (4.124); the SiC optical data are taken from [160] and those for hBN are taken from [82], see table 5.1. One therefore may wonder whether the bounds imposed by thermodynamics on the efficiency permit the process of conversion to be more efficient in the near-field regime as compared to the blackbody regime. For the case of blackbody radiation, the thermodynamic availability is given by

$$\dot{\mathcal{W}}_{\text{bb}} = \Phi_{\text{bb}} - T_c \Psi_{\text{bb}} = \sigma_{\text{SB}} (T_h^4 - T_c^4) - \frac{4}{3} \sigma_{\text{SB}} T_c (T_h^3 - T_c^3), \quad (5.13)$$

where we have used (4.99) and (4.100) with  $T_1 = T_h$  and  $T_2 = T_c$ . The upper bound for the efficiency in the blackbody limit is given by the Landsberg efficiency [113]

$$\bar{\eta}_{\text{bb}} = \frac{\dot{\mathcal{W}}_{\text{bb}}}{\sigma_{\text{SB}} T_h^4} = 1 - \frac{4}{3} \frac{T_c}{T_h} + \frac{1}{3} \left( \frac{T_c}{T_h} \right)^4. \quad (5.14)$$

<sup>1</sup>Efficiencies analogous to  $\bar{\eta}$  and  $\bar{\eta}_0$  can also be defined for solar energy conversion; a comparative discussion of these two efficiencies for this case can be found in [114].

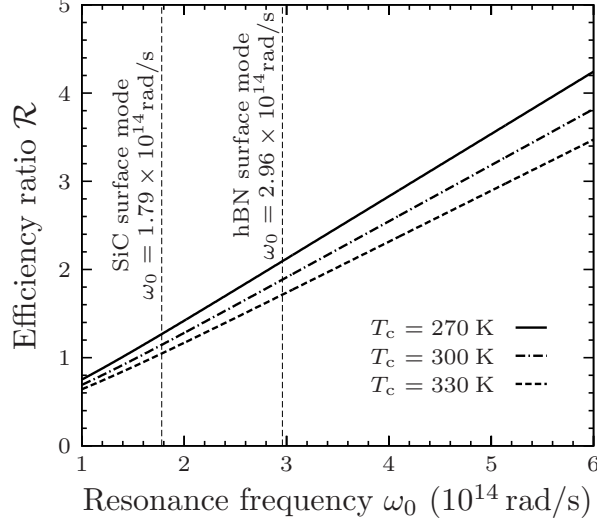


**Figure 5.2:** Ratio  $\bar{\eta}_0$  to  $\bar{\eta}_{\text{bb}}$  in the limit where the temperature of the hot source ( $T_h$ ) approaches the environmental temperature ( $T_c$ ) as a function of the frequency of the SPP. For  $T_c = 270$  K, in this limit  $\bar{\eta}_0$  is more than twice as large as  $\bar{\eta}_{\text{bb}}$  for hBN. Taken from [7].

Taking  $\bar{\eta}_{\text{bb}}$  as a reference provides a notion of how  $\bar{\eta}_0$  varies for different values of the resonant frequency  $\omega_0$ . For high enough temperatures,  $\bar{\eta}_{\text{bb}}$  can be larger than  $\bar{\eta}_0$ . However, here we concentrate on the case where the difference of temperatures of the surfaces is small in comparison with the average temperature. Such a situation is physically relevant, for instance, if a converter is implemented in a certain device with the purpose of harvesting energy from near-field radiation, taking advantage of the fact that one of its components has a temperature somewhat higher than the environment (at temperature  $T_c$ ) due to some independent process. The penalization in the efficiency of the conversion because of the small temperature difference can be compensated by the considerable amount of work flux obtained from near-field radiation. Thus, we take the limit where the temperature of the hotter surface approaches the environmental temperature  $T_c$  in the ratio  $\bar{\eta}_0/\bar{\eta}_{\text{bb}}$  and obtain [7]

$$\mathcal{R} \equiv \lim_{T_h \rightarrow T_c} \frac{\bar{\eta}_0}{\bar{\eta}_{\text{bb}}} = \frac{\hbar\omega_0}{4k_{\text{B}}T_c} \left[ 1 - \exp\left(-\frac{\hbar\omega_0}{k_{\text{B}}T_c}\right) \right]^{-1}. \quad (5.15)$$

The condition  $\bar{\eta}_0 > \bar{\eta}_{\text{bb}}$  in this limit, i.e.  $\mathcal{R} > 1$ , can be numerically solved and is satisfied if

$$\omega_0 > 3.921 \frac{k_{\text{B}}T_c}{\hbar}, \quad (5.16)$$

leading to a threshold frequency for which the conversion of near-field radiation can be more efficient than the conversion of blackbody radiation. Furthermore, this also

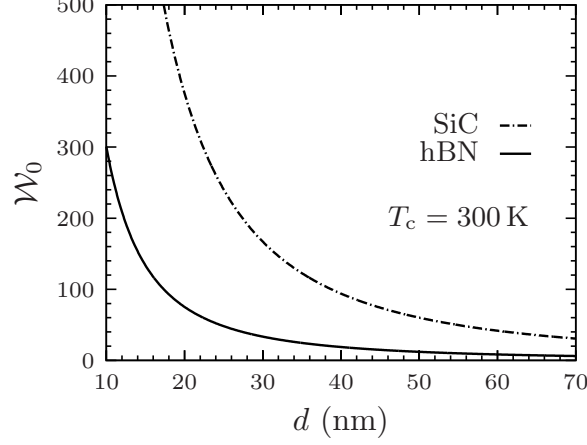


**Figure 5.3:** Ratio  $\mathcal{W}_0 = \dot{\mathcal{W}}/\dot{\mathcal{W}}_{\text{bb}}$  in the limit where the temperature of the hot source  $T_h$  approaches the environmental temperature  $T_c$  as a function of the gap width. In this asymptotic limit, the enhancement of the maximum work flux in the near-field regime as compared with that of blackbody radiation is shown for two different materials. Taken from [3].

means that the higher the value of  $\omega_0$ , the more  $\bar{\eta}_0$  increases at small temperature difference, see the figure 5.2. In contrast, the available work flux diminishes when the resonant frequency increases. To see this, we approximate  $\dot{\mathcal{W}}$  to leading order in  $\Delta T = T_h - T_c$  such that  $\Delta T/T_0 \ll 1$ , with  $T_0 = (T_c + T_h)/2$ , and obtain

$$\dot{\mathcal{W}} \simeq \frac{g_d(\omega_0)}{8k_{\text{B}}T_0} \left[ \hbar\omega_0 \text{csch} \left( \frac{\hbar\omega_0}{2k_{\text{B}}T_0} \right) \frac{\Delta T}{T_0} \right]^2, \quad (5.17)$$

which decreases for increasing  $\omega_0$  because of the hyperbolic cosecant. We see clearly that the choice of the material, characterized by  $\omega_0$ , directly affects the efficiency and determines the available work flux.

Further information can be obtained by comparing the maximum work flux in the near field with that of the blackbody regime. For small  $\Delta T$  one obtains  $\dot{\mathcal{W}}_{\text{bb}} \simeq 2\sigma_{\text{SB}}T_0^2(\Delta T)^2$ . Thus, we now define

$$\mathcal{W}_0 \equiv \lim_{T_h \rightarrow T_c} \frac{\dot{\mathcal{W}}}{\dot{\mathcal{W}}_{\text{bb}}}, \quad (5.18)$$

which, taking into account the expansions to leading order in  $\Delta T$  of both  $\dot{\mathcal{W}}$  and  $\dot{\mathcal{W}}_{\text{bb}}$ , can be written as [3]

$$\mathcal{W}_0 = \frac{\hbar^2\omega_0^2 g_d(\omega_0)}{4\sigma_{\text{SB}}k_{\text{B}}T_c^5} \frac{e^{\hbar\omega_0/k_{\text{B}}T_c}}{[e^{\hbar\omega_0/k_{\text{B}}T_c} - 1]^2}. \quad (5.19)$$

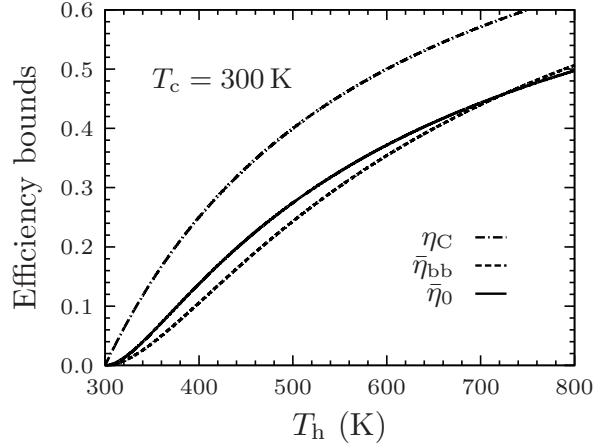


**Figure 5.4:** Efficiency bounds as a function of the temperature of the hot source  $T_h$  for fixed  $T_c = 300$  K. The near-field efficiency  $\bar{\eta}_0$  is plotted for hBN, and, for comparison purpose, also the Carnot efficiency  $\eta_C$  is plotted. Taken from [6].

Moreover, the functions  $\mathcal{W}_0$  and  $\mathcal{R}$  are related to each other, with the relation being given by

$$\mathcal{W}_0 = \frac{\hbar\omega_0}{\sigma_{\text{SB}}T_c^4} \frac{g_d(\omega_0)\mathcal{R}}{e^{\hbar\omega_0/k_B T_c} - 1}. \quad (5.20)$$

Of course, both the maximum work flux and the efficiency go to zero in the limit  $T_h \rightarrow T_c$ . However, the ratios  $\mathcal{W}_0$  and  $\mathcal{R}$  provide intrinsic information about the performance of the energy-conversion process in the asymptotic limit of small temperature difference. In figure 5.3, we show  $\mathcal{W}_0$  at  $T_c = 300$  K as a function of  $d$  for SiC and hBN. In figure it is clearly seen the enhancement in the work flux due to evanescent modes in the near-field regime;  $\dot{\mathcal{W}}$  is considerably larger than  $\dot{\mathcal{W}}_{\text{bb}}$  at room temperature at the nanoscale.

To conclude, we have alluded to the fact that for high enough temperatures,  $\bar{\eta}_{\text{bb}}$  can be larger than  $\bar{\eta}_0$ . We show this behavior in figure 5.4 for sources of hBN. There, for the sake of comparison, we also show the Carnot efficiency, which, of course, is always larger than both  $\bar{\eta}_{\text{bb}}$  and  $\bar{\eta}_0$ .

## 5.2 Many-body near-field heat engines

The properties of the thermal radiation driving an energy-conversion process depend on the distribution and the number of bodies interacting with the converter. As we shall see, the power delivered by heat engines driven photon tunneling in many-body systems can be higher than the power delivered by a two-body heat engine.

In particular, in Section 5.2.1, we study in detail the thermodynamics of a concrete example of a three-body heat engine and compare this device with its two-body counterpart. Then, it is shown that the thermodynamic availability in three-body systems can exceed the thermodynamic availability in two-body systems. Theoretical limits for energy and entropy fluxes in  $N$ -body systems are discussed at the end of this chapter, in Section 5.2.2. From here, the availability and efficiency in this theoretical limit can be deduced.

### 5.2.1 Three-body vs. two-body near-field heat engines

We are now interested in drawing a comparison between two-body (2B) and three-body (3B) radiative near-field heat engines, which are both sketched in figure 5.5. Let us define the thermodynamic scheme for those devices. In a 2B heat engine, a hot body at temperature  $T_h$  radiates towards a converter which is assumed to be coupled with a cold body in contact with a cold sink at temperature  $T_c < T_h$ . In the 3B configuration, a passive intermediate body of width  $\delta$  is placed between the hot and cold bodies. As shown in figure 5.5, this passive relay is maintained at the same separation distance  $d$  from both the hot and the cold bodies as the cavity width in the 2B system. Hence, we do not introduce in the 3B heat engine an exaltation mechanism which results from a simple reduction of distances. Moreover, we assume that the intermediate body reaches a local equilibrium temperature  $T_i$ , an assumption that is justified in practical applications for the sizes of the body that we consider here. This temperature  $T_i$  is not arbitrary. It is taken such that the net energy flux that the intermediate body exchanges with the hot and cold bodies vanishes. Hence,  $T_i$  is an implicit function of  $T_h$ ,  $T_c$ , and the two parameters  $d$  and  $\delta$  that specify the geometry of the problem. As a consequence, the energy flux radiated by the hot body coincides with the flux received by the cold body. This ensures that the energy supplied to the system comes only from the hot source, since, under these conditions, a thermostat at  $T_i$  in contact with the passive relay will provide a vanishing net energy flux. We will come back to this point later on.

The planar 2B and 3B structures considered here have an infinite transversal extension. According to the results of Sections 4.4.1 and 4.4.2, the net energy flux on the cold body, denoted here simultaneously for the two cases by  $\Phi_{iB}$  with  $i = 2, 3$ , can be written as an integral over monochromatic contributions of frequency  $\omega$ . In the near-field regime, that is, neglecting the contribution of propagative waves, this energy fluxes are given by

$$\Phi_{iB} = \int_0^\infty \frac{d\omega}{2\pi} \phi_{iB}(\omega, d, \delta) \quad (5.21)$$

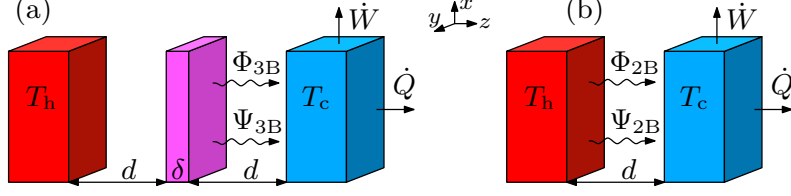


**Figure 5.5:** Sketch of a heat engine with a hot source at temperature  $T_h$  and a cold sink at temperature  $T_c < T_h$  that provides a usable work flux  $\dot{W}$  by converting near-field thermal radiation energy. The cold sink receives a heat flux  $\dot{Q}$ . (a) Three-body: One of the bodies (emitters) is thermalized with the hot source and another one with the cold sink, while a passive intermediate body (of width  $\delta$ ) is placed between them. The net energy and entropy fluxes on the cold body are  $\Phi_{3B}$  and  $\Psi_{3B}$ , respectively. (b) Two-body: The intermediate body is removed. The net energy and entropy fluxes on the cold body are  $\Phi_{2B}$  and  $\Psi_{2B}$ , respectively. The distance  $d$  between the bodies is indicated in both cases. Taken from [4].

with

$$\phi_{2B}(\omega, d) = \hbar\omega \sum_{\sigma} \int_{c\kappa > \omega} \frac{d^2\kappa}{(2\pi)^2} n_{h,c}(\omega) \mathcal{T}_{\sigma}^{h,c}(\kappa, \omega, d) \quad (5.22)$$

in the 2B case [12, 96] and

$$\begin{aligned} \phi_{3B}(\omega, d, \delta) = \hbar\omega \sum_{\sigma} \int_{c\kappa > \omega} \frac{d^2\kappa}{(2\pi)^2} & \left[ n_{h,i}(\omega) \mathcal{T}_{\sigma}^{h,i}(\kappa, \omega, d, \delta) \right. \\ & \left. + n_{i,c}(\omega) \mathcal{T}_{\sigma}^{i,c}(\kappa, \omega, d, \delta) \right] \end{aligned} \quad (5.23)$$

for the 3B configuration [88]. In order to obtain these expressions from those of Sections 4.4.1 and 4.4.2, we have set  $T_1 = T_h$  and  $T_2 = T_c$  in the 2B case and  $T_1 = T_h$ ,  $T_2 = T_i$ , and  $T_3 = T_c$  in the 3B case. In this way, the energy fluxes  $\Phi_{2B}$  and  $\Phi_{3B}$  corresponds to those given by equations (4.113) and (4.107), respectively. Thus, the transmission coefficients here take the form

$$\mathcal{T}_{\sigma}^{h,i} = \frac{4 |\tau_{\sigma}^i|^2 \operatorname{Im}(\rho_{\sigma}^h) \operatorname{Im}(\rho_{\sigma}^c) e^{-4|k_z|d}}{|1 - \rho_{\sigma}^{hi} \rho_{\sigma}^c e^{2ik_z d}|^2 |1 - \rho_{\sigma}^h \rho_{\sigma}^i e^{2ik_z d}|^2}, \quad (5.24)$$

$$\mathcal{T}_{\sigma}^{i,c} = \frac{4 \operatorname{Im}(\rho_{\sigma}^{hi}) \operatorname{Im}(\rho_{\sigma}^c) e^{-2|k_z|d}}{|1 - \rho_{\sigma}^{hi} \rho_{\sigma}^c e^{2ik_z d}|^2}, \quad (5.25)$$

$$\mathcal{T}_{\sigma}^{h,c} = \frac{4 \operatorname{Im}(\rho_{\sigma}^h) \operatorname{Im}(\rho_{\sigma}^c) e^{-2|k_z|d}}{|1 - \rho_{\sigma}^h \rho_{\sigma}^c e^{2ik_z d}|^2}, \quad (5.26)$$

where  $\rho_{\sigma}^h = \rho_{\sigma}^h(\kappa, \omega)$ ,  $\rho_{\sigma}^i = \rho_{\sigma}^i(\kappa, \omega, \delta)$ , and  $\rho_{\sigma}^c = \rho_{\sigma}^c(\kappa, \omega)$  are the reflection coefficients of the hot, intermediate, and cold bodies, respectively,  $\tau_{\sigma}^i = \tau_{\sigma}^i(\kappa, \omega, \delta)$  are the

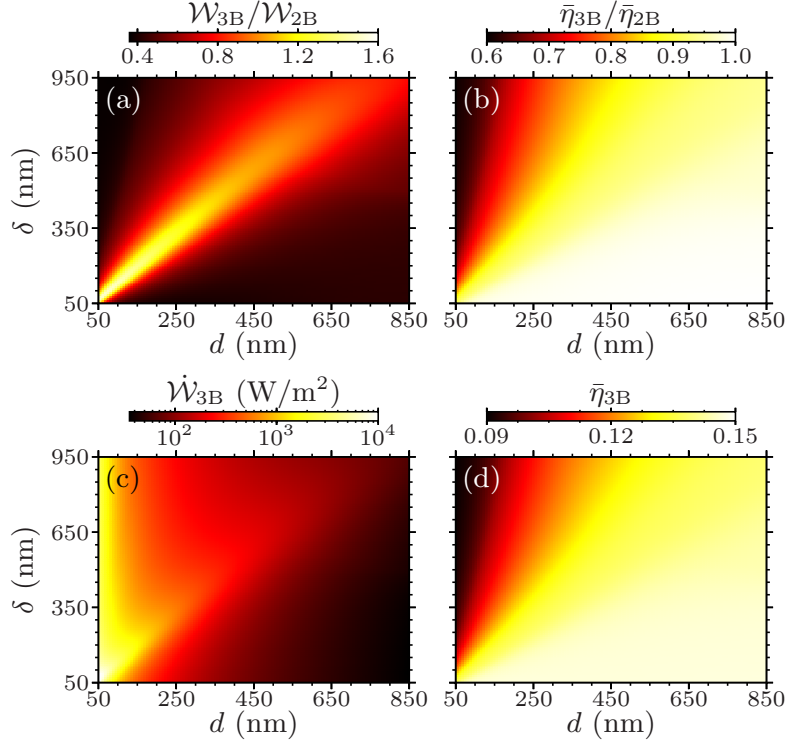


**Figure 5.6:** (a) Ratio of the maximum work flux in the 3B configuration to the maximum work flux in the 2B configuration,  $\dot{W}_{3B}/\dot{W}_{2B}$ , as a function of the separation  $d$  and width of the intermediate body  $\delta$  for  $T_h = 400$  K and  $T_c = 300$  K. A region of amplification due to 3B photon tunneling is clearly appreciated. (b) Efficiency ratio  $\bar{\eta}_{3B}/\bar{\eta}_{2B}$  in the same conditions. In (c) and (d), the plots show the corresponding maximum work flux and efficiency in the 3B configuration. Taken from [4].

transmission coefficients of the intermediate body, and

$$\rho_\sigma^{\text{hi}} = \rho_\sigma^{\text{i}} + \frac{\tau_\sigma^{\text{i}} \rho_\sigma^{\text{h}} \tau_\sigma^{\text{i}} e^{2ik_z d}}{1 - \rho_\sigma^{\text{h}} \rho_\sigma^{\text{i}} e^{2ik_z d}} \quad (5.27)$$

are the reflection coefficients of the hot and the intermediate bodies considered as a single entity. We stress that expressions (5.24) and (5.25) for the transmission coefficients in the 3B configuration show that the three bodies are coupled together due to multiple interaction mechanisms resulting in their nontrivial optical properties. Moreover, the temperature  $T_i$  of the intermediate body (which corresponds to body 2 in Section 4.4.1) can be numerically obtained by looking for the temperature  $T_2 = T_i$  that cancels out the energy flux (4.106) for the given  $T_1 = T_h$  and  $T_3 = T_c$  at fixed  $d$  and  $\delta$ . This guarantees the condition of passive relay for the intermediate

body, as discussed previously.

Furthermore, the net entropy fluxes on the cold body, denoted by  $\Psi_{2B}$  and  $\Psi_{3B}$  for the two different configurations, are given by equations (4.115) and (4.110), respectively. These entropy fluxes can therefore be written as

$$\Psi_{iB} = \int_0^\infty \frac{d\omega}{2\pi} \psi_{iB}(\omega, d, \delta), \quad (5.28)$$

for  $i = 2, 3$ , where the spectral entropy fluxes take the form

$$\psi_{2B}(\omega, d) = k_B \sum_\sigma \int_{c\kappa > \omega} \frac{d^2\kappa}{(2\pi)^2} m_{h,c}(\omega) \mathcal{T}_\sigma^{h,c}(\kappa, \omega, d), \quad (5.29)$$

$$\begin{aligned} \psi_{3B}(\omega, d, \delta) = k_B \sum_\sigma \int_{c\kappa > \omega} \frac{d^2\kappa}{(2\pi)^2} & \left[ m_{h,i}(\omega) \mathcal{T}_\sigma^{h,i}(\kappa, \omega, d, \delta) \right. \\ & \left. + m_{i,c}(\omega) \mathcal{T}_\sigma^{i,c}(\kappa, \omega, d, \delta) \right]. \end{aligned} \quad (5.30)$$

Once energy and entropy fluxes are known, the thermodynamics of the energy-conversion process can be analyzed as we have done in Section 5.1.1 (the 3B and the 2B configurations will be discussed simultaneously). First of all, notice that, due to the difference of temperatures between the bodies, the transport of heat through the cavity proceeds irreversibly and entropy is generated at a rate  $\Psi_g$  on the surface of the cold body. Since the bodies are thermalized, in particular, a heat flux  $\dot{Q}$  is transferred isothermally to the cold sink; we assume that this transference is done reversibly and, thus,  $\dot{Q} = T_c (\Psi_{iB} + \Psi_g)$ . In this scheme the heat engine can be considered as endoreversible, as discussed in [114] for the 2B problem in the far field. Taking into account the balances of energy and entropy fluxes, the work flux that can be delivered by the engine reads

$$\dot{W} = \Phi_{iB} - T_c (\Psi_{iB} + \Psi_g). \quad (5.31)$$

Since  $\Psi_g \geq 0$ , the maximum work flux, or thermodynamic availability, is given by

$$\dot{\mathcal{W}}_{iB} \equiv \Phi_{iB} - T_c \Psi_{iB}. \quad (5.32)$$

In addition, considering  $\Phi_{iB}$  as the input energy flux, the efficiency of the engine is given by  $\eta_{iB} = \dot{W}/\Phi_{iB}$ . According to this, an upper bound for the efficiency can be obtained by computing the ratio

$$\bar{\eta}_{iB} \equiv \frac{\dot{\mathcal{W}}_{iB}}{\Phi_{iB}}. \quad (5.33)$$

In the configuration we analyze, the hot and cold bodies are two 5- $\mu\text{m}$ -thick SiC samples [160] that support a SPP with a resonance at  $\omega_0 \simeq 1.79 \times 10^{14}$  rad/s.

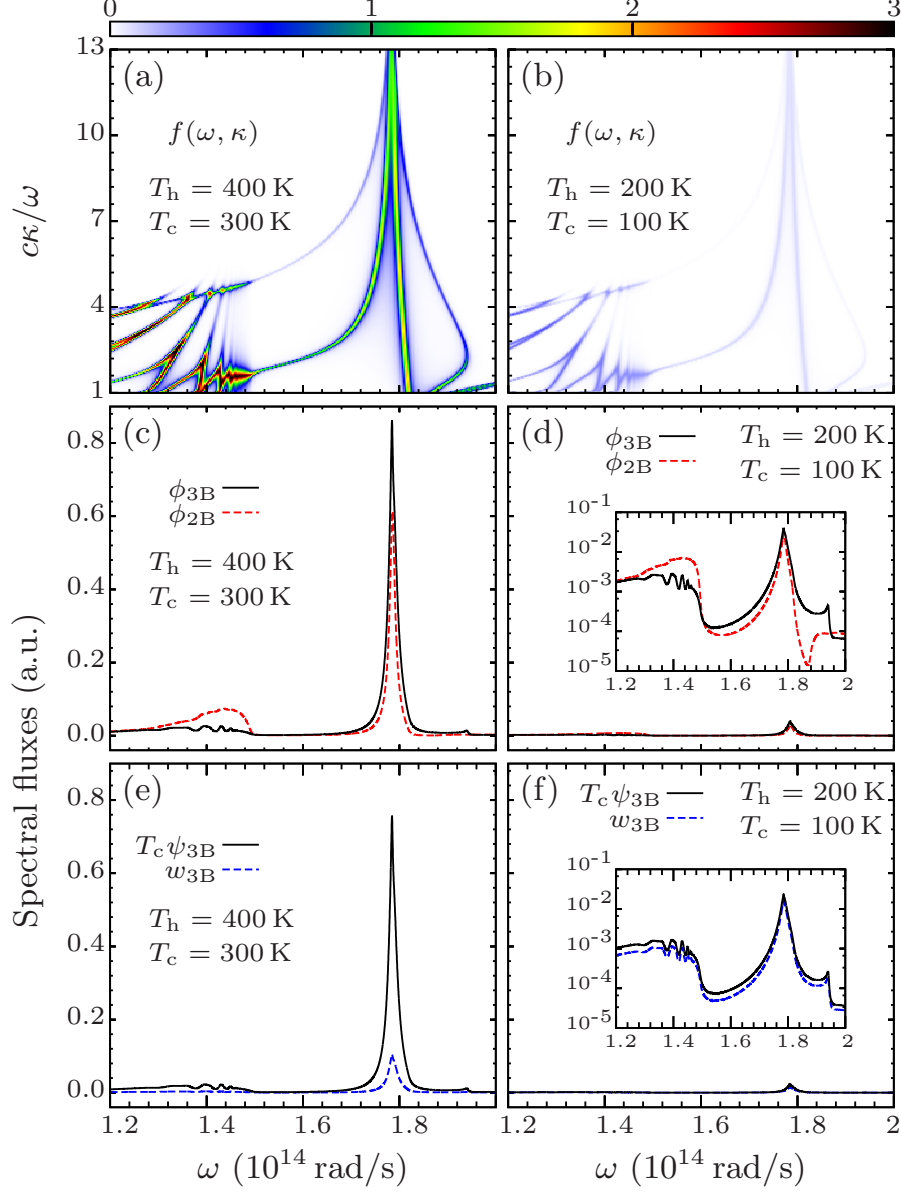


**Figure 5.7:** (a) Transmission coefficients weighted by the photon distributions taking  $d = 500$  nm and  $\delta = 667$  nm. We plot  $f(\omega, \kappa)$  for  $T_h = 400$  K and  $T_c = 300$  K, for which  $T_i = 357.01$  K. In (b),  $f(\omega, \kappa)$  is shown for  $T_h = 200$  K and  $T_c = 100$  K with  $T_i = 180.54$  K. (c) Spectral energy fluxes  $\phi_{3B}$  and  $\phi_{2B}$  corresponding to the same setting used in (a). (d) Spectral energy fluxes  $\phi_{3B}$  and  $\phi_{2B}$  corresponding to (b); the inset shows the same spectra in log scale. In (e) and (f) we plot the entropic contribution  $T_c \psi_{3B}$  and the spectral work flux  $w_{3B} = \phi_{3B} - T_c \psi_{3B}$  corresponding to the same setting used in (a)–(c) and in (b)–(d), respectively. Taken from [4].

Moreover, as done in [88], we use in the 3B configuration for the intermediate slab a metallike medium which supports a surface mode (a plasmon) at the same frequency  $\omega_0$ . The permittivity of this intermediate medium is described by the Drude model

$$\varepsilon(\omega) = 1 - \frac{\omega_p^2}{\omega(\omega + i\Gamma)}, \quad (5.34)$$

where  $\omega_p$  is the plasma frequency and  $\Gamma$  the relaxation rate. Since the plasmon frequency is given by  $\omega_p/\sqrt{2}$  [161], we take  $\omega_p = \sqrt{2}\omega_0$  [88], in such a way that the heat transfer is maximized by matching these two resonance frequencies. In addition, the relaxation rate is set to  $\Gamma = 10^{-3}\omega_p$ .

The figure 5.6(a) shows the ratio of the maximum work flux in the 3B system to the maximum work flux in the 2B system, i.e., with and without an intermediate relay. It can be seen that a 3B engine can produce about 60% more work than a classical 2B system. If the width of the intermediate body becomes sufficiently large, the 3B interaction disappears (in the near-field regime), and both cavities, located between the source and the intermediate relay and between the relay and the sink, become independent. Then, the work production by the 3B heat engine becomes comparable to or even smaller than the one of a 2B engine. As for the efficiency of those engines, we see in figure 5.6(b) that they are comparable in both configurations provided the separation distances are large enough compared to the width of the intermediate slab. It is interesting to note that the 2B efficiency seems always to be larger than the 3B efficiency even in the parameter range where the extracted work of the 3B system exceeds that of the 2B system.

In order to get some insight on these results, we plot in figures 5.7(a) and 5.7(b) the transmission coefficients for  $p$ -polarized waves (the main contribution) in the  $(\omega, \kappa)$  plane associated to the 3B engine by weighting them with the corresponding photon distribution functions. In concrete, in these figures we plot

$$f(\omega, \kappa) = 10^{22} \times \left[ n_{h,i}(\omega) \mathcal{T}_p^{h,i}(\kappa, \omega) + n_{i,c}(\omega) \mathcal{T}_p^{i,c}(\kappa, \omega) \right]. \quad (5.35)$$

As a first observation, we see the presence of different surface-mode branches of the four coupled surface modes (symmetric and antisymmetric modes) in the 3B system [161] around the surface-mode resonance frequency of SiC. For these surface modes, the transmission is apparently high. These branches support high transmissions for large wave vectors, which means that a large number of modes contribute to the heat transfer in this spectral region [115, 116]. The closer the frequency of the surface mode gets to Wien's frequency of the heat source  $\omega_W = 2.82k_B T_h/\hbar$ , the higher the number of excitations that contribute to the transfer. Accordingly, if the hot body is cooled down to a temperature for which  $\omega_W$  is far from  $\omega_0$ , the modes in the region around the SPP stop to contribute to the transfer, as can be seen in

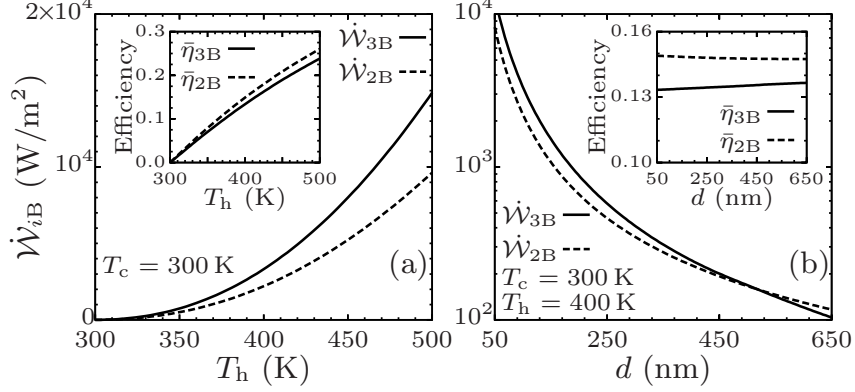


**Figure 5.8:** (a) Maximum work fluxes  $\dot{\mathcal{W}}_{3B}$  and  $\dot{\mathcal{W}}_{2B}$  for the 3B and 2B configurations, respectively, as a function of the temperature of the hot source  $T_h$ . The temperature of the cold sink is set to  $T_c = 300$  K, the separation distance to  $d = 100$  nm, and the width of the intermediate body to  $\delta = 133$  nm. The inset shows the corresponding upper bounds for the efficiency,  $\bar{\eta}_{3B}$  and  $\bar{\eta}_{2B}$ . (b) Dependence of the maximum work fluxes and efficiencies on the separation distance  $d$  for fixed temperatures and the optimal  $\delta$ . Taken from [4].

figure 5.7(b). The spectral energy fluxes plotted in the figures 5.7(c) and 5.7(d) corroborate this tendency. Since the 3B photon-tunneling enhancement occurs in the SPP region, we thus observe in figure 5.7(c) an increase of the quasimonochromatic spectral energy flux  $\phi_{3B}$  as compared with  $\phi_{2B}$ . Furthermore, the spectral entropy flux  $\psi_{3B}$  and the spectral work flux  $w_{3B} \equiv \phi_{3B} - T_c \psi_{3B}$  are also peaked around the SPP frequency. As shown in the figure 5.7(e), the negative entropic term drastically reduces the monochromatic contribution  $w_{3B}$  to the thermodynamic availability in the 3B configuration,

$$\dot{\mathcal{W}}_{3B}(d, \delta) = \int_0^\infty \frac{d\omega}{2\pi} w_{3B}(\omega, d, \delta). \quad (5.36)$$

This entropic term represents a non-negligible energy flux that the system transfers to the cold sink, thus diminishing the amount of usable work production.

Finally, we study the maximal work flux  $\dot{\mathcal{W}}_{iB}$  that can be extracted from such a 3B heat engine compared with that of a 2B heat engine. To this end, we fix  $T_c = 300$  K, while the temperature of the hot source  $T_h$  is varied. For the thickness of the vacuum gaps and the intermediate passive relay we choose  $d = 100$  nm and  $\delta = 133$  nm for which  $\dot{\mathcal{W}}_{3B}/\dot{\mathcal{W}}_{2B}$  is maximum when  $T_h$  has reached a temperature of 400 K, as shown in figure 5.6(a) (in that case, the ratio  $\dot{\mathcal{W}}_{3B}/\dot{\mathcal{W}}_{2B}$  slowly increases for increasing  $T_h$ ). The results are plotted in figure 5.8(a). They show that the discrepancy between  $\dot{\mathcal{W}}_{3B}$  and  $\dot{\mathcal{W}}_{2B}$  grows monotonically with respect to temperature while the 2B and 3B efficiencies remain very close to each other ( $\bar{\eta}_{2B} \geq \bar{\eta}_{3B}$ ). In

addition, the dependence of the work fluxes and efficiencies on the distance  $d$  for the optimal  $\delta$  are presented in figure 5.8(b), where the temperatures are set to  $T_h = 400$  K and  $T_c = 300$  K. This example illustrates that in a 3B system the energy flux and the maximal work flux that can be extracted are enhanced by the interactions of the surface modes in the hot and cold body with that of the intermediate relay.

The maximum transfer in a 3B configuration takes place when the transmission coefficients attain their maximum value. The theoretical limit is thus achieved by the condition  $\mathcal{T}_\sigma^{h,i} = \mathcal{T}_\sigma^{i,c} = 1$ , as also occurs for 2B systems [94, 115, 162] when  $\mathcal{T}_\sigma^{h,c} = 1$ . Using this in (5.22), (5.23), (5.29), and (5.30) and taking into account a cutoff wave vector  $\kappa_{c,iB} \gg \omega/c$ , for which the modes are effectively confined, we get

$$\Phi_{iB}^{\max} = \xi_{iB} (T_h^2 - T_c^2) \quad (5.37)$$

and

$$\Psi_{iB}^{\max} = 2\xi_{iB} (T_h - T_c), \quad (5.38)$$

where  $\xi_{iB} = \kappa_{c,iB}^2 k_B^2 / 24\hbar$ . Notice that maximizing the energy flux implies also that the flow of entropy per channel is maximum [94]. The maximum work flux is thus

$$\dot{\mathcal{W}}_{iB}^{\max} = \xi_{iB} (T_h - T_c)^2, \quad (5.39)$$

and, in consequence, the upper bound for the efficiency reads

$$\bar{\eta}_{2B}^{\max} = \bar{\eta}_{3B}^{\max} = \frac{T_h - T_c}{T_h + T_c}. \quad (5.40)$$

Therefore, the efficiencies for the 2B and 3B systems are equal in this limit. However, we remark that the difference between a 3B and a 2B system is manifested through  $\kappa_{c,iB}$ . The cutoff wave vector in a 3B system can be larger than that of the 2B configuration as shown in our numerical examples. Although the efficiencies and the ratios  $\Phi_{iB}^{\max} / \Psi_{iB}^{\max}$  are the same in the 3B and 2B system, it follows that

$$\frac{\dot{\mathcal{W}}_{3B}^{\max}}{\dot{\mathcal{W}}_{2B}^{\max}} = \frac{\Phi_{3B}^{\max}}{\Phi_{2B}^{\max}} = \frac{\kappa_{c,3B}^2}{\kappa_{c,2B}^2} \geq 1. \quad (5.41)$$

Hence, a larger maximum work flux in the 3B system is due to the larger energy flux which, in turn, results from the larger number of contributing modes.

## 5.2.2 Theoretical limits in many-body systems

For the general case of an  $N$ -body ( $NB$ ) engine, we can always write the heat flux exchanged between the different parts of the system by using the Landauer formalism

derived in Refs. [94, 115, 116], the transmission coefficients being simply related to the scattering of the electromagnetic field radiated by each part of the system. In fact, it is easy to induce the form of the fluxes in this case from the results we obtained in the preceding chapter.

Consider that now we have  $N$  bodies at equilibrium temperatures  $T_\alpha$  with  $\alpha = 1, 2, \dots, N$  and let the temperature of the left environment be  $T_0$  and that of the right environment be  $T_{N+1}$ . This distribution of bodies defines  $N + 1$  vacuum regions that can be denoted by  $\gamma = 0, 1, \dots, N$ . Thus, the system is composed, consecutively, by region 0, body 1, region 1, body 2,  $\dots$ , region  $N - 1$ , body  $N$ , and, finally, region  $N$ .

From the discussion in Section 4.1.4 and, in particular, from equation (4.59), the energy flux in region  $\gamma$  can be written as

$$\Phi_\gamma = \int_0^\infty \frac{d\omega}{2\pi} \hbar\omega \sum_\sigma \int \frac{d^2\boldsymbol{\kappa}}{(2\pi)^2} \sum_{\alpha=0}^N n_{\alpha,\alpha+1} \mathcal{T}_{\sigma,\gamma}^{\alpha,\alpha+1}, \quad (5.42)$$

where now  $\mathcal{T}_{\sigma,\gamma}^{\alpha,\alpha+1}$  are the set of  $N + 1$  transmission coefficients of the  $N$ -body system associated with region  $\gamma$  for a given polarization  $\sigma$ . Moreover, the total energy flux on the body  $N$  is given by

$$\Phi^{(N)} = \int_0^\infty \frac{d\omega}{2\pi} \hbar\omega \sum_\sigma \int \frac{d^2\boldsymbol{\kappa}}{(2\pi)^2} \sum_{\alpha=0}^N n_{\alpha,\alpha+1} \left( \mathcal{T}_{\sigma,N-1}^{\alpha,\alpha+1} - \mathcal{T}_{\sigma,N}^{\alpha,\alpha+1} \right), \quad (5.43)$$

which is the expression analogous to (4.64) and (4.84) for 3B and 2B systems, respectively. Thus, in the  $N$ -body system, the total entropy flux on the body  $N$  reads

$$\Psi^{(N)} = \int_0^\infty \frac{d\omega}{2\pi} k_B \sum_\sigma \int \frac{d^2\boldsymbol{\kappa}}{(2\pi)^2} \sum_{\alpha=0}^N m_{\alpha,\alpha+1} \left( \mathcal{T}_{\sigma,N-1}^{\alpha,\alpha+1} - \mathcal{T}_{\sigma,N}^{\alpha,\alpha+1} \right). \quad (5.44)$$

The expressions (5.43) and (5.44) contain both propagative and evanescent wave contributions. Since the interaction of the system with the environmental fields is only due to propagative waves, the terms containing the corresponding fluxes do not contribute in the near-field regime. This is also reflected in the fact that the transmission coefficients associated with regions 0 and  $N$  do not contribute when projected on the evanescent sector. According to this, in the near-field regime we are left with

$$\Phi^{(N)} = \int_0^\infty \frac{d\omega}{2\pi} \hbar\omega \sum_\sigma \int_{c\kappa > \omega} \frac{d^2\boldsymbol{\kappa}}{(2\pi)^2} \sum_{\alpha=1}^{N-1} n_{\alpha,\alpha+1} \mathcal{T}_{\sigma,N-1}^{\alpha,\alpha+1}, \quad (5.45)$$

$$\Psi^{(N)} = \int_0^\infty \frac{d\omega}{2\pi} k_B \sum_\sigma \int_{c\kappa > \omega} \frac{d^2\kappa}{(2\pi)^2} \sum_{\alpha=1}^{N-1} m_{\alpha,\alpha+1} \mathcal{T}_{\sigma,N-1}^{\alpha,\alpha+1}. \quad (5.46)$$

Besides, in the scheme of the energy-conversion process, as has been done in Section 5.2.1, the body 1 can be assumed to be the hot body, the bodies 2 to  $N-1$  can be taken as passive relays if they are thermalized at the appropriate local equilibrium temperature, and the body  $N$  plays the role of the cold body where the converted is coupled. Thus, we set  $T_1 = T_h$ ,  $T_N = T_c < T_h$ , and the temperatures  $T_\alpha$  for  $\alpha = 2, \dots, N-1$  must be taken as functions of  $T_h$  and  $T_c$  such that the total energy flux on the body  $\alpha = 2, \dots, N-1$  vanish.

Here we are only interested in the theoretical limit for which the energy and entropy fluxes are maximal. As before, this limit takes place when all the transmission coefficients reach their maximum value. In order to fulfill this condition in our case, we assume that  $\mathcal{T}_{\sigma,N-1}^{\alpha,\alpha+1} = 1$ . With this assumption, the energy and entropy fluxes attain their maximum value  $\Phi^{(N)} = \Phi_{NB}^{\max}$  and  $\Psi^{(N)} = \Psi_{NB}^{\max}$ , respectively, which can be written as

$$\Phi_{NB}^{\max} = \xi_{NB} (T_h^2 - T_c^2) \quad \text{and} \quad \Psi_{NB}^{\max} = 2\xi_{NB} (T_h - T_c), \quad (5.47)$$

where  $\xi_{NB} = \kappa_{c,NB}^2 k_B^2 / 24\hbar$  and  $\kappa_{c,NB} \gg \omega/c$  is a suitable cutoff wave vector for the  $N$ -body system. Therefore, the maximum work flux takes the form

$$\dot{\mathcal{W}}_{NB}^{\max} = \xi_{NB} (T_h - T_c)^2. \quad (5.48)$$

When  $\kappa_{c,NB} > \kappa_{c,2B}$  for  $N > 2$ , an enhancement in the maximum work flux  $\dot{\mathcal{W}}_{NB}^{\max}$  is thus expected with respect to the 2B case, while the efficiency

$$\bar{\eta}_{NB}^{\max} = \frac{T_h - T_c}{T_h + T_c} \quad (5.49)$$

remains the same for all  $N$ .

As a concluding remark, we note that the heat conductance in this  $NB$  endoreversible engine is, in general, nonlinear in the difference of temperatures  $\Delta T = T_h - T_c$ . However, the linear regime can be achieved if  $\Delta T \ll T_h$ , and, under this assumption, the efficiency becomes

$$\bar{\eta}_{NB}^{\max} = \frac{\Delta T}{2T_h}, \quad (5.50)$$

which is half the Carnot efficiency. For engines with linear heat conductance such as the Novicov engine, the efficiency is given by the Curzon-Ahlborn efficiency [163]  $\eta_{CA} = 1 - \sqrt{T_c/T_h}$ , which for  $\Delta T \ll T_h$  becomes  $\eta_{CA} = \Delta T / (2T_h)$ . We thus observe that the efficiency of our engine, in the appropriate limit, coincides with that of a Novicov engine.

## SUMMARY AND CONCLUSIONS

---

In this thesis we have studied statistical thermodynamics of classical systems with long-range interactions and thermal radiation in the near-field regime. Below we summarize our results and present the corresponding conclusions separately for each one of these two topics, ending with some possibilities of future research.

### 6.1 Replica energy as a degree of freedom

We have shown that nonadditive systems can be treated in the standard equilibrium thermodynamic framework if it is properly formulated. While in a statistical mechanics formulation the nonadditivity is naturally codified in the characteristic function of the ensemble under consideration [11], we have seen that it emerges through an additional degree of freedom in the thermodynamic treatment, the replica energy  $\mathcal{E}$ . According to the differences between isolated systems and systems in contact with a thermostat (ensemble inequivalence), the replica energy depends on the physical situation under consideration. Nevertheless, in nonadditive systems it is always different from zero. Here we have considered that the nonadditivity is caused by long-range interactions among the constituents of the system, but it can be originated from any other finite-size effect. The approach we have presented is based on Hill's thermodynamics of small systems [65]. Macroscopic systems with short-range interactions are particular cases of the systems considered here in which the replica energy vanishes, and can also be obtained as a limiting case in the treatment of systems with a small number of particles. Therefore, both long- and short-range interacting systems with a large number of particles as well as small systems can be described with the same thermodynamic approach.

As a consequence of the degree of freedom introduced by the nonadditivity, the usual Gibbs-Duhem equation is modified and the temperature, pressure, and

chemical potential may become independent variables. In turn, this fact leads to the possibility of taking the previous variables as control parameters. We have shown that systems with long-range interactions and a large number of particles can attain configurations of thermodynamic equilibrium in the unconstrained ensemble. In this ensemble the control parameters are the temperature, pressure, and chemical potential, and the associated free energy is the replica energy. In addition, a solvable model that is stable in the unconstrained ensemble has been introduced (the modified Thirring model). The equilibrium states of this model in the unconstrained ensemble have been compared with those of the grand canonical and canonical ensembles. From this comparison we observe that the space of parameters defining the possible stable configurations is enlarged when the system is constrained by fixing the volume and the number of particles. The latter quantities fluctuate in the unconstrained ensemble, as well as the energy of the system.

Macroscopic systems with short-range interactions cannot attain equilibrium states if the control parameters are the temperature, pressure, and chemical potential. According to the usual Gibbs-Duhem equation, these quantities cannot be taken together as independent variables. In this case, the temperature, pressure, and chemical potential are truly intensive properties and therefore, they cannot define the size of the system corresponding to an equilibrium state. In systems with long-range interactions, however, the temperature, pressure, and chemical potential are not intensive properties and can implicitly define the size of the system in equilibrium configurations. Thus, the typical scaling of the thermodynamic variables in long-range interacting systems makes it possible to have states of thermodynamic equilibrium under completely open conditions.

Furthermore, we have studied the phase diagrams of the Thirring model [18] in both the microcanonical and canonical ensembles, which in this case are not equivalent. Using the Landau theory of phase transitions, as done in [141], the coefficients of the Landau expansion of the canonical free energy can be written in terms of the coefficients of the microcanonical entropy, which permits an analysis of the critical conditions in which these coefficient vanish. Hence, the critical point at which each first-order transition line terminates can be computed exactly in this case, evincing that they are indeed different. Moreover, the comparison of the two phase diagrams shows that the energies at which phase transitions take place in the microcanonical ensemble are not allowed in the canonical ensemble. Conversely, the temperatures at which the transitions take place in the canonical ensemble are accessible to microcanonical equilibrium configurations.

The thermodynamic framework we have presented here emphasizes that finite-size effects can lead to equilibrium configurations in situations where configurations of the usual additive systems would be realized. This offers the possibility of new scenarios for exploring finite systems under completely open conditions.

## 6.2 Heat engines driven by photon tunneling

Near-field heat engines are devices that, through some suitable mechanism, convert the evanescent thermal field supported by a primary source into usable mechanical energy. We have formulated a thermodynamic scheme for energy-conversion processes in the near-field regime that can be implemented using such heat engines. Thermodynamic functions as energy and entropy fluxes have been constructed by computing the transmission coefficients for the thermal radiation emitted by the materials defining the system. In the situations we have considered, the thermal radiation is emitted by three or two bodies in mutual interaction [88, 103, 104]. All the transmission coefficients for three- and two-body systems have been computed explicitly, from which energy and entropy fluxes can be obtained in any of the vacuum regions defined by the distribution of bodies constituting the corresponding configuration. From energy and entropy fluxes, upper bounds for the usable work flux (thermodynamic availability) and the efficiency of the energy-conversion process have also been obtained in three- and two-body systems.

In two-body systems, we have studied the thermodynamics of thermal radiation between two semi-infinite polar media separated by a nanoscale vacuum gap. Emphasis has been placed on the case where the difference of temperatures of the materials is small in comparison with the average temperature. Such a situation is physically relevant, for instance, if a converter is implemented in a certain device with the purpose of harvesting energy from near-field radiation. On the one hand, the thermodynamic efficiency of the process strongly depends on the temperature difference and it is expected to be small in such cases. On the other hand, although small efficiencies is the price to pay under these conditions, the amount of work flux obtained from near-field thermal radiation is considerable higher than the corresponding one obtained from blackbody thermal radiation [113]. The latter corresponds to a limiting situation in which the thermal source and the converter are far from each other. In the near field, both maximum work flux and efficiency depend on the optical properties of the materials, and the explicit dependence on the frequency of the resonant mode supported by the media (surface phonon polariton) has been obtained. Thus, our analysis highlights how the properties of the material influence the performance of the energy harvesting process.

By investigating the thermodynamic performance of three-body near-field heat engines, we have demonstrated that the power they supply can be substantially larger than that of two-body systems, showing their strong potential for energy harvesting. Theoretical limits for energy and entropy fluxes in three-body systems, for which the transmission coefficients are assumed to attain their maximum value [94, 115, 162], have been discussed and compared with their corresponding two-body counterparts. Such considerations confirm that the thermodynamic availability

in energy-conversion processes driven by photon tunneling in three-body systems can exceed the thermodynamic availability in two-body systems. In the configurations we have analyzed, the efficiency of the three-body heat engine is, however, lower than its two-body analogue. Besides, and as a complementary result, the theoretical limit in which the transmission coefficients are assumed to attain their maximum value for the general case of many-body heat engines implies that the efficiency does not depend the number of bodies in interaction. The previous limit also leads to the conclusion that the thermodynamic availability can indeed be increased when increasing the number of bodies in the system. These results pave the way for a generation of nanoscale energy converters based on the physics of many-body interacting systems, instead of the conventional two-body systems. In addition, this work provides perspectives for investigating the thermodynamics of systems with long-range electromagnetic interactions.

### 6.3 Future directions

To conclude this monography, here we discuss some possible extensions and applications of the treatments developed in the preceding chapters.

First, in the modification of the Thirring model introduced in Section 3.2.1, and more specifically when studying the canonical ensemble in Section 3.2.4, it has been shown that the model exhibit first-order phase transitions. This is expected, since the case  $b = 0$  does exhibit phase transitions, as studied in detail in Section 3.1. It would be interesting to extend the analysis done in Section 3.1 to the case  $b \neq 0$  and study the full phase diagram in both the microcanonical and canonical ensembles. Moreover, the occurrence of negative response functions in this model could be studied in the different ensembles as well, to explore some of the relations given in Section 2.4. In addition, including hard-core repulsions in the model could give some insight into stability conditions in the unconstrained ensemble, since we have seen that the interactions need to be repulsive in the outer parts of the system to avoid collapse. All these questions may have some theoretical relevance.

Second, implementing different materials and configurations to look for optimal conditions in near-field thermal radiation energy conversion may be a valuable contribution to the field. The scheme we have presented could be generalized to include an specific conversion mechanism. With a concrete converter and given operating conditions, the entropy production in the process could be, in principle, estimated. This would lead to accurate bounds for the efficiency and usable work flux in the case at hand. In addition, the formal generalization for arbitrary number of bodies is almost immediate; one has to compute the associated transmission coefficients for the specific case under consideration. This can be done following the procedure

used to obtain the coefficients of the three-body systems. General expressions for the transmission coefficients for arbitrary number of bodies is also desirable.

Finally, the study of the thermodynamic properties of the near-field thermal radiation here has been restricted to situations that are globally out of thermal equilibrium. However, as mentioned in the introduction, in the near field certain effects can also be observed at global thermal equilibrium. Due to the contribution of evanescent modes and in situations in which the radiation is confined at scales below the characteristic thermal wavelength, the distribution of photon states in the cavity is not spatially homogeneous, even at thermal equilibrium. This is a well-known fact usually quantified by taking into account a position-dependent electromagnetic local density of states [107–109]. As a consequence of this nonhomogeneity, from a thermodynamic viewpoint the confined photon gas may exhibit some of the properties of classical systems with long-range interactions. Clearly, photon-photon interactions may be regarded as completely absent in normal conditions [98], but the effective electromagnetic interaction between the bodies confining the radiation is long ranged for small separation distances (small as compared with the thermal wavelength). These long-range interactions are van der Waals interactions between atoms in the walls of the container and are expressed through long-wavelength components of the electromagnetic field in the cavity [147]. In addition, the contribution of the van der Waals interactions to the free energy of the system is nonadditive [147]. The latter leads to a confined photon gas that is nonadditive as well, since its free energy is not simply proportional to the volume of the cavity. This issue is currently under investigation. Exploring such a connection between the two topics exposed in this work could give some insight in the physics of the confined electromagnetic radiation, and may provide experimental access to some of the theoretical properties predicted for long-range interacting systems.



# MODIFIED THIRRING MODEL: CANONICAL CRITICAL POINT

---

Our aim here is to succinctly derive the critical point of the modified Thirring model in the canonical ensemble. The model has been considered in this ensemble in Section 3.2.4. The derivation presented below is an extension of the detailed treatment presented in Section 3.1 for the original Thirring model.

## A.1 Free energy expansion

Phase transitions in the modified Thirring model in the canonical ensemble can be studied by extending the analysis done in Section 3.1 using the Landau theory of phase transitions. In Section 3.1, the expansion parameter specifying the transition is taken as the deviation of the fraction  $n_g = 1 - N_0/N$  with respect to the value of this fraction at an equilibrium configuration. Here we consider the fraction of particles in  $V_0$ , given by  $x_0/x$ , and take

$$m = (x_0 - \bar{x}_0)/x \tag{A.1}$$

as the expansion parameter. Accordingly, to obtain the critical point we expand the canonical free energy (3.133) around  $\bar{x}_0/x$  as

$$\hat{\varphi}_C = \varphi_0 + \varphi_1 m + \varphi_2 m^2 + \mathcal{O}(m^3), \tag{A.2}$$

and look for a solution of the system of equations

$$\begin{aligned} \varphi_1(\bar{x}_0, x, v) &= 0, \\ \varphi_2(\bar{x}_0, x, v) &= 0, \end{aligned} \tag{A.3}$$

with the constrain  $0 \leq \bar{x}_0/x \leq 1$ .

## A.2 Critical point

The first of the equations (A.3) is exactly (3.131), while the second one can be written as

$$\frac{2(b+1)(x-\bar{x}_0)\bar{x}_0-x}{(x-\bar{x}_0)\bar{x}_0}=0. \quad (\text{A.4})$$

Thus, for  $b > -1$ , equation (A.4) has two real solutions,

$$\bar{x}_0 = x_{\pm}(x) = \left[1 + b \pm \sqrt{(1+b)(1+b-2/x)}\right]^{-1}, \quad (\text{A.5})$$

when  $x > 2/(1+b) \equiv x_c$ . The critical point is defined by the condition  $x_+(x_c) = x_-(x_c)$ , in such a way that at the critical point one has  $x = x_c$  and

$$\bar{x}_0 = x_{\pm}(x_c) = x_c/2. \quad (\text{A.6})$$

In terms of the thermodynamic variables, this means that the critical temperature is given by

$$T_c = \nu N(1+b)/2 \quad (\text{A.7})$$

and that the fraction  $\bar{N}_0/N$  at the critical point is  $1/2$ . Moreover, we note that when  $b = -1$ , the left-hand side of equation (A.4) does not vanish, and, therefore, there are no phase transitions in this case. For  $b < -1$ , the fractions  $x_{\pm}/x$  does not lie in the interval  $[0, 1]$ , so that neither in this case the model will exhibit phase transitions. We therefore observe that the model may present phase transitions in the canonical ensemble, depending of the value of  $v$ , if  $x$  is larger than  $x_c$  and if  $b > -1$ .

The critical value of the reduced volume  $v_c$  is obtained by replacing  $\bar{x}_0 = x_{\pm}(x_c)$  in equation (3.131) with  $v = v_c$ , yielding

$$v_c = \exp[2(1-b)/(1+b)]. \quad (\text{A.8})$$

Thus, the model may exhibits phase transitions when  $v > v_c$ .

## TRANSMISSION COEFFICIENTS FOR RADIATIVE HEAT TRANSFER

---

This appendix is devoted to give some intermediate results used to determine the transmission coefficients for radiative transfer of three- and two-body systems. In addition, these transmission coefficients are given explicitly for both the far and near fields, that is, taking into account the full contribution of propagative and evanescent waves.

### B.1 Coefficients for the electric field

In Section 4.1.2, we wrote the electric field  $E_\sigma^{(\gamma)\phi}$  in region  $\gamma$  in terms of the source fields  $E_\sigma^{(\alpha)\phi}$ . These fields are related through a linear combination of the form

$$E_\sigma^{(\gamma)\phi} = \sum_{\alpha,\eta} L_{(\alpha)\eta}^{(\gamma)\phi}(\sigma, \boldsymbol{\kappa}, \omega) E_\sigma^{(\alpha)\eta}, \quad (\text{B.1})$$

where  $\gamma = \text{A, B, C, D}$ ,  $\alpha = 0, 1, 2, 3, 4$ , and  $\phi, \eta = +, -$ . By making use of the many-body scattering coefficients introduced in Section 4.1.3, the coefficients  $L_{(\alpha)\eta}^{(\gamma)\phi}$  can be directly obtained from the system of equations (4.16) after some simple algebraic operations [104]. Here we give the result, whereas the coefficients that are not listed below vanish.

$$\begin{aligned} L_{(0)+}^{(\text{A})+} &= 1, & L_{(0)+}^{(\text{C})+} &= u_\sigma^{(12,3)} \tau_\sigma^{(12)}, \\ L_{(0)+}^{(\text{A})-} &= \rho_\sigma^{(123)-}, & L_{(1)+}^{(\text{C})+} &= u_\sigma^{(12,3)} u_\sigma^{(1,2)} \tau_\sigma^{(2)}, \\ L_{(1)+}^{(\text{A})-} &= u_\sigma^{(1,23)} \rho_\sigma^{(23)-} \tau_\sigma^{(1)}, & L_{(2)+}^{(\text{C})+} &= u_\sigma^{(12,3)}, \end{aligned}$$

$$\begin{aligned}
L_{(2)+}^{(A)-} &= u_{\sigma}^{(12,3)} \tau_{\sigma}^{(12)} \rho_{\sigma}^{(3)-}, & L_{(2)-}^{(C)+} &= u_{\sigma}^{(12,3)} \tau_{\sigma}^{(2)} u_{\sigma}^{(1,2)} \rho_{\sigma}^{(1)+}, \\
L_{(1)-}^{(A)-} &= 1, & L_{(3)-}^{(C)+} &= u_{\sigma}^{(12,3)} \rho_{\sigma}^{(12)+}, \\
L_{(2)-}^{(A)-} &= u_{\sigma}^{(1,23)} \tau_{\sigma}^{(1)}, & L_{(4)-}^{(C)+} &= u_{\sigma}^{(12,3)} \rho_{\sigma}^{(12)+} \tau_{\sigma}^{(3)}, \\
L_{(3)-}^{(A)-} &= u_{\sigma}^{(12,3)} \tau_{\sigma}^{(12)}, & L_{(0)+}^{(C)-} &= u_{\sigma}^{(12,3)} \tau_{\sigma}^{(12)} \rho_{\sigma}^{(3)-}, \\
L_{(4)-}^{(A)-} &= \tau_{\sigma}^{(123)}, & L_{(1)+}^{(C)-} &= u_{\sigma}^{(12,3)} u_{\sigma}^{(1,2)} \rho_{\sigma}^{(3)-} \tau_{\sigma}^{(2)}, \\
L_{(0)+}^{(B)+} &= u_{\sigma}^{(1,23)} \tau_{\sigma}^{(1)}, & L_{(2)+}^{(C)-} &= u_{\sigma}^{(12,3)} \rho_{\sigma}^{(3)-}, \\
L_{(1)+}^{(B)+} &= u_{\sigma}^{(1,23)}, & L_{(2)-}^{(C)-} &= u_{\sigma}^{(12,3)} u_{\sigma}^{(1,2)} \rho_{\sigma}^{(3)-} \tau_{\sigma}^{(2)} \rho_{\sigma}^{(1)+}, \\
L_{(2)+}^{(B)+} &= u_{\sigma}^{(1,23)} u_{\sigma}^{(2,3)} \rho_{\sigma}^{(1)+} \tau_{\sigma}^{(2)} \rho_{\sigma}^{(3)-}, & L_{(3)-}^{(C)-} &= u_{\sigma}^{(12,3)}, \\
L_{(2)-}^{(B)+} &= u_{\sigma}^{(1,23)} \rho_{\sigma}^{(1)+}, & L_{(4)-}^{(C)-} &= u_{\sigma}^{(12,3)} \tau_{\sigma}^{(3)}, \\
L_{(3)-}^{(B)+} &= u_{\sigma}^{(1,23)} u_{\sigma}^{(2,3)} \rho_{\sigma}^{(1)+} \tau_{\sigma}^{(2)}, & L_{(0)+}^{(D)+} &= \tau_{\sigma}^{(123)}, \\
L_{(4)-}^{(B)+} &= u_{\sigma}^{(1,23)} \tau_{\sigma}^{(23)} \rho_{\sigma}^{(1)+}, & L_{(1)+}^{(D)+} &= u_{\sigma}^{(1,23)} \tau_{\sigma}^{(23)}, \\
L_{(0)+}^{(B)-} &= u_{\sigma}^{(1,23)} \rho_{\sigma}^{(23)-} \tau_{\sigma}^{(1)}, & L_{(2)+}^{(D)+} &= u_{\sigma}^{(12,3)} \tau_{\sigma}^{(3)}, \\
L_{(1)+}^{(B)-} &= u_{\sigma}^{(1,23)} \rho_{\sigma}^{(23)-}, & L_{(3)+}^{(D)+} &= 1, \\
L_{(2)+}^{(B)-} &= u_{\sigma}^{(1,23)} u_{\sigma}^{(2,3)} \rho_{\sigma}^{(3)-} \tau_{\sigma}^{(2)}, & L_{(2)-}^{(D)+} &= u_{\sigma}^{(1,23)} \tau_{\sigma}^{(23)} \rho_{\sigma}^{(1)+}, \\
L_{(2)-}^{(B)-} &= u_{\sigma}^{(1,23)}, & L_{(3)-}^{(D)+} &= u_{\sigma}^{(12,3)} \rho_{\sigma}^{(12)+} \tau_{\sigma}^{(3)}, \\
L_{(3)-}^{(B)-} &= u_{\sigma}^{(1,23)} u_{\sigma}^{(2,3)} \tau_{\sigma}^{(2)}, & L_{(4)-}^{(D)+} &= \rho_{\sigma}^{(123)+}, \\
L_{(4)-}^{(B)-} &= u_{\sigma}^{(1,23)} \tau_{\sigma}^{(23)}, & L_{(4)-}^{(D)-} &= 1.
\end{aligned}$$

## B.2 Transmission coefficients

Using the expressions for the correlation functions of the source fields  $C_{\sigma}^{(\alpha)\eta\eta'}$ , given by equations (4.33), (4.34), and (4.35), and the definition of the coefficients  $K_{\phi\phi'}^{(\alpha)\eta\eta'}$

given in (4.53), the latter can be written as

$$\begin{aligned}
K_{\phi\phi'}^{(\alpha)\eta\eta'} &= \Pi^{(\text{pw})} \delta_{\phi\phi'} \left[ \delta_{\eta\eta'} \left( 1 - \rho_{\sigma}^{(\alpha)\eta} \rho_{\sigma}^{(\alpha)\eta*} - \tau_{\sigma}^{(\alpha)} \tau_{\sigma}^{(\alpha)*} \right) \right. \\
&\quad \left. - (1 - \delta_{\eta\eta'}) \left( \rho_{\sigma}^{(\alpha)\eta} \tau_{\sigma}^{(\alpha)*} + \rho_{\sigma}^{(\alpha)\eta'*} \tau_{\sigma}^{(\alpha)} \right) \right] \\
&\quad + \Pi^{(\text{ew})} (1 - \delta_{\phi\phi'}) \left[ \delta_{\eta\eta'} \left( \rho_{\sigma}^{(\alpha)\eta} - \rho_{\sigma}^{(\alpha)\eta*} \right) + (1 - \delta_{\eta\eta'}) \left( \tau_{\sigma}^{(\alpha)} - \tau_{\sigma}^{(\alpha)*} \right) \right]
\end{aligned} \tag{B.2}$$

for  $\alpha = 1, 2, 3$ . In the same way, for  $\alpha = 0, 4$ , one obtains

$$K_{\phi\phi'}^{(\alpha)\eta\eta'} = \Pi^{(\text{pw})} \delta_{\phi\phi'} \delta_{\eta\eta'}. \tag{B.3}$$

Furthermore, we recall the definition of the coefficients  $X_{\sigma(\alpha)}^{(\gamma)}$ ,

$$X_{\sigma(\alpha)}^{(\gamma)} \equiv \sum_{\phi, \phi'} \sum_{\eta, \eta'} \phi L_{(\alpha)\eta}^{(\gamma)\phi} L_{(\alpha)\eta'}^{(\gamma)\phi'*} K_{\phi\phi'}^{(\alpha)\eta\eta'}, \tag{B.4}$$

and that only four of the five coefficients  $X_{\sigma(\alpha)}^{(\gamma)}$  need to be computed, since the remaining coefficient can be found with the help of the relation (4.57), namely,

$$\sum_{\alpha} X_{\sigma(\alpha)}^{(\gamma)} = 0. \tag{B.5}$$

Once computed the coefficients  $X_{\sigma(\alpha)}^{(\gamma)}$ , the transmission coefficients of the system can be obtained through equation (4.60), that is,

$$\mathcal{T}_{\sigma, \gamma}^{\alpha, \alpha+1} \equiv \sum_{\beta=0}^{\alpha} X_{\sigma(\beta)}^{(\gamma)}. \tag{B.6}$$

Moreover, using (B.5), we also can write

$$\mathcal{T}_{\sigma, \gamma}^{0,1} = X_{\sigma(0)}^{(\gamma)}, \tag{B.7}$$

$$\mathcal{T}_{\sigma, \gamma}^{1,2} = X_{\sigma(0)}^{(\gamma)} + X_{\sigma(1)}^{(\gamma)}, \tag{B.8}$$

$$\mathcal{T}_{\sigma, \gamma}^{2,3} = -X_{\sigma(3)}^{(\gamma)} - X_{\sigma(4)}^{(\gamma)}, \tag{B.9}$$

$$\mathcal{T}_{\sigma, \gamma}^{3,4} = -X_{\sigma(4)}^{(\gamma)}, \tag{B.10}$$

which can be used to obtain the desired result. Below we list the coefficients in each region.

Region A:

$$\mathcal{T}_{\sigma, \Lambda}^{0,1} = \Pi^{(\text{pw})} \left( 1 - \left| \rho_{\sigma}^{(123)-} \right|^2 \right), \tag{B.11}$$

$$\mathcal{T}_{\sigma,A}^{1,2} = \Pi^{(\text{pw})} \frac{|\tau_{\sigma}^{(1)}|^2 \left(1 - |\rho_{\sigma}^{(23)-}|^2\right)}{\left|1 - \rho_{\sigma}^{(1)+} \rho_{\sigma}^{(23)-}\right|^2}, \quad (\text{B.12})$$

$$\mathcal{T}_{\sigma,A}^{2,3} = \Pi^{(\text{pw})} \frac{|\tau_{\sigma}^{(12)}|^2 \left(1 - |\rho_{\sigma}^{(3)-}|^2\right)}{\left|1 - \rho_{\sigma}^{(12)+} \rho_{\sigma}^{(3)-}\right|^2}, \quad (\text{B.13})$$

$$\mathcal{T}_{\sigma,A}^{3,4} = \Pi^{(\text{pw})} \left|\tau_{\sigma}^{(123)}\right|^2. \quad (\text{B.14})$$

Region B:

$$\mathcal{T}_{\sigma,B}^{0,1} = \Pi^{(\text{pw})} \frac{|\tau_{\sigma}^{(1)}|^2 \left(1 - |\rho_{\sigma}^{(23)-}|^2\right)}{\left|1 - \rho_{\sigma}^{(1)+} \rho_{\sigma}^{(23)-}\right|^2}, \quad (\text{B.15})$$

$$\begin{aligned} \mathcal{T}_{\sigma,B}^{1,2} &= \Pi^{(\text{pw})} \frac{\left(1 - |\rho_{\sigma}^{(1)+}|^2\right) \left(1 - |\rho_{\sigma}^{(23)-}|^2\right)}{\left|1 - \rho_{\sigma}^{(1)+} \rho_{\sigma}^{(23)-}\right|^2} \\ &\quad + \Pi^{(\text{ew})} \frac{4 \text{Im} \left(\rho_{\sigma}^{(1)+}\right) \text{Im} \left(\rho_{\sigma}^{(23)-}\right)}{\left|1 - \rho_{\sigma}^{(1)+} \rho_{\sigma}^{(23)-}\right|^2}, \end{aligned} \quad (\text{B.16})$$

$$\begin{aligned} \mathcal{T}_{\sigma,B}^{2,3} &= \Pi^{(\text{pw})} \frac{|\tau_{\sigma}^{(2)}|^2 \left(1 - |\rho_{\sigma}^{(1)+}|^2\right) \left(1 - |\rho_{\sigma}^{(3)-}|^2\right)}{\left|1 - \rho_{\sigma}^{(1)+} \rho_{\sigma}^{(23)-}\right|^2 \left|1 - \rho_{\sigma}^{(2)+} \rho_{\sigma}^{(3)-}\right|^2} \\ &\quad + \Pi^{(\text{ew})} \frac{4 \left|\tau_{\sigma}^{(2)}\right|^2 \text{Im} \left(\rho_{\sigma}^{(1)+}\right) \text{Im} \left(\rho_{\sigma}^{(3)-}\right)}{\left|1 - \rho_{\sigma}^{(1)+} \rho_{\sigma}^{(23)-}\right|^2 \left|1 - \rho_{\sigma}^{(2)+} \rho_{\sigma}^{(3)-}\right|^2}, \end{aligned} \quad (\text{B.17})$$

$$\mathcal{T}_{\sigma,B}^{3,4} = \Pi^{(\text{pw})} \frac{|\tau_{\sigma}^{(23)}|^2 \left(1 - |\rho_{\sigma}^{(1)+}|^2\right)}{\left|1 - \rho_{\sigma}^{(1)+} \rho_{\sigma}^{(23)-}\right|^2}. \quad (\text{B.18})$$

Region C:

$$\mathcal{T}_{\sigma,C}^{0,1} = \Pi^{(\text{pw})} \frac{|\tau_{\sigma}^{(12)}|^2 \left(1 - |\rho_{\sigma}^{(3)-}|^2\right)}{\left|1 - \rho_{\sigma}^{(12)+} \rho_{\sigma}^{(3)-}\right|^2}, \quad (\text{B.19})$$

$$\begin{aligned} \mathcal{T}_{\sigma,C}^{1,2} &= \Pi^{(\text{pw})} \frac{|\tau_{\sigma}^{(2)}|^2 \left(1 - |\rho_{\sigma}^{(1)+}|^2\right) \left(1 - |\rho_{\sigma}^{(3)-}|^2\right)}{\left|1 - \rho_{\sigma}^{(12)+} \rho_{\sigma}^{(3)-}\right|^2 \left|1 - \rho_{\sigma}^{(1)+} \rho_{\sigma}^{(2)-}\right|^2} \\ &+ \Pi^{(\text{ew})} \frac{4 |\tau_{\sigma}^{(2)}|^2 \text{Im} \left(\rho_{\sigma}^{(1)+}\right) \text{Im} \left(\rho_{\sigma}^{(3)-}\right)}{\left|1 - \rho_{\sigma}^{(12)+} \rho_{\sigma}^{(3)-}\right|^2 \left|1 - \rho_{\sigma}^{(1)+} \rho_{\sigma}^{(2)-}\right|^2}, \end{aligned} \quad (\text{B.20})$$

$$\begin{aligned} \mathcal{T}_{\sigma,C}^{2,3} &= \Pi^{(\text{pw})} \frac{\left(1 - |\rho_{\sigma}^{(12)+}|^2\right) \left(1 - |\rho_{\sigma}^{(3)-}|^2\right)}{\left|1 - \rho_{\sigma}^{(12)+} \rho_{\sigma}^{(3)-}\right|^2} \\ &+ \Pi^{(\text{ew})} \frac{4 \text{Im} \left(\rho_{\sigma}^{(12)+}\right) \text{Im} \left(\rho_{\sigma}^{(3)-}\right)}{\left|1 - \rho_{\sigma}^{(12)+} \rho_{\sigma}^{(3)-}\right|^2}, \end{aligned} \quad (\text{B.21})$$

$$\mathcal{T}_{\sigma,C}^{3,4} = \Pi^{(\text{pw})} \frac{|\tau_{\sigma}^{(3)}|^2 \left(1 - |\rho_{\sigma}^{(12)+}|^2\right)}{\left|1 - \rho_{\sigma}^{(12)+} \rho_{\sigma}^{(3)-}\right|^2}. \quad (\text{B.22})$$

Region D:

$$\mathcal{T}_{\sigma,D}^{0,1} = \Pi^{(\text{pw})} \left| \tau_{\sigma}^{(123)} \right|^2, \quad (\text{B.23})$$

$$\mathcal{T}_{\sigma,D}^{1,2} = \Pi^{(\text{pw})} \frac{|\tau_{\sigma}^{(23)}|^2 \left(1 - |\rho_{\sigma}^{(1)+}|^2\right)}{\left|1 - \rho_{\sigma}^{(1)+} \rho_{\sigma}^{(23)-}\right|^2}, \quad (\text{B.24})$$

$$\mathcal{T}_{\sigma,D}^{2,3} = \Pi^{(\text{pw})} \frac{|\tau_{\sigma}^{(3)}|^2 \left(1 - |\rho_{\sigma}^{(12)+}|^2\right)}{\left|1 - \rho_{\sigma}^{(12)+} \rho_{\sigma}^{(3)-}\right|^2}, \quad (\text{B.25})$$

$$\mathcal{T}_{\sigma,D}^{3,4} = \Pi^{(\text{pw})} \left(1 - |\rho_{\sigma}^{(123)+}|^2\right). \quad (\text{B.26})$$

### B.2.1 Transmission coefficients in the two-body system

Taking into account the considerations discussed in Section 4.3.1, the transmission coefficients of the two-body system can be obtained from those of the three-body system in the appropriate limit. The resulting coefficients are listed below for each region.

Region A:

$$\mathcal{T}_{\sigma,A}^{0,1} = \Pi^{(\text{pw})} \left(1 - |\rho_{\sigma}^{(12)-}|^2\right), \quad (\text{B.27})$$

$$\mathcal{T}_{\sigma,A}^{1,2} = \Pi^{(\text{pw})} \frac{|\tau_{\sigma}^{(1)}|^2 \left(1 - |\rho_{\sigma}^{(2)-}|^2\right)}{\left|1 - \rho_{\sigma}^{(1)+} \rho_{\sigma}^{(2)-}\right|^2}, \quad (\text{B.28})$$

$$\mathcal{T}_{\sigma,A}^{2,3} = \Pi^{(\text{pw})} \left|\tau_{\sigma}^{(12)}\right|^2. \quad (\text{B.29})$$

Region B:

$$\mathcal{T}_{\sigma,B}^{0,1} = \Pi^{(\text{pw})} \frac{|\tau_{\sigma}^{(1)}|^2 \left(1 - |\rho_{\sigma}^{(2)-}|^2\right)}{\left|1 - \rho_{\sigma}^{(1)+} \rho_{\sigma}^{(2)-}\right|^2}, \quad (\text{B.30})$$

$$\begin{aligned} \mathcal{T}_{\sigma,B}^{1,2} = & \Pi^{(\text{pw})} \frac{\left(1 - |\rho_{\sigma}^{(1)+}|^2\right) \left(1 - |\rho_{\sigma}^{(2)-}|^2\right)}{\left|1 - \rho_{\sigma}^{(1)+} \rho_{\sigma}^{(2)-}\right|^2} \\ & + \Pi^{(\text{ew})} \frac{4\text{Im}\left(\rho_{\sigma}^{(1)+}\right) \text{Im}\left(\rho_{\sigma}^{(2)-}\right)}{\left|1 - \rho_{\sigma}^{(1)+} \rho_{\sigma}^{(2)-}\right|^2} \end{aligned} \quad (\text{B.31})$$

$$\mathcal{T}_{\sigma,B}^{2,3} = \Pi^{(\text{pw})} \frac{|\tau_{\sigma}^{(2)}|^2 \left(1 - |\rho_{\sigma}^{(1)+}|^2\right)}{\left|1 - \rho_{\sigma}^{(1)+} \rho_{\sigma}^{(2)-}\right|^2}. \quad (\text{B.32})$$

Region C:

$$\mathcal{T}_{\sigma,C}^{0,1} = \Pi^{(\text{pw})} \left|\tau_{\sigma}^{(12)}\right|^2, \quad (\text{B.33})$$

$$\mathcal{T}_{\sigma,C}^{1,2} = \Pi^{(\text{pw})} \frac{|\tau_{\sigma}^{(2)}|^2 \left(1 - |\rho_{\sigma}^{(1)+}|^2\right)}{\left|1 - \rho_{\sigma}^{(1)+} \rho_{\sigma}^{(2)-}\right|^2}, \quad (\text{B.34})$$

$$\mathcal{T}_{\sigma,C}^{2,3} = \Pi^{(\text{pw})} \left(1 - |\rho_{\sigma}^{(12)+}|^2\right). \quad (\text{B.35})$$

## RESUMEN

---

Esta tesis es un estudio sobre la termodinámica estadística de sistemas con interacciones de largo alcance y de radiación térmica de campo cercano. Tanto los sistemas con interacciones de largo alcance como la radiación térmica de campo cercano pueden considerarse casos particulares de una clase de sistemas más general, la cual contiene a los que podríamos denominar como sistemas finitos. La finitud asociada a estos sistemas, en general, puede ser producida por diferentes fenómenos con distinta naturaleza física. En el caso de los sistemas con interacciones de largo alcance, la finitud se manifiesta debido a que el tamaño del sistema es comparable al rango de las interacciones entre sus constituyentes. En el caso de la radiación térmica de campo cercano, en cambio, esta propiedad emerge porque el tamaño del sistema es comparable con la longitud de onda térmica dominante. Así pues, desde un punto de vista termodinámico y mecánico-estadístico, en estos sistemas la finitud da lugar a propiedades físicas que ciertamente no están presentes en sistemas que satisfacen el límite termodinámico ordinario, los cuales podríamos considerar como sistemas infinitos.

A continuación discutiremos el primero de los casos mencionados, expuesto en la primera parte de la tesis: los sistemas con interacciones de largo alcance. Éstos están caracterizados por potenciales de interacción que decaen lentamente, al menos en una región del sistema comparable a su extensión total. Más específicamente, este decaimiento es menor que el inverso de la distancia entre partículas elevada a la dimensión del espacio en el cual el sistema está definido. Por ejemplo, el potencial de interacción gravitatorio es de largo alcance. Los sistemas autogravitantes, de hecho, son probablemente el caso más paradigmático dentro de este tipo de sistemas, los cuales han sido ampliamente estudiados en la literatura. A raíz de la finitud introducida por las las interacciones de largo alcance, estos sistemas son intrínsecamente no aditivos. La no aditividad es responsable de ciertas propiedades termodinámicas y mecánico-estadísticas que no se dan en sistemas aditivos; a remarcar, las diferentes colectividades estadísticas no son, en general, equivalentes, ya que los estados observables en los sistemas no aditivos dependen fuertemente de qué conjunto de parámetros de control definen la configuración de equilibrio asociada.

A modo de ejemplo, estados observables cuando el sistema está aislado (colectividad microcanónica), pueden no realizarse cuando el sistema está termalizado con el ambiente (colectividad canónica).

En la tesis presentamos un formalismo termodinámico apropiado para los sistemas con interacciones de largo alcance, el cual tiene en cuenta explícitamente la no aditividad. El concepto central detrás de este formalismo es considerar una colectividad de réplicas del sistema donde la formulación estándar de la termodinámica puede aplicarse naturalmente, y desde allí inferir las propiedades de cada uno de los miembros de la colectividad. La colectividad de réplicas es en sí misma un sistema aditivo, mientras que un sistema individualmente no lo es. Esta formulación de la termodinámica está estrechamente relacionada con el tratamiento introducido por T. Hill para sistemas pequeños. El calificativo pequeño en este caso indica que el sistema tiene pocas partículas, lo cual es claramente otra fuente de finitud. En contraste, en los sistemas aquí tratados siempre se asume que el número de partículas es grande.

De manera concisa podríamos decir que la no aditividad introduce un grado de libertad termodinámico, que en este formalismo es representado por una energía característica llamada *energía de réplica*. La energía de réplica es nula para los sistemas aditivos. Cuando la energía de réplica es no trivial, existe la posibilidad de que la temperatura, la presión y el potencial químico del sistema puedan ser considerados como variables independientes. La energía de réplica modifica la ecuación de Gibbs-Duhem que relaciona la variaciones de estas cantidades. A su vez, esto da lugar a que, dependiendo del sistema concreto, la temperatura, la presión y el potencial químico puedan ser tomados como parámetros de control independientes para definir las configuraciones de equilibrio del sistema. La colectividad estadística en la que estos parámetros de control son las variables naturales asociadas puede ser considerada una colectividad “sin restricciones” (también llamada generalizada), en el sentido de que en este caso la energía, el volumen y el número de partículas fluctúan; en estas circunstancias, el sistema está completamente abierto. La energía de réplica es precisamente la energía libre asociada a esta colectividad sin restricciones. Para mostrar que tales condiciones pueden realizarse, hemos introducido un modelo que exhibe estados de equilibrio en esta colectividad. Éste es una modificación del modelo de Thirring, originalmente introducido como una versión simplificada de un gas autogravitante. Los estados de equilibrio del modelo de Thirring modificado en la colectividad sin restricciones han sido comparados con los correspondientes a las colectividades canónica y gran canónica. Se observa que cuanto más restricciones, fijando el volumen y/o el número de partículas, más grande es el espacio de posibles configuraciones estables. El modelo de Thirring original, de hecho, no es estable si se lo considera como completamente abierto. Este último presenta transiciones de fase de primer orden en las colectividades microcanónica y canónica, las cuales han sido

estudiadas con detalle. Los correspondientes diagramas de fase son diferentes entre sí, evidenciando la inequivalencia de colectividades en este modelo.

Por otro lado, centraremos nuestra atención ahora en el tema considerado en la segunda parte de la tesis: radiación térmica de campo cercano. En el intercambio de calor entre cuerpos separados por distancias mucho mayores que la longitud de onda térmica dominante, la potencia emitida por radiación térmica viene dada por la ley de Stefan-Boltzmann. Este es el llamado límite de cuerpo negro, el cual es debido exclusivamente a contribuciones de modos propagativos del campo electromagnético radiado. A diferencia de esto, el intercambio de calor por radiación térmica de campo cercano, que ocurre para separaciones menores que la longitud de onda térmica característica, está dominado por el “tuneo” de modos no propagativos del campo electromagnético. Estos modos corresponden a ondas evanescentes localizadas cerca de las superficies de los cuerpos en interacción radiativa. Debido al rápido decaimiento de estos modos, tales efectos aparecen a escalas por debajo de unos pocos micrómetros a temperatura ambiente. La radiación térmica de campo cercano, además, depende considerablemente de las propiedades ópticas de los materiales involucrados. Si los materiales que se utilizan soportan modos resonantes de superficie (*surface plasmons* o *surface phonon polaritons*), la radiación térmica de campo cercano es fuertemente monocromática, lo cual es muy ventajoso en procesos de conversión de energía en trabajo útil si se utilizan, por ejemplo, células fotovoltaicas apropiadas. Como consecuencia de la contribución de las ondas evanescentes, el intercambio de calor por radiación en el campo cercano puede ser varios órdenes de magnitud mayor que en el límite de cuerpo negro. Asimismo, cuando se consideran varios cuerpos en interacción radiativa, dependiendo de los materiales implementados, puede obtenerse una amplificación del flujo de energía, lo cual permite también una amplificación del trabajo útil que puede extraerse de la radiación.

En la tesis elaboramos un esquema termodinámico capaz de describir procesos de conversión de energía por radiación térmica de campo cercano en sistemas de varios cuerpos. De esta manera, como se ha hecho ampliamente en la literatura para radiación de cuerpo negro, obtenemos cotas dadas por la termodinámica para el trabajo útil y para la eficiencia del proceso de conversión. Tal esquema se obtiene cuantificando los flujos de energía y entropía transportados por la radiación, posibilitando la obtención de la disponibilidad energética del sistema. El flujo de energía en una región de vacío viene dado por el promedio estadístico de la componente del vector de Poynting perpendicular a la superficie de los cuerpos. Reescribiendo de manera adecuada el flujo de energía, es posible deducir los coeficientes de transmisión asociados al proceso radiativo en cada una de las regiones conformadas por la distribución de cuerpos en el sistema. Usando estos coeficientes de transmisión, los flujos de entropía asociados se obtienen de acuerdo con las relaciones usuales de

la termodinámica a partir de los flujos de energía.

Al implementar tal esquema termodinámico, hemos mostrado explícitamente que el trabajo útil que puede extraerse de la radiación térmica de campo cercano es considerablemente mayor que el obtenido con radiación de cuerpo negro, incluso varios órdenes de magnitud mayor, dependiendo de la configuración analizada. A esto debemos agregar que en sistemas de varios cuerpos es posible obtener amplificación del flujo de energía y, por ende, de la disponibilidad termodinámica, como habíamos remarcado previamente. En particular, en las configuraciones estudiadas hemos mostrado que en un sistema de tres cuerpos puede obtenerse una amplificación de un 60 % con respecto al correspondiente sistema de dos cuerpos. Esto provee nuevas perspectivas para explotar la física de la radiación térmica de campo cercano en sistemas de varios cuerpos, por ejemplo, como medio de recuperación o control de energía en dispositivos en la escala nanoscópica.

## REFERENCES

---

- [1] I. Latella, A. Pérez-Madrid, A. Campa, L. Casetti, and S. Ruffo. Long-range interacting systems in the unconstrained ensemble (*in preparation*).
- [2] A. Campa, L. Casetti, I. Latella, A. Pérez-Madrid, and S. Ruffo. Phase transitions in Thirring's model, arXiv:1603.02602 (*submitted*).
- [3] I. Latella, A. Pérez-Madrid, L. C. Lapas, and J. M. Rubi. Near-field thermodynamics and nanoscale energy harvesting. *Phys. Scr.* **T165**, 014026 (2015).
- [4] I. Latella, A. Pérez-Madrid, J. M. Rubi, S.-A. Biehs, and P. Ben-Abdallah. Heat engine driven by photon tunneling in many-body systems. *Phys. Rev. Applied* **4**, 011001 (2015).
- [5] I. Latella, A. Pérez-Madrid, A. Campa, L. Casetti, and S. Ruffo. Thermodynamics of nonadditive systems. *Phys. Rev. Lett.* **114**, 230601 (2015).
- [6] I. Latella, A. Pérez-Madrid, and J. M. Rubi. Thermodynamics and energy conversion of near-field thermal radiation: maximum work and efficiency bounds. *Eur. Phys. J. Conferences* **79**, 01001 (2014).
- [7] I. Latella, A. Pérez-Madrid, L. C. Lapas, and J. M. Rubi. Near-field thermodynamics: Useful work, efficiency, and energy harvesting. *J. Appl. Phys.* **115**, 124307 (2014).
- [8] I. Latella and A. Pérez-Madrid. Local thermodynamics and the generalized Gibbs-Duhem equation in systems with long-range interactions. *Phys. Rev. E* **88**, 042135 (2013).
- [9] I. Latella and A. Pérez-Madrid. Long-range interacting systems and the Gibbs-Duhem equation. In M. Pilotelli and G. P. Beretta, editors, *Proceedings of the 12th JETC*, page 437 (2013).
- [10] A. Campa, T. Dauxois, and S. Ruffo. Statistical mechanics and dynamics of solvable models with long-range interactions. *Phys. Rep.* **480**, 57 (2009).
- [11] A. Campa, T. Dauxois, D. Fanelli, and S. Ruffo. *Physics of Long-Range Interacting Systems*. Oxford University Press, Oxford (2010).
- [12] D. Polder and M. Van Hove. Theory of Radiative Heat Transfer between Closely Spaced Bodies. *Phys. Rev. B* **4**, 3303 (1971).
- [13] F. Bouchet, S. Gupta, and D. Mukamel. Thermodynamics and dynamics of systems with long-range interactions. *Physica A* **389**, 4389 (2010).

- [14] Y. Levin, R. Pakter, F. B. Rizzato, T. N. Teles, and F. P. C. Benetti. Nonequilibrium statistical mechanics of systems with long-range interactions: Ubiquity of core-halo distributions. *Phys. Rep.* **535**, 1 (2014).
- [15] V. A. Antonov. Most Probable Phase Distribution in Spherical Star Systems and Conditions for Its Existence. *Vest. Leningrad Univ.* **7**, 135 (1962).
- [16] D. Lynden-Bell and R. Wood. The gravo-thermal catastrophe in isothermal spheres and the onset of red-giant structure for stellar systems. *Mon. Not. R. Astron. Soc.* **138**, 495 (1968).
- [17] D. Lynden-Bell. Negative specific heat in astronomy, physics and chemistry. *Physica A* **263**, 293 (1999).
- [18] W. Thirring. Systems with negative specific heat. *Z. Phys.* **235**, 339 (1970).
- [19] T. Padmanabhan. Statistical mechanics of gravitating systems. *Phys. Rep.* **188**, 285 (1990).
- [20] P.-H. Chavanis. Gravitational instability of finite isothermal spheres. *Astron. Astrophys.* **381**, 340 (2002).
- [21] P.-H. Chavanis. Statistical Mechanics of Two-Dimensional Vortices and Stellar Systems. In T. Dauxois, S. Ruffo, E. Arimondo, and M. Wilkens, editors, *Dynamics and Thermodynamics of Systems with Long-Range Interactions*, volume 602 of *Lecture Notes in Physics*, page 208. Springer-Verlag Berlin Heidelberg (2002).
- [22] P.-H. Chavanis. On the lifetime of metastable states in self-gravitating systems. *Astron. Astrophys.* **432**, 117 (2005).
- [23] P.-H. Chavanis. Phase transitions in self-gravitating systems. *Int. J. Mod. Phys. B* **20**, 3113 (2006).
- [24] P.-H. Chavanis and J. Sommeria. Statistical mechanics of the shallow water system. *Phys. Rev. E* **65**, 026302 (2002).
- [25] J. Miller. Statistical mechanics of Euler equations in two dimensions. *Phys. Rev. Lett.* **65**, 2137 (1990).
- [26] L. Onsager. Statistical hydrodynamics. *Nuovo Cim. Suppl. 2* **6**, 279 (1949).
- [27] R. Robert and J. Sommeria. Statistical equilibrium states for two-dimensional flows. *J. Fluid. Mech.* **229**, 291 (1991).
- [28] P. Chomaz and F. Gulminelli. Phase Transitions in Finite Systems. In T. Dauxois, S. Ruffo, E. Arimondo, and M. Wilkens, editors, *Dynamics and Thermodynamics of Systems with Long-Range Interactions*, volume 602 of *Lecture Notes in Physics*, page 68. Springer-Verlag Berlin Heidelberg (2002).
- [29] A. Campa, A. Giansanti, and D. Moroni. Canonical solution of a system of long-range interacting rotators on a lattice. *Phys. Rev. E* **62**, 303 (2000).
- [30] A. Campa, A. Giansanti, and D. Moroni. Canonical solution of classical magnetic models with long-range couplings. *J. Phys. A: Math. Gen.* **36**, 6897 (2003).
- [31] T. Mori. Analysis of the exactness of mean-field theory in long-range interacting systems. *Phys. Rev. E* **82**, 060103(R) (2010).

- [32] T. Mori. Instability of the mean-field states and generalization of phase separation in long-range interacting systems. *Phys. Rev. E* **84**, 031128 (2011).
- [33] T. Mori. Phase transitions in systems with non-additive long-range interactions. *J. Stat. Mech.*, P10003 (2013).
- [34] M. K. H. Kiessling and T. Neukirch. Negative specific heat of a magnetically self-confined plasma torus. *Proc. Natl. Acad. Sci.* **100**, 1510 (2003).
- [35] D. R. Nicholson. *Introduction to Plasma Theory*. Krieger Publishing, Malabar, Florida (1992).
- [36] Y. Levin, R. Pakter, and T. N. Teles. Collisionless Relaxation in Non-Neutral Plasmas. *Phys. Rev. Lett.* **100**, 040604 (2008).
- [37] M. Antoni and S. Ruffo. Clustering and relaxation in Hamiltonian long-range dynamics. *Phys. Rev. E* **52**, 2361 (1995).
- [38] T. Dauxois, V. Latora, A. Rapisarda, S. Ruffo, and A. Torcini. The Hamiltonian Mean Field Model: From Dynamics to Statistical Mechanics and Back. In T. Dauxois, S. Ruffo, E. Arimondo, and M. Wilkens, editors, *Dynamics and Thermodynamics of Systems with Long-Range Interactions*, volume 602 of *Lecture Notes in Physics*, page 458. Springer-Verlag Berlin Heidelberg (2002).
- [39] C. Nardini and L. Casetti. Energy landscape and phase transitions in the self-gravitating ring model. *Phys. Rev. E* **80**, 060103 (2009).
- [40] T. M. Rocha Filho, M. A. Amato, B. A. Mello, and A. Figueiredo. Phase transitions in simplified models with long-range interactions. *Phys. Rev. E* **84**, 041121 (2011).
- [41] D. H. E. Gross. *Microcanonical thermodynamics: phase transitions in "small" systems*. Lecture Notes in Physics **66**, World Scientific (2001).
- [42] F. Leyvraz and S. Ruffo. Ensemble inequivalence in systems with long-range interactions. *J. Phys. A: Math. Gen.* **35**, 285 (2002).
- [43] F. Bouchet and J. Barré. Classification of Phase Transitions and Ensemble Inequivalence, in Systems with Long Range Interactions. *J. Stat. Phys.* **118**, 1073 (2005).
- [44] A. Campa and A. Giansanti. Canonical and microcanonical partition functions in long-range systems with order parameter space of arbitrary dimension. *Physica A* **340**, 170 (2004).
- [45] A. Campa, S. Ruffo, and H. Touchette. Negative magnetic susceptibility and nonequivalent ensembles for the mean-field  $\varphi^4$  spin model. *Physica A* **385**, 233 (2007).
- [46] A. Campa. The study of the equilibrium and of the dynamical properties of long-range interacting systems. In A. Campa, A. Giansanti, G. Morigi, and F. Sylos Labini, editors, *Dynamics and Thermodynamics of Systems with Long-Range Interactions: Theory and Experiments*, volume 970, page 3. AIP Conference Proceedings (2008).
- [47] R. S. Ellis, K. Haven, and B. Turkington. Large Deviation Principles and Complete Equivalence and Nonequivalence Results for Pure and Mixed Ensembles. *J. Stat. Phys.* **101**, 999 (2000).
- [48] J. Barré, D. Mukamel, and S. Ruffo. Inequivalence of Ensembles in a System with Long-Range Interactions. *Phys. Rev. Lett.* **87**, 030601 (2001).

- [49] M. Schmidt, R. Kusche, T. Hippler, J. Donges, W. Kronmüller, B. von Issendorff, and H. Haberland. Negative Heat Capacity for a Cluster of 147 Sodium Atoms. *Phys. Rev. Lett.* **86**, 1191 (2001).
- [50] F. P. C. Benetti, T. N. Teles, R. Pakter, and Y. Levin. Ergodicity Breaking and Parametric Resonances in Systems with Long-Range Interactions. *Phys. Rev. Lett.* **108**, 140601 (2012).
- [51] Y. Levin, R. Pakter, and F. B. Rizzato. Collisionless relaxation in gravitational systems: From violent relaxation to gravothermal collapse. *Phys. Rev. E* **78**, 021130 (2008).
- [52] P.-H. Chavanis. Hamiltonian and Brownian systems with long-range interactions: II. Kinetic equations and stability analysis. *Physica A* **361**, 81 (2006).
- [53] T. N. Teles, Y. Levin, and R. Pakter. Statistical mechanics of 1D self-gravitating systems: the core-halo distribution. *Mon. Not. R. Astron. Soc.* **417**, L21 (2011).
- [54] C. H. Silvestre and T. M. Rocha Filho. Ergodicity in a two-dimensional self-gravitating many-body system. *Phys. Lett. A* **380**, 337 (2016).
- [55] T. N. Teles, Y. Levin, R. Pakter, and F. B. Rizzato. Statistical mechanics of unbound two-dimensional self-gravitating systems. *J. Stat. Mech.*, P05007 (2010).
- [56] J. Katz. Thermodynamics of Self-Gravitating Systems. *Found. Phys.* **33**, 223 (2003).
- [57] H. J. de Vega and N. Sánchez. Statistical mechanics of the self-gravitating gas: I. Thermodynamic limit and phase diagrams. *Nuclear Physics B* **625**, 409 (2002).
- [58] H. J. de Vega and N. Sánchez. Statistical mechanics of the self-gravitating gas: II. Local physical magnitudes and fractal structures. *Nucl. Phys. B* **625**, 460 (2002).
- [59] J. Katz and I. Okamoto. Fluctuations in isothermal spheres. *Mon. Not. R. Astron. Soc.* **317**, 163 (2000).
- [60] D. Lynden-Bell and R. M Lynden-Bell. On the negative specific heat paradox. *Mon. Not. R. Astron. Soc.* **101**, 405 (1977).
- [61] G. Horwitz and J. Katz. Steepest-descent technique and stellar equilibrium statistical mechanics. I Newtonian clusters in a box. *Astrophys. J.* **211**, 226 (1977).
- [62] G. Horwitz and J. Katz. Steepest descent technique and stellar equilibrium statistical mechanics. III Stability of various ensembles. *Astrophys. J.* **222**, 941 (1978).
- [63] I. Ispolatov and E. G. D. Cohen. Collapse in Systems with Attractive Nonintegrable Potentials. *Phys. Rev. Lett.* **87**, 210601 (2001).
- [64] I. Ispolatov and E. G. D. Cohen. Phase transitions in systems with  $1/r^\alpha$  attractive interactions. *Phys. Rev. E* **64**, 056103 (2001).
- [65] T. L. Hill. *Thermodynamics of Small Systems, Parts I and II*. Dover, New York (2013).
- [66] M. Planck. *The Theory of Heat Radiation*. Dover, New York (1991).
- [67] J. J. Loomis and H. J. Maris. Theory of heat transfer by evanescent electromagnetic waves. *Phys. Rev. B* **50**, 18517 (1994).

- [68] E. Rousseau, A. Siria, G. Jourdan, S. Volz, F. Comin, J. Chevrier, and J.-J. Greffet. Radiative heat transfer at the nanoscale. *Nature Photon.* **3**, 514 (2009).
- [69] S. Shen, A. Narayanaswamy, and G. Chen. Surface Phonon Polaritons Mediated Energy Transfer between Nanoscale Gaps. *Nano Lett.* **9**, 2909 (2009).
- [70] S. Shen, A. Mavrokefalos, P. Sambegoro, and G. Chen. Nanoscale thermal radiation between two gold surfaces. *Appl. Phys. Lett.* **100**, 233114 (2012).
- [71] A. Pérez-Madrid, J. M. Rubi, and L. C. Lapas. Heat transfer between nanoparticles: Thermal conductance for near-field interactions. *Phys. Rev. B* **77**, 155417 (2008).
- [72] A. Pérez-Madrid, L. C. Lapas, and J. M. Rubi. Heat Exchange between Two Interacting Nanoparticles beyond the Fluctuation-Dissipation Regime. *Phys. Rev. Lett.* **103**, 048301 (2009).
- [73] S. Basu and Z. M. Zhang. Maximum energy transfer in near-field thermal radiation at nanometer distances. *J. Appl. Phys.* **105**, 093535 (2009).
- [74] A. Kittel, W. Müller-Hirsch, J. Parisi, S.-A. Biehs, D. Reddig, and M. Holthaus. Near-Field Heat Transfer in a Scanning Thermal Microscope. *Phys. Rev. Lett.* **95**, 224301 (2005).
- [75] Y. De Wilde, F. Formanek, R. Carminati, B. Gralak, P.-A. Lemoine, K. Joulain, J.-P. Mulet, Y. Chen, and J.-J. Greffet. Thermal radiation scanning tunnelling microscopy. *Nature* **444**, 740 (2006).
- [76] P. Ben-Abdallah and S.-A. Biehs. Near-Field Thermal Transistor. *Phys. Rev. Lett.* **112**, 044301 (2014).
- [77] A. Narayanaswamy and G. Chen. Surface modes for near field thermophotovoltaics. *Appl. Phys. Lett.* **82**, 3544 (2003).
- [78] M. Laroche, R. Carminati, and J.-J. Greffet. Near-field thermophotovoltaic energy conversion. *J. Appl. Phys.* **100**, 063704 (2006).
- [79] K. Park, S. Basu, W. P. King, and Z. M. Zhang. Performance analysis of near-field thermophotovoltaic devices considering absorption distribution. *J. Quant. Spectrosc. Radiat. Transfer* **109**, 305 (2008).
- [80] S. Basu, Z. M. Zhang, and C. J. Fu. Review of near-field thermal radiation and its application to energy conversion. *Int. J. Energ. Res.* **33**, 1203 (2009).
- [81] O. Ilic, M. Jablan, J. D. Joannopoulos, I. Celanovic, and M. Soljačić. Overcoming the black body limit in plasmonic and graphene near-field thermophotovoltaic systems. *Opt. Express* **20**, A366 (2012).
- [82] R. Messina and P. Ben-Abdallah. Graphene-based photovoltaic cells for near-field thermal energy conversion. *Sci. Rep.* **3**, 1383 (2013).
- [83] P. Ben-Abdallah. Photon Thermal Hall Effect. *Phys. Rev. Lett.* **116**, 084301 (2016).
- [84] B. Song, A. Fiorino, E. Meyhofer, and P. Reddy. Near-field radiative thermal transport: From theory to experiment. *AIP Advances* **5**, 053503 (2015).
- [85] X. Liu, L. Wang, and Z. M. Zhang. Near-Field Thermal Radiation: Recent Progress and Outlook. *Nanosc. Microsc. Therm.* **19**, 98 (2015).

- [86] P. Ben-Abdallah, S.-A. Biehs, and K. Joulain. Many-Body Radiative Heat Transfer Theory. *Phys. Rev. Lett.* **107**, 114301 (2011).
- [87] Z. H. Zheng and Y. M. Xuan. Enhancement or Suppression of the Near-Field Radiative Heat Transfer Between Two Materials. *Nanoscale Microscale Thermophys. Eng.* **15**, 237 (2011).
- [88] R. Messina, M. Antezza, and P. Ben-Abdallah. Three-Body Amplification of Photon Heat Tunneling. *Phys. Rev. Lett.* **109**, 244302 (2012).
- [89] R. Messina, M. Tschikin, S.-A. Biehs, and P. Ben-Abdallah. Fluctuation-electrodynamic theory and dynamics of heat transfer in systems of multiple dipoles. *Phys. Rev. B* **88**, 104307 (2013).
- [90] M. Nikbakht. Radiative heat transfer in anisotropic many-body systems: Tuning and enhancement. *J. Appl. Phys.* **116**, 094307 (2014).
- [91] Y. Wang and J. Wu. Radiative heat transfer between nanoparticles enhanced by intermediate particle. *AIP Advances* **6**, 025104 (2016).
- [92] V. Kubytskyi, S.-A. Biehs, and P. Ben-Abdallah. Radiative Bistability and Thermal Memory. *Phys. Rev. Lett.* **133**, 074301 (2014).
- [93] L. Novotny and B. Hecht. *Principles of nano-optics*. Cambridge University Press, Cambridge (2006).
- [94] J. B. Pendry. Radiative exchange of heat between nanostructures. *J. Phys. Condens. Matter* **11**, 6621 (1999).
- [95] S. M. Rytov. *Theory of electric fluctuations and thermal radiation*. Air Force Cambridge Research Center, Bedford, MA (1953).
- [96] S. M. Rytov, Y. A. Kravtsov, and V. I. Tatarskii. *Principles of Statistical Radiophysics*. Springer-Verlag, Berlin Heidelberg (1989).
- [97] H. B. Callen and T. A. Welton. Irreversibility and generalized noise. *Phys. Rev.* **83**, 34 (1951).
- [98] L. D. Landau and E. M. Lifshitz. *Statistical Physics, Part 1, Vol. 5, 3rd ed.* Butterworth-Heinemann, Oxford (1980).
- [99] J.-P. Mulet, K. Joulain, R. Carminati, and J.-J. Greffet. Enhanced radiative heat transfer at nanometric distances. *Microscale Thermophys. Eng.* **6**, 209 (2002).
- [100] E. M. Lifshitz. The Theory of Molecular Attractive Forces between Solids. *Sov. Phys. JETP* **2**, 73 (1956).
- [101] I. E. Dzyaloshinskii, E. M. Lifshitz, and L. P. Pitaevskii. General Theory of Van Der Waals' Forces. *Sov. Phys. Uspekhi* **4**, 153 (1961).
- [102] H. B. G. Casimir. On the attraction between two perfectly conducting plates. *Proc. Kon. Nederland. Akad. Wetensch.* **51**, 793 (1948).
- [103] R. Messina and M. Antezza. Scattering-matrix approach to Casimir-Lifshitz force and heat transfer out of thermal equilibrium between arbitrary bodies. *Phys. Rev. A* **84**, 042102 (2011).

- [104] R. Messina and M. Antezza. Three-body radiative heat transfer and Casimir-Lifshitz force out of thermal equilibrium for arbitrary bodies. *Phys. Rev. A* **89**, 052104 (2014).
- [105] K. Joulain, J.-P. Mulet, F. Marquier, R. Carminati, and J.-J. Greffet. Surface electromagnetic waves thermally excited: Radiative heat transfer, coherence properties and Casimir forces revisited in the near field. *Surf. Sci. Rep.* **57**, 59 (2005).
- [106] A. I. Volokitin and B. N. J. Persson. Near-field radiative heat transfer and noncontact friction. *Rev. Mod. Phys.* **79**, 1291 (2007).
- [107] G. S. Agarwal. Quantum electrodynamics in the presence of dielectrics and conductors. III. Relations among one-photon transition probabilities in stationary and nonstationary fields, density of states, the field-correlation functions, and surface-dependent response functions. *Phys. Rev. A* **11**, 253 (1975).
- [108] W. Eckhardt. Radiation Laws in the Vicinity of Metallic Boundaries. *Z. Phys. B - Cond. Matter* **46**, 85 (1982).
- [109] K. Joulain, R. Carminati, J.-P. Mulet, and J.-J. Greffet. Definition and measurement of the local density of electromagnetic states close to an interface. *Phys. Rev. B* **68**, 245405 (2003).
- [110] I. Dorofeyev. Thermodynamic functions of fluctuating electromagnetic fields within a heterogeneous system. *Phys. Scr.* **84**, 055003 (2011).
- [111] A. Narayanaswamy and Y. Zheng. Theory of thermal nonequilibrium entropy in near-field thermal radiation. *Phys. Rev. B* **88**, 075412 (2013).
- [112] A. Babuty, K. Joulain, P.-O. Chapuis, J.-J. Greffet, and Y. De Wilde. Blackbody Spectrum Revisited in the Near Field. *Phys. Rev. Lett.* **110**, 146103 (2013).
- [113] P. T. Landsberg and G. Tonge. Thermodynamic energy conversion efficiencies. *J. Appl. Phys.* **51**, R1 (1980).
- [114] A. De Vos, P. T. Landsberg, P. Baruch, and J. E. Parrott. Entropy fluxes, endoreversibility, and solar energy conversion. *J. Appl. Phys.* **74**, 3631 (1993).
- [115] P. Ben-Abdallah and K. Joulain. Fundamental limits for noncontact transfers between two bodies. *Phys. Rev. B* **82**, 121419 (R) (2010).
- [116] S.-A. Biehs, E. Rousseau, and J.-J. Greffet. Mesoscopic Description of Radiative Heat Transfer at the Nanoscale. *Phys. Rev. Lett.* **105**, 234301 (2010).
- [117] H. B. Callen. *Thermodynamics and an introduction to thermostatistics*. John Willey & Sons, Singapore (1985).
- [118] T. L. Hill. Thermodynamics of small systems. *J. Chem. Phys.* **36**, 3182 (1962).
- [119] D. Bedeaux. Private communication, December 2014.
- [120] T. L. Hill and R. V. Chamberlin. Extension of the thermodynamics of small systems to open metastable states: An example. *Proc. Nat. Acad. Sci.* **95**, 12779 (1998).
- [121] S. K. Schnell, T. J. H. Vlugt, J.-M. Simon, D. Bedeaux, and S. Kjelstrup. Thermodynamics of a small system in a  $\mu T$  reservoir. *Chem. Phys. Lett.* **504**, 199 (2011).

- [122] S. K. Schnell, T. J. H. Vlugt, J.-M. Simon, D. Bedeaux, and S. Kjelstrup. Thermodynamics of small systems embedded in a reservoir: a detailed analysis of finite size effects. *Mol. Phys.* **110**, 1069 (2012).
- [123] R. V. Chamberlin. Mean-field cluster model for the critical behaviour of ferromagnets. *Nature* **408**, 337 (2000).
- [124] T. L. Hill. *Statistical Mechanics: Principles and Selected Applications*. Dover, New York (1987).
- [125] E. A. Guggenheim. Grand Partition Functions and so-called “Thermodynamic Probabilities”. *J. Chem. Phys.* **7**, 103 (1939).
- [126] H. Fowler and E. A. Guggenheim. *Statistical Thermodynamics*. Cambridge, London (1939).
- [127] T. L. Hill. A Different Approach to Nanothermodynamics. *Nano Lett.* **1**, 273 (2001).
- [128] T. L. Hill. Perspective: Nanothermodynamics. *Nano Lett.* **1**, 111 (2001).
- [129] T. L. Hill and R. V. Chamberlin. Fluctuations in energy in completely open small systems. *Nano Lett.* **2**, 609 (2002).
- [130] E. A. Guggenheim. *Thermodynamics: An Advanced Treatment for Chemists and Physicists*. North-Holland Publishing Company, Amsterdam (1967).
- [131] A. Planes and E. Vives. Entropic formulation of statistical mechanics. *J. Stat. Phys.* **106**, 827 (2002).
- [132] K. Huang. *Statistical Mechanics, 2nd ed.* John Wiley & Sons, New York (1987).
- [133] S. de Groot and P. Mazur. *Non-Equilibrium Thermodynamics*. Dover Publications, New York (1984).
- [134] P. Glansdorff and I. Prigogine. *Thermodynamic theory of structure, stability and fluctuations*. Wiley-Interscience, London (1977).
- [135] P.-H. Chavanis. Brownian particles with long- and short-range interactions. *Physica A* **390**, 1546 (2011).
- [136] P.-H. Chavanis. Hamiltonian and Brownian systems with long-range interactions: I Statistical equilibrium states and correlation functions. *Physica A* **361**, 55 (2006).
- [137] T. Mori. Thermodynamics of Extensive but Nonadditive Systems: Modified Gibbs-Duhem Equation in the Dipolar gas, arXiv:1510.07109.
- [138] L. Velazquez. Remarks about the thermodynamics of astrophysical systems in mutual interaction and related notions. *J. Stat. Mech.*, 033105 (2016).
- [139] H. Touchette, R. S. Ellis, and B. Turkington. An introduction to the thermodynamic and macrostate levels of nonequivalent ensembles. *Physica A* **340**, 138 (2004).
- [140] H. Touchette. The large deviation approach to statistical mechanics. *Phys. Rep.* **478**, 1 (2009).
- [141] O. Cohen and D. Mukamel. Ensemble inequivalence: Landau theory and the ABC model. *J. Stat. Mech.*, P12017 (2012).
- [142] L. Casetti and C. Nardini. A solvable model of a self-gravitating system. *J. Stat. Mech.*, P05006 (2010).

- [143] S. Chandrasekhar. *An introduction to the study of stellar structure*. The University of Chicago press (1939).
- [144] R. Landauer. Electrical resistance of disordered one-dimensional lattices. *Philos, Mag.* **21**, 863 (1970).
- [145] Büttiker, M. Four-Terminal Phase-Coherent Conductance. *Phys. Rev. Lett.* **57**, 1761 (1986).
- [146] S.-A. Biehs, P. Ben-Abdallah, and F. S. S Rosa. *Nanoscale Radiative Heat Transfer and Its Applications*. In V. Morozhenko, editor, *Infrared Radiation*, InTech (2012).
- [147] E. M. Lifshitz and L. P Pitaevskii. *Statistical Physics, Part 2, Vol. 9*. Butterworth-Heinemann, Oxford (1980).
- [148] A. I. Volokitin and B. N. J. Persson. Radiative heat transfer between nanostructures. *Phys. Rev. B* **63**, 205404 (2001).
- [149] K. Joulain. Near-field heat transfer: A radiative interpretation of thermal conduction. *J. Quant. Spectrosc. Ra.* **109**, 294 (2008).
- [150] P.-O. Chapuis, S. Volz, C. Henkel, K. Joulain, and J.-J. Greffet. Effects of spatial dispersion in near-field radiative heat transfer between two parallel metallic surfaces. *Phys. Rev. B* **77**, 035431 (2008).
- [151] C. Henkel and K. Joulain. Electromagnetic field correlations near a surface with a nonlocal optical response. *Appl. Phys. B* **84**, 61 (2006).
- [152] G. W. Ford and W. H. Weber. Electromagnetic interactions of molecules with metal surfaces. *Phys. Rep.* **113**, 195 (1984).
- [153] J. D. Caldwell, L. Lindsay, V. Giannini, I. Vurgaftman, T. L. Reinecke, S. A. Maier, and Glembocki O. J. Low-loss, infrared and terahertz nanophotonics using surface phonon polaritons. *Nanophotonics* **4**, 44 (2015).
- [154] E. Rousseau, M. Laroche, and J.-J. Greffet. Asymptotic expressions describing radiative heat transfer between polar materials from the far-field regime to the nanoscale regime. *J. Appl. Phys.* **111**, 014311 (2012).
- [155] L. Hu, A. Narayanaswamy, X. Chen, and G. Chen. Near-field thermal radiation between two closely spaced glass plates exceeding Planck's blackbody radiation law. *Appl. Phys. Lett.* **92**, 133106 (2008).
- [156] R. S. Ottens, V. Quetschke, S. Wise, A. A. Alemi, R. Lundock, G. Mueller, D. H. Reitze, D. B. Tanner, and B. F. Whiting. Near-Field Radiative Heat Transfer between Macroscopic Planar Surfaces. *Phys. Rev. Lett.* **107**, 014301 (2011).
- [157] T. Kralik, P. Hanzelka, V. Musilova, A. Srnka, and M. Zobac. Cryogenic apparatus for study of near-field heat transfer. *Rev. Sci. Instrum.* **82**, 055106 (2011).
- [158] R. S. DiMatteo, P. Greiff, S. L. Finberg, K. A. Young-Waithe, H. K. H. Choy, M. M. Masaki, and C. G. Fonstad. Enhanced photogeneration of carriers in a semiconductor via coupling across a nonisothermal nanoscale vacuum gap. *Appl. Phys. Lett.* **79**, 1894 (2001).
- [159] S. Kjelstrup, D. Bedeaux, E. Johannessen, and J. Gross. *Non-equilibrium Thermodynamics for Engineers*. World Scientific Publishing Company (2010).

- [160] E. Palik (editor). *Handbook of optical constants of solids*. Academic Press, London (1998).
- [161] E. N. Economou. Surface Plasmons in Thin Films. *Phys. Rev.* **182**, 539 (1969).
- [162] A. I. Volokitin and B. N. J. Persson. Resonant photon tunneling enhancement of the radiative heat transfer. *Phys. Rev. B* **69**, 045417 (2004).
- [163] K. H. Hoffmann, J. M. Burzler, and S. Schubert. Endoreversible Thermodynamics. *J. Non-Equilib. Thermodyn.* **22**, 311 (1997).